Esophageal Extracellular Matrix Hydrogel to Restore Dysregulated Microenvironment-Cell Signaling for Treatment of Pre-Malignant and Neoplastic Esophageal Disease

by

Lindsey Tamiko Saldin

Bachelor of Science, University of California, Berkeley, 2013

Submitted to the Graduate Faculty of

Swanson School of Engineering in partial fulfillment

of the requirements for the degree of

Doctor of Philosophy

University of Pittsburgh

2018

UNIVERSITY OF PITTSBURGH

Swanson School of Engineering

This dissertation was presented

by

Lindsey Tamiko Saldin

It was defended on

August 29, 2018

and approved by

Dr. Lance Davidson, PhD, Professor
Department of Bioengineering

Dr. Vera Donnenberg, PhD, Associate Professor
Department of Cardiothoracic Surgery

Dr. Cyrus Ghajar, PhD, Assistant Member
Public Health Sciences, Fred Hutchinson Cancer Research Center

Dr. Partha Roy, PhD, Associate Professor
Department of Bioengineering

Dissertation Director: Dr. Stephen F. Badylak, DVM, PhD, MD, Professor
Departments of Surgery and Bioengineering

ESOPHAGEAL EXTRACELLULAR MATRIX HYDROGEL TO RESTORE DYSREGULATED MICROENVIRONMENT-CELL SIGNALING FOR TREATMENT OF PRE-MALIGNANT AND NEOPLASTIC ESOPHAGEAL DISEASE

Lindsey Tamiko Saldin, PhD

University of Pittsburgh, 2018

Esophageal adenocarcinoma (EAC) has a 20% five-year survival rate, and the standard of care esophagectomy has a 20% mortality and 50% morbidity. EAC pathogenesis involves dysplastic and metaplastic changes within the mucosa in response to dysregulated microenvironmental cues, i.e., gastric reflux and chronic inflammation. Extracellular matrix (ECM) is a primary component of the microenvironment that influences cell phenotype through dynamic reciprocity.

ECM bioscaffolds have been used to treat 14 EAC patients after mucosal resection resulting in preservation of esophageal function, restoration of a near normal mucosa, and no recurrence of cancer for 1-8 years. The implanted ECM bioscaffolds completely degraded within 2 weeks, suggesting that the ECM degradation products normalized cell phenotype in the post-cancer resection niche. ECM bioscaffolds can be digested by pepsin *in vitro* to simulate ECM degradation products, and furthermore these degradation products can be formulated as a hydrogel for clinical therapy.

The objectives of the present dissertation were to determine the effects of solubilized non-malignant, metaplastic, and neoplastic esophageal ECM upon macrophage activation and epithelial cell function, to further understand the role of ECM-cell crosstalk in EAC progression. Solubilized, non-malignant ECM hydrogel was evaluated for its potential to mitigate diseased esophageal epithelial cells *in vitro* and *in vivo*.

Metaplastic and neoplastic ECM contained distinctive matrix-bound nanovesicle (MBV) miRNA cargo and ECM protein signatures that activated macrophages toward a pro-

inflammatory, TNFα+ state, and increased epithelial cell migration. Non-malignant esophageal ECM (eECM) hydrogel downregulated cancer cell proliferation and signaling pathways (e.g., PI3K-Akt, cell cycle/DNA replication), with a minimal effect on normal esophageal epithelial cells. eECM hydrogel treatment mitigated macroscopic esophagitis, regressed Barrett's epithelium toward normal squamous epithelium, and downregulated the pro-inflammatory TNFα+ cell infiltrate in a pre-clinical, large animal model of Barrett's esophagus. Similar results were seen with eECM hydrogel treatment in an *in vivo* rodent model of EAC. Finally, practical aspects of the clinical translation of eECM hydrogels were determined. eECM hydrogel mechanical properties can be tailored to facilitate oral, endoscopic, or submucosal injection delivery.

Taken together, we conclude that eECM hydrogel is a suitable therapy for esophageal disease based upon the accepted concepts of cell-matrix interactions.

TABLE OF CONTENTS

LIST OF TABLES

LIST OF FIGURES

1.0 INTRODUCTION

1.1 ESOPHAGEAL ADENOCARCINOMA ARISES FROM DYSREGULATED MATRIX-CELL SIGNALING

The incidence of esophageal adenocarcinoma (EAC) is increasing faster than any other type of cancer in the United States [1]. More than 50% of EAC patients have unresectable or metastatic disease upon EAC diagnosis, and overall 5-year survival is poor (less than 20%) [2]. The default response to tissue injury in the esophagus following resection is inflammation and scarring, which eventually leads to stricture; therefore, even pre-malignant tissues and early stage cancer cannot be excised without compromising esophageal function [3]. The current standard of care is monitoring for Barrett's esophagus, and esophagectomy for EAC, a procedure associated with high morbidity, post-surgical complications, and decreased quality of life.

Current evidence indicates EAC progresses spatially and temporally in response to the environmental injury caused by gastroesophageal reflux. Five to 8% of gastroesophageal reflux disease (GERD) patients develop inflammatory Barrett's esophagus (BE), where refluxed stomach acid and bile enters the esophagus, transforming normal, stratified squamous epithelium to villiform, columnar epithelium with appearance of goblet cells ("metaplasia"), characteristic of the stomach or small intestine [1]. Chronic and repetitive injury of this type leads to EAC, marked by glandular cell growth and invasion into the basement membrane ("neoplasia"). Because each patient's cells are genetically identical, precancerous and

cancerous gene expression patterns may be the result of epigenetic changes induced by altered microenvironments. EAC provides the opportunity to investigate non-malignant, metaplastic, and neoplastic disease states within the same tissue, wherein the non-malignant adjacent tissue can serve as the patient's own control.

A primary component of the microenvironment is the extracellular matrix (ECM), the structural and functional proteins secreted by all living cells [4]. ECM is now recognized as essential to govern tissue-specific function by a process termed "dynamic reciprocity": the bidirectional crosstalk between a cell and its surrounding matrix to dictate cell behavior [5]. Specifically, cell receptors for ECM components transduce signals from the microenvironmental niche, to the cytoskeleton, to the nuclear matrix, to chromatin, and back again. Normal tissue homeostasis is a function of dynamic reciprocity; however, in chronic inflammation and cancer the ECM becomes dysregulated. Disruption of physiologic cell-ECM signaling facilitates the initiation and progression of epithelial cancer in lung, kidney, prostate, saliva gland, and breast [4].

Although the pathogenesis of EAC is relatively well established [1], the biochemical changes to the ECM occurring during EAC progression are not well known. The changes to the ECM composition, including ECM proteins and cargo of recently described, matrix-bound nanovesicles (MBV) [6], would likely affect candidate cell types in the EAC niche via dynamic reciprocity. Two cell types that are directly regulated by the ECM and are important in EAC progression are: 1) macrophages and 2) epithelial cells.

Macrophages are plastic, innate immune cells recruited to sites of inflammation, injury, and cancer [7]. At a lesion or tumor site, macrophages may activate to the pro-inflammatory phenotype ("M1") or immunomodulatory phenotype ("M2") in response to microenvironmental signals [8]. M1 and M2 represent the extremes of a continuum and are characterized by distinctive functional programs involving released growth factors, chemokines, and MMPs.

Macrophages are activated to an M1 phenotype by molecules such as IFNγ, LPS, and TNFα; and secrete copious amounts of nitric oxide, reactive oxygen species (ROS), and pro-inflammatory cytokines i.e., IL-12high, IL-10low, IL-6 and TNFα to protect against pathogens. In contrast, macrophages are activated to an M2 phenotype by molecules such as IL-4 and IL-13 and secrete large amounts of TGFβ1 and arginase; secrete IL-10high and IL-12low; and scavenge debris, promote angiogenesis, and recruit cells involved in constructive tissue remodeling. “Tumor-associated macrophages" (TAM) are considered a subtype of M2 macrophages, which express phenotypic M2 activation factors and show little cytotoxicity for tumors [9]. However, TAMs also promote chronic “smoldering" pro-inflammation that accompanies cancer initiation [10]. Macrophage phenotype in chronic inflammatory and neoplastic microenvironments has been characterized, but the isolated effect of metaplastic and neoplastic ECM on macrophage phenotype and function remains unknown, and could become an important EAC therapeutic target. The persistence of chronic inflammation in EAC and its progression is important because it is associated with the persistence of metaplasia in Barrett’s patients, despite these patients being chronically treated for the secretion of acidic gastric contents with proton pump inhibitors (PPI) [11, 12]. Macrophages can also be modulated by immunotherapy-based approaches, making an understanding of their activation by the metaplastic and neoplastic ECM clinically important.

Esophageal epithelial cells form a continuous layer of squamous cells that line the esophagus, and are in intimate contact with the basement membrane. Some theories support the concept that abnormal microenvironmental conditions (e.g., bile salts, acid) promotes metaplastic and neoplastic transformation of esophageal epithelial cells (and esophageal epithelial stem cells [13]) by activating esophageal developmental pathways (Hedgehog) [14]; oncogenic pathways (PI3K-Akt) [15], epithelial-mesenchymal transition (EMT) [16]; and genetic and epigenetic changes (silencing, mutation, or loss of p16, p53, and APC, and overexpression

of cyclin D1 and EGFR, downregulation of Ecadherin) [14, 17]. The esophageal epithelial cells can therefore acquire tumorigenic features such as avoiding apoptosis, maintaining growth self-sufficiency, and overriding cell cycle control checkpoints [18]. Epithelial cells are also sensitive to paracrine effects from immune cells in chronic inflammatory microenvironments [10, 19, 20]. However, the isolated effect of the non-malignant, metaplastic, and neoplastic ECM upon the differentiation state of epithelial cells, and paracrine effects of macrophages, remain unknown.

1.2 RESTORING DYSREGULATED MATRIX-CELL SIGNALING WITH NON-MALIGNANT ECM THERAPY

Understanding the dysregulated matrix-cell signaling changes that occur during EAC progression could inform current treatment strategies, and could provide a rationale to treat pre-malignant Barrett's and EAC patients with non-malignant ECM. Dysregulated matrix-cell signaling in breast cancer, such as non-physiologic integrin signaling (β1 and β4 integrins) [21, 22] or abnormal cell signaling pathway activation (PI3K) [23], can be restored by inhibitory integrin antibodies or PI3K pathway inhibitors, respectively, and show a dramatic reversion to basally polarized, growth arrested cell phenotype similar to non-malignant cell controls. Correcting dysregulated-microenvironmental signaling was dominant over the cancer cell genotype to direct cell behavior [21-23]. Stated differently, the interaction between cancer cells and the surrounding ECM during malignancy can be manipulated toward a more normal pattern by restoring normal matrix-cell signals.

Non-malignant ECM can be considered "Mother Nature's template" and is capable of maintaining initiating and inhibitory signals for cell growth, differentiation, and apoptosis, in balanced stoichiometric ratios [21, 24]. Non-malignant ECM can be harvested from mammalian tissues by decellularization. ECM was shown to retain the bioactivity and majority of the

ultrastructure and composition of the native tissue. The decellularization protocol should be tailored as a balance between removing cellular material, while preserving ECM structure and composition. A more comprehensive background on the concepts of decellularization of mammalian tissues can be found in the book chapter by [25].

Non-malignant ECM bioscaffolds have been extensively characterized and used in esophageal reconstruction over the past decade, as shown in Table 1. Both homologous and heterologous ECM promotes constructive esophageal tissue remodeling and prevents stricture in various pre-clinical models [26-33]. The success of the earlier pre-clinical studies led to a human cohort study, where ECM bioscaffolds were used to treat 5 EAC patients (T1A) (nodule size <20 mm) after aggressive long-segment mucosal resection [30]. Mature normal epithelium was present as early as 4 months after treatment, with minimal stricture and scarring, after ECM treatment. Follow-up for 4-24 months showed no recurrent EAC. Patients returned to a normal diet and avoided esophagectomy. The ECM bioscaffolds had completely degraded in 2 weeks [30], suggesting that ECM degradation products may have influenced cell phenotype in the cancer niche. Fourteen EAC patients have been treated to date, with similar results and are 7-8 years disease free. However, the molecular mechanisms by which non-malignant ECM ultimately alters the default tissue response to injury in the context of normal, metaplastic, and neoplastic microenvironments remains to be determined. Some studies show an ECM-induced downregulation of neoplastic phenotype in non-esophageal cancer types [30, 34-40]. Understanding the mechanisms by which non-malignant ECM bioscaffold degradation products and hydrogels downregulate neoplastic phenotype is crucial to further advance the potential use of ECM-based materials in the treatment of neoplasia.

Table 1. Studies using ECM in esophageal reconstruction.

Year	Study	Ref.
2000	ECM bioscaffold for repair of 50% circumferential esophageal defect in a dog model	[41]
2005	Full circumference esophageal reconstruction with ECM plus muscle tissue in a dog model	[27]
2006	Reinforcement of esophageal anastomoses with an extracellular matrix scaffold in a canine model	[28]
2009	An extracellular matrix scaffold for esophageal stricture prevention after circumferential EMR	[29]
2011	Esophageal preservation with ECM in five male patients after endoscopic circumferential resection in the setting of superficial cancer	[30]
2013	Bone marrow-derived cells participate in the long-term remodeling in a mouse model of esophageal reconstruction	[31]
2013	Characterization of esophageal mucosa ECM bioscaffold	[42]
2014	Patch Esophagoplasty: Esophageal reconstruction using biologic scaffolds	[32]
2015	Tissue-specific effect of esophageal mucosa ECM upon stem cell chemotaxis and differentiation	[33]
2017	ECM heals a large, chronically infected esophageal perforation	[43]

The protocol used to generate ECM degradation products *in vitro*, pepsin solubilization, can also be used to prepare hydrogel forms that could be delivered to the esophagus without surgery. Solubilized ECM would obviate the need for mucosal resection and placement of a stent (to hold the scaffold in place), and could expand its clinical utility: such as delivering ECM hydrogel at the time of diagnosis as an outpatient procedure, or provided over-the-counter for oral administration. Solubilized ECM degradation products and ECM hydrogels are a central concept of the present dissertation, and a review is provided in the following chapter, of their characterization and considerations for clinical translation.

2.0 STRUCTURE AND FUNCTION OF EXTRACELLULAR MATRIX HYDROGELS[1]

2.1 ABSTRACT

Extracellular matrix (ECM) bioscaffolds prepared from decellularized tissues have been used to facilitate constructive and functional tissue remodeling in a variety of clinical applications. The discovery that these ECM materials could be solubilized and subsequently manipulated to form hydrogels expanded their potential *in vitro* and *in vivo* utility; i.e. as culture substrates comparable to collagen or Matrigel, and as injectable materials that fill irregularly-shaped defects. The mechanisms by which ECM hydrogels direct cell behavior and influence remodeling outcomes are only partially understood, but likely include structural and biological signals retained from the native source tissue. The present chapter describes the utility, formation, and physical and biological characterization of ECM hydrogels. Two examples of clinical application are presented to demonstrate *in vivo* utility of ECM hydrogels in different organ systems. Finally, new research directions and clinical translation of ECM hydrogels are discussed.

---

[1] Portions of this chapter were adapted from the following publication:

L.T. Saldin and M.C. Cramer, S.S. Velankar, L.J. White, S.F. Badylak, Extracellular matrix hydrogels from decellularized tissues: Structure and function, Acta biomaterialia 49 (2017) 1-15.

2.2 INTRODUCTION

Hydrogels are defined as highly hydrated polymer materials (>30% water by weight), which maintain structural integrity by physical and chemical crosslinks between polymer chains [44]. The polymer chains can be synthetic [e.g., polyethylene oxide (PEO), poly(vinyl alcohol) (PVA), poly(acrylic acid) (PAA), poly(propylenefumarate-co-ethylene glycol) P(PF-co-EG)] or natural (e.g., alginate, chitosan, collagen, hyaluronic acid). Synthetic and natural hydrogels have been widely used to fill space, deliver bioactive molecules/drugs, and/or deliver cells to stimulate tissue growth [44].

Many hydrogels have been derived from components of the extracellular matrix (ECM) such as collagen, hyaluronic acid and elastin or complex mixtures of ECM proteins such as Matrigel. The focus of the present chapter is ECM hydrogels and specifically, hydrogels that are 1) derived from decellularized mammalian tissue, and 2) enzymatically solubilized and neutralized to physiologic pH and temperature. Hence, ECM materials that fulfill one of these criteria, such as decellularized tissues that are “gel-like” but not further solubilized (for example decellularized human lipoaspirate [45] , intervertebral disc [46, 47], and devitalized cartilage [48, 49]) are beyond the scope of this chapter. In contrast to hydrogels composed of individual ECM components, ECM hydrogels retain the full biochemical complexity of the native tissue, and unlike Matrigel, are not composed of a protein source that is a product of a tumorigenic cell line.

To date, ECM hydrogels have been primarily used as 3D organotypic culture models and to stimulate tissue growth after injury. The present chapter describes the utility, formation and physical and biological characterization of ECM hydrogels. Two examples of clinical application in selected organ systems are presented. Finally, new research directions and clinical translation of ECM hydrogels are discussed.

2.2.1 Why ECM?

The ECM consists of the structural and functional molecules secreted by the resident cells of each tissue, hence the 3D organization and biochemical composition of the ECM is distinctive for each tissue type. ECM has been influencing cell behavior, dynamically and reciprocally [5] since single cell organisms evolved more than 600 million years ago, and likely played a central role in the transition from unicellular organisms to multicellular organisms [50]. Mimicking aspects of the structure and composition of the ECM has guided the rational design of biomaterials over the past several decades in attempts to proactively influence cell behavior [51].

Although decellularization of tissue was first reported in 1973 as a technique to preserve tissue intended to be used as a protective barrier for burn patients [52], the first reported production of ECM by decellularization of a source tissue for subsequent use as a bioscaffold for tissue reconstruction was the use of small intestinal submucosa (SIS) for vascular applications [53-57]. These initial studies removed cellular material while preserving the structural and functional proteins of the ECM such as glycosaminoglycans (GAGs), proteoglycans, and growth factors [58]. When processed appropriately, ECM materials harvested by such methods retain the biochemical complexity, nanostructure, and bioinductive properties of the native matrix, and have been shown to promote the *in vivo* creation of site-specific, functional tissue [59]. ECM-derived materials are FDA approved, can be preserved and used ‘off the shelf,’ have been implanted in millions of patients to date; and have been extensively characterized in both the 2D sheet and powder forms [59, 60].

The discovery that ECM bioscaffolds could be transformed into hydrogels expanded their potential *in vitro* and *in vivo* utility [58]. For example, minimally invasive delivery becomes possible wherein a pre-gel viscous fluid is injected with a catheter or syringe and polymerizes at physiologic temperature into a hydrogel conforming to the shape of any defect site. Compared

to suspensions of ECM powders, ECM hydrogels can be injected with a more homogenous concentration and with greater ease [61].

Hydrogels derived from SIS and urinary bladder matrix (UBM) have been shown to retain the inherent bioactivity of the native matrix with the ability to promote constructive remodeling in heterologous tissue applications [58, 62-68]. In the last decade more than 70 papers have been published on the use of ECM hydrogels in almost every organ system. The mechanisms by which the ECM hydrogel modulates cell behavior are not fully understood but likely include release of bound growth factors [69], cytokines, and chemokines [70], presentation of cryptic peptides [71-74], exposure of bioactive motifs, and as recently reported, through bioactive matrix-bound nanovesicles [6].

2.3 ECM HYDROGEL FORMATION

ECM hydrogel formation is a collagen-based self-assembly process that is regulated in part by the presence of glycosaminoglycans, proteoglycans, and ECM proteins [75]. Polymerization kinetics will be influenced by the native biochemical profile of the source tissue and of the proteins that remain after decellularization and solubilization. Therefore, it is important to achieve sufficient cell removal from source tissues [76, 77] while maintaining ECM composition and ultrastructure. The choice of solubilization protocol is crucial to not adversely affect the ability to subsequently form an ECM hydrogel. Appendix A provides an overview of the many methods used to decellularize source tissues and solubilize the remaining ECM. ECM hydrogels are primarily derived from porcine tissue but some hydrogel types, e.g., adipose, tendon, umbilical cord are sourced from human tissue (Appendix A).

Formation of a hydrogel involves two key steps: 1) solubilization of the ECM material into protein monomeric components, and 2) temperature- and/or pH-controlled neutralization to

induce spontaneous reformation of the intramolecular bonds of the monomeric components into a homogeneous gel. The most prevalent method used to form an ECM hydrogel is via pepsin mediated solubilization of a comminuted (powder) form of ECM (also called “ECM digestion”). Pepsin is an enzyme derived from porcine gastric juices that has been used since 1972 to solubilize a substantial portion (up to 99%) of acid-insoluble collagen [78, 79]. Pepsin cleaves the telopeptide bonds of the collagen triple helix structure to unravel collagen fibril aggregates [80]. The ECM material is first powdered and stirred in pepsin with dilute hydrochloric acid over 48 hours, as reported by Freytes et al. and designated herein as the “Freytes method” [62]. Another method involves the use of 0.5 M acetic acid instead of 0.1 M HCl as a base medium for the pepsin enzyme (“Voytik-Harbin method”) [58]. Pepsin digestion or solubilization is complete when the liquid is homogenous with no visible particles [62]. Different digestion times will produce a different profile of cryptic molecules, some of which possess bioactive properties [73, 81], suggesting the preferred digestion period will need to be tailored for each clinical application; times of 24 – 96 hours have been reported (Appendix A). The “solubilized ECM” or “ECM digest” forms a gel when the liquid is neutralized to physiologic pH, salt concentration (“ECM pre-gel”) and temperature *in vitro* (“ECM hydrogel”) in an entropy-driven process dominated by collagen kinetics. Specifically, there is an increase in entropy when collagen monomers lose water, form aggregates, and bury surface-exposed hydrophobic residues within the fibril *in vitro,* in a self-assembly process [80, 82]. In practice, the “solubilized ECM” is neutralized to physiologic pH and salt concentration and kept at a low temperature well-below 37°C, until the application of interest is identified for temperature-controlled gelation; e.g., injected by needle or catheter to gel in situ, or placed in an incubator for 3D cell culture.

Johnson et al. investigated the effect of changing a single neutralization parameter (pH, temperature, ionic strength) from standard conditions (pH 7.4, 37°C, 1x PBS) on the material properties of an ECM hydrogel, specifically myocardial ECM hydrogel [83]. In brief, the gelation time could be modulated from ~ 20 minutes at decreased salt concentration (0.5x PBS) or to > 8

hours at increased salt concentration (1.5x PBS). Increasing the salt concentration also decreased the storage modulus by ~ 2-3 fold. Interestingly, lowering the gelation temperature below 22°C was shown to inhibit gelation unlike pure collagen hydrogels that can gel between 4-37°C. The impact of gelation parameters on material properties underscores the importance of understanding ECM hydrogel structure-function relationships.

Alternative methods for ECM digestion include an extraction process to solubilize and form an ECM hydrogel from soft tissue [84, 85]. Proteins and glycoproteins can be extracted using a homogenization process involving pestle and mortar or high speed shear mixed within a high salt buffer that physically disrupts the ECM particles and collagen fiber structure at physiologic pH [84-88]. Homogenization involves a dispase enzymatic step that cleaves fibronectin, collagen IV, and collagen I and digests the ECM, a urea extraction step which further disrupts the non-covalent bonding and increases the solubility of the ECM proteins, and centrifugation that removes any residual non-soluble ECM components. The resulting solubilized extracts form an ECM hydrogel when increasing the temperature of the extract to 37°C or by decreasing the pH with acetic acid to pH 4.0 (“Uriel method”) [84]. The Uriel method is based on the technique established to isolate commercial products Matrigel, Myogel, and Cartigel [85]. Basement membrane complexes are believed to be formed by cells secreting a certain threshold of basement proteins at 37°C or by decreasing the local pH at the cell surface to trigger laminin-111 arrangement; although the exact mechanism or combination thereof of pH and temperature gelation has yet to be determined [85].

While collagen kinetics and basement membrane assembly have been used to describe ECM hydrogel formation *in vitro*, the other components of the complex ECM unavoidably influence the hydrogel formation process. Brightman et al. showed that ECM hydrogels have distinct matrix assembly kinetics, fiber networks, and fibril morphology compared to purified collagen I hydrogels [75]. Addition of GAGs (heparin) or proteoglycans (decorin) to purified

collagen I hydrogel show that the heparin moiety causes the collagen to gel faster and form larger fibers that are less tightly packed, while addition of decorin causes the collagen to gel faster but does not affect fibril network. The results are consistent with the known role of heparin as a nucleation site for collagen fibrillogenesis and for decorin as a known regulator of fibril self-assembly [75, 80]. In addition to heparin and decorin, many other ECM proteins are known to contribute to collagen polymerization: fibronectin is known to organize collagen fibers, and minor collagens (collagen V and XI) are nucleation sites that must be present for collagen fibrillogenesis *in vivo* [89]. The Brightman et al. study [75] shows ECM glycoproteins and proteoglycans play a dynamic role in regulation of ECM hydrogel fibrillogenesis, and therefore the importance of preserving the ECM proteins in their stoichiometric ratios from the native tissues during the decellularization and solubilization steps (Appendix A).

2.4 ECM HYDROGEL CHARACTERIZATION

Source tissue type and subsequent processing steps affect the topological, biochemical, mechanical, and biological properties of an ECM hydrogel. These properties have been well characterized for SIS and UBM hydrogels, as well as many different tissue-derived hydrogels. Figure 1 provides an overview of methods that have been used for various tissue types and is a general guide to the state of the field. Figure 1 is not a comprehensive list since hydrogels made from various species, tissues, concentrations and processing methods have been classified only by the source tissue.

There are certain characteristics of ECM hydrogels that are widely conserved regardless of source tissue; however, some properties vary markedly and are influenced by many factors, including source tissue, source species, ECM concentration, ECM processing method, method of sterilization, and even natural variability among biologic samples.

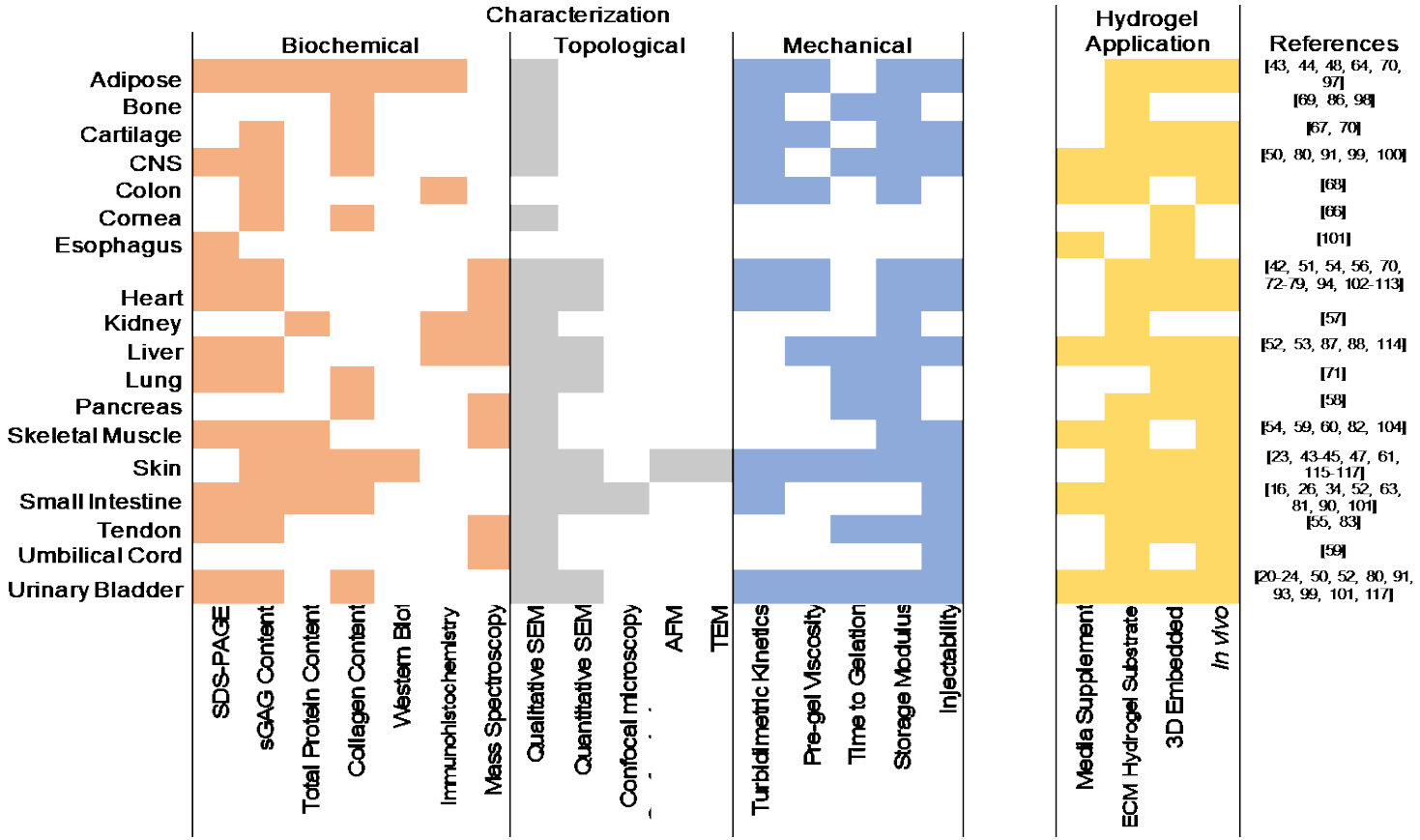

Figure 1. Overview of characterization techniques.
Overview of techniques used to characterize and to evaluate the cellular response to ECM hydrogels thus far. ECM hydrogels derived from various species, concentrations and processing methods are categorized only by source tissue.

2.4.1 Biochemical Composition

The ECM is composed of a complex mixture of both structural and functional molecules that can be largely retained following the decellularization and solubilization processes if appropriate methods are used. However, the enzymatic solubilization process undoubtedly alters the proteins within the ECM hydrogel. Pouliot et al. directly compared the protein profile of lung ECM powder and pepsin digested lung ECM pre-gel with SDS-PAGE [90]. The protein profile shows a smear of smaller proteins in the pre-gel solution, which must be due to fragmentation of larger proteins by the enzyme since there is no extraction or purification step involved in the pepsin-based solubilization process. The extent to which this protein fragmentation affects the bioactivity of ECM hydrogels is currently unknown.

Even so, the biochemical composition of the hydrogel forms of SIS [75] and UBM [62, 65] are similar to that of the intact bioscaffolds with respect to collagen and sulfated GAG (sGAG) content. Intact SIS scaffolds are composed mainly of collagen I with lesser amounts of collagens III, IV, V, and VI [59]. SIS hydrogels are known to at least contain collagens I, III, and IV and sGAGs [75]. Gel electrophoresis of UBM hydrogels shows similar bands to SIS hydrogels and both show additional bands corresponding to other ECM proteins [62]. Intact growth factors have also been confirmed in adipose [91], colon [92], liver [93], and SIS [94] ECM hydrogels, although present in reduced amounts compared to native tissue or ECM scaffolds. The impact of solubilization on cryptic peptide and matrix-bound nanovesicle content or activity has yet to be evaluated.

In spite of the similarities, the composition of the ECM is distinctive for each tissue and organ. For example, the soluble collagen content of brain ECM is significantly less than UBM and spinal cord ECM [95], but that of dermis is significantly greater than UBM [65]. Both spinal cord and dermal ECM have lower sGAG content than UBM [95]. Species-specific differences in

the composition of the same tissue type ECM, such as pericardium [96] and liver [97], have also been shown.

A commonly used technique to characterize the biochemical composition of ECM hydrogels is mass spectroscopy. Reverse phase high-performance liquid chromatography interfaced with tandem mass spectroscopy (LC-MS/MS) was used to determine the proteomic profile of pepsin-solubilized hydrogels by comparing the generated protein fragments to a protein data bank. Thus far, LC-MS/MS has been used to characterize liver [98], skeletal muscle [99], tendon [100], heart [96, 99, 101], kidney [102], pancreas [103] and umbilical cord [104] ECM hydrogels.

2.4.2 Gel Ultrastructure

The native ECM structure is comprised of a 3D network of fibers with both tightly and loosely associated proteoglycans and GAGs. Fiber diameter, pore size, and fiber orientation can all influence cell behavior [85]. During the decellularization and solubilization processes, the collagen fiber structure is disrupted, resulting in loss of the native fiber network. The collagen monomers self-assemble into a fibrillar network which does not exist in the pre-gel solution [105]. Scanning electron microscopy (SEM) is the most common method of visualizing the topology of hydrogels, but transmission electron microscopy (TEM) [85], atomic force microscopy (AFM) [106], and confocal microscopy [75] have also been used. SEM images of fully-formed ECM hydrogels generally show a loosely organized nanofibrous scaffold with interconnecting pores [62]. The nano-scale topography provides a high surface area to volume ratio that allows increased area for integrin binding, and is small enough to be sensed and manipulated by infiltrating cells [83, 101]. An algorithm has been developed to perform automated and high-throughput analysis of SEM images with quantification of fiber diameter, pore size, and fiber alignment of hydrogels [65, 97, 107]. UBM hydrogels show an average fiber

diameter of 74 nm [65]. Various source tissue ECMs showing an average fiber diameter of approximately 100 nm have been reported (e.g. cardiac [83], SIS [94], adipose [108]).

As stated earlier, ECM hydrogels share many common features, but the tissue of origin, processing methods, and protein concentration of the hydrogel all influence the structure of these materials. For example, pore size and fiber diameter are independent of concentration in UBM [65] and liver ECM gels [97], but vary with ECM concentration in dermal ECM gels [65]. UBM hydrogels also show randomly organized fibers, whereas more aligned fiber architecture has been observed in SIS hydrogels [94]. Qualitative analysis of SEM images show easily recognizable differences in structure depending upon the gelation mechanism (temperature- vs. pH-induced) used to create dermal hydrogels [85]. Variation in structure with species source has also been reported for liver hydrogels derived from human, rat, dog and pig [97].

Some structural characteristics of the native ECM are retained in ECM hydrogels. For example the pore size, fiber diameter and primarily flocculent fiber structure of dermal ECM hydrogels are comparable to the native basement membrane [85]. Additionally, periodic striations characteristic of the D-band morphology of native collagen can be seen in fiber networks of liver [98] and tendon [100] hydrogels.

2.4.3 Viscoelastic Properties

Low viscosity of the pre-gel solution and application-appropriate gelation kinetics are important criteria for minimally invasive delivery. Stated differently, sufficient time is required for delivery of the pre-gel to selected anatomic sites before gelation is complete. Substrate stiffness is also known to direct stem cell differentiation and function in *in vitro* culture and also influences the remodeling outcome *in vivo* [109]. Therefore, use of an ECM hydrogel intended to define the microenvironment for stem cell delivery or recruitment can be dependent upon pre-determined hydrogel properties. Furthermore, all three of these properties (i.e. pre-gel viscosity, gelation

kinetics and gel stiffness) can affect whether the injected gel is retained within the defect site or instead diffuses into the surrounding host tissue [63, 64]. Turbidimetric gelation kinetics and rheology are the primary methods used to assess the viscoelastic properties of ECM hydrogels. Other methods, such as indentation [110] and compression [87, 105, 111] testing, AFM [106], and macroscopic rigidity [62, 65, 112] have been explored but will not be further reviewed herein.

The turbidimetric gelation kinetics of UBM show a sigmoidal shape similar to that of purified collagen I gels [62]. Sigmoidal gelation behavior is also observed with bone [113], cartilage [111] and spinal cord ECM [95] hydrogels, whereas brain ECM hydrogels [95] show exponential behavior. The lag phase (t_{lag}) and the time to reach half of the final turbidity ($t_{1/2}$) is greater in UBM than collagen I gels, ostensibly due to the presence of GAGs and other molecules that may modulate self-assembly [62]. The t_{lag} and $t_{1/2}$ vary with gelation mechanism [84, 85] and concentration [65, 112] in some cases, and are concentration-independent in others [111].

Rheology is typically utilized to determine the storage modulus, or stiffness, of the hydrogel following gelation, but can also provide the pre-gel viscosity and time to gelation. ECM pre-gel solutions show low viscosity that increases with protein concentration of the pre-gel [62, 64, 112]. Shear thinning behavior is also a common feature of ECM hydrogels, characterized by a decrease in the steady shear viscosity of the pre-gel with increasing shear rate [114]. This characteristic may be desirable for ECM pre-gels intended for delivery through a catheter or syringe.

Upon increasing the temperature from storage of the pre-gel at 4°C to 37°C, gelation of the ECM pre-gel is initiated and the resulting change in properties can be measured. The rate of gelation is greater with increasing concentration in UBM [65], bone [113], liver [98] and dermal [65] ECM hydrogels. The gelation time determined by rheology is also shorter than that determined by turbidimetric methods [62]. The final storage modulus is related to the stiffness,

and solid-like behavior of the gel is confirmed when the storage modulus is greater than the loss modulus by approximately one order of magnitude, and the storage modulus is largely independent of frequency [62]. An increase in storage modulus occurs with increasing protein concentration for multiple source tissues including UBM [62, 64, 65], lung [90], heart [83], bone [113], colon [112], and liver [98]. Frequency sweep analysis after gelation shows very little frequency dependence of the storage modulus, indicative of a stable and uniform gel [64, 65, 98].

A substantial strain-dependence is observed in some ECM hydrogels, with an increase in modulus occurring with increased strain [90, 113] and an irreversible change in modulus above 5% [90]. The storage modulus of hydrogels has been determined for gels formed directly on the rheometer, and for gels pre-formed in an incubator as long as 24 hours prior to rheological testing. The influence of strain and gelation method on observed modulus has yet to be studied, but the large variations could be partially due to different testing methods used by each group [90]. Table 2 shows the concentration, testing parameters, and final storage modulus of porcine-derived ECM hydrogels. The pre-gel steady shear viscosity and time to gelation as determined by rheology are included where available. The dependence of storage modulus on source tissue, concentration, testing parameters and natural variability between samples is evident. The storage modulus of the ECM hydrogel is frequently lower than the respective tissue from which the hydrogel is derived. The hydrogel should be thought of, at least in part, as an inductive template to recruit cells that will secrete *de novo* ECM comprising the stiffness of the new tissue. Though ECM hydrogels derived only from porcine tissues are included in this table, species-dependence of viscoelastic properties has also been noted [97].

Table 2. Viscoelastic properties of ECM hydrogels.
Italicized values were estimated from representative images. Steady shear viscosities refer to the pre-gel solution. “Pre-formed” indicates that gelation was induced prior to rheologic testing. * indicates time to 50% gelation. “NR” indicates “not recorded.”

Tissue	**Conc. (mg/ml)**	**Protocol (strain, frequency)**	**G’ (Pa)**	**Steady Shear Viscosity (Pa*s)**	**Gelation time (min)**	**Ref**
Cartilage	30	2%, 1rad/s	*4000*	*3*		[114]
Brain	4	5%, 1rad/s	20.3		34.8	[95]
	6	5%, 1rad/s	49.9		2.4	[95]
	8	5%, 1rad/s	61.8		8.3	[95]
Colon	4	0.5%, 1rad/s	*9*	*0.75*		[112]
	8	0.5%, 1rad/s	*50*	*1.7*		[112]
Heart	6	2.5%, 0.4rad/s	11.3	**Pre-formed**		[115]
		2.5%, 1rad/s	6.5	**Pre-formed**		[116]
		NR, 1rad/s,	5.28	**Pre-formed**		[83]
		NR, 6.28rad/s	6.08	**Pre-formed**		[101]
	8	2.5%, 0.5rad/s	5.3	**Pre-formed**		[117]
		NR, 1rad/s,	9.52	**Pre-formed**		[83]
	30	2%, 1 rad/s	*800*	*33*		[114]
Liver	8	0.5%, 1rad/s	*630*	*4.25*	*8.5*	[97]
Lung	4	0.5%, 6.28rad/s	15.3			[90]
	6	0.5%, 6.28rad/s	32.0			[90]
	8	0.5%, 6.28rad/s	59.0			[90]
Pancreas	16.7	2.5%, 1rad/s	*190*		*4.5*	[103]
Skeletal Muscle	6	NR, 1rad/s	6.5	**Pre-formed**		[118]
Skin	4	0.5%, 1rad/s	*110*	*2*		[65]
	6	0.5%, 1rad/s	*200*	*2*		[65]
	8	0.5%, 1rad/s	466	*7*		[65]
Spinal cord	4	5%, 1rad/s	138		11.7	[95]
	6	5%, 1rad/s	235		7	[95]
	8	0.5%, 1rad/s	757		28.9	[95]

Table 2 (continued)

Tissue	Conc. (mg/ml)	Protocol (strain, frequency)	G' (Pa)	Steady Shear Viscosity (Pa*s)	Gelation time (min)	Ref
Urinary Bladder	3	5%, 1rad/s	*6*		*10*	[62]
	4	0.5%, 1rad/s	*110*	*0.06*		[65]
			76.6	0.084	3.2*	[64]
		5%, 1rad/s	11.4		52.5	[95]
	6	0.5%, 1rad/s	*40*	*0.9*		[65]
		5%, 1rad/s	*26*		*10*	[62]
			72.8		8.47	[95]
	8	0.5%, 1rad/s	182	*0.9*		[65]
			460	0.443	3.0*	[64]
		5%, 1rad/s	143		19.8	[95]

Another important ECM hydrogel design criterion is injectability. While injectability may be related to the viscoelastic properties (ECM pre-gel viscosity and gelation time), injectability has been independently confirmed *in vitro* and/or *in vivo* for heart [96, 101, 115-117, 119-123], spinal cord [124], small intestine [68, 92], umbilical cord [104], skeletal muscle [104, 105, 118], tendon [100, 125], dermal [65], lung [90], liver [98], cartilage [111], urinary bladder [63, 64, 66, 124] and adipose [91, 108] ECM hydrogels with reported 18-27 gauge syringes or catheters. For example, porcine myocardial gel (6 mg/mL) was confirmed to be injectable through a 27 gauge catheter [119], and then confirmed to be injectable via NOGA guided MyoSTAR catheter (27 gauge), which is the current gold standard delivery device used in cellular cardiomyoplasty procedures [119]. The material remained injectable for 1 hour at room temperature during injection, a clear advantage compared to other natural materials such as collagen and fibrin that gel too quickly and cannot be delivered by catheter [119].

2.5 CELLULAR RESPONSE TO ECM HYDROGELS

The ECM represents, in large part, the microenvironmental niche of every cell. The mechanism by which the native ECM influences cell behavior likely includes the physical and mechanical properties of the ECM, embedded cytokines and chemokines, cryptic peptides formed during ECM remodeling, and matrix-bound nanovesicle mediated events, among others. The signaling mechanisms that are preserved during production of an ECM hydrogel from a source tissue are only partially understood and will obviously influence cell viability, proliferation, migration, morphology, differentiation and phenotype. Established methods to evaluate the cellular response to ECM hydrogels both *in vitro* and *in vivo* are summarized in
Figure 2.

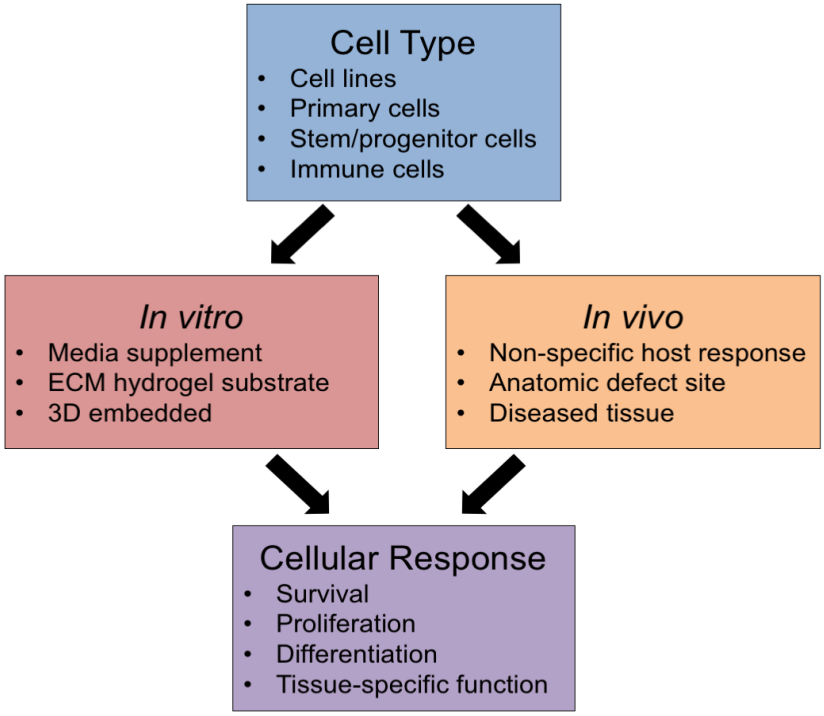

Figure 2. Approaches to interrogate cellular responses to ECM hydrogels.
General approaches to assess cellular response to ECM hydrogels. The response of various cell types *in vitro* or *in vivo* can be evaluated.

The viability of cells cultured on the surface of ECM hydrogels *in vitro* has been consistently shown for cell lines [65, 95, 104, 105, 111, 112, 118], primary cells [98, 104, 110, 112, 118, 119, 126], and stem cells [85, 90, 91, 114, 124, 127]. In addition, the innate bioactivity of soluble factors within the ECM has been demonstrated using *in vitro* culture with media supplemented with solubilized ECM to remove the influence of hydrogel structure on the function of cells.

Wolf et al. studied the response of 3T3 fibroblasts and C2C12 myoblast cells to UBM and dermal ECM hydrogels by three different methods: cells seeded on the surface of pre-formed gels (ECM hydrogel substrate), cells embedded within gels (3D embedded), and gel

placement in an anatomic defect site *in vivo* [65]. Almost 100% viability of 3T3 fibroblasts and C2C12 myoblasts was observed after 7 days of culture for all configurations investigated *in vitro*. C2C12 myoblast cells seeded on the surface of the dermal ECM hydrogels fused into large diameter, multinucleated myotubes with radial alignment, whereas cells cultured on the surface or embedded within UBM and embedded within dermal ECM formed smaller elongated cell structures. Implantation of the hydrogels within a rodent partial thickness abdominal wall defect produced a significantly greater area of *de novo* muscle formation when the defects were treated with UBM hydrogel compared to unrepaired defects. This result likely represents the combination of microstructure, mechanical properties, and bioactivity. The collagen fiber ultrastructure and low storage modulus of UBM hydrogels allows for cell infiltration and fibroblast mediated contraction of the gel, two important aspects of wound healing [65].

2.5.1 Comparison to Collagen and/or Matrigel

Cell behavior in response to ECM hydrogels has consistently been shown to be comparable to Matrigel and/or collagen substrate for liver [128, 129], skeletal muscle [99], heart [99] and fat [84-86, 88, 108] applications. Uriel et al. [84] showed that primary rat pre-adipocytes cultured on the surface of adipose ECM hydrogels (1 mg/mL) formed colonies that were significantly larger compared to Matrigel (1 mg/mL) indicative of enhanced pre-adipocyte expansion and differentiation into fat after 7 days. Furthermore, the adipose ECM hydrogels (1 mg/mL) that were formed by reducing pH to 4.0 showed significantly greater adipose area compared to Matrigel (1 mg/mL) at 1, 3, and 6 weeks *in vivo* in an epigastric pedicle model.

2.6 IN VIVO APPLICATIONS OF ECM HYDROGELS

Structure-function relationships of ECM hydrogels can provide a basis for predicting the appropriate hydrogel formulation for given applications. Although *in vitro* structure-function relationships are important to understand, their relationship to *in vivo* applications are largely unknown. There have been limited experiments with ECM hydrogels in two anatomic locations: the heart and the brain.

2.6.1 Heart

Cardiac-derived gels are being investigated for cardiac reconstruction following ischemic injury [83, 96, 99, 101, 116, 119-121, 123]. Heterologous ECM hydrogels have been evaluated in the heart but formed cartilaginous tissue suggesting that tissue-specific cues may be necessary for appropriate cardiac tissue remodeling [119]. The Christman laboratory has investigated different cardiac tissue types for cardiac application including 1) the effect of species (porcine versus human) [101], and 2) the effect of pericardium versus myocardium [96].

Both porcine and human source tissue has been evaluated for clinical translation. Harvested porcine cardiac tissue is more homogeneous for variables such as diet, age, and strain unlike human cadaveric donor heart tissue which involves a range of ages, disease states, and co-morbidities [101, 120]. A human ECM source tissue has been cited as mitigating the risk for xenogeneic disease transfer [101], although there has not been a reported case of zoonotic disease in the millions of patients that have received porcine ECM scaffolds or porcine tissue (e.g., porcine heart valves) to date [130]. Both porcine and human myocardial ECM formed similar hydrogel ultrastructure *in vivo* after injection into the rat left ventricular myocardium [101]. However, perhaps most importantly, over half of the human myocardial pre-gel solutions did not form gels even allowing for the same DNA and lipid content. The

differences may be attributed to the requirement for a “more harsh” decellularization protocol (e.g., longer SDS incubation, lipid/DNA removal steps) required as a result of the increased ECM crosslinking and adipose tissue of the human tissue (donor age of human tissue ranged from 41-69 years). Johnson et al. eventually recommended porcine myocardial ECM hydrogel as the preferred source for clinical translation over human myocardial ECM hydrogel because of the increased tissue availability, relatively more gentle decellularization protocol, and more reliable gelation [101]. Human tissue was recommended as a useful model system for *in vitro* study of the role of human ECM in cardiac disease.

Two different tissue types within the heart were evaluated for myocardial repair. The pericardium is the fibrous sac surrounding the heart primarily composed of compact collagen and elastin fibers. While not tissue specific, the pericardium was explored as a potentially autologous therapy because the pericardium can be resected from the heart without adverse effect on heart function and is currently FDA approved for structural reinforcement in other body applications. The pericardial ECM hydrogel (6.6 mg/mL) and myocardial ECM hydrogel (6 mg/mL) were evaluated in the non-diseased, orthotopic location, and injected into the rat LV wall in separate studies. Both pericardial ECM and myocardial ECM hydrogels supported vascular cell infiltration (endothelial cells, smooth muscle cells) and almost identical arteriole formation within 2 weeks (51 +/- 42 vessels/mm^2, 52+/- 20 arterioles/mm^2 respectively) [96, 119]. In conclusion, it was suggested that pericardial ECM may be a candidate for same-patient ECM sourcing [96, 120], but myocardial ECM hydrogel was preferred for pre-clinical studies in the rat and pig [121, 122].

Porcine myocardial ECM hydrogel has been evaluated in both small and large animal models of myocardial infarction (MI). The *in vivo* pathogenic microenvironment poses unique challenges such as the sustained release of pro-inflammatory cytokines thought to promote cell apoptosis or necrosis, matrix metalloproteinase (MMP) production that degrades the matrix, and an ischemic/hypoxic microenvironment. Myocardial ECM preserved cardiac function in a rat

model of MI while the saline treated rats worsened 4 weeks after injection compared to baseline 1 week prior to injection. Specifically, myocardial ECM showed an increased ejection fraction (EF) and a relatively decreased percent change in end-systolic volume (ESV) and end-diastolic volume (EDV) compared to saline treated control; however, none of the three markers were significantly different compared to controls [122]. In an established large animal model, the myocardial ECM was delivered by the clinical standard transendocardial catheter two weeks after MI. After three months, myocardial ECM treated groups showed significant improvement in three measures of cardiac function: 1) echocardiography, 2) global wall motion index scoring, and 3) electromechanical NOGA mapping [121]. Corroborating the functional improvement, myocardial ECM treated animals promoted healthy muscle and blood vessel formation in infarcted areas: a distinct band of muscle that stained positive for troponin T below the endocardium was present in the myocardial ECM treated groups, and the muscle was significantly larger than control muscle. The myocardial ECM treated group showed significantly reduced fibrosis and neovascularization foci below the endocardium compared to controls.

Recently, Wassenaar et al. investigated the molecular mechanisms underlying the ability of myocardial ECM to mitigate negative LV remodeling using whole transcriptome analysis in the rat model of MI [123]. This was the first study to determine global gene expression changes with ECM hydrogel treatment. The myocardial ECM compared to saline control after 1 week of treatment showed several significantly altered pathways at the tissue level including: altered inflammatory response; decreased cardiomyocyte apoptosis, altered myocardial metabolism, enhanced blood vessel development, increased cardiac transcription factor expression, and increased progenitor cell recruitment. Angiogenesis is one of the processes modulated by ECM hydrogel treatment and a critically important process relevant to other *in vivo* applications. Wassenaar et al. speculate the ECM hydrogel may directly recruit endothelial progenitor cells through pro-angiogenic growth factors or matricryptic peptides, provide a scaffold for blood vessel formation, or modulate the recruited macrophages' secretory profile [123].

2.6.2 Brain

While the use of homologous ECM has been investigated for cardiac applications, the use of heterologous ECM, specifically UBM hydrogel, has been evaluated in brain applications to treat traumatic brain injury (TBI) [66] and stroke [63, 64].

In a rat model of TBI [66], UBM hydrogel (5 mg/mL) was delivered one day after controlled cortical impact injury. UBM mitigated adverse tissue damage with decreased lesion volume, decreased white matter injury, and increased vestibulomotor function at 21 days. However, no cognitive improvement was shown by the Morris water maze task tests. While the UBM hydrogel showed functional improvement in tissue repair, it has yet to demonstrate its utility in the “holy grail” of cognitive improvement. It was suggested the brain may be a type of clinical application which requires the addition of neural stem cells to the ECM hydrogel, or other tailoring of ECM hydrogel properties.

ECM concentration-specific properties of UBM hydrogels were also used to selectively affect the material retention [64] and the immune cell infiltrate [63] in a small animal model of chronic stroke. Specifically, UBM hydrogel (1-8 mg/mL) was delivered 14 days after middle cerebral artery occlusion in the rat. UBM hydrogels < 3 mg/mL did not form a gel within the stroke lesion and instead diffused into the surrounding brain tissue as early as 24 hours, the earliest time point investigated [64]. In a follow-up study, it was shown that with the use of UBM hydrogels < 3 mg/mL, the cells did not have a medium through which to infiltrate the lesion and instead accumulated around the lesion site [63]. UBM hydrogels > 3 mg/mL formed a hydrogel within the stroke cavity that interfaced with the adjacent tissue [63, 64]. Because a distinct host/tissue interface was formed, > 3 mg/mL treatment also showed extensive cell infiltration 1 day after delivery [63]. Macrophages and microglia were accompanied by neural progenitor cells, endothelial cells, oligodendrocytes, and astrocytes. An understanding of the cell infiltrate based upon the viscoelastic properties of the hydrogel in the brain is crucial since these cells

will ultimately remodel the ECM and replace it with *de novo* matrix. While this application would suggest that the > 3 mg/mL UBM hydrogels would be preferred, other tissue applications may show improved outcomes if ECM signaling molecules would be released and permeate the surrounding tissue.

For ECM hydrogels > 3 mg/mL that may be retained within the lesion and allow for immune cell infiltration, there are several concentration-dependent properties that may be important in the context of clinical delivery [64]. Four and 8 mg/mL UBM hydrogels were tested *in vitro* as candidates for brain repair after stroke injury. Both 4 and 8 mg/mL hydrogels showed ideal properties of an injectable therapy: viscosities ranging from that of water to honey (0.084 Pa*s and 0.443 Pa*s respectively), stably formed gels (G' > G'' by ~ 10 fold), and 50% gelation times (~3 min) considered to be a reasonable time frame in the operating room. The storage moduli or "stiffness" differed more dramatically for the 4 and 8 mg/mL hydrogel, at 76 and 460 Pa respectively. Brain tissue storage moduli has been reported between 200-500 Pa as a target moduli range [64], however it is important to state again the recruited cells will ultimately remodel the matrix.

2.6.3 Safety

The *in vivo* safety of an ECM hydrogel for any clinical application is obviously an important consideration. ECM hydrogels were considered safe in the aforementioned heart and brain *in vivo* applications. The ECM treated MI induced pigs did not show arrhythmias, thromboembolism or ischemia 3 months after myocardial ECM injection [121]. Hemocompatibility was further corroborated *in vitro* when the myocardial ECM gels were tested at a physiologically relevant concentration and shown not to accelerate coagulation.

Zhang et al. also showed that the UBM hydrogel (5 mg/mL) did not have a deleterious effect when injected into the normal brain [66]. There was no reactive astrocytosis (GFAP+),

and no neuronal degeneration at 1, 3, and 7 days after UBM hydrogel injection. Microglial activation and degenerate neurons were shown at 1 and 3 days along the needle track and injection site, but was no different than PBS control; and was resolved by 21 days.

The potential unintended presence of ECM hydrogels in peripheral organs was evaluated in the studies of myocardial injection, and would be a safety concern relevant to all ECM hydrogel applications. Myocardial ECM hydrogels were not found at 2 hours in the pig lung, liver, spleen, kidney and brain [122], nor at 3 months [121]. Each clinical application of ECM hydrogels would likely have a distinctive profile of safety measures.

2.6.4 *In vivo* Host Response

The clinical applications of ECM involving the heart and brain did not elicit an adverse immune response. In general, ECM hydrogels have been well-tolerated in a wide variety of *in vivo* applications. No adverse immune response was shown after ECM hydrogels were injected in the heart [96, 101, 115, 116, 119-123], fat [84, 86, 88, 91, 108], liver [98], brain [63, 64, 66] skeletal muscle [65, 104, 105, 118], tendon [68, 100, 125], spinal cord [124], lung [90], cartilage [111], or colon [92, 112], and these studies included both homologous and heterologous ECM hydrogels. The findings *in vivo* are consistent with *in vitro* studies that have shown the pepsin-digested ECM (“pre-gel”) promotes a regulatory (“M2-like”) macrophage activation state, which is associated with a constructive remodeling response *in vivo* [112, 131, 132]. For example, macrophages activated toward an M2-like phenotype with solubilized ECM promoted downstream effects such as stimulating the migration and myogenesis of skeletal muscle progenitor cells [131]. In SIS hydrogel treatment of ulcerative colitis *in vivo,* the ECM modulated the macrophage response towards a predominately regulatory state by decreasing the number of pro-inflammatory (“M1-like”) activated macrophages, as opposed to increasing the number of

M2-like macrophages [112]. This effect of altering the innate immune response by shifting the M2:M1 ratio is observed in the host response to solid ECM scaffolds as well [131].

2.6.5 Summary of *In vivo* Applications

Heart and brain were selected as two organ systems with a need for a minimally invasive, injectable therapy. The heart showed safety and efficacy of myocardial ECM hydrogel in small and large animal model of disease up to 3 months, and is currently being evaluated in a Phase I clinical trial (ClinicalTrial.gov Identifier: NCT02305602) [133]. The brain case study showed the importance of investigating multiple ECM concentrations to determine preferred characteristics of an injectable therapy for central nervous system (CNS) applications, including delivery, facilitation of the immune cell infiltrate, and mitigation of the default response to injury. Future work in the brain will likely identify the balance of factors required for cognitive improvement. Overall, each new therapeutic application will need a thorough understanding of the ECM hydrogel structure-function relationships for successful clinical translation. Relevant references to other organ *in vivo* applications can be found in **Error! Reference source not found.**.

2.7 FUTURE PERSPECTIVES

With more than 70 papers published in the last decade, it is evident that the therapeutic potential of ECM hydrogels is recognized. Characterization of hydrogel structure and function *in vitro* have provided a basis for selection of appropriate source tissue and hydrogel formulation in selected body systems. However, the relationship between *in vitro* structure-function and *in vivo* application is still largely unknown for most other clinical applications.

The mechanisms by which ECM hydrogels mediate cell behavior are not fully understood. Several hypotheses have been suggested including the possibility that the architecture of the gelled hydrogel comprises a pore size and fiber diameter suitable for endogenous cell infiltration [134]. Additionally, the bioinductive hydrogel provides tissue-specific cues, likely through the release of bound growth factors [69], or the creation of cryptic peptides or the exposure of bioactive motifs [71-74]. The recent report of bioactive matrix-bound nanovesicles within biologic scaffolds [6] provides a new possibility for study to determine the mechanisms contributing to the constructive tissue remodeling facilitated by ECM hydrogels.

The use of ECM hydrogels as a delivery vehicle is an obvious area for future study. Although a standalone ECM biomaterial therapy offers practical advantages by way of reduced regulatory concerns, ease of manufacturing and route to market, combinations of ECM hydrogels with growth factors and/or cells may provide significant mutual enhancement. Recent studies have shown that sulfated GAGs within ECM hydrogels bind to growth factors with prolonged release of basic fibroblast growth factor and heparin-binding growth factor that enhances therapeutic effects [116, 135]. ECM hydrogels have also been used as a delivery system for growth factor containing microparticles to enhance skeletal tissue repair within an *ex vivo* chick femur defect model [136]. Cell therapy for neurological conditions may require integration with an appropriate biomaterial to support cells during transplantation and provide a structural support system post implantation. Recent investigations of ECM hydrogels for CNS applications have included the assessment of different source tissues to direct cell differentiation [137] and the transplantation of human neural stem cells embedded within ECM hydrogels to support the creation of *de novo* tissue [67]. Stem cells and primary cells have also been embedded within lung [90], liver [98], spinal cord [124], and adipose [91] ECM hydrogels to improve the tissue remodeling outcome.

In conclusion, the use of ECM hydrogels for a variety of clinical applications is in its infancy, but has shown promise. The combination of *in vitro* and *in vivo* studies designed to understand mechanical and material properties, the effects of processing methods upon hydrogel performance, the mechanisms by which such hydrogels influence cell behavior and tissue remodeling, and the safety of ECM hydrogels should advance their clinical utility.

2.8 ACKNOWLEDGMENTS

LTS was supported by the National Institute of Biomedical Imaging and Bioengineering of the National Institutes of Health (2T32 EB001026-11). LJW was funded by a Marie Curie International Outgoing Fellowship under REA grant agreement no. 624841.

3.0 OBJECTIVES

Esophageal adenocarcinoma (EAC) is a cancer that progresses in response to microenvironmental-induced injury (e.g., gastric reflux) and the pathogenesis (gastroesophageal reflux disease-metaplastic Barrett's-neoplastic EAC) is relatively well understood; however, changes to the esophageal extracellular matrix (ECM) during EAC progression are not fully known. Neoplastic ECM directs abnormal cell phenotype in other cancer types (e.g., breast, brain), and ECM from normal tissue can dramatically revert abnormal cell phenotype toward a more polarized, normal phenotype by restoring dysregulated ECM-cancer cell signaling. The esophageal epithelial cells are the candidate cells transformed during metaplastic and neoplastic progression. Macrophages are plastic cells that are recruited to the site of inflammatory injury and cancer, and their phenotype influences downstream tissue remodeling.

The objectives of the present dissertation were to characterize non-malignant, metaplastic and neoplastic ECM biochemical signals (ECM protein signature, matrix-bound nanovesicle miRNA) and to investigate the effect of solubilized ECM from these 3 disease states upon macrophage phenotype and esophageal epithelial cell behavior. Non-malignant, solubilized esophageal ECM ("ECM hydrogel") was then evaluated as a therapy to mitigate or revert metaplastic and neoplastic disease by providing non-malignant biochemical signals to epithelial cells. The ECM hydrogel modulated neoplastic epithelial cell function, signaling pathways, and differentiation status *in vitro* and *in vivo*; and downregulated the pro-inflammatory infiltrate *in vivo*. The present dissertation also determined practical aspects of clinical therapy i.e., the tissue source, ECM concentration for the preferred characteristics of the hydrogel

therapy for oral/endoscopic delivery, and identified an alternative method to treat patients at the time of mucosal resection by injecting the eECM hydrogel into the submucosa. The long-term goal of the present dissertation is to provide a molecular basis for the use of a non-malignant ECM hydrogel from decellularized tissues for the treatment of metaplastic and neoplastic diseases for which there are currently no satisfactory cures.

4.0 CENTRAL HYPOTHESIS AND SPECIFIC AIMS

Extracellular matrix (ECM) isolated from non-malignant, metaplastic, and neoplastic esophageal tissue will have distinct effects upon macrophage activation and epithelial cell phenotype. Delivering non-malignant ECM hydrogel to the diseased esophagus will halt or revert disease progression *in vivo* via macrophage-mediated effects and restore dysregulated matrix-cell signaling.

Specific Aim 1: To determine the effect of non-malignant, metaplastic, and neoplastic ECM upon macrophage activation *in vitro*.

Subaim 1.1. To characterize the ultrastructure and biochemical composition (i.e., protein profile and matrix-bound nanovesicle miRNA cargo) of non-malignant, metaplastic, and neoplastic ECM.

Corollary Hypothesis: Metaplastic ECM will activate macrophages toward an "M1-like" state and neoplastic ECM will activate macrophages toward an "M2-like" state compared to non-malignant ECM. Metaplastic and neoplastic ECM will have a distinctive protein profile and matrix-bound nanovesicle miRNA profile compared to non-malignant ECM, with functionality related to inflammatory response and tumorigenic processes.

Corollary Rationale: Macrophages are plastic, innate immune cells recruited to the site of inflammation and injury and likely play an important role in the chronic inflammatory-driven pathogenesis of EAC [1]. Macrophages are activated along a spectrum from pro-inflammatory ("M1-like") to immunomodulatory ("M2-like") in response to microenvironmental signals [7].

Metaplastic Barrett's esophagus represents a chronic inflammatory ("M1") microenvironment, while the neoplastic esophagus has been associated with a tumor associated macrophage (TAM) phenotype and an M2-like microenvironment [9]. However, the isolated effect of non-malignant, metaplastic, and neoplastic ECM upon macrophage activation has not been characterized in vitro.

Furthermore, despite the pathogenesis of esophageal adenocarcinoma (EAC) being relatively well established; changes to the ECM during EAC progression are not as well characterized. Matrix-bound nanovesicles (MBV) are a recently described, bioactive component of the matrix, and shown to recapitulate some of the biologic effects of the parent ECM [6], including modulation of macrophage phenotype [138]. Identification of dysregulated ECM protein expression and MBV miRNA expression in neoplastic esophageal tissues, and the role of such molecules in macrophage activation, may suggest novel therapeutic targets for EAC patients.

Specific Aim 2: To determine the effect of non-malignant ECM hydrogel from two distinct tissue sources upon normal, metaplastic, and neoplastic esophageal cell phenotype and neoplastic signaling pathways *in vitro*.

Subaim 2.1: To determine the cell surface receptors activated in neoplastic cells compared to non-malignant cells by the non-malignant ECM hydrogel.

Corollary Hypothesis: Heterologous urinary bladder matrix (UBM) and homologous esophageal mucosa ECM (eECM) molecules would have the potential to normalize neoplastic cell behavior and cancer signaling pathways, while having a minimal effect upon non-malignant cell phenotype. The homologous eECM would provide a more pronounced downregulation of neoplastic cell behavior compared to heterologous UBM.

Corollary Rationale: Heterologous ECM, including UBM, has been used to treat 14 EAC patients after mucosal resection, with positive, constructive tissue remodeling; preservation of

esophageal function; and perhaps most importantly, without recurrence of cancer. Non-malignant, heterologous ECM has been shown to downregulate pancreatic, sinonasal, bladder, melanoma, and esophageal cancer; but the mechanisms involved have not been fully determined. Homologous eECM is a more recently described biomaterial, and was shown to increase esophageal stem cell migration and organoid formation *in vitro* compared to heterologous ECM sources. UBM and eECM will be evaluated to identify a preferred source for an esophageal therapy.

Specific Aim 3: To determine the effect of non-malignant ECM hydrogel upon macrophage activation and epithelial cell phenotype in a canine model of Barrett's esophagus and rat model of esophageal adenocarcinoma *in vivo*.

Subaim 3.1. To tailor the material properties of a non-malignant ECM hydrogel for oral delivery to the esophagus.

Subaim 3.2. To investigate the use of non-malignant ECM hydrogel to mechanically elevate mucosal tissue for resection and to prevent stricture.

Corollary Hypothesis: A preferred hydrogel formulation can be selected that is mucoadhesive and has viscoelastic properties compatible for oral and/or endoscopic delivery to the esophagus, by testing two variables: ECM concentration and tissue source. Non-malignant ECM hydrogel will mitigate or revert metaplastic Barrett's esophagus and high grade dysplasia in two animal models compared to control.

Corollary Rationale: An ideal therapy to the esophagus would be 1) non-invasive, 2) halt or revert neoplastic esophageal cell phenotype, 3) promote re-epithelialization, and 4) mitigate stricture. ECM bioscaffolds have been shown to prevent the recurrence of esophageal cancer in 14 human patients [30], and prevent stricture/promote re-epithelialization in a canine model of esophageal repair [27, 29]. The present study will answer the question whether or not the ECM hydrogel can provide the same properties as the ECM bioscaffold. ECM concentration and

tissue source are two important variables used to tailor ECM hydrogel material properties for specific applications [139]. Finally, ECM hydrogel has successfully halted acute ulcerative colitis in a rat model, with concomitant downregulation of pro-inflammatory TNF+ macrophages [140]. These results suggest that similar mechanisms may occur in Barrett's esophagus and high grade dysplasia animal models to provide a prolonged therapeutic response.

5.0 THE EFFECT OF NORMAL, METAPLASTIC, AND NEOPLASTIC ESOPHAGEAL EXTRACELLULAR MATRIX UPON MACROPHAGE ACTIVATION[2]

5.1 HYPOTHESIS

ECM isolated from non-malignant, metaplastic, and neoplastic esophageal tissue will have distinctive biochemical profiles and activate macrophages toward distinct pro-inflammatory and anti-inflammatory activation states. Specifically, it is hypothesized that metaplastic ECM will activate macrophages toward a chronic inflammatory, “M1-like” state and neoplastic ECM will activate macrophages toward an immunomodulatory, “M2-like” state compared to normal esophageal ECM. Neoplastic ECM will modulate the macrophage secretome to increase esophageal epithelial cell migration, or stated differently, influence the behavior of a non-malignant cell to behave like a neoplastic cell. The interplay between non-malignant, metaplastic, and neoplastic ECM and macrophage activation state can inform treatment strategies for esophageal cancer patients treated with non-malignant ECM.

---

[2] This chapter was adapted from the following manuscript in preparation:

L.T. Saldin, M. Klimak, R. Hill, M.C. Cramer, L. Huleihel, M. Quidgley-Martin, D. Cardenas, T.J. Keane, R. Londono, G. Hussey, L. Kelly, J.E. Kosovec, E. Lloyd, A.N. Omstead, L.Zhang, A. Nieponice, B.A. Jobe, K. Hansen, A. Zaidi, S.F. Badylak. The effect of normal, metaplastic, and neoplastic esophageal extracellular matrix upon macrophage activation*. In preparation*.

5.2 ABSTRACT

Macrophages are extremely plastic cells that change their activation state in response to inflammation, tumorigenesis and tissue remodeling to promote or reject tumors. Macrophages have been characterized in response to non-malignant extracellular matrix (ECM), but their response to diseased ECM is not fully understood. Esophageal adenocarcinoma (EAC) is a chronic inflammatory driven cancer; thus this disease provides the opportunity to investigate the effects of normal, metaplastic, and neoplastic ECM harvested from decellularized tissues on macrophage phenotype. The present study shows that metaplastic and neoplastic esophageal ECM increased TNFα by gene expression, secreted proteins, and immunolabeling. The effect of metaplastic and neoplastic ECM upon macrophage secreted products increased the migration of normal esophageal epithelial cells, acquiring similar behavior of a tumor cell. Metaplastic ECM showed similar but less pronounced effects than neoplastic ECM suggesting the neoplastic signals can start at the pre-cancerous state. ECM proteins functionally related to cancer and tumorigenesis were identified in the esophageal neoplastic tissue including COL8A1, lumican, and elastin. An “ECM progression series” (normal, metaplastic, and neoplastic ECM) can provide insights into the isolated effects of ECM upon cell phenotype, including novel biomarkers and macrophage signaling pathways to target for therapeutic treatment.

5.3 INTRODUCTION

Macrophages are mononuclear cells associated with the innate immune system and can originate in the bone marrow, circulate as monocytes, and enter the extravascular space in response to potential pathogens, foreign bodies, or tissue injury [141-143]. In the past two

decades, the recognized functional roles of these cells have markedly expanded. In addition to their role in host defense, macrophages are now known to be required for normal fetal development [144], tissue and organ regeneration in regenerative species such as the axolotl [145, 146], and regulation and resolution of inflammation in most body systems [147]. Each of these functional activities is associated with a distinct macrophage phenotype or activation state.

The phenotype of all cells, including macrophages, is responsive to the surrounding microenvironment [141, 148], many aspects of which are embodied in the extracellular matrix (ECM): the collection of structural and functional molecules secreted by each cell [69, 149]. The ECM is intimately connected to the cell surface and communicates with the cytosol by transmembrane molecules that instruct cell behavior via epigenetic mechanisms. Modification of secreted cell products in turn influences the composition and mechanical properties of the surrounding matrix [5]. The ECM of each tissue is distinctive since the mixture of parenchymal, mesenchymal, and endothelial cells, among other cell types in each tissue is unique [150]. The secreted matrix is constantly, albeit slowly, turning over during health, and changes more rapidly during disease including states of inflammation and neoplasia [151-153]. Since macrophages play an essential role in physiologic and pathologic processes [8, 154], and because immunomodulatory strategies for affecting macrophage phenotype are being investigated for potential therapeutic applications [155, 156], the effect of ECM derived from tissues in various states of health and disease upon macrophage activation state is of great interest.

Esophageal adenocarcinoma (EAC) is a chronic inflammatory-driven cancer and an ideal model to determine the effect of ECM from progressively diseased tissue upon macrophage phenotype. Furthermore, despite the reflux-metaplastic-neoplastic pathogenesis being reasonably well established [1], there is a limited understanding of the biochemical changes to the extracellular matrix during EAC progression. The objective of the present study

was to evaluate the effect of ECM harvested from normal, metaplastic, and neoplastic esophageal tissue upon the activation state of macrophages and paracrine effects upon esophageal epithelial cells.

5.4 MATERIALS AND METHODS

5.4.1 ECM hydrogel preparation

Normal, metaplastic, and neoplastic esophageal tissue was harvested from a rat surgical model of EAC ("Levrat") [157]. The distal esophagus of Sprague-Dawley rats was anastomosed to the jejunum of the small intestine in the Levrat model, creating constant acid reflux in the distal esophagus. Over a period of 17-33 weeks, normal squamous epithelium transforms to metaplastic Barrett's Esophagus and then to a neoplastic, glandular cell type (EAC). The progression of changes in cell phenotype in the rat model mimics the pathophysiology of esophageal disease. Esophagi were explanted, opened longitudinally and frozen on edge in Optimal Cutting Temperature (OCT) using liquid nitrogen. Full-thickness tissue sections of the length of each esophagus were stained with hematoxylin and eosin (H&E) to confirm the presence of the three disease regions. Normal, metaplastic, and neoplastic esophageal tissues were isolated. The three tissues were separately decellularized using a protocol modified from Sutherland et al [158]. Briefly, the tissue was soaked in distilled water at -80°C overnight, and subsequently agitated for 1 h with distilled water, rocked at 37°C for 1 h in 0.25% trypsin/0.05% EDTA, stirred for 4 hrs in 4% sodium deoxycholate, and rocked at 37°C for 2 hrs in 1 M NaCl + 50 U/mL DNAse, repeated 3 times. The tissue was then agitated for 1 h with distilled water, disinfected with 4% PAA at 300 rpm for 2 hrs, and rinsed in alternating 1x PBS and distilled water 4 times, 15 min each shaking at 300 rpm. The resulting ECM biomaterials were

lyophilized. ECM hydrogels were prepared from the normal, metaplastic, and neoplastic ECM as previously described [62]. Briefly, the ECM was powdered, digested by pepsin for 48 hours in 0.01 M HCl, and neutralized (temperature-controlled, pH 7.4) to produce normal, metaplastic, and neoplastic ECM hydrogels.

The same decellularization protocol was used for human tissues. De-identified human tissues were provided by West Penn Allegheny Hospital System and Fundacion Favloro (MTA I#0044782). Table 3 shows the procedures and assays conducted with the two ECM sources. The limited quantity of rat and human samples available prevented complete duplication between species.

Table 3. ECM sources for experiments.
The procedures and assays conducted with the rat and human ECM sources are listed.

	Rat (Levrat)	Human
Decellularization efficacy (H&E, DAPI stain)	√	√
Gel ultrastructure	√	
SDS-PAGE	√	
Absolute proteomic quantification		√
Macrophage (gene expression, protein expression, immunolabeling)	√	
Migration of normal esophageal epithelial cells	√	

5.4.1.1 Decellularization efficacy

Crapo, Gilbert [76] have recommended a set of decellularization criteria. Two of the criteria were used in the present study to determine decellularization efficacy. A subset of the lyophilized ECM materials was fixed in 10% neutral buffered formalin for 24 h. The fixed samples were

paraffin embedded and 5 um sections were stained with hematoxylin and eosin (H&E) or 40 ,6-diamidino-2-phenylindole (DAPI) to identify any remaining cellular structures.

5.4.2 ECM hydrogel characterization

5.4.2.1 ECM hydrogel ultrastructure

The ultrastructure of normal, metaplastic, and neoplastic ECM hydrogels (6 mg/mL) was characterized with scanning electron microscopy (SEM), as previously described [65]. Briefly, ECM hydrogels were fixed in cold 2.5% glutaraldehyde for 24 hours, rinsed in PBS, dehydrated with graded ethanol (30, 50, 70, 90, 100% ethanol in PBS) at 45 min per wash, and critical point dried for 5 hours (Leica EM CPD030 Critical Point Dryer, Leica Microsystems, Buffalo Grove, IL). After drying, gels were sputter coated (Sputter Coater 108 Auto, Cressington Scientific Instruments, Watford, UK) with a 4.6 nm thick gold/palladium alloy coating and imaged with a scanning electron microscope (JEOL JSM6330f, JEOL Ltd., Peabody, MA) at 2,000 and 10,000x magnification.

5.4.2.2 Solubilized ECM chromatographic profile

The solubilized normal, metaplastic, and neoplastic ECM and pepsin control were subjected to SDS-PAGE (polyacrylamide gel electrophoresis) and visualized using silver stain (Thermo Fisher) according to manufacturer's instructions. Solubilized ECM protein concentration was determined using bicinchoninic acid assay (BCA) quantification (Pierce Chemical). Ten (10) ug of normal, metaplastic, and neoplastic solubilized ECM and pepsin control was suspended in Laemmli buffer (R&D Systems) containing 5% β-mercaptoethanol (Sigma-Aldrich), and separated in a 4-20% gradient SDS-PAGE gel (Mini-PROTEAN TGX protein gel, Bio-Rad) at 150 mV in running buffer (25 mM tris base, 192 mM glycine, and 0.1% SDS), and transferred to polyvinylidene difluoride membranes (Millipore) using semi-dry technique for 45 min at constant

voltage in transfer buffer [25 mM tris (pH 7.5), 192 mM glycine, 20% methanol, and 0.025% SDS]. Silver staining was applied to the gels using the Silver Stain Plus Kit (Bio-Rad) according to the manufacturer's instruction and imaged using a ChemiDoc Touch Imaging System (Bio-Rad).

5.4.2.3 Solubilized ECM mass spectrometry

The proteomic profile of patient-matched human normal and tumor tissue and corresponding ECM was determined. Native tissue and ECM samples were cryomilled using liquid nitrogen and lyophilized before mass spectrometry analysis.

One mg of lyophilized tissue was weighed and processed as previously described [159]. Briefly, tissues were homogenized by mechanical agitation (Bullet Blender®, Next Advance) in a CHAPS buffer containing 2mm glass beads. Following homogenization, tissues were sequentially extracted with vortexing and high-speed centrifugation in 8 M Urea, and CNBr buffers resulting in 3 fractions for each sample: (1) cellular fraction, (2) soluble ECM, and (3) insoluble ECM. ECM representative stable isotope labeled (SIL) polypeptides (QconCATs [160]) were spiked into each fraction at known concentrations prior to proteolytic digestion. Enzymatic digestion was carried out as previously described [161]. In short, samples were reduced, alkylated and digested via filter assisted sample prep (FASP) and desalted by solid phase extraction using C18 resin.

Samples were analyzed by both liquid chromatography-selected reaction monitoring (LC-SRM) and liquid chromatography-tandem mass spectrometry (LC-MS/MS) for targeted (quantitative) and global proteomics respectively. Equal volumes of each post-digestion sample were combined and injected every fifth run and used to monitor technical reproducibility. LC-SRM and LC-MS/MS data was processed as previously described [162].

5.4.3 THP-1 macrophage cell culture

A human mononuclear cell line (THP-1, ATCC) was expanded as previously described [163] in culture media (RPMI, 10% FBS, 1% pen/strep). THP-1 cells were plated at 2 million cells/well and activated to naïve macrophages (M0) by 320 nM phorbol-12-myristate-13-acetate (PMA) for 24 hrs. Activated THP- cells were washed and rested for 3d, and treated with one of the following for 24 hrs: solubilized normal, metaplastic, or neoplastic ECM hydrogel (250 ug/mL), positive control “M1"-like stimulus IFNγ (20 ng/mL)/LPS (100 ng/mL), positive control “M2"-like stimulus IL4 (20 ng/mL), negative controls pepsin (25 ug/mL) or medium alone, as previously described [164].

5.4.3.1 ECM effect on THP-1 macrophage gene expression

RNA was isolated (Qiagen RNEasy) and transcribed to cDNA (Invitrogen cDNA RT kit) for qPCR using the SYBR green probe (BioRad) and tested for a panel of pro-inflammatory (“M1-like") and anti-inflammatory (“M2-like") genes in technical duplicates (n=4). Results were expressed with the $\Delta\Delta$Ct method, normalized to housekeeping gene βgus, and fold change was calculated against medium treatment at 24 hrs. The significant genes were repeated with the same experimental set-up at 6 and 72h to investigate the effect of time for gene expression.

Endotoxin, a ubiquitous environmental contaminant and known M1 activator was tested using Limulus Amebocyte Lysate assay (LAL) in the neutralized ECM hydrogels (5 mg/mL), and sample endotoxin concentration was calculated using an endotoxin standard curve.

5.4.3.2 ECM effect on THP-1 macrophage secreted proteins

Enzyme-linked immunosorbent assay (ELISA) was used to determine the concentration of IFNγ, TNFα, and IL1RN in the supernatant of macrophages treated with metaplastic and neoplastic

ECM after 6 or 24 hrs. Supernatants were first centrifuged at 1500 rpm at 4°C for 10min to remove any particulate material. The ELISA for IFNγ (Human IFNγ ELISA Kit II, BD OptEIA), TNFα (Human TNF ELISA Kit II, BD OptEIA), and IL1RN (Human IL-1ra/IL-1F3, R&D Systems) were each performed according to the manufacturer's instructions. Each sample was run in technical duplicate with the appropriate dilution.

5.4.3.3 Immunolabeling

THP-1 cells were immunolabeled with the TNFα and IL1RN antibodies after ECM, cytokine, or control treatment for 24h (n=5), as described in 5.4.3. Cells were rinsed with PBS, fixed with 2.5% glutaraldehyde for 20 min, and rinsed with PBS. Wells were blocked (0.1% Triton x 100, 0.1% Tween 20, 2% bovine serum, and 4% goat serum in PBS) for 1 hour at room temperature. Cells were incubated with the following primary antibodies polyclonal rat CD11b (1:150, Abcam 8878), polyclonal rabbit IL1RN (1:1000, Abcam 2573), and monoclonal mouse TNFα (1:100, Abcam 6671) in blocking buffer overnight at 4°C. Wells were rinsed with PBS three times and cells were incubated with secondary antibodies AlexaFluor donkey anti-mouse 488, goat anti-rabbit 546, and goat anti-rat 596 (1:200 in blocking buffer) for 1 hour at room temperature in the dark. Wells were rinsed three times with PBS, incubated with DAPI for 5 min, rinsed with PBS and imaged at 20x magnification using a live-cell microscope. Exposure times were standardized by cytokine treated macrophage controls (i.e., "M1"-like and "M2"-like treatments). Three technical images were taken per sample. Images were quantified using a CellProfiler pipeline that analyzed black and white images of the unmixed channels and quantified the number of positive CD11b, TNFα, and IL1RN cells that showed positive labeling to determine the ratio of cells that were IL1RN+/CD11b+ or TNFα+/CD11b+. Ratios of ILRN+ or TNFα+ over the total number of CD11b+ positive cells were used to normalize counts.

5.4.3.4 Effect of ECM conditioned macrophage secretome on Het-1A normal esophageal epithelial cell line

Chemotaxis of an immortalized normal esophageal epithelial cell (Het-1A, ATCC) was investigated using the Boyden chamber assay (Transwell, 6.5 mm diameter; Corning, Lowell, MA). Het-1A cells were cultured in Bronchial Epithelial Basal Media (Lonza), with Bronchial Epithelial Growth Media Bullet Kit (Lonza) according to ATCC guidelines. Gentamycin-amphotericin B mixture from the Bullet Kit was not added to the medium based on ATCC recommendations. The medium was supplemented with 1% penicillin/streptomycin (Fisher). Het-1A cells were expanded on flasks pre-coated with a solution of 0.01 mg/mL fibronectin, 0.03 mg/mL bovine collagen, and 0.01 mg/mL bovine serum albumin solution. Het-1A cells were split at 70-80% confluency, and detached with a solution of 0.05% (w/v) Trypsin-.53 mM EDTA, 0.5% polyvinylpyrrolidone (PVV), and 0.35 mM EDTA solution in 1x PBS; and trypsinization was stopped with an equal volume of 0.1% Het-1A trypsin inhibitor.

"Conditioned medium" is defined as the secretome of THP-1 cells that have been pre-treated for 24h as described in 5.4.3, rinsed with PBS, and incubated in serum-free RPMI medium for a period of 5h. The Boyden Chamber was a polycarbonate membrane with 8 μm pores that were coated on both sides with rat collagen (0.05 mg/mL) in 0.02 N acetic acid for 1 hour at room temperature, rinsed 1x with PBS, and air dried before being used in the Boyden Chamber assay. Conditioned medium was added to the bottom of each Boyden well. Thirty thousand Het-1A cells in serum free medium were added to the top of each Boyden well and allowed to migrate to the underside of the porous membrane for 24 hrs at 37°C in technical quadruplicates (n=3). The non-migratory cells on the upper membrane surface were removed with a scraper, the membrane was fixed for 5 minutes in 95% methanol, and the migratory cells attached to the bottom surface of the membrane were stained with 0.1% crystal violet in 0.1 M borate, pH 9.0, and 2% ethanol at room temperature. The membrane was mounted on a slide

and stained with southern blot DAPI (SouthernBiotech). The number of migrated cells per well was imaged using absorbance 350 nm on the fluorescent live cell microscope (Zeiss Axiovert) and Cell Profiler was used to count the number of nuclei/well.

5.4.4 Statistical Analysis

All results are expressed as mean ± SEM.

Gene expression –A two-way ANOVA for the independent variables treatment and time was performed for the dependent variable fold change of gene expression. The Dunnett's post hoc multiple comparisons test was used to determine significant differences ($p<0.05$) between treatment and medium control at 6, 24, and 72 hours.

ELISA – A Kruskal Wallis nonparametric test was used because the standard deviation was significantly different between treatment groups. One-way ANOVA was performed for the independent variable treatment at 6 and 24h for the dependent variable protein expression. Dunn's multiple comparisons post hoc test was used to determine significant differences ($p<0.05$) between treatment and medium control.

Immunolabeling - A one-way ANOVA was used for all comparisons against both medium and normal ECM treatments with Dunnett's multiple comparison post hoc analysis.

Boyden Chamber – A one-way ANOVA for the independent factor treatment was performed for the dependent variable number of migrated Het-1A cells. The Dunnett's post hoc multiple comparisons test was used to determine significant differences ($p<0.05$) between treatment and medium or treatment and normal ECM.

5.5 RESULTS

5.5.1 Normal, metaplastic, and neoplastic tissue from rat and human species can be decellularized with the same protocol

Normal, metaplastic, and neoplastic ECM was isolated from rat and human tissue. First, normal, metaplastic and neoplastic tissue was identified for the rat model of EAC macroscopically (Figure 3A) and the pathology confirmed histologically with H&E staining (Figure 3B). Normal tissue shows a stratified, squamous epithelium; metaplastic tissue shows a villiform, columnar epithelium with goblet cells, reminiscent of that present in normal jejunum tissue; and neoplastic tissue shows glandular cells invading into the submucosa. The rat normal, metaplastic, and neoplastic tissues were decellularized using the same protocol and shown to achieve decellularization by absence of nuclei by H&E and DAPI staining (Figure 3C). The optimized decellularization protocol for rat tissue was shown to similarly achieve decellularization in normal and neoplastic human tissue by absence of nuclei (Figure 3D).

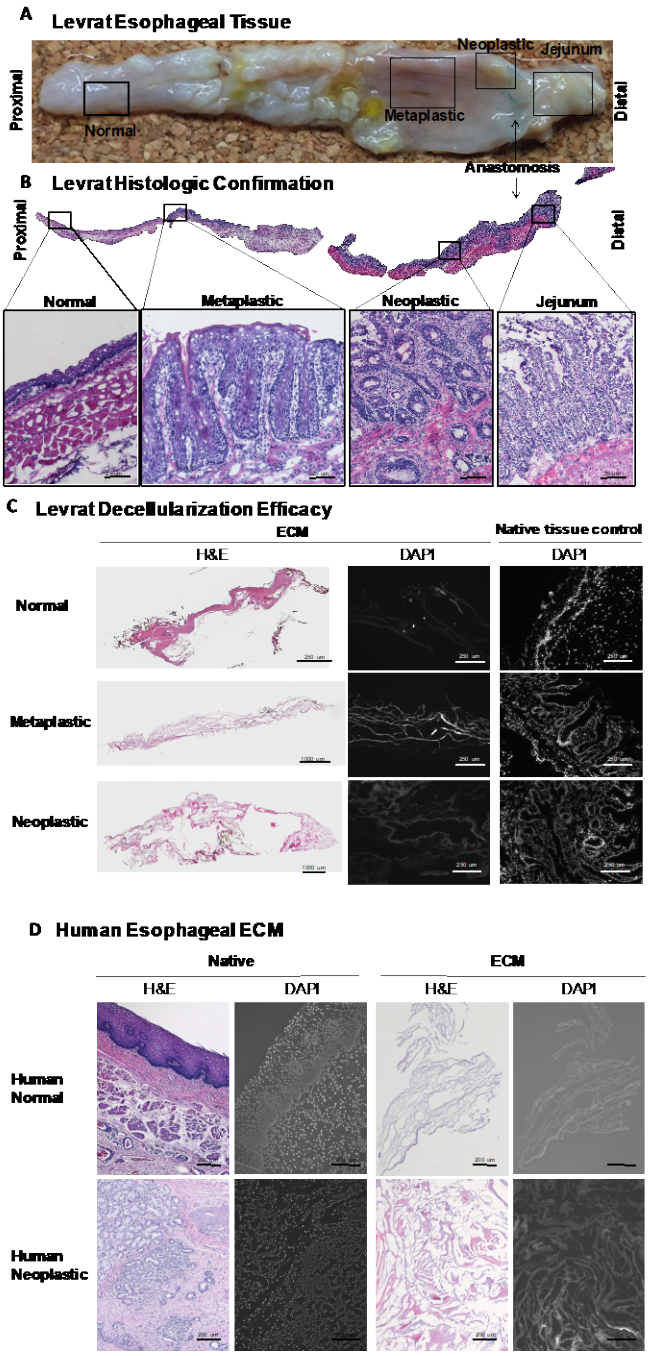

Figure 3. ECM preparation

(A) An established rat surgical model of EAC (Levrat) progresses from normal squamous epithelium to metaplastic, villiform, columnar epithelium (Barrett's Esophagus) to neoplastic, glandular cell growth with invasion into the basement membrane (esophageal adenocarcinoma) over a period of 33 weeks. **(B)** Representative H&E confirmation of diseased regions. Normal, metaplastic, and neoplastic tissue were dissected and pooled by diseased region. **(C)** Decellularization efficacy assessed by absence of nuclei (H&E and DAPI stain). **(D)** Representative H&E and DAPI stains of human normal and human neoplastic native tissue, and ECM showing decellularization efficacy.

5.5.2 ECM hydrogel characterization

5.5.2.1 ECM hydrogel nanostructure between disease states is distinctive

Hydrogels of the normal, metaplastic, and neoplastic ECM were prepared by pepsin digestion and characterized for the fibrous structure. While enzymatic cleavage of collagen by pepsin results in loss of the 3-dimensional architecture, the nanofibrous monomeric structure is retained and can still be visualized by SEM (Figure 4).

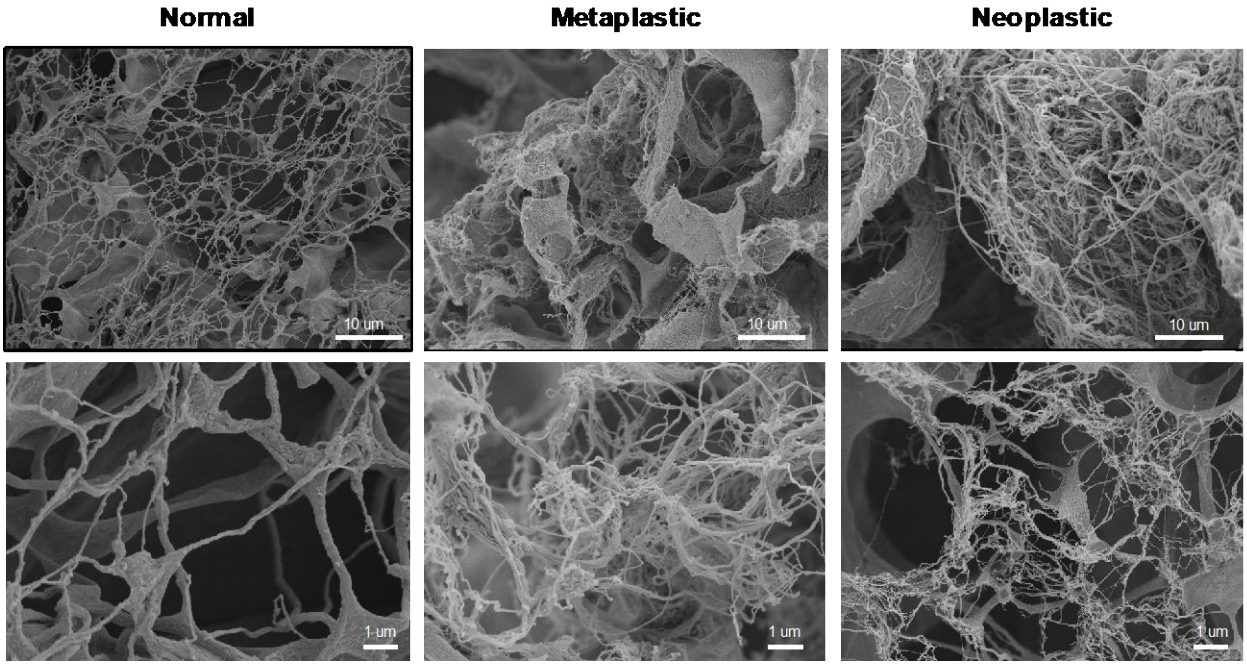

Figure 4. ECM hydrogel ultrastructure.
Normal, metaplastic and neoplastic ECM hydrogels were prepared for scanning electron microscopy and imaged at 2,000x and 10,000x magnification. The three types of ECM hydrogels show a porous fibrillar network. Scale bars shown are 10 um for 2,000 x magnification and 1 um for 10,000 x magnification.

5.5.2.2 Solubilized metaplastic and neoplastic ECM show a distinct chromatographic profile compared to solubilized normal ECM

Normal, metaplastic, and neoplastic ECM showed distinct chromatographic profiles by SDS-PAGE and silver stain (Figure 5). Noticeably, higher molecular weight protein bands >250 kDa present in normal ECM were absent in metaplastic ECM and neoplastic ECM. The distinctive chromatographic profile of each ECM suggests that biochemical differences exist and are retained following decellularization since the same decellularization protocol was used for all sources tissues. Other differences may exist between the protein banding patterns that are not readily apparent with SDS-PAGE/silver stain, such as amount of protein and protein isoforms, and hence mass spectrometry with absolute quantification was performed on all samples, as described in the following section.

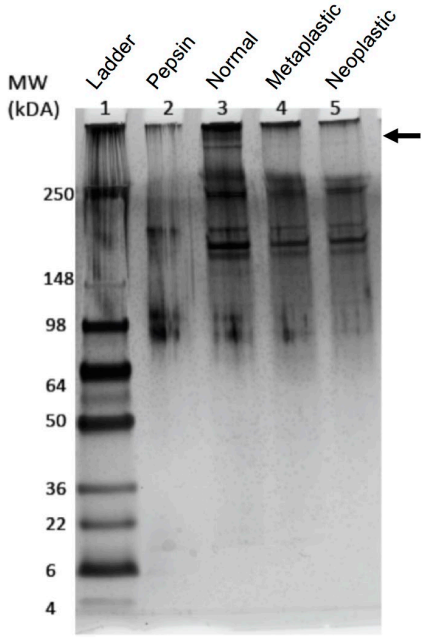

Figure 5. ECM hydrogel chromatographic profiles.
Solubilized ECM was separated using SDS-PAGE (polyacrylamide gel electrophoresis) and visualized using silver stain. Noticeably, higher molecular weight protein bands >250 kDa present in normal ECM were absent in metaplastic ECM and neoplastic ECM. The silver stain results suggest disease specific protein profiles are present for each ECM type.

5.5.2.3 Targeted mass spectrometry and global mass spectrometry can identify a distinctive neoplastic ECM signature (COL8A1, lumican, elastin)

Targeted mass spectrometry showed that the quantitative profile of ECM-associated proteins between the human normal and neoplastic ECM was relatively similar, despite the banding differences seen via SDS-PAGE for the rat normal, metaplastic, and neoplastic ECM. However, the human normal and neoplastic native samples had protein profiles that were distinguishable by partial least squared discriminate analysis (Figure 6A).

The human neoplastic native samples produced nearly two times the total ECM as the normal native samples (FC of 1.76, $p = .0345$) (Figure 6B). Decellularization resulted in near complete depletion of cellular proteins (<0.1% remaining), in addition to the depletion of the majority of basement membrane and other structural ECM proteins outside of fibrillar collagen. COL1A1/2 and COL5A1/2 accounted for over 98% of the quantifiable proteins in the resulting normal and neoplastic ECM. Comparison of residual proteins separate from fibrillar collagen in the normal and neoplastic ECM showed notably more collagen type VIII alpha 1 chain (COL8A1), fibulin-1 (FBLN1), fibrillin-1 (FBN1), and lumican (LUM) in the neoplastic ECM (Figure 6C). Lumican was retained at amounts nearly 4 fold higher ($p=0.0132$) in the neoplastic ECM compared to normal ECM.

Global mass spectrometry was used to corroborate the targeted proteomics and identify other proteins that were characteristic of the neoplastic ECM signature (Table 4). Several proteins of interest from the targeted proteomics could not be immediately validated by global mass spectrometry because the targeted proteomics methodology is nearly an order of magnitude more sensitive. However, COL8A1 was increased in neoplastic ECM compared to normal ECM ($p=0.0007$) consistent with the results of targeted proteomics. The closely associated protein COL8A2 was also increased ($p=0.0156$). In addition, elastin was increased in neoplastic ECM compared to normal ECM ($p=0.000424$) and showed a 25% increase in non-

specific cleavage compared to normal ECM. Finally, LOXL1 was only shown to be present in neoplastic ECM but not normal ECM.

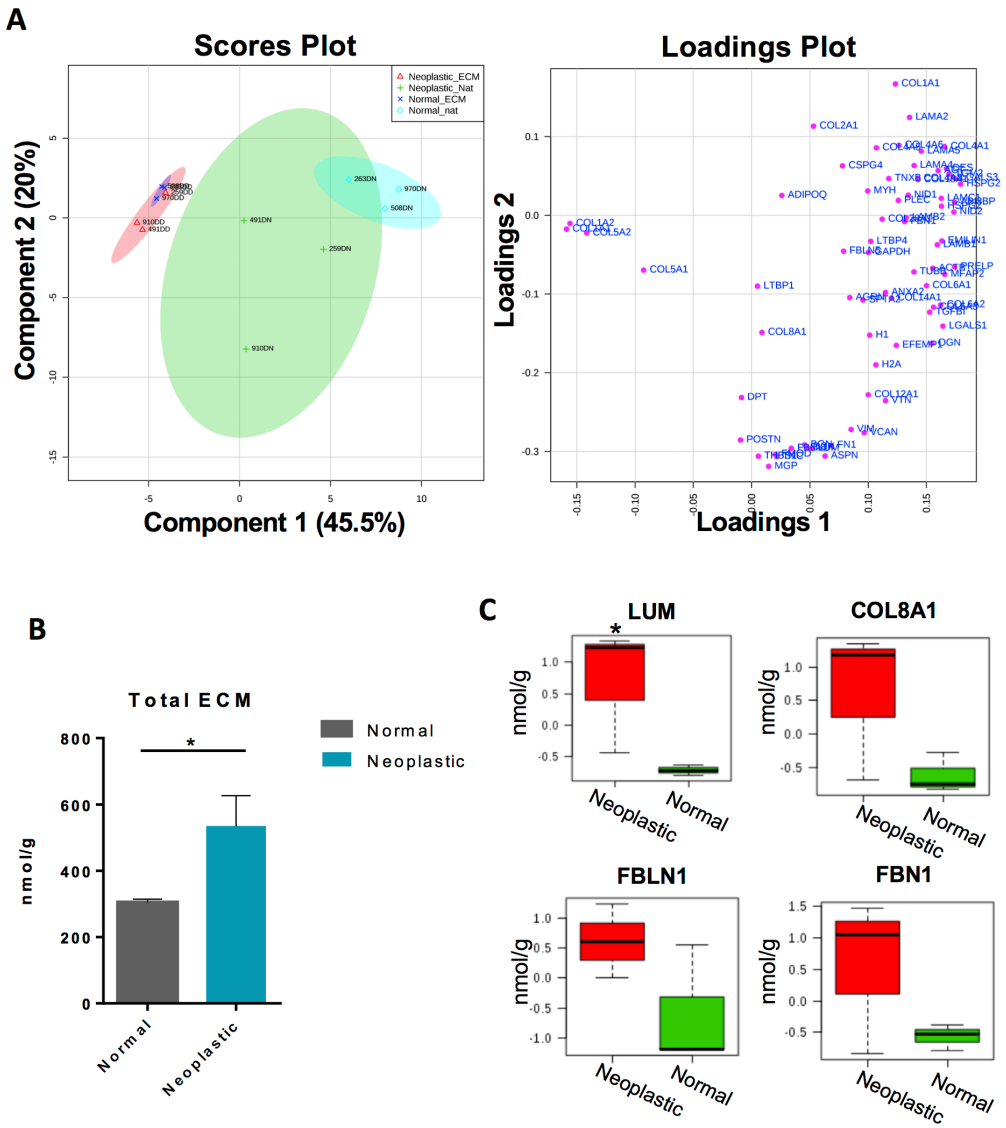

Figure 6. ECM hydrogel proteomic quantification in comparison to native tissue.
(A) Principal component analysis of quantitative ECM proteomics for neoplastic and normal tissue and ECM. Scores plot (left) and corresponding loading plot (right) show the ECM proteins contributing to the principal components. (B) Nanomolar concentration per gram of tissue for normal and neoplastic tissue. (C) Lumican (LUM), collagen 8A1 (COL8A1), Fibulin 1 (FBLN1), Fibrillin 1 (FBN1) in neoplastic and normal ECM. Lumican was significantly increased in neoplastic ECM compared to normal ECM. Values were expressed as mean ± SEM.

Table 4. Global mass spectrometry of normal and neoplastic tissue and ECM.
The top 20 significantly upregulated proteins in neoplastic ECM compared to normal ECM are shown (p value < 0.05, shown in green). Ratio of neoplastic to normal peptide spectral counts are shown for the raw values and values normalized to dry weight of the starting material (g). Red shows upregulated proteins in neoplastic compared to normal tissue or ECM, blue shows downregulated proteins in neoplastic compared to normal tissue or ECM. ND – Not detected.

			Peptide Spectral Counts (Neoplastic/Normal)				ttest (Neoplastic vs Normal)	
			Native		ECM		Native	ECM
	Proteins	Gene	Raw	Normalized	Raw	Normalized	Raw	Raw
1	Keratin, type II cytoskeletal 1	KRT1	0.86	0.89	0.75	0.62	0.737482548	0.000119761
2	Elastin	ELN	1.54	1.42	4.11	3.46	0.269976249	0.000423654
3	Collagen alpha-1(VIII) chain	COL8A1	0.53	0.62	4.43	3.80	0.357540495	0.000745307
4	Myosin regulatory light polypeptide 9	MYL9	1.31	1.19	6.00	4.34	0.254209637	0.001337909
5	Keratin, type II cytoskeletal 6A	KRT6A	1.33	1.34	7.92	6.24	0.711480681	0.002598833
6	Histone H2A type 1-C	HIST2H2AA3	0.84	0.77	2.79	1.98	0.29867707	0.005267808
7	Laminin subunit alpha-5	LAMA5	2.26	2.04	3.00	2.57	0.32250446	0.007490434
8	Pseudokinase FAM20A	FAM20A	0.63	0.57	0.56	0.47	0.485170293	0.008970902
9	Creatine kinase B-type	CKB	0.89	0.79	14.79	10.25	0.657449724	0.010514894
10	Fibulin-5	FBLN5	2.81	2.67	1.63	1.37	0.301864239	0.011056493
11	Filamin-A	FLNA	1.17	1.10	3.67	2.56	0.56953829	0.013480957
12	Collagen alpha-2(VIII) chain	COL8A2	0.00	0.00	1.94	1.62	ND	0.015587358
13	Myosin light polypeptide 6	MYL6	1.10	1.00	14.75	10.41	0.675526185	0.0158151
14	Ig lambda-2 chain C regions	IGLC2	2.33	2.24	4.83	3.24	0.310601762	0.03066557
15	Keratin, type I cytoskeletal 10	KRT10	0.92	0.91	0.79	0.65	0.861890262	0.036733887
16	Maestro heat-like repeat-containing protein family member 2	MROH2B			0.52	0.47	ND	0.0379966
17	Transgelin	TAGLN	0.74	0.67	6.68	4.47	0.131248949	0.03837828
18	Gelsolin	GSN	1.24	1.11	8.00	5.70	0.484673355	0.041174163
19	UPF0450 protein C17orf58	C17orf58	2.57	2.16	2.80	2.44	ND	0.044093614
20	Vinculin	VCL	1.35	1.21	11.75	8.12	0.380902468	0.044878608

5.5.3 Metaplastic and neoplastic ECM can activate TNFα and IL1RN signaling in macrophages, and neoplastic ECM increased macrophage TNFα secretion

Transcription factors and downstream genes are shown for the pro-inflammatory (Figure 7A) and anti-inflammatory (Figure 7B) panel of markers. For the pro-inflammatory IFNγ signaling pathway, neoplastic ECM increased Stat2 transcription factor expression (p=0.0001) at 24h. The metaplastic and neoplastic ECM increased the downstream gene iNOS at 24 hours (p=0.0313, p=0.0047 respectively). However, secreted IFNγ protein was not changed with normal, metaplastic, or neoplastic ECM treatment at 24 hours. For the pro-inflammatory TLR-4 signaling pathway, there was basal expression of TNFα with normal ECM treatment at 24 hours

(p=0.0415), but increased TNFα gene expression was shown for metaplastic (p=0.0001) and neoplastic ECM (p=0.0001) treatment at 24 hours, and for metaplastic (p=0.0002) and neoplastic (p=0.002) ECM treatment at 72 hours. TNFα secreted protein was increased with neoplastic ECM treatment at 24h (p=0.0497). The increase in M1-related genes with metaplastic and neoplastic ECM was not due to a difference in endotoxin concentration between samples (Figure 38). For the anti-inflammatory IL4 signaling pathway, there was increased expression of the transcription factor IRF4 with metaplastic (p=0.0086) and neoplastic ECM treatment at 24h (p=0.001). Secreted IL1RN protein trended towards an increase with neoplastic ECM treatment at 24 hours, but was not significant (p=0.0671). Other genes tested that did not show significant differences by one-way ANOVA at 24h were: Stat5b, Stat5a, IRF3 (M1) and KLF4, Stat6, PPARγ, Stat3, and CD206 (M2) (Figure 39), and were not further evaluated. Table 5 summarizes the macrophage activation markers in the present study with respect to canonical markers of M1, M2, and Tumor-Associated Macrophages (TAM).

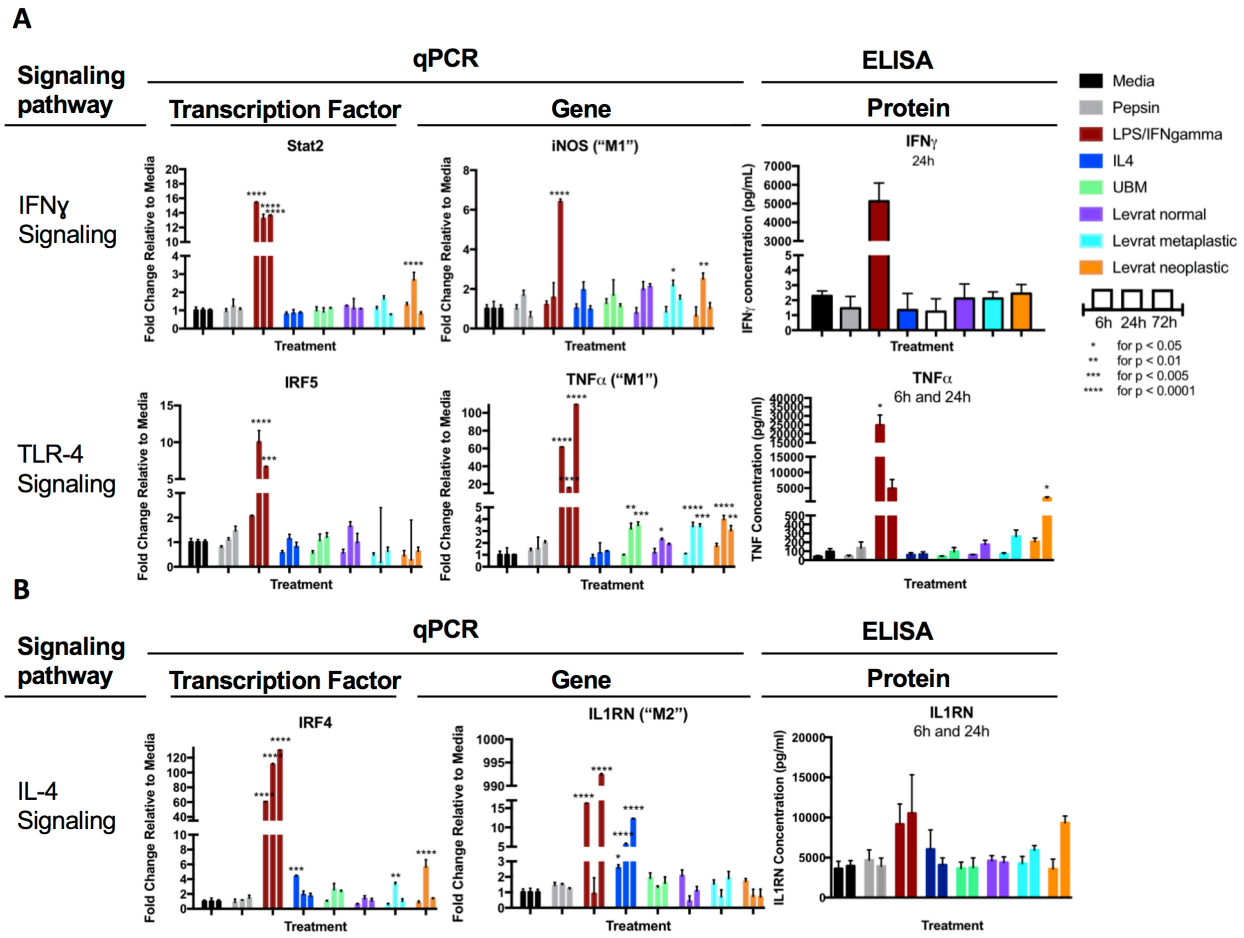

Figure 7. Normal, metaplastic, and neoplastic ECM promotes a distinctive M1-like and M2-like signature.
A human mononuclear cell line (THP-1) was activated to naïve macrophages (M0). The M0 macrophages were treated with normal, metaplastic, and neoplastic ECM hydrogels (250 ug/mL) or positive controls for M1-like activation (LPS/IFNγ) and M2-like activation (IL4) or negative controls (pepsin, medium) for 24 hours and tested for a panel of (A) Pro-inflammatory and (B). Anti-inflammatory genes and transcription factors. ELISA confirmed increased TNFα expression at 24 hours in the neoplastic ECM treated groups, and IL1RN expression trended towards an increase at 24h but not significant (p=0.0671). * p< 0.05, ** p< 0.01, *** p< 0.005, **** p<0.0001. Values are expressed as mean ± SEM.

Table 5. Summary of macrophage activation markers.

		Description	Markers	Ref
Literature	**"M1"-like**	• Activated by IFNγ, LPS, and TNFα • Protect against pathogens	• Secrete high nitric oxide (NO), reactive oxygen species (ROS) and cytokines • IL-12^{high}, IL-10^{low}, IL-6 ^{high} and TNFα ^{high}	[7]
	"M2-like"	• Activated by IL-4 and IL-13 • Scavenge debris, promote angiogenesis, and recruit cells involved in constructive tissue remodeling.	• Secrete high TGF-β1 and arginase • IL-10^{high} IL-12^{low}; IL-1RA^{high}, and IL-1 decoy^{high}	[7]
	Tumor Associated Macrophage	• Subtype of M2 • Non-cytotoxic toward tumor cells; inefficient to trigger an adaptive immune response	• Secrete low NO and reactive oxygen intermediates (ROI) • 1L-10 ^{high}; IL-12^{low}, IL-1β ^{low}, TNFα^{low}, IL-6 ^{low} • Low antigen presenting	[165] [7, 9]
Present Study	**M(normal ECM)**	• Activated by 250 ug/mL	• TLR-4: TNFα ^{high} 24h	
	M(metaplastic ECM)	• Activated by 250 ug/mL	• IFNγ: Stat2^{high} 24h • TLR-4: TNFα ^{high} 24 and 72h • IL-4: IRF4 ^{high} at 24h • Increase epithelial cell migration	
	M(neoplastic ECM)	• Activated by 250 ug/mL	• IFNγ: Stat2^{high} 24h, iNOS^{high} 24h • TLR-4: TNFα ^{high} 24 and 72h, secrete TNFα high 24h, immunolabel TNFα ^{high} • IL-4: IRF4 ^{high} at 24h • Increase epithelial cell migration	
	M(UBM)	• Activated by 250 ug/mL	• TLR-4: TNFα ^{high} 24 and 72h	

5.5.3.1 Neoplastic ECM treatment increased nuclear and cytosolic TNFα expression in macrophages

Immunolabeling of pro-inflammatory TNFα and immunomodulatory IL1RN after 24h of treatment was performed to corroborate the qPCR and ELISA results (Figure 8A). TNFα increased with neoplastic ECM treatment compared to medium ($p=0.036$), and increased with neoplastic ECM compared to normal ECM ($p=0.019$). IL1RN did not show any change between ECM treatments (Figure 8B).

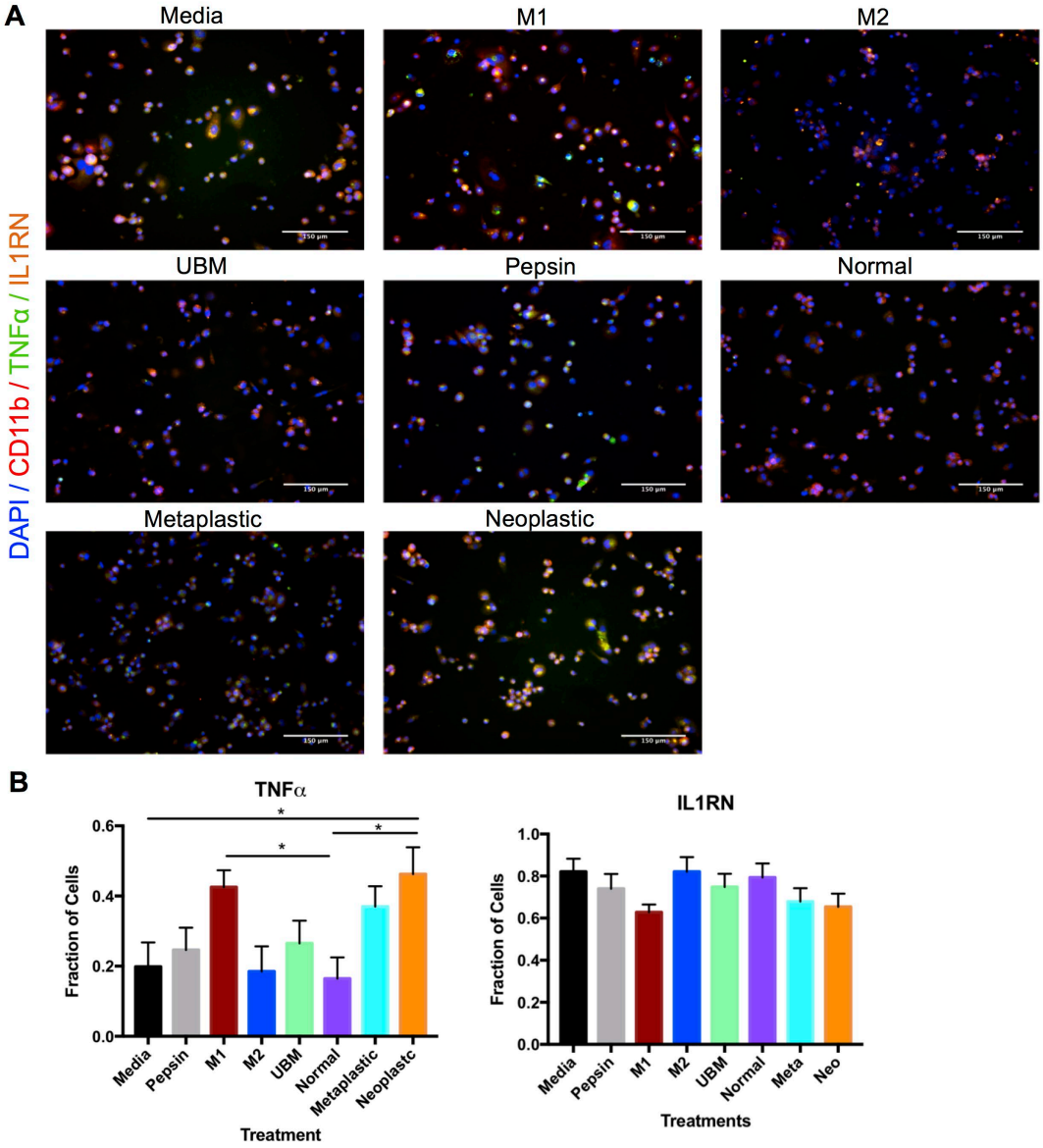

Figure 8. Immunolabeling of ECM treated macrophages.
A human mononuclear cell line THP-1 was activated to naïve macrophages (M0). The M0 macrophages were treated with normal, metaplastic, and neoplastic ECM hydrogels (250 ug/mL) or positive controls for M1-like activation (LPS/IFNγ) and M2-like activation (IL4) or negative controls (pepsin, medium) for 24 hours. (A) Macrophages were fixed and labeled with TNFα ("M1" like) in green, IL1RN ("M2 like") in orange, pan macrophage marker CD11b in red, and DAPI in blue. Representative images are shown (n=3, with 3 images per sample). (B) Images were quantified in CellProfiler (n=3, with 3 images per sample). Fraction of cells refers to cells that were TNFα+/CD11b+ out of the total CD11b+ cells or IL1RN+/CD11b+ out of the total CD11b+ cells. * $p<0.05$. Values are expressed as mean ± SEM.

5.5.3.2 Macrophages pre-treated with metaplastic and neoplastic ECM increased normal esophageal epithelial cell migration through paracrine effects

The paracrine effect of normal, metaplastic, and neoplastic ECM treated macrophages was investigated. “Conditioned media” (i.e., the secretome of macrophages that have been pre-treated for 24h) was used in a Boyden Chamber assay to quantify chemotaxis upon normal esophageal epithelial cells (Het-1A) (Figure 9). Metaplastic ($p=0.0033$) and neoplastic ECM ($p=0.0001$) conditioned media increased esophageal epithelial cell Het-1A chemotaxis compared control. Importantly, neoplastic ECM conditioned medium increased migration compared to normal ECM conditioned medium ($p=0.0393$), showing increasing migration with increasing ECM tumorigenicity.

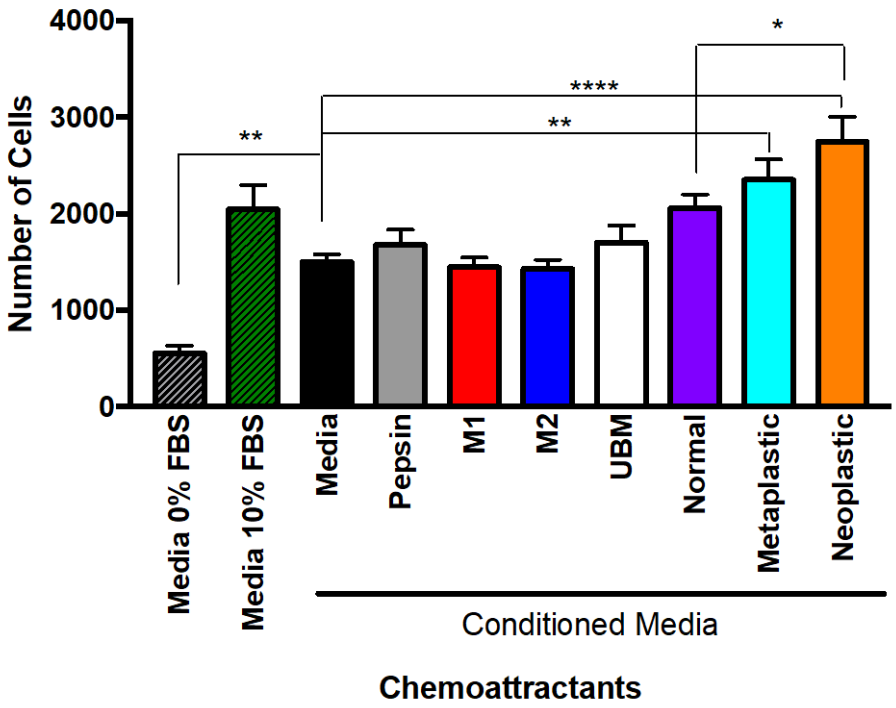

Figure 9. Metaplastic and neoplastic ECM increased migration of normal esophageal epithelial cells through macrophage paracrine effects.
Macrophages were conditioned with medium, M1-like positive stimulus (LPS/IFNγ), M2-like positive stimulus (IL4), pepsin (25 ug/mL), UBM (250 ug/mL), or normal, metaplastic, and neoplastic ECM (250 ug/mL) for 24 hours. The secretome of the conditioned macrophages was collected for 4 hours in serum-free medium and used as a chemoattractant in a Boyden chamber assay using normal esophageal epithelial cells (Het-1a). Het-1a cells migrated to medium with 10% FBS as expected, and more towards metaplastic and neoplastic ECM, suggesting a tissue-specific effect for the esophageal ECM. Normal esophageal epithelial cells migrated more towards neoplastic ECM than normal ECM. * $p \leq 0.05$, ** $p \leq 0.01$, *** $p \leq 0.001$, **** $p \leq 0.0001$. Values are expressed as mean ± SEM.

5.6 DISCUSSION

The results of the present study show that normal, metaplastic, and neoplastic ECM have distinctive biochemical signatures and resulting effects upon macrophage activation. Specifically, neoplastic ECM had notably higher concentrations of lumican, COL8A1, and

elastin. The three types of ECM were decellularized using the same protocol to eliminate the variable of processing, suggesting that the distinct effects upon macrophage phenotype were due to ECM signals retained following decellularization. Metaplastic and neoplastic ECM increased pro-inflammatory (IFNγ, TNFα) and immunomodulatory (IL1RN) gene expression and increased esophageal epithelial cell migration compared to control. Neoplastic ECM had the most pronounced effect upon naïve macrophage activation towards TNFα+, and influenced a non-malignant esophageal epithelial cell to behave more like a neoplastic cell with increased migration, consistent with the premise of dynamic reciprocity. Metaplastic ECM showed similar but less pronounced effects than neoplastic ECM suggesting that the neoplastic ECM signals start at the pre-cancerous state. The results importantly show the isolated role of progressively diseased ECM ("ECM progression series") to influence key macrophage signaling pathways associated with chronic inflammation and neoplasia, and influence epithelial cell behavior.

5.6.1 Solubilized ECM from normal, metaplastic, and neoplastic esophageal ECM induce a distinct macrophage activation state. Metaplastic and neoplastic ECM promoted TNFα+ macrophage activation and increased epithelial cell migration in a stepwise manner.

Macrophages activate at a site of tissue injury or within a tumor on a spectrum from pro-inflammatory ("M1"-like) to immunomodulatory ("M2"-like) in response to microenvironmental signals [166]. M1 and M2 are characterized by different functional programs involving released growth factors, chemokines, and MMPs [167]. Tumor-associated macrophages (TAM) are characterized as a subtype of M2, involved in immunomodulation to promote neoplastic cells to proliferate and survive [7, 9, 154]. It was hypothesized that ECM derived from Barrett's esophagus, as a chronic inflammatory state, would activate macrophages toward an "M1-like" state, and the neoplastic ECM would activate macrophages toward an "M2"-like state [9].

Signaling pathways were characterized by expression of transcription factors, downstream genes, and secreted products. For the pro-inflammatory ("M1") TLR-4 signaling pathway, metaplastic and neoplastic ECM increased TNFα gene expression at 24 and 72h, and normal ECM increased THP-1 TNFα gene expression at 24h. Only neoplastic ECM increased TNFα secreted protein expression by ELISA compared to medium at 24h. Immunolabeling corroborated these results with neoplastic ECM increasing TNFα compared to medium control and compared to normal ECM treatment after 24h. TNFα is upregulated in GERD [12], along with other pro-inflammatory cytokines IL1B, IL8, and IL10; and upregulated from BE to EAC [19]. TNFα is released by macrophages as well as cancer cells, fibroblasts, and epithelial cells in EAC and other cancer types, with the possibility for paracrine and autocrine feedback [10, 19, 20]. In the context of other inflammatory driven cancers (e.g., ovarian, breast, prostate, bladder, colorectal) [19], TNFα increased epithelial cell proliferation [19], MMP secretion [19], ROS production to directly oxidize DNA [20], epithelial-mesenchymal transition [10], cancer cell invasion [10], and macrophage-mediated T cell suppression [168]. These pro-tumoral TNFα functions observed for other cancer types may be contributing toward EAC progression. The present study adds to the literature by showing the isolated role of metaplastic and neoplastic ECM as an initiating signal to activate macrophages toward TNFα+.

Metaplastic and neoplastic ECM induced a macrophage secretome ("conditioned media") that increased epithelial cell migration compared to control conditioned medium. Neoplastic ECM conditioned medium also increased epithelial cell migration compared to normal ECM conditioned medium. The chemotactic signals in the macrophage secretome remain to be determined, but TNFα could be contributing because it increased neoplastic cell invasiveness when co-cultured with macrophages in functional antibody-blocking experiments [9].

Pro-inflammatory IFNγ signaling was also implicated in the present study, specifically an increase in iNOS gene expression with metaplastic and neoplastic ECM treatment at 24h (Figure 7). Stat2, an upstream transcription factor in the IFNγ signaling pathway, was upregulated at 24h for neoplastic ECM. However, secreted IFNγ was not increased at 24h by ELISA. iNOS and Stat2 may be activating other downstream pro-inflammatory secreted products. IFNγ inducible cytokines can also be inhibited by IL-4 signaling [7], and it is possible cross talk may have occurred between the IL-4 and IFNγ pathways in the present study.

For the immunomodulatory ("M2") IL-4 signaling, metaplastic and neoplastic ECM increased THP-1 IRF4 transcription factor at 24h, but was not significant at the protein level.

How do the macrophage activation results compare to canonical tumor associated macrophage (TAM) markers? It was surprising that the neoplastic ECM activated one "M2-like" transcription factor IRF4, and increased pro-inflammatory ("M1-like") Stat2, iNOS, and TNFα gene expression and TNFα protein expression. TNFα is not a canonical TAM marker [9]. There are several possibilities for this discrepancy. The TAM response has been characterized after exposure to specific cytokines [9] or to singular ECM fragments [148, 156], but not to the isolated role of the biochemically complex ECM *in vitro* as in the present study. Evaluating the macrophage response to the ECM, alone and in combination with cytokines *in vitro*, can lead to a more complete understanding for the synergy of these signals occurring *in vivo.*

The finding that neoplastic ECM, and to a lesser degree metaplastic ECM, can activate TNFα signaling can have clinical implications. An effective "M1-like" tumor rejection therapy may be possible by changing the concentration or temporal presentation of TNFα. For example, a chronic, low dose of TNFα can promote tumor progression, but a high, concentrated TNFα dose can destroy tumor blood vessels [20].

Because ECM bioscaffolds are M2 promoting biomaterials and are being investigated as a therapy after cancer resection [30], another important question is do neoplastic ECM and

ECM bioscaffolds promote similar M2 macrophage activation markers? In the present study, we investigated UBM as a heterologous ECM control which also promotes M2-like immunomodulation and tissue remodeling [132, 169]. Neoplastic ECM and urinary bladder matrix showed distinct gene and protein expression for the pro-inflammatory pathways IFNγ, TLR-4 and immunomodulatory IL1RN markers (Figure 7). The results of the present study suggest that the two ECM are distinctive subtypes. The findings also reinforce that more than one M1 or M2 marker should be used to distinguish these subtypes.

5.6.2 Neoplastic ECM signature contains collagen type VIII alpha 1 chain, lumican, and elastin

The protein profiles of the ECM were characterized to address which components of metaplastic and neoplastic ECM could be activating macrophages. SDS-PAGE showed distinct protein profiles between the normal, metaplastic, and neoplastic ECM, specifically bands >250 kDa were absent in the metaplastic and neoplastic ECM compared to normal ECM (Figure 5). The normal and neoplastic ECM prepared in the present study shows the biochemical complexity of the native tissue is retained by quantitative and global proteomics. The increased ECM protein per dry weight measured in the neoplastic tissue is consistent with the known increased ECM deposition by fibroblasts during tumorigenesis [152]. Over 98% quantifiable proteins in the resulting normal and neoplastic ECM were COL1A 1/2 and COL5A 1/2. Collagen is one of the top increased proteins in cancer [170], and associated with increased stiffness of the matrix, which could increase integrin signaling/proliferation and activate cancer signaling pathways ERK, PFAK, and PI3K [153]. Collagen 1 has been implicated in increasing infiltration, and inhibiting macrophage polarization [153]. Macrophages could polarize to an M1 activation in the present study, despite the high expression of collagen, suggesting that the other proteins in the biochemically complex ECM are necessary for macrophage activation. Several ECM proteins

related to gastrointestinal cancers and inflammation were identified as being increased in the neoplastic ECM including but not limited to COL8A1, lumican, and elastin.

COL8A1 is a non-fibrillar, short chain collagen 60 kDa that is pepsin-resistant. It serves as a major component of the specialized ECM basement membranes; and is increased in tumorigenesis [171], including gastrointestinal cancers [172] and breast cancer [173]. Lumican is a small, leucine rich proteoglycan 90 kDa that is upregulated with chronic inflammation [152] and GI cancers [174]. Lumican is a core protein in the keratin sulfate proteoglycans (KSPG). Lumican can regulate collagen fibrillization, cell adhesion, epithelial cell migration, and macrophage attachment [174]. Finally, elastin, is important for the distensibility of the esophagus, with increased expression in the lower third of the esophagus [175]; where EAC most frequently occurs [1]. Elastin fragments recruit and elicit a TH1/M1 macrophage response [153, 176, 177], and many MMPs increased in EAC specifically target elastin [178]. Positive feedback loops may be created wherein an inflammatory response is activated and elastin further degrades [177]. Future work will determine the role of these ECM proteins to activate macrophages toward TNFα+, individually or synergistically.

5.6.3 Limitations, Future Directions, and Significance

There were limitations to the present study. Rat ECM was used for all experiments except for targeted and global proteomics wherein human ECM was used. ECM proteins are conserved across species [179-182], however the neoplastic signature identified in human (e.g., COL8A1, lumican, elastin) may be distinct from the rat neoplastic signature. The present study used solubilized ECM added to the medium of macrophages cultured in 2D, therefore only the effect of the ECM biochemical signals were investigated. The limitation of culturing cells on 2D tissue culture plastic is well understood [4, 183] and furthermore, does not evaluate ECM stiffness [152], density [152], geometries [151], and ECM fiber organization [152, 170] which play a key

role in influencing cell behavior. Two immortalized cell lines were used in the present study, the THP-1 mononuclear cell line and Het-1A esophageal epithelial cell line. In addition, other important cell types in the EAC niche including stem cells, fibroblasts, and other immune cells (neutrophils, dendritic cells, T cells, Tregs, and MDSCs), would likely be influenced by the normal, metaplastic, and neoplastic ECM.

Despite these limitations, the distinctive effect of normal, metaplastic, and neoplastic ECM upon macrophage gene and protein expression, and the paracrine effect upon an esophageal epithelial cell migration is strongly supported. Even though ECM components are known to be central to inflammation and cancer progression [148], there is a need to isolate the biochemically complex ECM and determine neoplastic ECM:cell interactions. Fractionating the ECM could further identify key ECM proteins in tumorigenesis as a reductionist approach. ECM hydrogels from decellularized cancer tissues can be prepared from a diversity of human cancer types and are compatible with 3D culture, tumor spheroids, and organ on a chip models [184].

How could the findings of the present study be applied clinically? The results suggest that TNFα is worthy of further investigation as a biomarker for metaplastic and neoplastic disease. Future work could determine the prevalence of COL8A1, lumican, and elastin in EAC biopsies as potential biomarkers. In addition, a current paradigm is to promote anti-tumor immunity by modulating macrophages from “M2” to “M1” activation for cancer treatment [10]. However, neoplastic ECM promoted M1-like TNFα activation in the present study. The results suggest that perhaps the objective should be to modulate macrophage phenotype from neoplastic ECM activation toward normal ECM activation, such as by providing normal ECM to the tumor niche. Future work can determine macrophage receptor(s) activated in response to normal, metaplastic, and neoplastic ECM to inform a more targeted approach and intervene at

ECM-macrophage receptor. The present study also supports that while current chemotherapy targets the neoplastic cells, the neoplastic ECM remains in the microenvironment and is a potent signaling molecule to consider.

5.7 CONCLUSION

Macrophages in neoplastic microenvironments and tissue regeneration both promote immunomodulatory “M2” macrophage activation [7]. However, ECM bioscaffolds have been successfully used to treat 14 esophageal cancer patients, and promoted constructive tissue remodeling, without recurrence of cancer [30]. It is therefore important to characterize the isolated role of non-malignant, metaplastic, and neoplastic ECM upon macrophage activation. The present study isolated ECM from normal, metaplastic, and neoplastic tissue and showed an increase in lumican, COL8A1, and elastin in neoplastic ECM compared to non-malignant ECM. The biochemical changes to the esophageal ECM during cancer progression are not well characterized, and these ECM proteins could be new therapeutic targets. Metaplastic and neoplastic ECM increased macrophage pro-inflammatory TNFα signaling and increased non-malignant epithelial cell migration *in vitro*. Contrary to our hypothesis, neoplastic ECM did not promote “M2”-like anti-inflammatory gene and protein expression. The results of the present study support further investigation for an esophageal cancer therapy that downregulates pro-inflammatory TNFα+ signaling, possibly by providing non-malignant esophageal ECM to the tumor niche.

6.0 BIOACTIVE COMPONENTS OF NORMAL, METAPLASTIC, AND NEOPLASTIC ECM

6.1 HYPOTHESIS

Neoplastic ECM had a distinctive biochemical protein profile (COL8A1, lumican, elastin) and increased macrophage TNFα signaling compared to non-malignant ECM (Chapter 5.0 It was hypothesized that bioactive components of neoplastic ECM could be identified that can recapitulate the effects of the parent neoplastic ECM. First, it was hypothesized that matrix-bound nanovesicle (MBV) isolated from non-malignant, metaplastic, and neoplastic ECM will have distinctive miRNA cargo functionally related to esophageal cancer progression. Second, it was hypothesized that neoplastic ECM can be fractionated by molecular weight as a strategy to identify enriched proteins that can recapitulate the macrophage TNFα+ signature.

6.2 INTRODUCTION

Solubilized metaplastic and neoplastic esophageal ECM progressively increased TNFα+ signaling in macrophages *in vitro (*Figure 7*)*. The results led us to ask the question: What are the bioactive component(s) in the metaplastic and neoplastic ECM that are influencing macrophage phenotype? Two possibilities explored in the present chapter are 1) the recently described, matrix-bound nanovesicle (MBV) cargo, and 2) the composition of ECM proteins.

MBV are a type of lipid-protected extracellular vesicle, sized 30-1000 nm, secreted by cells that contain miRNA and proteins such as cytokine-chemokine cargo [6]. The primary distinguishing characteristic of MBV from other extracellular vesicles, such as exosomes, is the medium of residence: exosomes are secreted into biologic fluids (e.g., saliva, plasma, cerebrospinal fluids) [185], while MBV are secreted and embedded within matrix fibers [6]. MBV can recapitulate the effects of the solubilized ECM, including differentiation of neural stem cells [6] and “M2-like” activation of macrophages [138]. Separate from the established mechanisms by which ECM influences cell behavior (e.g., ECM ligand presentation, released growth factors, and mechanical properties), it is plausible MBV represent a primary mechanism by which ECM influences cell behavior locally. MBV can be isolated by differential ultracentrifugation [6] similarly to extracellular vesicles [185], but with the additional first step of enzymatic digestion (e.g., collagenase) to loosen the ECM fibers and liberate the MBV.

In Chapter 5.5.3 we showed activation of macrophages using ECM isolated from a rat model of EAC. Targeted and global proteomics identified COL8A1, elastin, and lumican overexpressed in human neoplastic ECM samples compared to normal ECM samples.

Herein we characterized the miRNA profile of non-malignant, metaplastic, and neoplastic ECM. Macrophages were exposed to normal, metaplastic, and neoplastic ECM isolated from human tissue to validate the activation results seen with rat ECM. The human normal, metaplastic, and neoplastic ECM samples were fractionated by molecular weight to identify a fraction that could recapitulate the TNFα signature. This chapter details the interim conclusions of these studies.

6.3 MATERIALS AND METHODS

6.3.1 MBV miRNA profile

MBV were isolated from ECM with the intent to extract RNA for small RNA sequencing as previously described [6]. The normal, metaplastic, and neoplastic powdered ECM (10 mg/mL) was digested with collagenase from *Clostridium histolyticum* (1 mg/mL, Sigma-Aldrich) for 24 h to release the MBV trapped within the ECM fibers. A graded series of centrifugation steps (500 g for 10 min, 2500 g for 20 min, and 10,000 g for 30 min, two times each at 4°C) was performed to remove ECM fibril remnants, followed by an ultracentrifugation step (100,000 g for 1 hr at 4°C) to concentrate the MBV into a pellet. The MBV were re-suspended in PBS and treated with RNAse A (1:100, Qiagen) at 37°C for 20 min to remove RNA attached to the surface of the MBV, i.e., residual RNA contaminants from the decellularization process. MBV were lysed, and RNA was extracted using a commercial kit (SeraMir, System Bioscience), in brief involving RNA purification steps on columns. The normal, metaplastic, and neoplastic MBV RNA was submitted to the RNA sequencing core to be run on a size exclusion gel (<100 nt) to purify miRNA for small RNA sequencing (Ion Torrent Xpress).

The small RNA sequencing results yielded “reads” that were extracted, trimmed by the adapter sequences, annotated using the rat miRNome (miRBase v21) and merged counts to identify conserved miRNA sequences. The total reads for each miRNA in metaplastic and neoplastic ECM MBV were normalized to “normal" ECM MBV miRNA. To visualize the biological variation of miRNA signatures across the normal, metaplastic, and neoplastic ECM, the fold change miRNA reads (neoplastic:normal, metaplastic:normal) were log2 transformed; centered on the median; normalized by the standard deviation; clustered using an unsupervised hierarchical clustering program (Cluster 3.0), with Euclidean distance as the similarity metric and average linkage as the clustering method [186]; and visualized as a heat map (Java

TreeView). Ingenuity Pathway (IPA) functional analysis was performed on the differentially regulated miRNA.

6.3.2 Human normal, metaplastic, and neoplastic ECM

Human normal, metaplastic, and neoplastic esophageal tissues were decellularized and solubilized as described in Chapter 5.4.1, and macrophages were treated as described in Chapter 5.4.3 with rat ECM. The ECM samples used are listed in Table 6.

6.3.3 Fractionation

The ECM samples used for the biological replicates re listed in Table 6. ECM was neutralized to 5 mg/mL. 50 uL of ECM was used for the fractionation by molecular weight. Each ECM type (normal, metaplastic, and neoplastic) had three molecular weight cut-off columns (VivaSpin 500): 3 kDa, 10 kDa, and 30 kDa for n1 and n2, and 3 kDa, 30 kDa, and 50 kDa for n3. Samples were spun at 15,000 g for 20 minutes at 4°C. After centrifugation, retentate and flow through were collected in separate tubes and reconstituted to the original volume (50 uL) with cold PBS. THP-1 macrophages were treated with the fractions.

Table 6. ECM used for human cancer ECM and fractionation experiments.
The numbers in the table refer to individual patient samples. Samples were "patient matched" when possible such as "N1"; and "N3" and "N4" samples were combinations of samples that were patient matched. "N2" was not patient matched.

		Normal	Metaplastic	Neoplastic
Human Cancer ECM	N1	925	BE-1	925
	N2	397	BE-1	928
	N3	648, 925, 1011	BE-1	648, 925,1011
	N4	948, 925	BE-1	948, 925
Fractionation	N1	925	BE-1	925
	N2	397	BE-1	928
	N3	648, 925, 1011	BE-1	648, 925, 1011

6.3.4 TNFα ELISA

TNFα ELISA was performed on the macrophage conditioned media after 24h treatment as described in Chapter 5.4.3.2.

6.4 RESULTS

6.4.1 MBV miRNA profile

miRNA isolated from MBV are in the size range of 25-100 nt, as expected (Figure 10A). The miRNA from metaplastic and neoplastic ECM MBV were normalized to normal ("non-malignant") MBV miRNA (Figure 10B), and showed striking fold change differences between groups. Pathway analysis on the differentially regulated metaplastic and neoplastic MBV miRNA notably identified epithelial-mesenchymal transition (EMT) (Notch and TGFβ1-mediated), cancer, and inflammatory disease and inflammatory response among the top networks, pathways, and

functions (Figure 10C). Functional analysis of miRNA involved in the “inflammatory response,” specifically “M1 activation of macrophages,” showed opposite regulation of let-7 miRNA in metaplastic and neoplastic ECM MBV (Figure 10D).

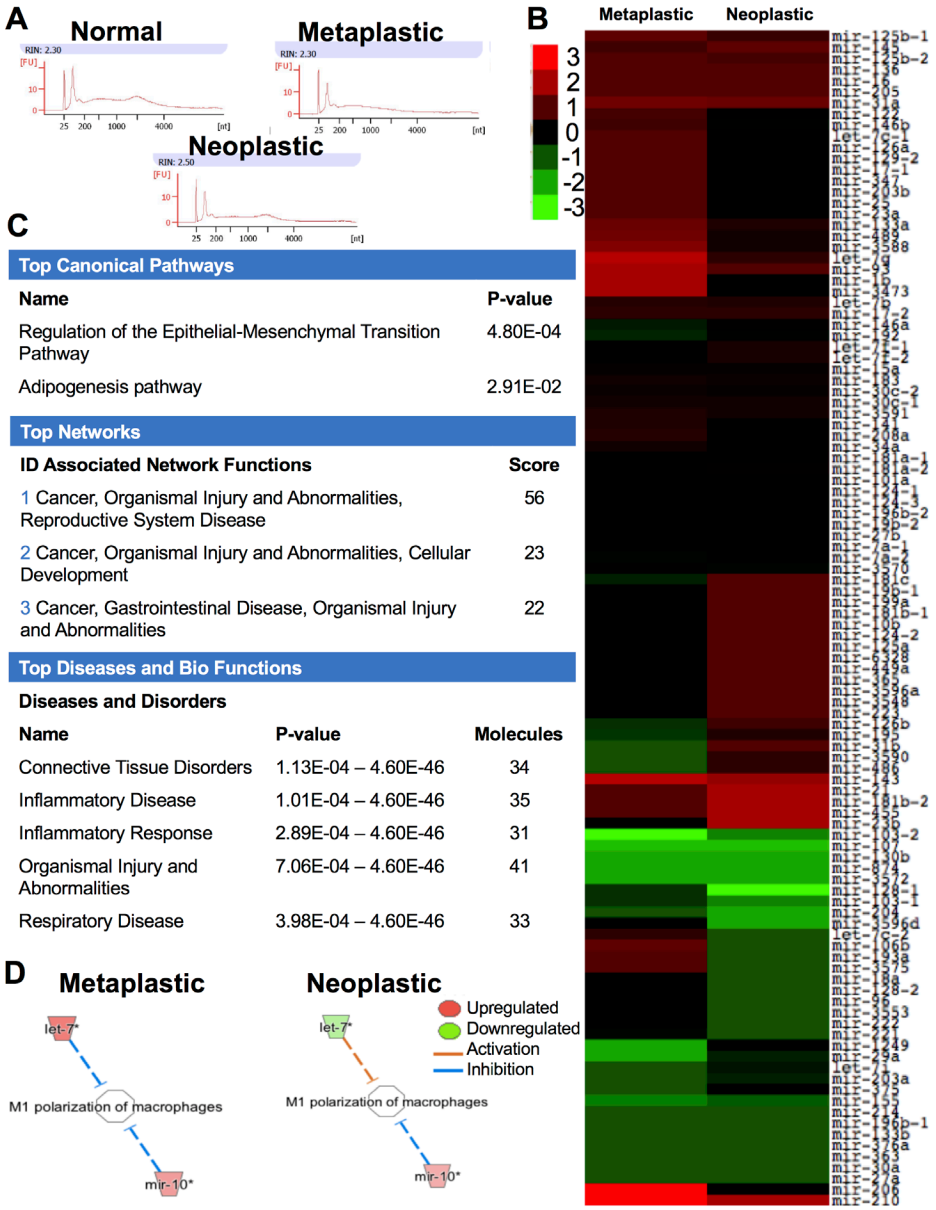

Figure 10. Non-malignant, metaplastic, and neoplastic MBV miRNA profile and functional analysis.
(A). MBV miRNA bioanalyzer results. (B) Heat map of differentially regulated miRNA for metaplastic and neoplastic ECM MBV, fold change relative to normal. (C) MBV miRNA functional analysis of top pathways, networks, and functions. (D). “Macrophage activation” is a top function of MBV miRNA.

6.4.2 TNFα activation of THP-1 macrophages by human normal, metaplastic, and neoplastic ECM

Human neoplastic ECM corroborated the results of the rat neoplastic ECM, showing an increase in THP-1 TNFα expression compared to media control by ELISA (Figure 11). Metaplastic ECM showed an increase in TNFα expression compared to media control in 2 of the 4 samples, however, because of the limited availability of Barrett's tissue, only 1 biological patient source was obtainable.

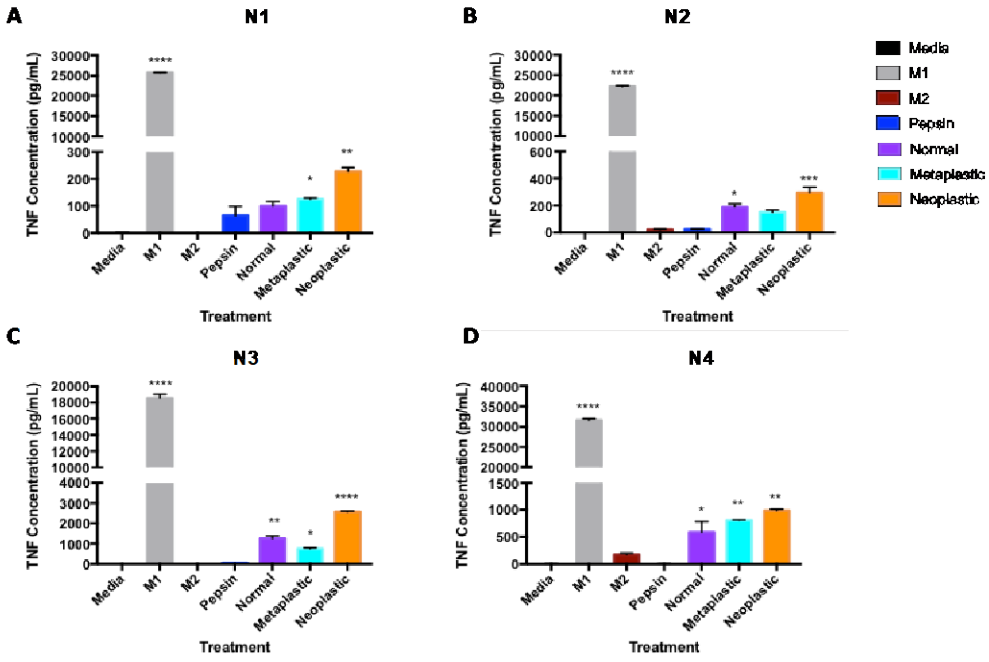

Figure 11. TNFα activation of THP-1 macrophages with human normal, metaplastic, and neoplastic ECM.
A human mononuclear cell line (THP-1) was activated to naïve macrophages (M0). The M0 macrophages were treated with human normal, metaplastic, and neoplastic ECM hydrogels (250 ug/mL) or positive controls for M1-like activation (LPS/IFNγ) and M2-like activation (IL4) or negative controls (pepsin, medium) for 24 hours. The human normal and neoplastic ECM was isolated from 4 patients (n1-4), and only one metaplastic Barrett's sample was available and tested for n1-4. ELISA for TNFα was performed. * $p < 0.05$, ** $p < 0.01$, *** $p < 0.005$, **** $p < 0.0001$. Values are expressed as mean ± SD.

6.4.3 TNFα activation of THP-1 Macrophages by Fractionated human normal, metaplastic, and neoplastic ECM

The human normal, metaplastic, and neoplastic ECM were fractionated by 3 cut-off columns in the range of 3-50 kDa, where the retentate (“R”) and flow-through (“F”) were used to treat THP-1 macrophages, and THP-1 TNFα expression was measured by ELISA (Figure 12).

The “whole” ECM recapitulated the signature shown with the human ECM for n1 and n3 (i.e., neoplastic ECM showed the increased activation of TNFα compared to media). The neoplastic 3R and 30R fractions showed consistently high TNFα expression compared to media across the three biological replicates, and will be tested by mass spectrometry for enriched ECM proteins and protease remodeling.

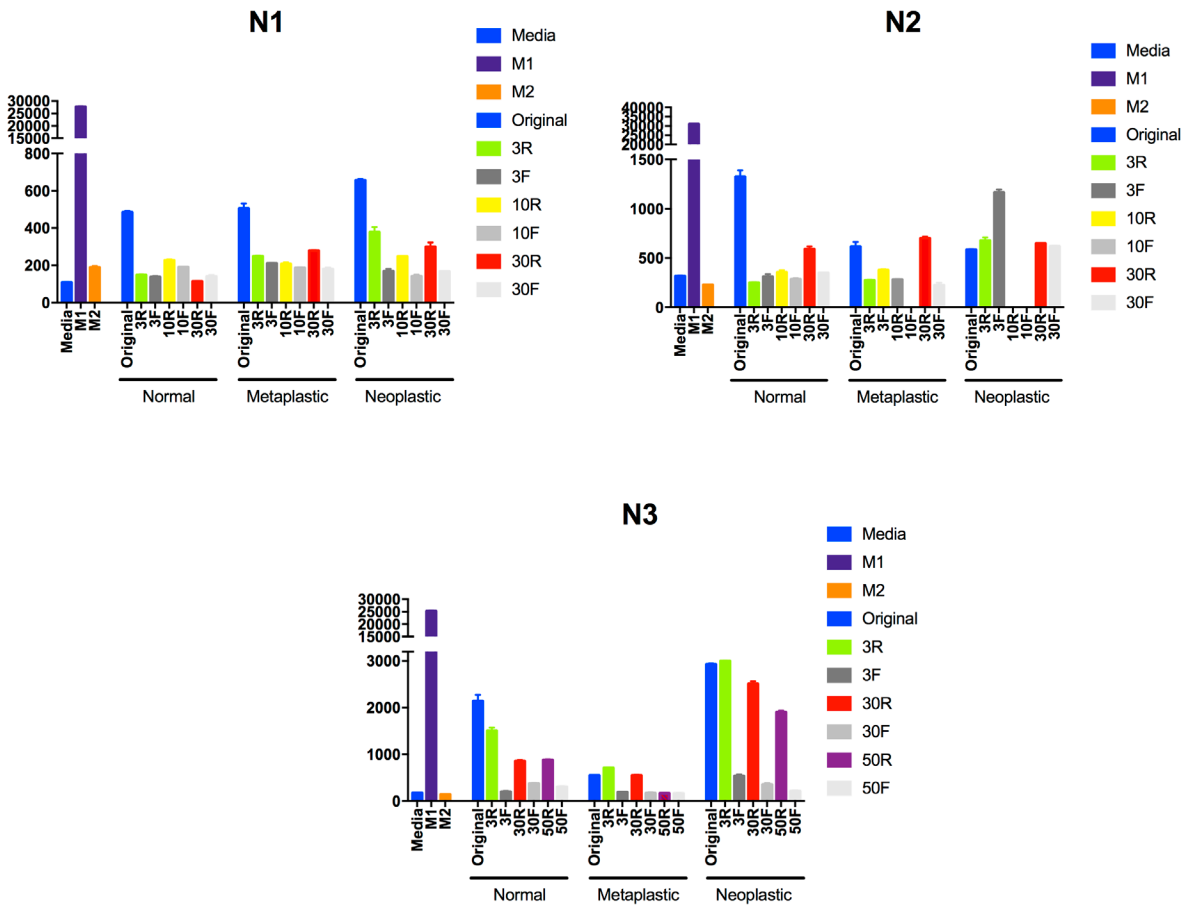

Figure 12. TNFα activation of THP-1 macrophages by fractions of normal, metaplastic, and neoplastic ECM.
A human mononuclear cell line (THP-1) was activated to naïve macrophages (M0). The M0 macrophages were treated with fractionated human normal, metaplastic, and neoplastic ECM hydrogels (250 ug/mL) or positive controls for M1-like activation (LPS/IFNγ) and M2-like activation (IL4) or negative controls (pepsin, medium) for 24 hours. Fractions were prepared with cut-off columns in the range of 3-50 kDa. ELISA for TNFα was performed. * p< 0.05, ** p< 0.01, *** p< 0.005, **** p<0.0001. Values are expressed as mean ± SD.

6.5 DISCUSSION

ECM composition and ultrastructure is known to change with neoplastic progression [4] in breast [187, 188], brain [189], ovary [190-193], and esophagus [194-196]. It was shown In Chapter 5.0 that metaplastic and neoplastic ECM isolated from decellularized esophageal tissue activated macrophages toward a pro-inflammatory, TNFα+ state. Because ECM represents a complex mixture of proteins, bound growth factors, and cryptic peptide sequences, there are likely multiple bioactive components of the matrix that are directing cell behavior acting synergistically. To start addressing which of these components could be a main effector of the observed phenotype, two likely candidates were investigated: matrix-bound nanovesicle cargo including miRNA, and composition. Identifying the component(s) could identify a potential signaling microenvironment-mediated mechanism and inform novel therapeutic treatments for the esophagus.

miRNA are potent post-transcriptional regulators of gene expression that are often dysregulated in tumorigenesis [197]. The present study showed the presence of extracellular miRNA, protected and embedded within the matrices, that can target key EAC signaling pathways. For example, let-7 targets TLR-4 and IL-4 pathways [198], and miR-10 targets TLR-4 [199]. TLR-4 and IL-4 were two of the intracellular pathways shown to be activated by macrophages exposed to neoplastic ECM (Chapter 5.5.3), further suggesting the potential importance of the MBV miRNA in ECM-mediated EAC progression. Metaplastic and neoplastic MBV miRNA would be a new therapeutic target or biomarker.

Future work will determine the functional relevance of non-malignant, metaplastic and neoplastic MBV upon candidate cell types in the tumor niche including THP-1 macrophage

activation (TNFα+), Het-1A epithelial cell expression of epithelial-mesenchymal transition (EMT) markers (Vimentin, Twist) and disease markers (normal, Barrett's, EAC), and primary-derived fibroblasts expression of ECM proteins upregulated in neoplastic ECM (COL8A1, lumican, and elastin). It is hypothesized that the neoplastic MBV would induce tumorigenic-like behavior in the respective cell types (increased TNFα+, increased mesenchymal/esophageal adenocarcinoma markers, increased production of ECM proteins). Optimization experiments performed to date are listed in Appendix C.

Future work will also identify the relevance of the 30R and 3R ECM fractions activating THP-1 cells toward TNFα+. The 30R and 3R ECM fractions could identify enriched ECM proteins, and the secretome of macrophages exposed to the ECM fraction could identify increased MMP and cryptic peptide sequences. It is hypothesized that COL8A1, lumican, and elastin will be enriched in these bioactive fractions, and that these proteins will be remodeled by specific MMPs secreted by macrophages. Future work will also test the effects on non-transformed primary macrophages because the THP-1 cells used in the present study are a cell line.

The interim results and plans for future work (Appendix C) present a working model hypothesis as shown in Figure 13. In this model, COL8A1, lumican, and elastin are all components of non-malignant esophageal ECM. Upregulated MMP production during neoplastic progression remodels the matrix, which produces cryptic peptides and also releases MBV. The cryptic peptides induce macrophage TNFα+ activation, inducing more MMP expression, more cryptic peptide creation, and perpetuates in a positive feedback loop. The MBV induce fibroblasts to secrete increased amounts of lumican, elastin, and COL8A1.

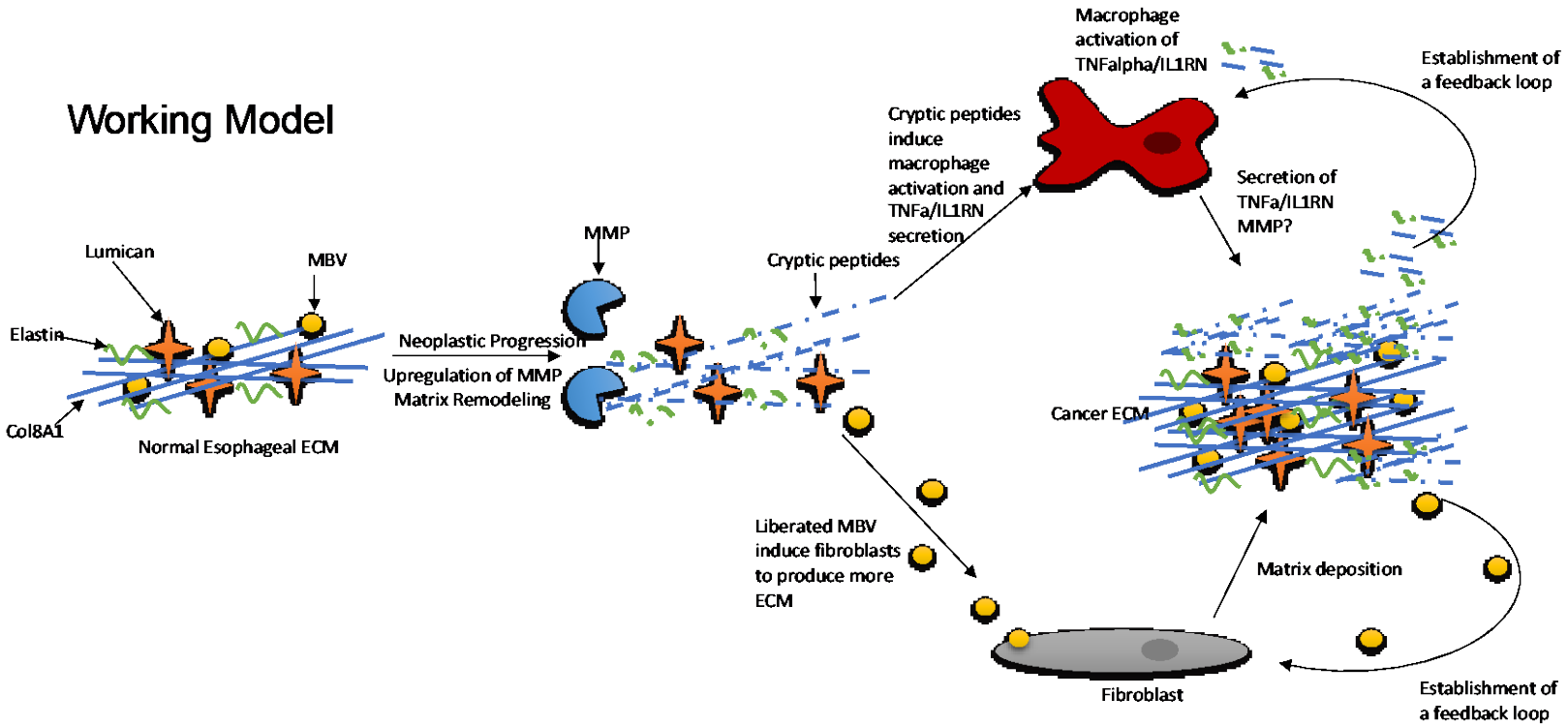

Figure 13. Working hypothesis of normal, metaplastic, and neoplastic MBV
COL8A1, lumican, and elastin are all components of non-malignant esophageal ECM. Upregulated MMP production during neoplastic progression remodels the matrix, which produces cryptic peptides and also releases MBV (in yellow). The cryptic peptides induce macrophage TNF+ activation, inducing more MMP expression, more cryptic peptides, in a positive feedback loop. The MBV induce fibroblasts to secrete increased amounts of lumican, elastin, and COL8A1.

6.6 CONCLUSION

The results show that extracellular miRNA, protected within MBV and embedded within the metaplastic and neoplastic matrix, target key signaling pathways involved in esophageal cancer progression and immune cell activation. Differentially regulated miRNA in metaplastic and neoplastic MBV, including let-7 and miR-10, should be further investigated as novel therapeutic targets, distinct from the commonly characterized intracellular miRNA. The present study confirmed the macrophage TNFα+ signature in human ECM, similarly to rat ECM in Chapter 5.0 , suggesting that the neoplastic ECM signaling molecules are conserved across species. The human ECM was fractionated by molecular size, and the 3R and 30R fractions increased macrophage TNFα expression. The 30R and 3R fractions will be further characterized to identify specific proteins that can activate macrophages toward TNFα+ and provide a mechanism for the observed *in vitro* results.

6.7 ACKNOWLEDGEMENTS

This study, including the progress in the Appendix, is in progress and acknowledges the contributions of the following people: Dr. Xue Li, Dr. Lina Quijano, Dr. Jonas Erikkson, Dr. Luai Huleihel, Dr. George Hussey, Dr. Ali Zaidi, Dr. Blair Jobe, Ashten Omstead, Dr. Alejandro Nieponice, Dr. Ryan Hill, Dr. Kirk Hansen, and Dr. Stephen F. Badylak.

7.0 ECM DOWNREGULATES NEOPLASTIC ESOPHAGEAL CELL PHENOTYPE[3]

7.1 HYPOTHESIS

ECM isolated from different stages of disease distinctively activated macrophage phenotype and influenced epithelial cell behavior to behave like a neoplastic cell (Chapter 5.0). It was hypothesized that the converse would also be true, i.e., solubilized non-malignant ECM would downregulate neoplastic epithelial cell function and cancer signaling pathways, while having a minimal effect on non-malignant cells based upon dynamic reciprocity.

---

[3] Portions of this chapter were adapted from the following manuscript:

L.T. Saldin, S. Patel, L. Zhang, L. Huleihel, G. S. Hussey, D.G. Nascari, L.M. Quijano, X. Li, D. Raghu, A.K. Bajwa, N.G. Smith, C.C. Chung, A.N. Omstead, J.E. Kosovec, B.A. Jobe, N.J. Turner, A.H. Zaidi, S.F. Badylak, Extracellular matrix degradation products downregulate neoplastic esophageal cell phenotype, Tissue Eng A, 2018.

7.2 ABSTRACT

Extracellular matrix (ECM) bioscaffolds have been successfully used to treat 5 esophageal adenocarcinoma (EAC) patients following resection of neoplastic mucosal tissue. The present study evaluated the *in vitro* effect of ECM harvested from non-malignant, decellularized tissue on EAC cell phenotype to understand the molecular mechanisms underlying the clinical findings. Non-malignant (Het-1A), metaplastic (CP-A), and neoplastic (SK-GT-4, OE33) esophageal epithelial cells were exposed to ECM degradation products (250 ug/mL) prepared from heterologous urinary bladder tissue or homologous esophageal mucosa tissue, and evaluated for cell morphology, cell function, and EAC signaling pathways. The two ECM sources both downregulated neoplastic cell phenotype, but had distinctive tissue-specific effects. Urinary bladder ECM decreased OE33 and SK-GT-4 metabolism and increased CP-A apoptosis. Esophageal ECM decreased SK-GT-4, CP-A, and Het-1A proliferation; robustly downregulated PI3K-Akt-mTOR, cell cycle/DNA replication signaling and upregulated autophagy signaling in OE33 cells; and increased cell cycle/DNA replication signaling in Het-1A cells. Both ECM sources decreased OE33 proliferation, decreased phosphorylated AKT in OE33 cells; and in contrast, increased phosphorylated AKT in Het-1A cells. The results support the concept that the biochemical signals in non-malignant ECM can downregulate neoplastic cell phenotype with minimal, and sometimes opposite, effects on normal cells. PI3K-Akt signaling has been implicated in EAC progression and these ECM-mediated effects may be favorable for an esophageal therapy following cancer resection.

7.3 IMPACT STATEMENT

Extracellular matrix (ECM) biomaterials were used to treat esophageal cancer patients after cancer resection and promoted re-growth of normal mucosa without recurrence of cancer. The present study investigates the mechanisms by which these materials were successful to prevent the cancerous phenotype. ECM downregulated neoplastic esophageal cell function (proliferation, metabolism), but normal esophageal epithelial cells were unaffected *in vitro*, and suggests a molecular basis (downregulation of PI3K-Akt, cell cycle) for the promising clinical results. The therapeutic effect appeared to be enhanced using homologous esophageal ECM. This study suggests that ECM can be further investigated to treat cancer patients after resection or in combination with targeted therapy.

7.4 INTRODUCTION

Biologic materials composed of extracellular matrix (ECM) [59, 200], or individual components of ECM such as collagen [201, 202] or hyaluronan (HA) [203] have been successfully used in every body system for the repair and reconstruction of injured tissues. However, such materials have been used only sparingly in the gastrointestinal tract. The ECM is composed of natural secreted products of the resident cells of each tissue and organ and constitutes the solid component of every cell's microenvironmental niche. The ECM is a potent regulator of cell homeostasis, proliferation, migration, differentiation, and spatial organization or patterning.

Abnormal or dysregulated cell phenotype can be mitigated by exposure to ECM or components of ECM harvested from normal tissues [30, 34-40]. The pathogenesis of gastroesophageal reflux disease (GERD) with progression to metaplastic Barrett's esophagus (BE) and esophageal adenocarcinoma (EAC) is well established [204]. Microenvironmental

changes induce progressively more severe changes in cell phenotype and culminate in EAC [17], a disease with a 20% 5-year survival regardless of therapy [205].

Preclinical studies [27-29, 32, 33, 41, 206] and a cohort study of five patients [30] show that placement of a xenogeneic ECM bioscaffold at the site of long-segment, full circumferential resection of the esophageal mucosa and submucosa facilitated the restoration of a near normal esophageal mucosa, with preservation of esophageal structure and function, and without clinically significant stricture. The 5 patient cohort had T1A EAC before resection and placement of the ECM bioscaffold [30], and are still 7-8 years cancer-free. The ECM bioscaffold completely degraded within 2 weeks, suggesting the matrix was not required to be physically present long-term for effective results, but rather the bioinductive cues of the native matrix or matrix degradation products influenced cell phenotype in the post-tumor resection niche. The results are consistent with “dynamic reciprocity:” a bi-directional crosstalk between a cell and its surrounding matrix to influence cell behavior [5]. The molecular mechanisms by which the embedded signaling molecules of the ECM influence cell behavior are only partially understood. A more complete understanding of these mechanisms may allow more targeted therapy with ECM-based materials.

The objective of the present study was to determine the response of normal, metaplastic, and neoplastic esophageal epithelial cells to the degradation products of ECM harvested from porcine homologous (site-specific) esophageal mucosa ECM (eECM) and heterologous (non site-specific) urinary bladder matrix (UBM-ECM). Biologic scaffolds composed of allogeneic and xenogeneic ECM have been successfully used in a variety of clinical applications and have involved both homologous and heterologous tissues [207]. These materials have been manufactured by a variety of methods and all consist of a large number of structural and functional molecules such as collagen, laminin, fibronectin, glycosaminoglycans, and various cytokines and chemokines [207]. The heterologous UBM-ECM and homologous eECM materials used in the present study are comprised of similar molecular species, although

the protein compositions would likely be distinct between tissue sources [33]. We hypothesized that pepsin-digested degradation products of UBM-ECM and eECM would have the potential to normalize neoplastic cell behavior and cancer signaling pathways, and that the homologous eECM would provide a more pronounced downregulation of neoplastic cell behavior compared to heterologous UBM-ECM. Outcome measures included cell phenotype; cell function including proliferation, metabolism, and apoptosis; and key cancer signaling pathways involved in EAC progression.

7.5 MATERIALS AND METHODS

7.5.1 ECM degradation products

Urinary bladder matrix (UBM-ECM) and esophageal mucosa ECM (eECM) were decellularized from porcine tissues using tissue-specific protocols to meet criteria of decellularization as previously described [42, 62]. ECM (10 mg/mL) was solubilized using pepsin (1 mg/mL) in 0.01 M HCl for 48 h [62] as previously described. Pepsin control (1 mg/mL) was similarly prepared without the addition of ECM.

7.5.2 SDS-PAGE with silver stain

Pepsin-digested UBM-ECM, eECM and pepsin control proteins were separated by gel electrophoresis and stained using silver stain as detailed in Supplementary Methods (D.1.1).

7.5.3 Cell culture and ECM treatment

Het-1A is an immortalized non-malignant “normal” esophageal epithelial cell line and CP-A is an immortalized non-dysplastic, metaplastic Barrett’s esophageal epithelial cell line, both obtained from American Type Culture Collection (ATCC). Cells were cultured according to manufacturer’s guidelines and the media supplemented with 1% penicillin/streptomycin. OE33 and SK-GT-4 are immortalized EAC epithelial cell lines (Sigma-Aldrich), and were cultured according to manufacturer’s guidelines.

Cells were seeded at 70% confluency for experiments: Het-1A (400,000 cells/well), CP-A (250,000 cells/well), SK-GT-4 (200,000 cells/well), or OE33 (250,000 cells/well) in 6 well plates; or scaled appropriately for 96 well plates.

Cells were treated with media supplemented with UBM-ECM (250 ug/mL), eECM (250 ug/mL), or pepsin control (25 ug/mL) for 24h for the cellular assays, unless otherwise noted.

7.5.4 Cell morphology

Brightfield micrographs were taken of 6 well plates after 6, 24, and 48 h of treatment. Live cell time-lapse microscopy was used to visualize the cell bridges over a period of 18 hours after treatment, with a picture taken every 20 minutes. Immunolabeling was performed on the fixed OE33 cancer cell bridges for actin, and immunolabeling was performed for tubulin overlaid with differential interference contrast (DIC) microscopy after 24h of culture to determine the bridge biochemical content as described in Supplementary Methods (D.1.2).

7.5.5 Proliferation

Cell proliferation was quantified with a 5-bromo-2-deoxyuridine (BrdU) colorimetric immunoassay based on manufacturer's guidelines (Roche) in 96 well plates. Each assay was performed in technical quadruplicates, and representative graphs of the biological replicates (n=3) are shown.

7.5.6 Metabolism

Cell metabolic activity was assayed with the Vybrant MTT colorimetric assay according to manufacturer's instruction (Thermo Fisher) for the MTT Quick Protocol Option in 96 well plates. Each assay was performed in technical quadruplicates, and representative graphs of the biological replicates (n=3) are shown.

7.5.7 Apoptosis

Flow cytometry was performed to determine the percentage of early and late apoptotic cells after ECM treatment using Annexin V/Propidium iodide (PI) staining in 6 well plates (n=3) as detailed in Supplementary Methods (D.1.3).

7.5.8 Gene expression

Het-1A cells and OE33 cells were seeded in 6 well plates and 24h after treatment cells were collected in TRIzol (Invitrogen), with technical duplicates (n=3). RNA was isolated using the RNeasy Mini Kit (Qiagen) according to manufacturer's instructions. RNA concentration and

purity were measured with the NanoDrop 1000. Gene expression was determined by whole transcriptome analysis and qPCR as described in the following sections.

7.5.8.1 Whole transcriptome analysis

RNA was prepared for whole transcriptome analysis using the Human Clariom S Pico array as detailed in Supplementary Methods (D.1.4). Differentially expressed genes (>2 or <-2 fold change, $p < 0.05$) were analyzed with the Affymetrix Transcriptome Analysis Console Pathway software. Six pathways were selected for further analysis based upon the following criteria: 1) Within the top 15 signaling pathways of OE33 cancer cells treated with UBM-ECM or eECM, and 2) related to the functional changes tested (i.e., proliferation, metabolism, apoptosis) and/or EAC tumorigenesis. Treeview was used to generate heat maps for the differentially expressed genes grouped by top signaling pathways.

7.5.8.2 Selection of candidate genes and validation by qPCR

The biological function of the differentially expressed genes associated with the selected signaling pathways are shown in Supplementary Table 10. Thirty candidate genes across the 9 signaling pathways consistent with the hypothesis were selected for validation by qPCR. Genes were excluded if ECM treatment changed the normal and neoplastic cell in the same direction, unless the relative fold change between the normal and neoplastic cell was >2 or <-2. Primer sequences are shown in Supplementary Table 11 and primers were optimized as detailed in Supplementary Methods (D.1.5). RNA was transcribed to cDNA (Invitrogen cDNA RT Kit), and qPCR was performed using SYBR Green Master Mix (Bio-RAD) in technical duplicates (n=3). Results were analyzed by the $\Delta\Delta$Ct method, and normalized to housekeeping gene *ACTB*. Fold change were calculated for each treatment compared to pepsin control.

7.5.9 Western immunoblotting

Detailed methods are provided in Supplementary Methods (D.1.6) for the collection of OE33 and Het-1A cell lysates at 0, 6, and 24h and Western Immunoblotting for pAKT, AKT, and ACTB. The experiment was performed for n=2 independent lysates and technical duplicates. Representative images are shown.

7.5.10 Statistical analysis

Functional data sets were analyzed with a one-way analysis of variance (ANOVA) with post hoc Tukey test using GraphPad Prism 7.0 statistical software (GraphPad Software, Inc., San Diego, CA). Data are reported as the mean ± standard deviation. Whole transcriptome statistics was performed by the Affymetrix Transcriptome Analysis Console software using one-way between-subject ANOVA (unpaired) based on the gene level intensities (bi-weight average signal (log2)). qPCR gene expression data was log 2 transformed and one-way analysis of variance was performed, with Sidak multiple comparisons test. Significance was determined using the 95% confidence interval and p-values were adjusted for the multiple comparisons.

7.6 RESULTS

7.6.1 UBM-ECM and eECM show similar but distinctive protein compositions

The protein profiles of the soluble fraction of UBM-ECM and eECM were largely similar, but also showed distinctive bands such as those present at ~ 60 kDa for eECM and at ~65 kDa for UBM-ECM (Supplementary Figure 45).

7.6.2 ECM degradation products promote morphologic changes in neoplastic cells

Cell morphology did not change after 6h of treatment (Supplementary Figure 46A), but OE33 cells treated with UBM-ECM and eECM showed markedly reduced confluency after 24h of treatment compared to pepsin control (Figure 14A). Upon closer inspection, the OE33 and SK-GT-4 cells showed a striking morphologic change after ECM treatment with the appearance of "cell bridges" at 24h (Figure 14B) which were absent in the pepsin control and Het-1A and CP-A cells (Supplementary Figure 48B). The cell bridges had a membranous appearance and served as a physical connection between cells, as shown by brightfield microscopy and differential interference contrast (DIC) microscopy. These bridges typically had a length of several cell diameters (Figure 14B). The cellular bridges did not stain positive for actin (Supplementary Figure 48D) or tubulin (Figure 14B).The cell bridges were transient, forming and re-forming between groups of cells, and lasting on the order of minutes-hours, as shown by the time-lapse microscopy video of the cell bridge formation in OE33 cells treated with UBM-ECM (Supplementary Movie). OE33 cells treated with UBM-ECM and eECM for 48h showed a reduced confluency compared to pepsin control, similarly to 24h, with little change in the Het-1A or CP-A cells. SK-GT-4 cells also showed a slightly reduced confluency with UBM-ECM and eECM treatment compared to pepsin at 48h (Supplementary Figure 46C).

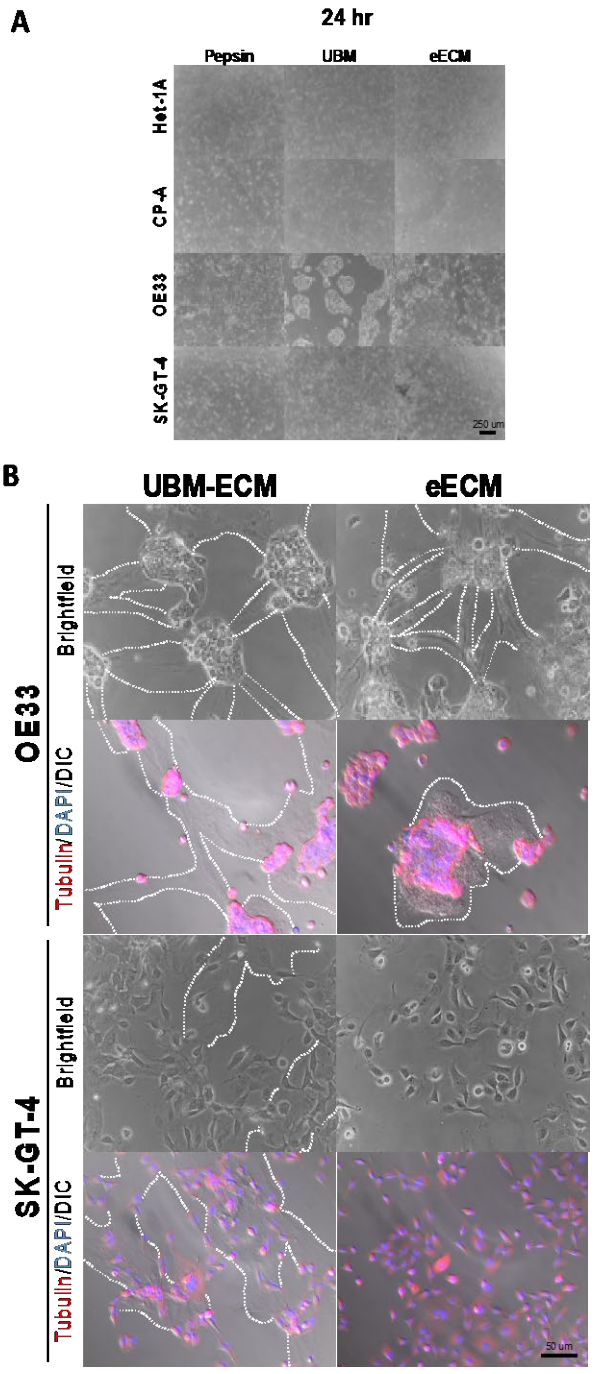

Figure 14. Cell morphology.
OE33 cells showed reduced confluency with UBM-ECM and eECM treatment compared to pepsin control, while Het-1A, CP-A, and SK-GT-4 cells showed no change after 24h. Scale bar = 250 um (**A**). OE33 cells form bridges with UBM-ECM and eECM treatment and SK-GT-4 cells form bridges with UBM-ECM treatment (**B**), visible with brightfield and differential interference contrast (DIC) microscopy at 24h. Bridges are outlined with white dotted lines. The bridges do not stain positively for cytoskeletal marker tubulin. Pictures shown are representative brightfield micrographs after 24h of treatment. Scale bar = 50 um**.**

7.6.3 UBM-ECM decreases OE33 cell proliferation; eECM decreases normal, metaplastic, and neoplastic cell proliferation

UBM-ECM decreased the proliferation of OE33 cancer cells compared to pepsin control ($p=0.0008$), but showed no change in proliferation compared to pepsin control for Het-1A, CP-A, or SK-GT-4 cells. eECM decreased proliferation of all cell types compared to pepsin control: Het-1A ($p<0.0001$), CP-A ($p<0.0001$), OE33 ($p=0.0003$), and SK-GT-4 ($p<0.0001$) (Figure 15A). Comparing ECM tissue types, eECM significantly decreased proliferation of all cell types compared to UBM-ECM for Het-1A ($p<0.0001$), CP-A ($p<0.0001$), and SK-GT-4 ($p<0.0001$). There was no difference between eECM and UBM-ECM to decrease OE33 proliferation (Figure 15A).

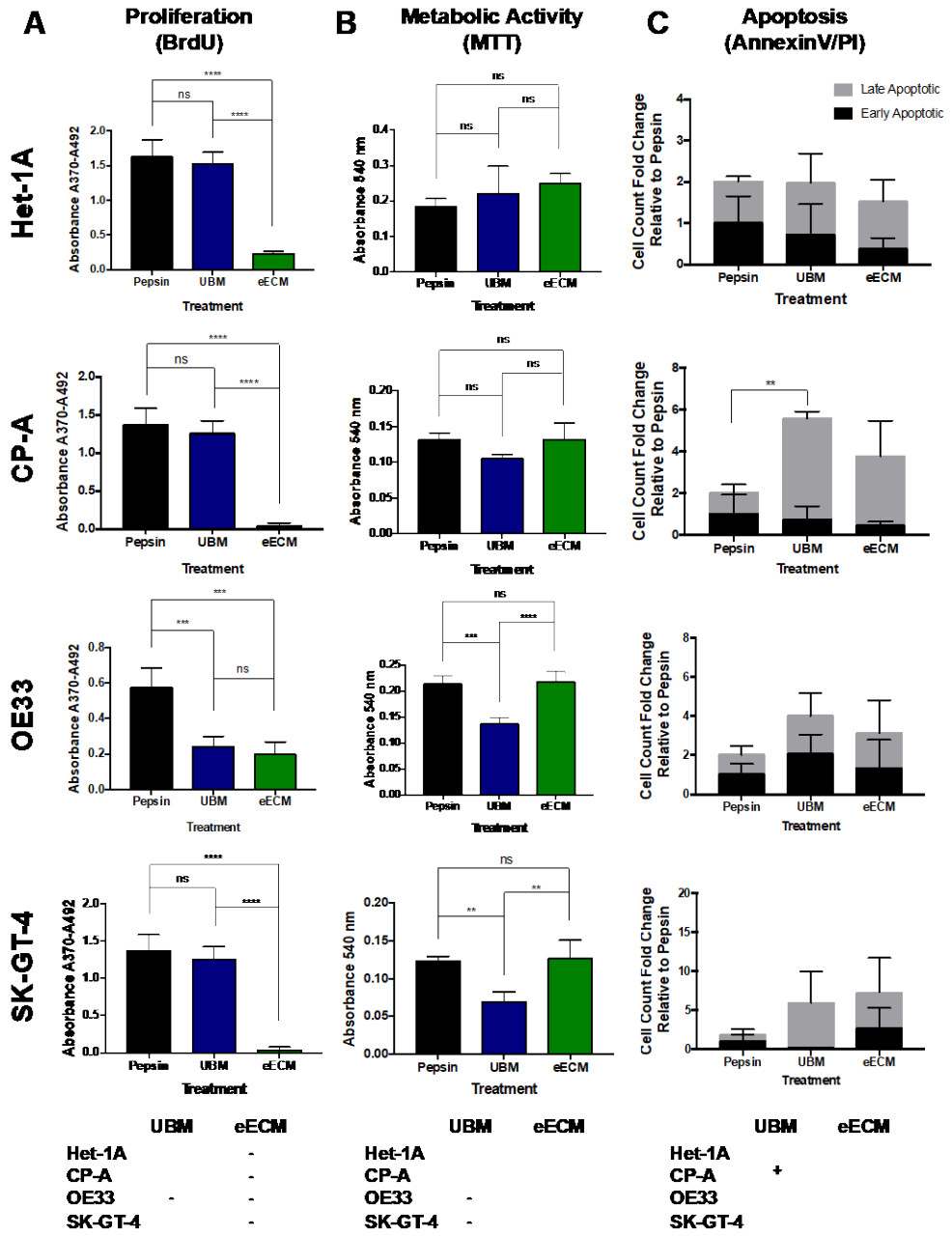

Figure 15. Cell function.
Het-1A, CP-A, OE33, and SK-GT-4 cells were cultured with media supplemented with pepsin (25 ug/mL), UBM-ECM (250 ug/mL), or eECM (250 ug/mL) for 24h. Cell proliferation was measured by BrdU (**A**), cell metabolic activity was measured by MTT assay (**B**), and cell apoptosis was measured by flow cytometry using AnnexinV/Propidium Iodide (PI) stain (**C**). Representative graphs are shown for n=3, technical quadruplicates for the BrdU and MTT assays. Cell count fold change is shown normalized to pepsin for apoptosis (early and late apoptosis) (n=3). Bar represents the mean ± standard deviation. Summary tables show positive (+) or negative (-) regulation for UBM-ECM or eECM treatment compared to pepsin control for each cell line. (ns - not significant $p>0.05$; ** $p<0.01$; *** $p<0.001$; **** $p<0.0001$).

7.6.4 UBM-ECM decreases neoplastic cell metabolism

UBM-ECM and eECM did not affect the metabolic activity of Het-1Aor CP-A cells compared to pepsin control. UBM-ECM decreased the metabolic activity of the OE33 ($p=0.0001$) and SK-GT-4 ($p=0.0035$) cells compared to pepsin control. UBM-ECM also decreased the metabolic activity of OE33 ($p<0.0001$) and SK-GT-4 ($p=0.0024$) cells compared to eECM (Figure 15B).

7.6.5 UBM-ECM increases metaplastic cell apoptosis

The fold change of early and late apoptotic cells with UBM-ECM or eECM treatment compared to pepsin is shown for Het-1A, CP-A, OE33, and SK-GT-4 (Figure 15C). For CP-A cells, UBM-ECM treatment increased late apoptosis ($p=0.0095$) compared to pepsin control. UBM-ECM and eECM did not show differences for early or late apoptosis in Het-1A, OE33, or SK-GT-4 cells compared to pepsin control.

7.6.6 eECM can downregulate PI3K-Akt, cell cycle, and DNA replication pathways; and can increase autophagy signaling in OE33 cells. eECM can upregulate cell cycle and DNA replication signaling in Het-1A cells

The gene expression workflow is shown (Figure 16A). Genes that were differentially expressed (defined as greater or less than 2-fold change, with significance by one-way ANOVA $p<0.05$) were identified (Supplementary Figure 47A). Notably, eECM had 1,445 differentially expressed genes in OE33 cells and 2,274 differentially expressed genes in Het-1A cells. In contrast, UBM-ECM had 149 differentially expressed genes in OE33 cells and 24 differentially expressed genes in Het-1A cells.

The top differentially expressed pathways are shown (Supplementary Figure 47B). The six differentially expressed pathways in OE33 cells with UBM-ECM and eECM treatment selected for further analysis included the focal adhesion-PI3K-Akt-mTOR, Cell Cycle, DNA replication, and autophagy (Figure 16B), and G1 to S phase transition and Wnt (Supplementary Figure 48). Signaling pathway networks for other cancers i.e., gastric cancer, breast cancer, and glioblastoma signaling pathways, were also shown to be downregulated in OE33 cells with eECM treatment (Supplementary Figure 49), but not further validated. qPCR validation of 30 candidate genes selected from the top signaling pathways largely agreed with the whole transcriptome analysis (Figure 16B); wherein eECM had a more pronounced effect compared to UBM-ECM at 24h, and Het-1A and OE33 cells responded differently to the same ECM treatment. eECM showed a net effect of decreasing PI3K-Akt-mTOR signaling and increasing autophagy signaling in OE33 cells. eECM robustly downregulated cell cycle, DNA replication, and G1 to S phase signaling in OE33 cells, and in contrast, upregulated these signaling pathways in Het-1A cells.

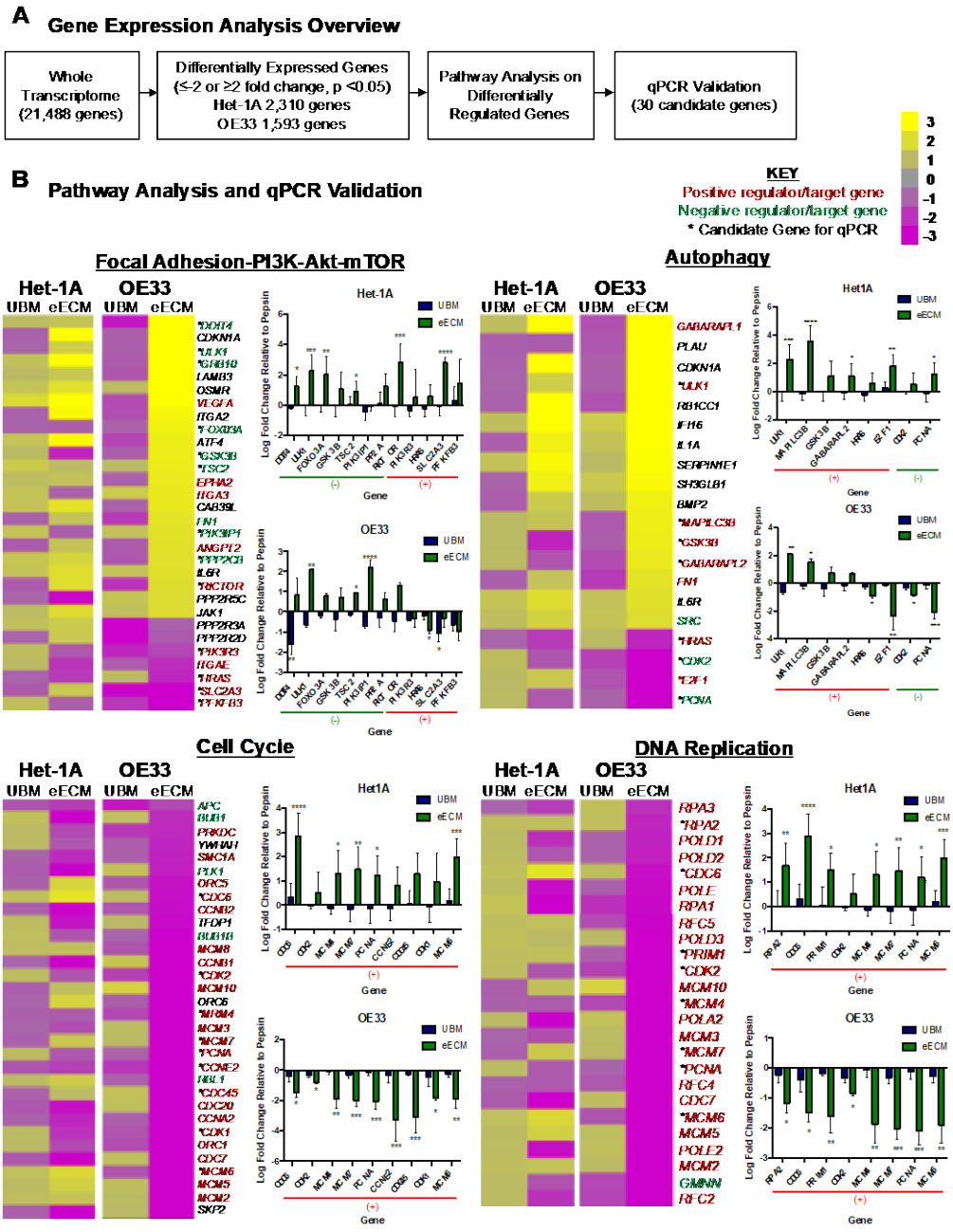

Figure 16. Gene expression.

(A) Overview of gene expression analysis. **(B)** Differentially expressed genes (>2 or <-2 fold change, with p< 0.05) grouped by signaling pathway for Het-1A and OE33 cells treated with UBM-ECM (250 ug/mL) or eECM (250 ug/mL) for 24h, normalized to pepsin control treatment (25 ug/mL) (n=3). Heat maps show the whole transcriptome analysis with corresponding qPCR for each signaling pathway: Focal adhesion-PI3K-Akt-mTOR, autophagy, cell cycle and DNA replication. Purple bars represent downregulated genes, and yellow bars represent upregulated genes compared to pepsin control. Genes are labeled as positive regulators (red) or negative regulators (green) and candidate genes that were further validated by qPCR are marked (*). (* p<0.05; ** p<0.01; *** p<0.001; **** p<0.0001). Values are expressed as mean ± SD.

7.6.7 UBM-ECM and eECM decrease phosphorylated AKT protein expression in OE33 cells and increase phosphorylated AKT in Het-1A cells

Western immunoblot was performed on the OE33 and Het-1A lysates for pAKT, a key upstream regulator of proliferation, cell cycle, and metabolism. OE33 cells and Het-1A cells showed no change in pAKT in the pepsin control. OE33 cells show a downregulation in pAKT expression with UBM-ECM treatment at 24h, and a downregulation in pAKT expression with eECM treatment at 6 and 24h (Figure 17A). In contrast, Het-1A cells showed an upregulation in pAKT expression with UBM-ECM and eECM treatment at 6 and 24h (Figure 17B). However, it is important to note that the initial/baseline levels of pAKT were much lower in OE33 compared to Het-1A and ~ 6x as much protein was needed to detect pAKT levels in OE33 cells.

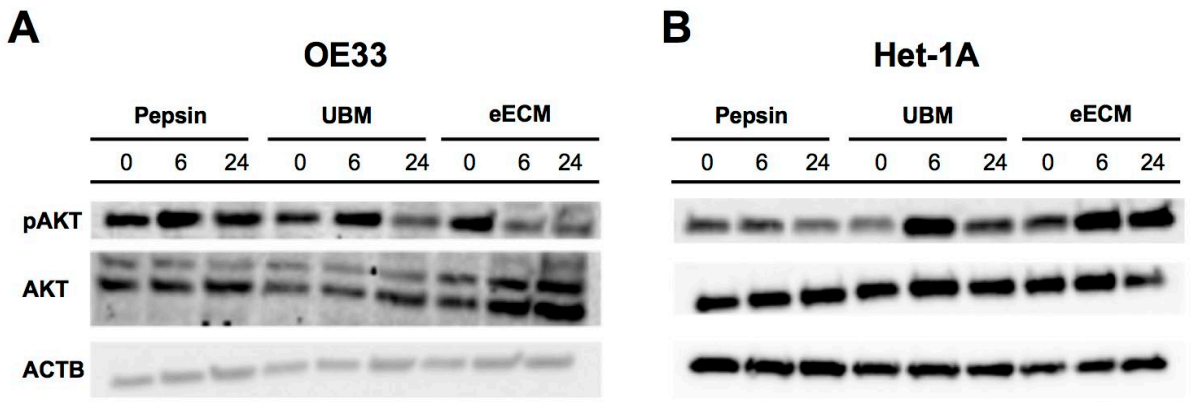

Figure 17. Phosphorylated AKT expression.
PI3K-Akt is a signaling pathway that regulates proliferation and metabolism, and shown to be upregulated in EAC cells. OE33 and Het-1A cells were treated with pepsin (25 ug/mL), UBM-ECM (250 ug/mL), or eECM (250 ug/mL) for 0, 6, or 24h. All time points were collected at the same time (t=0). Immunoblot for pAKT, AKT, and ACTB expression is shown for OE33 (**A**) and Het-1A (**B)** cells. Representative blots from a single experiment, n=2, technical duplicates. Independent blots were loaded with equal protein concentrations and confirmed for equal protein loading by ACTB. The initial/baseline levels of pAKT were much lower in OE33 compared to Het-1A and ~ 6x as much protein was needed to detect pAKT levels in OE33 cells.

7.7 DISCUSSION

The results of the present study show that signaling molecules present in solubilized ECM derived from non-malignant tissue can downregulate the neoplastic phenotype of EAC epithelial cells. “Downregulate” is defined herein as the active normalization of neoplastic epithelial cell behavior toward normal epithelial cell behavior. The same ECM had minimal, and sometimes opposite, effects on non-malignant “normal” esophageal epithelial cells. The rationale for the two types of xenogeneic (porcine) ECM used in the present study is based upon the results of two previous studies [30, 33]. UBM-ECM is commercially available (Matristem, ACell) and one of the ECM types used to treat 14 EAC patients (stage T1A) to date after aggressive, long segment mucosal resection. The patients, ineligible for esophagectomy due to co-morbidities, have survived for 1-8 years to date and returned to a normal diet. The bioscaffolds degraded completely within 2 weeks, suggesting the importance of ECM degradation products as an inductive cue for resident cells in the post tumor-resection niche [30]. The work is currently in a Phase I clinical trial (ClinicalTrial.gov Identifier: NCT02396745). eECM is a more recently developed biomaterial [42] and the logical tissue source for esophageal reconstruction. eECM enhanced esophageal stem cell migration and organoid formation compared to UBM-ECM and small intestinal submucosa (SIS-ECM) [33]. In the present study, the heterologous UBM-ECM and homologous eECM showed similar but distinctive effects on the normal, metaplastic, and neoplastic cells for phenotype, cell function, and gene expression, as summarized in Figure 18.

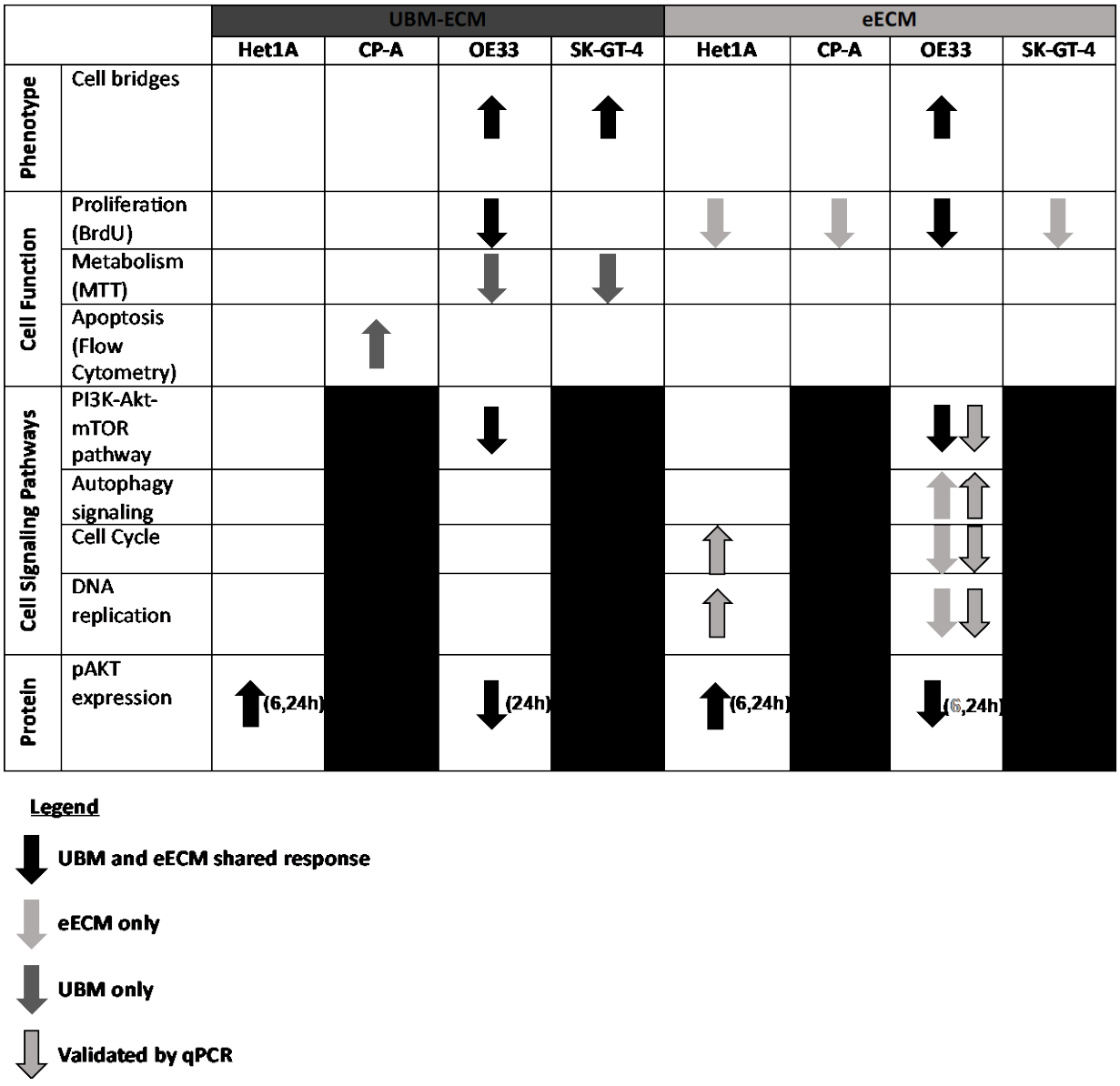

Figure 18. Summary graphic.
Summary of significant findings divided by treatment (UBM-ECM versus eECM) and by cell line. Arrows represent directionality of change with ECM treatment compared to pepsin control. ⬇ :similar response across ECM treatment types, ⬇ : specific response to UBM-ECM, ⬇ : specific response to eECM, ⇩: validated by qPCR, Blank box: no change, black box: Not tested.

7.7.1 Homologous and heterologous ECM: Similar and distinctive effects

The similar effects of both UBM-ECM and eECM included decreased proliferation in OE33 cells, decreased the focal adhesion-PI3K-Akt-mTOR signaling pathway in OE33 cells, and downregulated phosphorylated AKT at 24h in OE33 cells, and upregulated phosphorylated AKT in Het-1A cells at 6 and 24h. These similar responses elicited by the two ECM sources suggest the presence of common signaling molecules derived from non-malignant tissue with the ability to downregulate certain neoplastic cell behavior.

UBM-ECM and eECM treatment also showed reduced confluency and a striking morphologic change with the formation of cell bridges in OE33 and SK-GT-4 cells at 24h, which were absent in pepsin control and Het-1A and CP-A cells. Interestingly, the cell bridges in the present study did not positively label for actin or tubulin, as characteristic of other cell bridges, commonly referred to as “tunneling nanotubes” [208-210]. Tunneling nanotubes are a more recently described form of intercellular communication found in a variety of cell types including non-malignant and neoplastic cells *in vitro,* and *in vivo* [208]. Tunneling nanotubes have been shown to transfer healthy organelles and energy between cells in response to metabolic stress, mediated by PI3K-Akt activation, or prior to apoptosis [211]. It is plausible that the cell bridges in the present study are also related to a PI3K-Akt mediated stress response to the ECM treatment.

The distinctive effects of the two ECM materials included decreased metabolic activity of OE33 and SK-GT-4 cells, and increased late apoptosis of CP-A cells caused by UBM-ECM but not eECM. Previous studies have shown the effect of a heterologous ECM, specifically SIS-ECM, to suppress the malignant growth of neoplastic cells including pancreatic [34], sinonasal [35], bladder [36-39], melanoma [40], and esophageal [30] cancer cells in small animal studies [34, 39, 40] and human patients [30, 35]. Hurst et al. [39] showed SIS-ECM hydrogel delayed and reduced incidence of tumor growth when bladder cancer cells were directly mixed and

injected into the flank of mice compared to Matrigel. The present study corroborates Hurst et al. [39], by showing that heterologous UBM-ECM degradation products can specifically reduce proliferation and metabolic activity of neoplastic esophageal epithelial cells *in vitro* compared to pepsin control.

eECM showed distinctive effects compared to UBM-ECM by decreasing the proliferation of SK-GT-4 neoplastic and CP-A metaplastic cells, as well as Het-1A non-malignant esophageal epithelial cells. Only eECM downregulated the focal adhesion-PI3K-Akt-mTOR and cell cycle/DNA replication pathways, and upregulated autophagy signaling at 24h in OE33 cells by qPCR. It is important to note that while Het-1A proliferation was decreased with eECM treatment; Het-1A metabolic activity showed no change and Het-1A mitogenic signaling pathways including cell cycle, DNA replication, and pAKT signaling increased with eECM treatment at 24h. Explanations for the discrepancy can include the time point selected for the proliferation assay, or other downstream functions of the upregulated signaling pathways that remain to be determined.

Despite the tissue-specific differences in neoplastic cell function and gene expression results shown between UBM-ECM and eECM, the protein signature of UBM-ECM and eECM using SDS-PAGE showed that the banding patterns between the UBM-ECM and eECM were largely similar, except for a difference at ~60 kDa for eECM and at ~65 kDa for UBM-ECM. However, SDS-PAGE is not sensitive enough to detect if there are distinct protein isoforms present for the protein bands. The specific factors in normal ECM that actively suppress the neoplastic phenotype remain to be determined. The suppressive factor could be a soluble protein [163], cryptic peptide [73, 81], recently discovered matrix-bound nanovesicle (MBV) [6], combination of the aforementioned, or other factors.

7.7.2 Signaling pathways modulated by ECM degradation products: PI3K-Akt-mTOR, autophagy, cell cycle/DNA replication

eECM showed a downregulation of the PI3K-Akt-mTOR, cell cycle/DNA replication pathways and upregulation of autophagy pathways in OE33 cells by whole transcriptome analysis and qPCR. PI3K-Akt-mTOR has been shown to be upregulated in many cancers [212], including the progression from BE to EAC [213, 214]. Notably, PI3K-Akt-mTOR signaling regulates key cancer functions evaluated in the present study including metabolism, proliferation, and apoptosis [212]. The identification of PI3K-Akt-mTOR pathways, and more specifically upregulation of negative regulators of the pathway *PIK3IP1*, *ULK1*, and *TSC2* and downregulation of positive regulator *HRAS* in OE33 cells treated with eECM was shown by whole transcriptome analysis and qPCR. Other studies investigating the effect of (acellular) ECM on neoplastic cells have implicated the Akt pathway [38, 39]. Hurst et al. [39] showed that PI3K-Akt pathway was found to be the most significantly downregulated pathway at the protein level of bladder cancer cells grown on top of SIS gel, in comparison to grown on top of Matrigel or collagen. The identification of PI3K-Akt signaling in the present study could suggest a common pathway that is altered in neoplastic cells with ECM treatment; although the responsible signaling molecules would likely be distinct between cancer types and ECM tissue sources.

PI3K-Akt-mTOR negatively regulates autophagy signaling, and consistent with the present study results autophagy was shown to be increased in OE33 cells treated with eECM by whole transcriptome analysis and qPCR. The role of autophagy in EAC progression is not fully understood. However, a decrease in autophagy was proposed to be related to EAC cancer progression [215]. The net increase in autophagy, as a controlled form of cellular death, may further support the use of ECM to treat EAC.

UBM-ECM regulated fewer genes in the PI3K-Akt-mTOR pathway in OE33 cells by qPCR, despite the whole transcriptome predictions. In OE33 cells, UBM-ECM decreased a negative regulator of the PI3K-Akt-mTOR pathway (*DDIT4*) and decreased a positive regulator of PI3K-Akt-mTOR (*SLC2A3*). *SLC2A3* is a gene that facilitates uptake of glucose needed to support proliferation and metabolic activity, and could be related to the downregulation of metabolic activity and proliferation shown in OE33 cells with UBM-ECM treatment at 24h.

Cell cycle and DNA replication genes were strikingly regulated in opposite ways in Het-1A and OE33 cells treated with eECM, specifically the marked decrease of positive regulators in OE33 cells and marked increase of positive regulators in Het-1A cells. Similar to the present study, Barkan et al. [216] showed that basement membrane ECM could arrest the cell cycle of breast cancer cells cultured in 3D, specifically with an increase in cell cycle inhibitors CDKN2A (p16) and CDKN1A (p27). Adding a specific component of the basement membrane matrix, α2 non-collagenous Type IV collagen (canstatin), was shown by recombinant protein experiments to directly increase CDKN2A (p16) expression in cultured melanoma cells and promote cellular quiescence [217]. It remains unknown if the same basement membrane proteins are coordinating the changes in the cell cycle/DNA replication pathways in the present study, or if the effects are initiated by other proteins within the complex ECM.

At the protein level, UBM-ECM and eECM both downregulated phosphorylated AKT in OE33 cells at 24h, and eECM also downregulated phosphorylated AKT in OE33 cells as early as 6h. In contrast, UBM-ECM and eECM both upregulated phosphorylated AKT in Het-1A cells at 6 and 24h. PI3K-Akt is an EAC signaling pathway, but its activation is also shown to be vital in wound healing processes in non-malignant cells [218]. The differential regulation of phosphorylated AKT in Het-1A and OE33 cells in response to the same ECM bioscaffold degradation products could be favorable for a therapy promoting tissue reconstruction in a setting of occult adenocarcinoma.

Why would a normal and neoplastic cell show divergent intracellular signaling pathway responses to a normal ECM? Although the ability of the microenvironment to “normalize” neoplastic cell signaling pathways is not fully understood, the neoplastic cell may overexpress or downregulate cell surface receptors (e.g., integrins, growth factor receptors) that integrate ECM signaling molecules [219, 220], or show differences in downstream histone modifications and epigenetic remodeling [221]. A normal ECM likely causes changes in multiple signaling pathways to downregulate the neoplastic phenotype [23]. A corollary question is: why is understanding these intracellular signaling pathways important? Liu et al. [23] used specific PI3K pathway inhibitors on human mammary epithelial cancer cells and showed phenotypic reversion to normal phenotype with reduced proliferation, reduced size, and corrected basal polarity. Stated differently, even though the neoplastic breast cells retained their genetic mutations, the cells were biochemically normalized by manipulating a pathway that had previously shown to be initiated by deregulated matrix-cell contact. As the cell becomes normalized biochemically and phenotypically, the ECM that the cell secretes will change. Many ECM proteins including thrombospondin [222, 223], tenascin X, and tropoelastin among others [224] have p53 binding sites, which shows the coordination between tumor suppressor gene activation and the synthesis of new ECM. In this manner, the ECM can function as a tumor suppressing unit in response to dynamic intracellular signaling changes. Even a transient application of normal ECM can re-program the PI3K-Akt signaling pathway in OE33 cells, as early as 6h with eECM treatment or at 24h with UBM-ECM treatment, as demonstrated in the present study. The multi-factorial signaling pathways (PI3K-Akt, Cell cycle, DNA replication, autophagy, among others) that are targeted with ECM treatment could be advantageous for EAC with documented genetic heterogeneity [225].

7.7.3 Limitations and Future Work

There were limitations to the present study. First, immortalized cell lines were used, which are by definition transformed; however, other studies have shown similar effects with ECM on cancer cell lines [34, 36-39]. Second, the progression cell series were cultured on tissue culture plastic with ECM spiked in the media. The limitation of culturing cells on tissue culture plastic is well understood [4, 183], and future work can validate the functional differences and signaling pathways of normal and EAC cells in 3D models and *in vivo*. Spiking the cell culture media with ECM means that only the biochemical cues of the ECM were evaluated, and not the potential effect of the structural/mechanical cues. Third, only one time point (24h) was investigated for the functional tests. This study, along with other studies investigating the effect of solubilized ECM on cell behavior that used short time points (1-2d) [42, 95, 111, 112, 140], demonstrate the rapid effect of ECM degradation products upon cell phenotype. However, future work could investigate later time points. Finally, the isolated role of ECM on epithelial cells alone was investigated without the associated effects upon supporting stromal cells (e.g., fibroblasts, immune cells) in the tumor niche that also influence the final remodeling outcome.

Despite the limitations, the role of ECM bioscaffold degradation products in modulating neoplastic phenotype was strongly supported. Similar and distinctive effects between a heterologous UBM-ECM and homologous eECM to modulate neoplastic cell proliferation and metabolism were shown, and the PI3K-Akt-mTOR, autophagy, and cell cycle/DNA replication pathways were identified as possible regulating pathways. Future work will definitely prove the signaling pathways with pathway inhibitor/activation experiments. While both heterologous UBM and homologous eECM showed the potential to decrease neoplastic phenotype, it appears as if the homologous eECM may show a more pronounced therapeutic effect. Interestingly, the suppressive effects of ECM are primarily shown with neoplastic cells while normal cells were minimally affected. Normal cells have repeatedly been shown to not be adversely affected by

normal ECM degradation products [226], and ECM biomaterials have been safely implanted in millions of patients to date. ECM bioscaffolds can also form a hydrogel with pepsin-solubilization, which is liquid at room temperature and gels *in vivo*, expanding the potential clinical use for minimally invasive or oral delivery to treat the cancer precursor diseases Barrett's esophagus and high grade dysplasia. ECM could be used in combination with targeted therapy or immunotherapy, or as an adjunct therapy, to treat established esophageal cancer. As the mechanisms by which a normal ECM downregulates neoplastic phenotype are better understood, ECM-based therapies can be tailored for patients of this devastating disease.

7.8 CONCLUSION

Consistent with our hypothesis, exposure of metaplastic and neoplastic esophageal epithelial cells to a soluble form of normal esophageal ECM induced a marked downregulation of cancer-associated molecular pathways (e.g., PI3K-Akt, cell cycle, DNA replication) and normalization of cell phenotype (proliferation, metabolism, apoptosis) *in vitro*. The normalization of neoplastic phenotype was enhanced with tissue-specific esophageal ECM compared to heterologous urinary bladder matrix. The results support the use of non-malignant eECM as a potential therapy for esophageal cancer precursor and cancer patients.

7.9 ACKNOWLEDGEMENTS

This work was supported by the National Cancer Institute of the National Institutes of Health under Award Number F31CA210694 (LS). The content is solely the responsibility of the authors and does not necessarily represent the official views of the National Institutes of Health.

The authors thank Lynda Guzik from the McGowan Institute Flow Cytometry core at the University of Pittsburgh for access and assistance in the design and performance of flow cytometry experiments. The project used the University of Pittsburgh HSCRF Genomics Research Core Whole Transcriptome Array and gratefully acknowledges the technical assistance of Liane Fairfull for processing the samples and gene expression data; and Deborah Hollingshead and Dr. Janette Lamb for helpful discussions in whole transcriptome experimental design.

7.10 NEOPLASTIC ESOPHAGEAL CELL SURFACE RECEPTORS ACTIVATED BY NON-MALIGNANT ECM: PRELIMINARY RESULTS

7.10.1 Introduction

Cell surface receptors (e.g., integrins, receptor tyrosine kinases) transduce signals from the microenvironment, and blocking or inhibiting dysregulated surface receptors can dramatically revert breast neoplastic cells toward a polarized, non-malignant phenotype [21, 22].

eECM and UBM showed a tissue-specific downregulation of neoplastic esophageal cell phenotype (OE33), with minimal or opposite effects on non-malignant esophageal epithelial cell phenotype (Het-1A). It was hypothesized that the solubilized, non-malignant ECM distinctively modulated cell surface receptor expression in the two cell types, leading to the distinctive activation of downstream signaling pathways (PI3K-Ak, cell cycle, and DNA replication).

A screening panel of 228 cell surface markers was performed on OE33 cells treated with pepsin, UBM, and eECM to identify candidate receptors.

7.10.2 Materials and Methods

7.10.2.1 OE33 cell culture

OE33 cells were cultured according to manufacturer's guidelines and treated with solubilized eECM (250 ug/mL), UBM (250 ug/mL), or pepsin control (25 ug/mL) for 24h. Cells were washed with PBS, detached with Accutase, neutralized with media, counted (1 million/vial), and re-suspended in ice cold PBS-BSA (1%) and 2 mM EDTA to be analyzed by multicolor-flow cytometry for cell surface profiling.

7.10.2.2 Multicolor-flow cytometry-based cell surface profiling

Harvested cells (OE33) were washed twice with ice cold PBS and the viability was assessed by Trypan blue staining using a hemocytometer. Non-specific binding sites and Fc receptors were blocked with mouse serum for 20 min and cells were then divided in equal parts for fluorescence minus one (FMO) and DAPI only controls. The cells were divided to a 96-well plate containing FITC, PE and APC-conjugated antibodies specific to 228 cell proteins (BP80394, BDT FACSCAP Lyoplate, BD Biosciences, San Diego, CA, USA). Plates were incubated in the dark and centrifuged at 240 g for 7 min. Cells were fixed with 2% methanol-free formaldehyde for 20 min, permeabilized with 0.05% Saponin in IFA buffer and washed with IFA buffer. Finally, DAPI (Invitrogen, Cat. No. D1306) was added to the cells at a concentration of 8 µg/ml and plates were acquired on Fortessa SORP flow cytometer (BD Biosciences) equipped as described in MIFlowCyt. The instrument was set up using CS and T beads (BD Biosciences) and PMT voltages were adjusted to predetermined target channels using the 7^{th} peak of 8-peak Rainbow Calibration Particles (Spherotech, Lake Forest IL, RCP-30-5A) as a reference point. FITC, APC and PE Calibrite beads (BD Biosciences) and single stained antibody capture beads (BD Biosciences) were used as spectral compensation standards, along with cells stained with DAPI alone. Acquired data were analyzed using

VenturiOne software (Applied Cytometry Systems, Dinington UK) and plots were generated in Systat (San Jose, CA, USA).

7.10.3 Preliminary Results

OE33 eECM treatment reduced the expression of CD164 and OE33 UBM treatment reduced epidermal growth factor receptor (EGFR) expression compared to pepsin control as shown in Table 7.

Table 7. Cell surface receptor expression with UBM and eECM treatment compared to pepsin control.

	Sample		
Cell Surface Receptor	**OE33 Pepsin**	**OE33 eECM**	**OE33 UBM**
CD164	28.5% (CD164+)	6.4% (CD164-)	29.5% (CD164+)
EGFR	86.8% (EGFR+)	78% (EGFR+)	27.6% (EGFR-)

7.10.4 Discussion

EGFR expression in OE33 cells was decreased from 86.8% (pepsin) to 27.6% with 24h UBM treatment. EGFR is overexpressed in more than 50% of poorly differentiated EAC cases by immunohistochemical staining [227], and in Barrett's cases, a range of 30-100% patients reported upregulated EGFR [227], suggesting an early oncogenic event. EGFR controls cell proliferation, differentiation, and oncogenesis, and is relevant to the present dissertation because it can be upregulated by TNFα and is upstream of PI3K-Akt signaling [228].

CD164 expression in OE33 cells was decreased from 28.5% (pepsin) to 6.4% with eECM treatment, but was not affected by UBM treatment. CD164 is a glycoprotein and a type I integral transmembrane sialomucin, that is associated with endothelial cells and leukocytes [229]. Although less is known about the role of CD164 in esophageal adenocarcinoma, CD164 is upregulated in colon cancer and ovarian cancer, and is associated with increased ovarian epithelial cell proliferation, colony formation, and decreased apoptosis; and can promote PI3K-Akt signaling by upregulating the CXCR-4/stromal derived factor-1 (SDF-1) complex [229].

Future work will validate EGFR and CD164 cell surface receptors in OE33 cells and the non-malignant Het-1A control with UBM, eECM, and pepsin treatment. This work is clinically important to elucidate the molecular mechanism initiated by the non-malignant ECM interacting with the neoplastic cell surface receptor, and modulating downstream signaling pathways for the observed phenotypic changes.

7.11 ACKNOWLEDGEMENTS

This study is in progress and acknowledges the contributions of the following people: Dr. Vera Donnenberg, Dr. Xue Li, Dr. Lina Quijano, Dr. Albert Donnenberg, Popov Bosko, Ernest (Michael) Meyer, and Dr. Stephen F. Badylak.

8.0 ESOPHAGEAL EXTRACELLULAR MATRIX AS AN ORAL THERAPY FOR BARRETT'S ESOPHAGUS IN A DOG MODEL[4]

8.1 HYPOTHESIS

Considering the observed effect of solubilized non-malignant eECM to downregulate neoplastic esophageal epithelial cell phenotype *in vitro* (Chapter 7.0 it was hypothesized that non-malignant eECM hydrogel delivered orally in a canine model of Barrett's esophagus would mitigate or revert the metaplastic epithelium *in vivo*. Similarly, because TNFα signaling was increased in macrophages by metaplastic and neoplastic ECM *in vitro* (Chapter 5.0 it was hypothesized that the non-malignant eECM would downregulate TNFα+ macrophages in the canine model as a potential mechanism of action for a durable, therapeutic response.

---

[4] Portions of this chapter were adapted from the following manuscript in preparation:

J.D. Naranjo and L.T. Saldin, E. Sobieski, L.M. Quijano, P.G. Chan, C. Torres, R. Hill, J.L. Dziki, M.C. Cramer, Y.C. Lee, R. Das, A.K. Bajwa, R. Nossair, M. Klimak, L. Marshal, S. Patel, S. Velankar, K. Hansen, K. McGrath, and Stephen F. Badylak. Esophageal extracellular matrix hydrogel mitigates metaplastic change in a dog model of Barrett's esophagus. *In preparation*.

8.2 ABSTRACT

Proton-pump inhibitors (PPIs) are the mainstay of treatment for patients with chronic esophagitis associated with gastroesophageal reflux disease (GERD). However, proton pump inhibitors are non-curative and have debated efficacy. A synergistic approach is required to halt or reverse the potential progression to dysplasia, metaplastic Barrett's esophagus (BE), and esophageal adenocarcinoma (EAC). Biomaterials composed of extracellular matrix (ECM) in both solid and hydrogel forms have been shown to modulate the default response to tissue injury from a pro-inflammatory to a regulatory and constructive tissue remodeling phenotype. Esophageal ECM (eECM) hydrogel at 12 mg/mL has viscoelastic properties compatible with endoscopic and oral delivery, a gelation time of less than 5 min, and is adhesive to the esophageal mucosa. Targeted proteomic analysis confirmed the retention of structural proteins and a majority of basement membrane proteins related to matrix-cell signaling. eECM was administered orally for 30 days to dogs with experimentally induced BE and showed a reduction in esophagitis, a reversal of columnar metaplasia with decreased SOX9+/Alcian blue+ goblet cells, and an increase in CK13+/CK14+ differentiated esophageal epithelial cells. The results suggest that eECM may represent a viable strategy to prevent or reverse the dysplastic and metaplastic changes associated with chronic esophageal inflammation associated with reflux disease.

8.3 INTRODUCTION

Esophageal adenocarcinoma (EAC) has a five-year survival rate of approximately 20% [230], and the morbidity associated with current treatment options makes the clinical significance of this deadly disease particularly noteworthy. The disease progression of EAC has been well-studied and can involve progressive metaplastic and dysplastic changes within the esophageal

mucosa in response to the chronic and recurring insult inflicted by gastric reflux (i.e., stomach acid, bile salts) and the associated chronic inflammation [1, 12, 231]. The metaplastic change of the esophageal mucosal epithelium, referred to as Barrett's esophagus (BE), affects approximately 1-6% of the United States population [231-233], and is associated with an 11 – 125 fold increased risk of EAC [234, 235]. The therapeutic tenets for non-dysplastic BE include suppressing acid reflux with proton pump inhibitors (PPIs) and monitoring disease progression by endoscopy and frequent and unpleasant biopsy procedures [231]; and to a lesser extent the administration of non-steroidal anti-inflammatory drugs (NSAIDs) [236, 237]. Monitoring of disease progression by endoscopy provides the opportunity for timely treatment. Unfortunately, this approach has not only failed to mitigate the incidence of EAC, but has been associated with an increased incidence of this neoplastic disease [1].

Changes in the extracellular microenvironment have been proposed as the main driver of metaplastic, dysplastic, and neoplastic transformation of the esophageal mucosa [12]. Cell-microenvironment cross-talk mediates changes in cell phenotype and the resultant cell secretome that constitutes the composition and mechanical properties of the surrounding extracellular matrix (ECM) [5, 188]. Kratochwil and Bissell et. al have shown that cell phenotype and 3-dimensional spatial organization of tissue can be dramatically affected by the tissue-specific source of the ECM to which they are exposed [238, 239]. ECM harvested from various tissue and organ sources appears to include the universally shared ability to mitigate a pro-inflammatory phenotype of macrophages and lymphocytes [169, 240, 241], promote a regulatory and tissue healing phenotype [131, 240, 241], and the ability to recruit endogenous progenitor cells [63, 73, 242-245], and therefore facilitate tissue healing. Several studies in animals and humans have shown the constructive influence of the ECM upon esophageal healing following injury [26-33]. A cohort study of five patients with early stage EAC showed that surgical removal of the neoplastic mucosa followed by replacement with an ECM bioscaffold

resulted in formation of a new functional esophageal mucosa without recurrence of cancer [30]. A separate case report showed that the use of an ECM bioscaffold facilitated the healing of a large, chronically infected esophageal perforation [43].

Solubilized and degraded forms of ECM and hydrogels composed of ECM retain the immunomodulatory, progenitor cell attractant, and anti-microbial properties of the parent ECM [139]. The development of ECM hydrogels with “tunable” viscoelastic properties affords the possibility of minimally invasive delivery of ECM signaling molecules with their attendant biologic properties to anatomic sites that can otherwise be accessed only by more aggressive interventional procedures [64, 121, 139]. A recent study showed the mitigating effects of esophageal ECM harvested from normal tissue upon the aberrant properties of metaplastic and neoplastic esophageal epithelial cells (Chapter 7.0).

The objective of the present study was to determine the effect of orally administered esophageal ECM hydrogel in dogs with experimentally induced Barrett’s Esophagus (Figure 19).

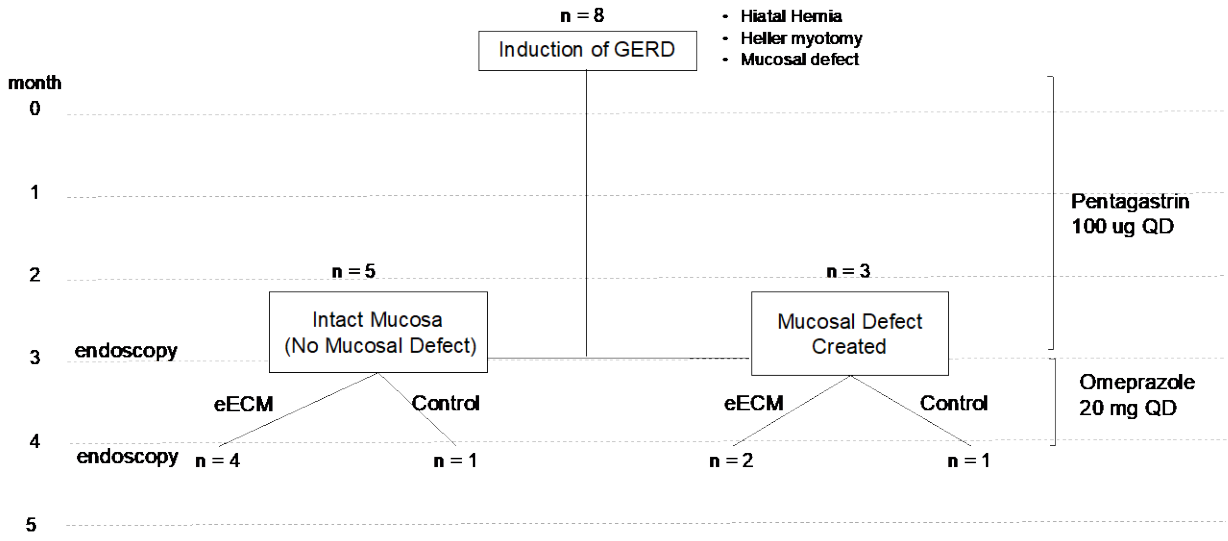

Figure 19. Study overview.
A total of 8 dogs underwent a reflux-inducing procedure in which a hiatal hernia, a Heller myotomy and a mucosal defect were created. Animals received pentagastrin daily for 3-4 months. Following pentagastrin administration, animals were evaluated by endoscopy and pentagastrin was replaced with omeprazole (PPI). Animals were randomly divided into two groups, no mucosal defect (intact mucosa) (n=5) or to receive a second mucosal defect (n=3). Each of the two groups had a randomly assigned control animal to evaluate the effect of removing pentagastrin and starting omeprazole. The remaining animals, 4 for the no mucosal defect group and 2 for the mucosal defect group received treatment with eECM for 30 days. Each animal was compared to itself before and after eECM treatment.

8.4 MATERIALS AND METHODS

8.4.1 Overview of experimental design

A pilot study was conducted to evaluate the potential therapeutic effect of an ECM hydrogel for Barrett's Esophagus in a dog model. BE was created in eight dogs by modification of a previously described surgical method that results in chronic gastric reflux. The dogs were then randomly separated into two groups, one of which had focal mucosal defects created to mimic

the clinical scenario of endomucosal resection (n=3), and the other of which left the mucosa intact (n=5). Four of five dogs in the intact mucosa group were administered ECM hydrogel orally, twice daily for 30 days, and two of three dogs in the mucosal defect group received the same dose regiment of ECM hydrogel. The remaining dog in each group was left untreated, with the exception of oral omeprazole, which all eight dogs received. The dogs were sacrificed after 30 days of ECM hydrogel treatment and evaluated by endoscopic, macroscopic, and microscopic methods.

8.4.2 ECM hydrogel preparation

Urinary bladder ECM (UBM) [62], dermal ECM (dECM) [65], and esophageal ECM (eECM) [33, 42] were prepared by decellularizing porcine tissues using tissue-specific protocols as previously described. ECM was solubilized using pepsin (1 mg/mL) in 0.01 M HCl, in a 10:1 ratio of ECM:pepsin, for 48h at room temperature as previously described ("ECM digest") [62]. The ECM digest was stored at -20°C. Samples were thawed at 4°C, and neutralized to physiologic pH and salt concentration with 0.1 M NaOH (1/10 volume of pre-gel solution) and 10x PBS (1/9 volume of pre-gel solution) and diluted to the desired ECM concentration (4, 8, 12, 16 mg/mL) with 1x PBS at 4°C ("ECM pre-gel") as previously described [62]. The temperatures were increased to 37°C for gelation to occur ("ECM hydrogel").

8.4.3 Rheology

The viscoelastic properties of the ECM pre-gel and formed ECM hydrogel were determined with a temperature-controlled, 40 mm parallel plate rheometer (AR2000) as previously described [65] and according to the American Society for Testing and Materials (ASTM) Standard F2900-11 [246]. The pre-gel form of three ECM tissue types (eECM, dECM, UBM) were prepared at 4

concentrations (4, 8, 12, 16 mg/mL) and tested (n=3) to determine a preferred formulation for oral and/or endoscopic delivery to the esophagus. Tissue type and ECM concentration have both been shown to influence viscoelastic properties [139].

ECM digests were neutralized and kept at 4ºC ("pre-gel") and tested within a 2 hour window. The pre-gel samples were loaded onto the AR2000 rheometer (TA Instruments) with a parallel plate geometry pre-cooled to 10 ºC, a temperature well below gelation. Mineral oil was used to seal the sample-plate interface and to minimize evaporation during the testing. A series of rheological tests were conducted for each sample in sequence. A steady state flow curve at 10°C was performed to determine the viscosity profile of the ECM pre-gel solution at a range of shear rates (0.1-1000 s^{-1}). Plate temperature was rapidly raised from 10°C to 37ºC to induce gelation, and an oscillatory time sweep was performed at 37ºC, by applying a small, 0.5% oscillatory strain at a frequency of 1 rad/s to measure the maximum storage modulus (G'), maximum loss modulus (G'') and gelation kinetics of the fully formed ECM hydrogel (occurring within 40-60 minutes). The time to 50% gelation was measured as the time to 50% of the maximum storage modulus. An oscillatory frequency sweep at 37ºC was performed after gelation was complete to determine the storage modulus (G'), loss modulus (G'') and complex viscosity $\eta^*(\omega)$ over a range of angular frequencies (ω) (0.1-100 rad/s) by applying a small, 0.5% oscillatory strain.

Data was extracted using the Rheology Advantage Data Analysis software (Version 5.7, TA Instruments, New Castle, DE), exported to Microsoft Excel and Prism (Version 6, GraphPad) for statistical analysis. Data is presented as average $\pm$ standard deviation.

8.4.4 Mucoadhesion

Mucoadhesion *in vitro* was assessed by determining the mucoadhesive strength and the thickness of ECM hydrogel remaining to the mucosa after applying laminar flow of type I water.

8.4.4.1 Mucoadhesive strength

A custom designed test was used to measure mucoadhesive strength. Porcine esophageal mucosa with attached submucosa were mechanically isolated from the underlying muscularis layer. 4 mL of ECM pre-gel (eECM, dECM, UBM) at 4 ECM concentrations (4, 8, 12, 16 mg/mL) (n=3) were placed at the bottom of each well of a 6 well plate. Porcine esophageal mucosa was glued to the outer convex surface of a half-sphere (40 mm diameter). The temperature was increased to 37°C to cause ECM hydrogel formation and adherence to the esophageal mucosa. The construct was then placed on the MTS Insight Tensile machine with 10N load cell and ball burst attachment, set to a measuring frequency of 10 Hz. The ball burst attachment was securely attached to the half-sphere and the half-sphere was raised up at a rate of 5 mm/min until separation of the hydrogel from the mucosa occurred. The maximum force value was considered the adhesion strength. Measurements were only accepted if the detachment occurred between the mucosa and the hydrogel.

8.4.4.2 Mucoadhesion with laminar flow

The intermediate ECM concentrations (8 and 12 mg/mL) for the 3 sources (eECM, dECM, UBM) were selected for mucoadhesion testing with laminar flow. A thin layer of ECM pre-gel (2 mL) was spread evenly across a porcine esophageal mucosa surface cut to specifications 6.5 cm long x 2.5 cm wide. The gel-mucosa surface was placed in a flow chamber and immediately subjected to flow of Type 1 water at 70 mL/min at 37ºC. The test was performed for 6 or 24h (n=3) and the sample was then formalin-fixed, stained with hematoxylin and eosin (H&E), imaged with a live cell microscope, and thickness of remaining gel as quantified by ImageJ.

8.4.5 Endoscopic and oral delivery *in vivo*

The ability of the ECM hydrogel to adhere to and be retained on the esophageal mucosa *in vivo* was evaluated in a canine model. The method was previously used in humans to test deliverability of different hydrogels to the esophageal mucosa [247]. In brief, the neutralized hydrogel was colored with McCormick blue dye for 9 hours with constant stirring at 4°C to prepare for administration. Animals were given 0.25 mL of acepromazine for mild sedation and 25 or 50 mL of 12 mg/mL neutralized hydrogel was delivered at 4, 15 and 25°C either orally by placing the syringe at the mouth of the animal and slowly delivering through a 60 mL catheter tip syringe (Monoject™, Covidien) or with the use of a 12Fr x 16” feeding tube (Medtronic) which was placed in the esophagus. Placement was confirmed by esophageal palpation. After delivery of the hydrogel, animals were denied access to any food or water until the start of the endoscopic procedure. Each dog was anesthetized by induction with ketamine (5-11 mg/kg), and surgical plane anesthesia was maintained with 1-5% Isoflurane via an endotracheal tube. The animal was placed in sternal recumbency with the neck extended to avoid pressure from the endoscope on the trachea or the nearby vessels. If necessary, insufflation with minimal amounts of air was done to facilitate appropriate visualization. The animal was placed at a 50° angle with the head lifted upwards. The endoscope was advanced slowly to identify the hydrogel.

For evaluation of endoscopic delivery of the hydrogel, a EDC190 delivery catheter (MILA International) was used. The gel at the desired temperature was injected onto the esophageal surface. Video recording was performed throughout the procedure.

8.4.6 Targeted mass spectrometry

Esophageal samples were processed as previously described [162]. Briefly, fresh frozen samples were milled in liquid nitrogen with a mortar and pestle and lyophilized to dryness. Approximately 2.5 mgs of samples were processed by step-wise extraction resulting in a cellular, soluble ECM (sECM), and insoluble (iECM) fraction for each sample. Protein concentration was determined by A660 Protein Assay (Pierce™). Enzymatic digestion was carried out by filter-aided sample processing [248] with 10kDa molecular weight cutoff filters. 30 µg of proteins form each sample was added to the filer in combination with 500 fmols of stable isotope labeled quantitative concatamers (QconCATs [160]) representing ECM, ECM-associated, and cellular proteins of interest [159]. Samples were then reduced, alkylated and digested with trypsin at 37˚C for 14 hrs. peptides were recovered with successive washed of ammonium bicarbonate and 0.1% formic acid, dried, and brought up to final volume for LC-MS injection.

Quantitative analysis of the ECM was carried out by liquid chromatography – selected reaction monitoring (LC-SRM) analysis on a QTRAP®5500 triple quadrupole mass spectrometer (ABSciex) coupled with a UHPLC Ultimate 3000 (Thermo Fisher) with acquisition methods as previously described [249]. Each sample was injected and separated by reversed phase chromatography (Waters, Acquity UPLC BEH C18, 1.7 µm 150 x 1 mm) by running a gradient from 2% to 28% acetonitrile in 0.1% formic acid for 28 minutes at a flow rate of 150 µL/min. The mass spectrometer was run in positive ion mode with the following settings: source temperature of 210ºC, spray voltage set to 5300V, curtain gas of 20 psi, and source gas of 35 psi (nitrogen gas). Data were acquired using the instrument controlled software, Analyst (v1.6.2). QconCAT transition selection, declustering potential, collision energies, and retention times were specifically optimized for each peptide of interest using Skyline's software [250] and settings can be found in previously published data.

Data Analysis for LC-SRM runs was carried out in the Skyline software package. Briefly, peaks were manually validated and light to heavy ratios ($^{12C}_{6}/^{13C}_{6}$) for each target peptide were used to back calculate concentration of each endogenous peptide targeted in the sample.

8.4.7 Intra-esophageal pH monitoring

Intraesophageal pH monitoring was performed on all animals before the reflux-inducing operation and 6 weeks after the reflux-inducing operation. The procedure was performed on fasted animals. The positioning of the pH probe (Ohmega pH Impedance recorder, Laborie) was done while the animals were awake. The position of the probe was determined by advancing the probe into the stomach until an acid readout was obtained. The probe was then withdrawn until the readout became alkaline, and from this point it was further withdrawn 5 cm to its final position. The reading was registered during a 1-hour period. Animals were pre-sedated with acepromazine, and low dose ketamine (5-11 mg/kg) was used at the moment of placing the probe.

8.4.8 Surgical procedures

8.4.8.1 Reflux inducing procedure

All animal procedures complied and were approved by the University of Pittsburgh Institutional Animal Care and Use Committee (IACUC #16119368).

Each dog was anesthetized by induction with acepromazine (0.01 mg/kg, SC), and surgical plane anesthesia was maintained with 1-5% Isofluorane via endotracheal tube. Aseptic procedures were followed, using sterile instruments and sterile preps. The animals were moved into the sterile surgical theatre and intubated. The animals were infused with 2 ml/kg/h of lactated Ringer's solution throughout the entire procedure. Physiologic parameters were

documented every 15 minutes. Before beginning the procedure, if needed, an orogastric tube was used to decompress the stomach. Peri-operative antibiotic prophylaxis was done with injection of 25mg/kg of Cefazolin before the first incision. The esophagus was approached through an upper mid-line laparotomy (extending from the umbilicus to the xiphoid process). The lower third of the esophagus was mobilized carefully to not injure the vagus nerve. The left crus of the diaphragm was separated from the esophagus, and through the enlarged hiatus, the cardia and upper third of the stomach were mobilized into the thoracic cavity. A fixed hiatal hernia was created by suturing the left crus of the diaphragm to the anterior wall of the stomach (that had been mobilized into the thoracic cavity) 2 cm below the gastroesophageal junction with non-absorbable 2-0 sutures. The muscle fibers of the lower esophageal sphincter were removed (Heller myotomy). If deemed necessary, the stomach was fixed to the lateral abdominal wall to prevent sliding into the thoracic cavity. The muscular plane was sutured in a continuous pattern with polyglactin or polypropylene 2-0 to 1 suture to close. Grafts were used to close the skin (Covidien).

During the same reflux-inducing surgery, an endoscopy was performed to create a mucosal defect. First an area of 2 cm circumferential by 3 cm longitudinal of the esophagus was identified 1 cm above the gastro-esophageal junction on the anterior side of the esophagus. Using a Duette™ band-ligation EMR kit (Cook Medical) this area of mucosa was removed. For posterior identification the area was marked by injecting Spot Endoscopic Marker at opposing corners. The animal was carefully monitored for 24 hours following the surgical procedure.

8.4.8.2 Postoperative animal care

All animals received buprenorphine (0.01 mg/kg BID) and oral cephalexin (35 mg/kg BID) after the procedure for 5 days. After completing the buprenorphine and cephalexin, all animals received 100 ug of Pentagastrin subcutaneously until the second procedure/endoscopy. Weight

after the initial surgery was recorded daily, and 3 times a week thereafter. All animals were evaluated daily for GI related complications.

8.4.8.3 Biopsy collection

Dogs were anesthetized by induction with acepromazine (0.01 mg/kg, SC), and surgical plane anesthesia was maintained with 1-5% isoflurane via endotracheal tube. During endoscopy, insufflation with minimal amounts of air was done to achieve appropriate visualization. Biopsy samples were collected for all animals around the circumference of the esophagus at the same height. For biopsy retrieval, first the z-line was identified to prevent collecting any stomach tissue. Under direct vision, biopsy forceps were advanced through the endoscope channel, opened and withdrawn, and the sample was retrieved from the endoscope. The location of the biopsy based on depth in the esophagus and laterality (anterior posterior, etc.), and the moment in the video was recorded for later identification and sample matching to location. All biopsy samples were formalin fixed.

8.4.8.4 Second mucosal resection for mucosal defect group

To answer the question if the diseased tissue would have to be resected prior to administration of eECM hydrogel, one study arm had a second mucosal resection before the start of treatment and approximately 12 weeks after the initial reflux-inducing procedure. A second mucosal defect was performed in the same manner under general anesthesia it was done in the first procedure opposite to the initial EMR. Treatment with the ECM hydrogel was applied at this point for the 2 mucosal defect treated animals. After the procedure, pentagastrin was suspended and omeprazole (20 mg QD) was given until the end of the study.

8.4.9 eECM hydrogel treatment

eECM treatment animals were administered ECM hydrogel per os for 30 days, BID. The eECM digest was thawed at 4°C, and the neutralizing solution was added, and the pre-gel was stirred at room temperature until it reached 15˚C. At that point, a 60 mL catheter tip syringe was used to deliver the pre-gel to the dogs per os.

Dogs were restricted for food and water for the hour following administration of the hydrogel. The treatment schedule was designed to keep the dogs from eating immediately after the pre-gel administration. Animals were fed once in the morning and once in the afternoon and the pre-gel was administered after the dogs had eaten to maximize exposure without food and without disturbing the animals' normal feeding schedule.

8.4.10 Necropsy

Thirty days after starting treatment, all animals underwent an endoscopy procedure to evaluate their esophagus before sacrifice. The procedure was recorded and the anterior and posterior sides of the esophagus were identified. Blood was also collected for serum protein analysis. The animals were euthanized with sodium pentobarbital (390 mg/kg).

After sacrifice, the esophagus was harvested and directionality and in-body dimensions were maintained. The esophagus was opened longitudinally from the side. The anterior and posterior surfaces were identified on the opened esophagus and biopsy samples were collected using a 12mm biopsy punch along the circumference of the esophagus (3 samples/height) starting at the GE junction (including stomach tissue) and proximal area until the end of the defect ensuring all the lower esophagus was covered. The height from the GEJ and a relation to the anterior side of all samples was recorded to locate the position of the sample during analysis. All samples were formalin fixed.

8.4.11 Analysis of harvested tissue samples

Serial sections (5 um) of biopsies (D0) and necropsy samples (D30) were stained with hematoxylin and eosin (H&E) and Alcian blue by standard histologic techniques [251]. A diagnosis of intestinal metaplasia requires the presence of goblet cells and Alcian blue staining marks the intracytoplasmic acidic mucin of goblet cells [252]. A brightfield microscope was used to image the H&E and Alcian blue slides.

H&E stained slides of all samples collected were blindly assessed and their characteristics (metaplasia, dysplasia, gastric tissue, etc) were recorded. The samples were matched with the animal and esophageal location where they had been harvested. This allowed to match the esophageal location of the biopsy to the same esophageal location at the moment of necropsy without introduction of bias. The samples at areas of interest (i.e. Barrett's metaplasia on biopsy or defect) were matched and analyzed based on the characteristics identified in the H&E staining. The same samples were used for further immunolabeling analysis.

8.4.12 Immunolabeling

Immunolabeling was performed using primary antibodies for squamous esophageal epithelial cell markers cytokeratin 13 [EPR3671] (rabbit monoclonal, Abcam, ab92551, 1:250) and cytokeratin 14 [LL002] (mouse monoclonal, Abcam, ab7800, 1:400); and the Barrett's epithelial cell marker Sox9 (rabbit polyclonal, Chemicon, AB5535, 1:1000). Immunolabeling was also performed for TNFα (rabbit polyclonal, Novus Biologicals, NBP1-19532, 1:200) to identify the pro-inflammatory cell infiltrate. The secondary antibodies used were goat anti-rabbit 488 (Abcam, ab150077, 1:200) for CK13 and Sox9, donkey anti-mouse 488 (Invitrogen, A21202, 1:200) for CK14, and goat anti-rabbit 594 (Invitrogen, A11037, 1:200) for TNFα. All primary and

secondary antibodies were diluted in blocking buffer solution (5% BSA with 1% Tween/1% Triton X-100).

Serial sections (5 um) of each tissue specimen identified previously were deparaffinized with xylene and rehydrated through a graded ethanol series. Antigen retrieval was performed using a citrate buffer (10 mM citric acid, 0.05% Tween20, pH 6) brought to boil and the slides were incubated for 20 minutes in the solution maintained at 95-100°C. The slides in the buffer solution were brought to room temperature and washed 3x5 min in 1x PBS, and blocked for 1h. The primary antibody solution was added and allowed to incubate overnight at 4°C. The slides were washed 3x5 min in PBS at room temperature, and the secondary antibody solution was added for 1h at room temperature. Slides were washed 5x5 min in PBS, and counterstained with 4'6-diamidino-2-phenylinidole (DAPI). Slides were washed 3x5 min in PBS, and mounted in fluorescent mounting media (Dako, Glostrup, Denmark) and cover slipped. The slides were imaged on a Nikon E600 fluorescence microscope with the Cri Nuance FX Multispectral Imaging System for fluorescence. Primary deletes were confirmed to be negatively stained.

Representative images were taken of the H&E, Alcian blue, CK13, CK14, and Sox9 staining at 10x and 20x fields. Three images per sample for TNFα were taken at 20x and quantified using a CellProfiler pipeline for positive TNFα and DAPI staining, with a threshold of 0.25 intensity or greater for the 594 channel to discount any background staining.

8.4.13 Statistical analysis

All values are expressed as mean ± SEM because at least 2 technical replicates were performed for each biological sample (n=3), except rheology values are expressed as mean ± SD because one technical replicate was performed for each biological sample.

Rheology - A 2-way ANOVA was performed for the main effects of ECM concentration and shear rate for the viscosity flow profile, and for the main effects of ECM concentration and modulus for the time sweep test. A 1-way ANOVA was performed for main effect of ECM concentration on gelation time. Values are expressed as mean ± SD because one technical replicate was performed for each biological sample.

Mucoadhesive Strength – A 2-way ANOVA was performed for the main effects ECM tissue type and ECM concentration. The Tukey multiple comparisons test was performed comparing mucoadhesion of each ECM concentration within each ECM tissue type, and mucoadhesion of each ECM tissue type within each ECM concentration. Values are expressed as mean ± SD.

Mucoadhesion with Laminar Flow – A 2-way ANOVA was performed for the main effects of sample and time. The Tukey multiple comparisons test was performed comparing gel thickness after laminar flow of each sample within each time. Values are expressed as mean ± SEM because at least 8 technical measurements were taken per sample.

Immunolabeling- Student's unpaired t test was performed comparing treatment animal specimens to control animal specimens. Values are expressed as mean mean ± SD.

8.5 RESULTS

8.5.1 Viscoelastic properties of ECM hydrogel are tissue-specific and can be tailored by ECM concentration

Rheology was performed on 3 tissue sources of solubilized ECM (i.e., pre-gels); specifically, esophagus (eECM), dermis (dECM), and urinary bladder (UBM) at 4 ECM concentrations (4, 8, 12, 16 mg/mL) to determine the preferred formulation that could be delivered orally and endoscopically to the esophagus (Figure 20**)**.

ECM pre-gel viscosity increased with increasing ECM concentration at low shear rates. Specifically, 16 mg/mL had a higher viscosity than 4, 8, and 12 mg/mL for all ECM hydrogels at 0.1 shear rate (1/s) (Figure 20A, D, G) ($p<0.0001$ for all except $p=0.0061$ for dECM 12 mg/mL versus 16 mg/mL). UBM hydrogel at 12 mg/mL was more viscous than 4 ($p=0.0071$) and 8 mg/mL ($p=0.0276$) concentrations at 0.1 shear rate (1/s) and UBM 16 mg/mL was more viscous than 4 mg/mL at 1 shear rate (1/s) ($p=0.0456$) (Figure 20G). eECM 12 mg/mL was more viscous than 8 mg/mL at 0.1 shear rate (1/s) ($p=0.0355$). No differences in viscosity were shown between ECM concentrations at higher shear rates (10, 100, and 1000/s) (Figure 20A,D,G). In general, all ECM tissue sources at each ECM concentration tested were "shear-thinning," defined as the decreased viscosity of the pre-gels with increasing shear rate.

eECM and UBM hydrogels at 16 mg/mL had higher storage moduli (G'') compared to 4, 8, and 12 mg/mL ($p<0.001$ for all except $p=0.0005$ for eECM 12 mg/mL versus eECM 16 mg/mL) hydrogels (Figure 20B, H). dECM had a higher storage modulus of 16 mg/mL compared to 4 ($p=0.0006$) and 8 mg/mL ($p=0.001$), and higher storage modulus of 12 mg/mL compared to 4 mg/mL ($p=0.0395$) (Figure 20E).

Gelation time was independent of ECM concentration for eECM (Figure 20C) and UBM (Figure 20**I**). For dECM, 4 mg/mL had a longer time to 50% gelation compared to 12 ($p=0.0093$) and 16 mg/mL ($p=0.0044$) hydrogels (Figure 20F).

UBM and eECM hydrogels were "stably formed" defined as the moduli being weakly dependent upon frequency, and the complex viscosity varying inversely with frequency. Furthermore, the G' storage modulus was greater than the G'' loss modulus over the angular frequencies (ω) tested (0.1-100 rad/s) for 4-16 mg/mL (Supplementary Figure 50).

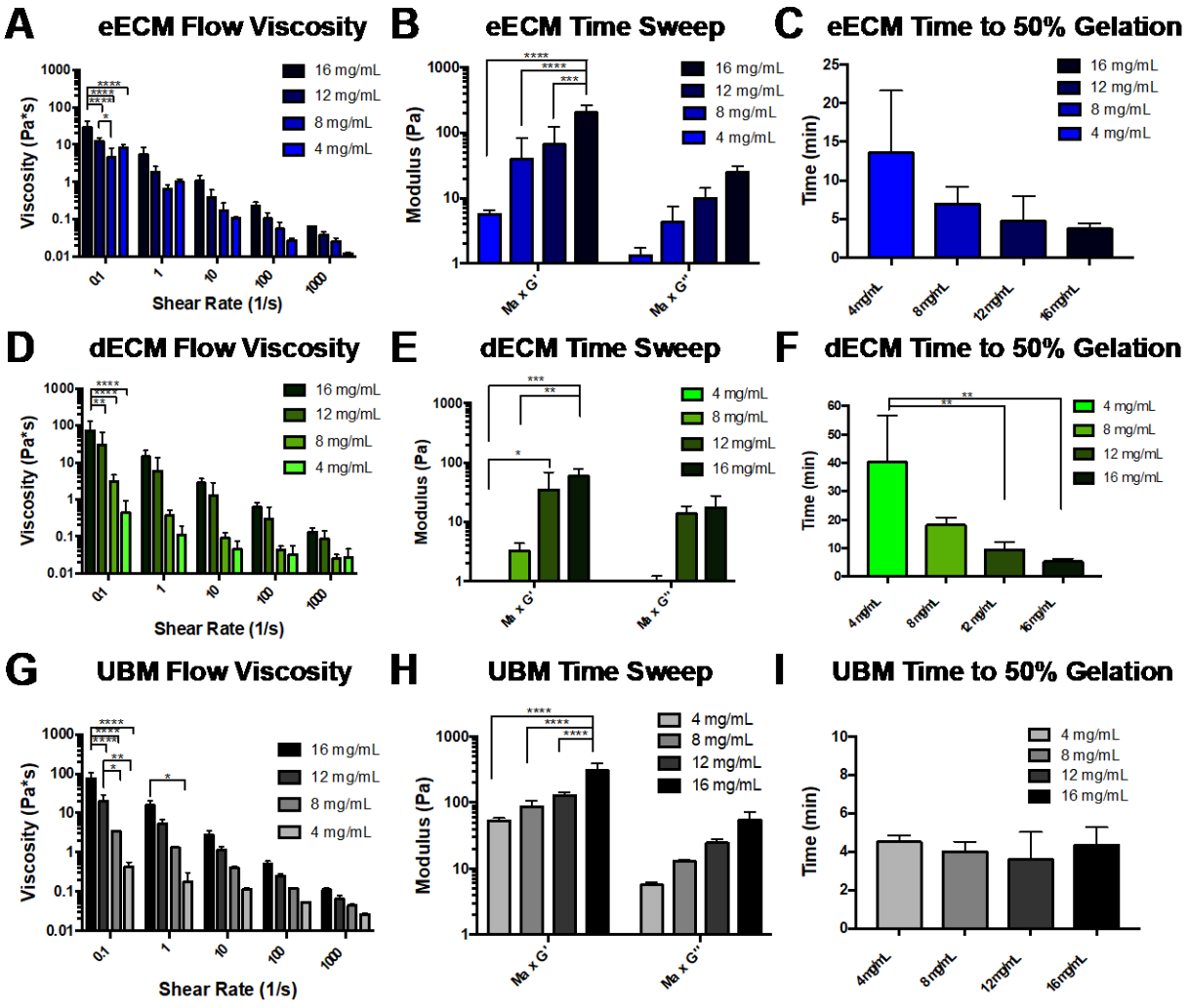

Figure 20. Tissue-specific viscoelastic properties for oral and endoscopic delivery. Rheology was performed on eECM (A, B, C), dECM (D, E,F), and UBM (G, H, I) pre-gels at 4 ECM concentrations (4, 8, 12, 16 mg/mL). ECM pre-gels were shear-thinning, i.e., viscosity decreased with increasing shear rate at 10°C (a temperature well below gelation), and viscosity increased with increasing ECM concentration at low shear rates (A, D, G). The maximum storage modulus ("stiffness") (G') and loss modulus (G'') was measured after temperature was raised to 37°C (B, E, H). Time to 50% gelation was measured as the time to 50% of the maximum storage modulus. Time to 50% gelation was independent of ECM concentration for UBM and eECM, and dependent upon ECM concentration for dECM (C, F, I). (* $p \leq 0.05$, ** $p \leq 0.01$, *** $p \leq 0.001$, **** $p \leq 0.0001$). Values expressed as mean ± SD.

8.5.2 Mucoadhesion

8.5.2.1 eECM has the highest mucoadhesive strength and is dependent upon ECM concentration

Mucoadhesive testing was performed to determine the ECM hydrogel adherence to the esophageal mucosa *ex vivo*. Mucoadhesive strength showed two main effects: tissue source ($F(2,24)=12.55$, $p=0.0002$) and ECM concentration ($F(3,24)=10.05$, $p=0.0002$) by 2-way ANOVA A). A multiple comparisons test was performed comparing ECM concentration within each ECM source, and comparing ECM tissue source within each ECM concentration to interrogate differences of the main effects. There was an increase in mucoadhesion for eECM between 4 and 12 mg/mL ($p=0.0007$), 4 and 16 mg/mL ($p=0.0026$), 8 and 12 mg/mL ($p=0.0053$), and 8 and 16 mg/mL ($p=0.0178$) but not between 4 and 8 mg/mL ($p=0.8508$), or 12 and 16 mg/mL ($p=0.9559$). eECM mucoadhesive strength was higher compared to dECM ($p=0.0007$) and UBM ($p=0.0314$) at 12 mg/mL. eECM mucoadhesive strength was higher compared to dECM ($p=0.0107$) at 16 mg/mL.

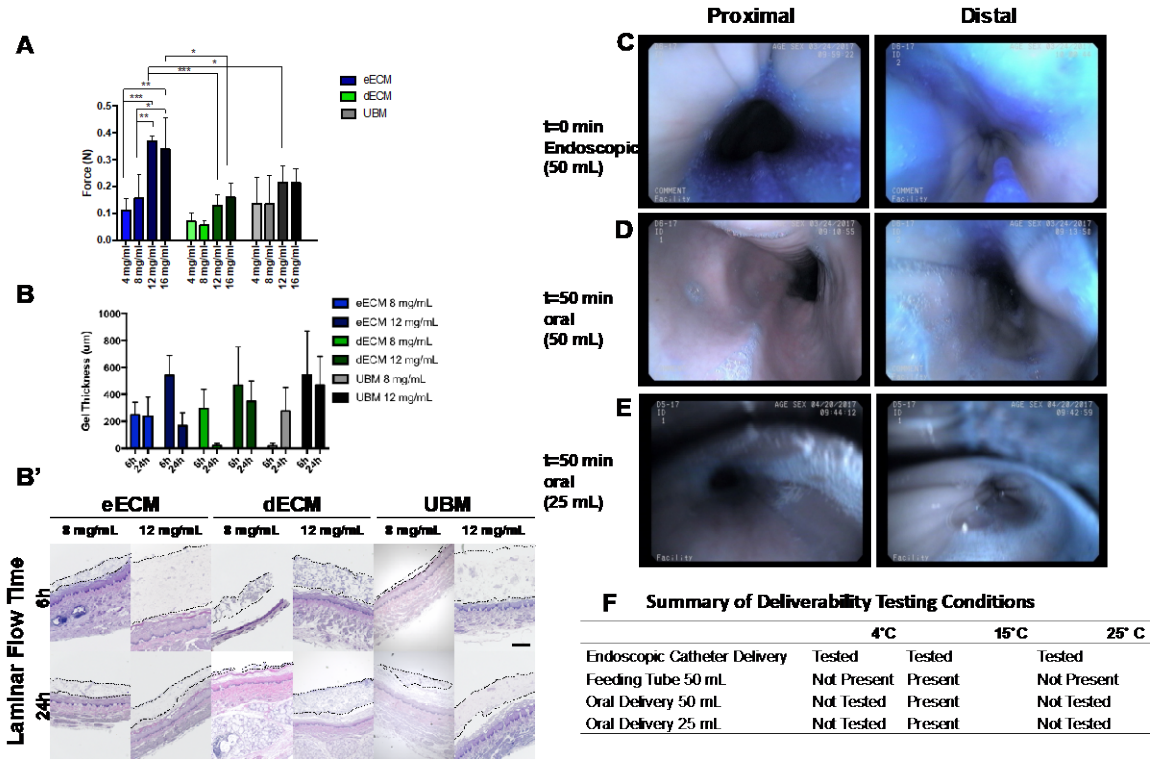

F Summary of Deliverability Testing Conditions

	4°C	15°C	25° C
Endoscopic Catheter Delivery	Tested	Tested	Tested
Feeding Tube 50 mL	Not Present	Present	Not Present
Oral Delivery 50 mL	Not Tested	Present	Not Tested
Oral Delivery 25 mL	Not Tested	Present	Not Tested

Figure 21. ECM hydrogel mucoadhesion *ex vivo* and *in vivo.*
Ex vivo mucoadhesion testing was performed to determine the adherence of the different ECM sources (eECM, dECM, UBM) to the esophageal mucosa. (A) The mucoadhesion force of ECM pre-gel (4, 8, 12, 16 mg/mL) to an esophageal mucosa was measured, and eECM showed increasing mucoadhesion with increasing ECM concentration. eECM at 12 mg/mL had higher mucoadhesion than UBM or eECM. (* $p \leq 0.05$, ** $p \leq 0.01$, *** $p \leq 0.001$). Values expressed as mean ± SD. (B) ECM pre-gel (8, 12 mg/mL) mucoadhesion with laminar flow was measured for 6 and 24h and showed presence of hydrogel for all ECM sources by H&E staining. Values expressed as mean ± SEM. (B') Representative images of the ECM hydrogel, outlined in black dotted lines, are shown. C. Blue dyed hydrogel delivered at initial temperature of 15˚C with the use of an endoscopic delivery catheter remains at the mucosa and can be delivered to specific locations. D. Hydrogel was present at the proximal (left panel) and distal (right panel) esophagus 50 minutes after delivery of 15˚C 50 mL. E. Hydrogel was present at the distal esophagus 50 minutes after delivery of 15˚C 25 mL. F. Summary of in-vivo deliverability testing at different temperatures forms and delivery volumes.

8.5.2.2 ECM hydrogel adheres to porcine esophageal mucosa for at least 24h under laminar flow conditions

The ECM hydrogel was placed on the surface of porcine esophageal mucosa and water was flowed continuously across the surface at 70mL/min to determine if the hydrogel would adhere with laminar fluid flow, simulating swallowing. Results showed that hydrogel remained adhered to the mucosa for each ECM tissue type and ECM concentration after 6 and 24h. The amount of gel remaining did not differ across the ECM tissue sources or ECM concentrations (Figure 21B). Representative figures of the gel remaining after continuous flow are shown in Figure 21B'.

8.5.3 eECM hydrogel remains at the esophagus after oral and endoscopic delivery in vivo

The rheology and *ex vivo* mucoadhesion testing showed the feasibility of *in vivo* delivery and adherence of the ECM hydrogel to the esophageal mucosa. eECM at 12 mg/mL was selected as the preferred hydrogel for *in vivo* testing due to its higher mucoadhesive strength when compared to other source ECM tissue, relative faster gelation time (~5 min), and its homology to the esophagus.

Deliverability testing was conducted in healthy dogs. A method similar to one previously reported [247] was used. The eECM hydrogel was dyed for 9 hours prior to the tests and delivered to the test animals by 1) an endoscopic catheter, or 2) oral administration. The effects of temperature and volume of ECM hydrogel were also evaluated.

The eECM hydrogel proved to be deliverable through the endoscopic catheter at 4, 15, and 25°C. Representative images for 15°C are shown in the proximal and distal esophagus at the time of application (t=0 min) (Figure 21C).

The eECM hydrogel was delivered using the feeding tube and was not clearly identifiable by endoscopy after delivery at 4 or 25˚C, however it was clearly identifiable 40 minutes after feeding tube delivery at 15˚C (Supplementary Figure 51).

When an initial delivery volume of 25 or 50 mL of eECM hydrogel was administered orally at 15˚C, the hydrogel was present at the proximal and distal esophagus for at least 40 minutes after delivery (Figure 21D, E). A summary of the deliverability testing conditions and results is shown in Figure 21F.

8.5.4 Proteomic signature of eECM shows retention of structural, cell-matrix attachment, and basement membrane proteins

Quantitative targeted proteomics was performed on eECM and the native esophageal tissue. There was notable retention of proteins in the eECM that contribute to the physical characteristics of the source tissue including the fibrillar collagens type I, III, and V (Figure 22A,C) and those proteins that participate in cell-matrix adhesion, such as the basement membrane proteins laminin, perlecan, nidogen, agrin and collagen type IV (Figure 22A,B). The fibrillar collagens were almost completely retained (Figure 22C, Table 12), as were microfibril associated proteins that play an important role in anchoring cells to the collagen rich matrix such as fibronectin 1, dermatopontin, and fibrillin-1 (Figure 22D, Table 12). Matricellular proteins as well as structural proteins that contribute to microfibrillar and elastic fiber formation were still present but almost an order of magnitude lower in concentration in the eECM when compared to the source esophageal tissue (Table 12). Decellularization of the source tissue resulted in an efficient removal of cellular material, in agreement with a previous report [42]; specifically, H1, H2A, MYH, and GAPDH were no longer detected, and ACT/B, LMNA, VIM, and TUBB were present but at an average concentration decrease of 98.91% (Table 15).

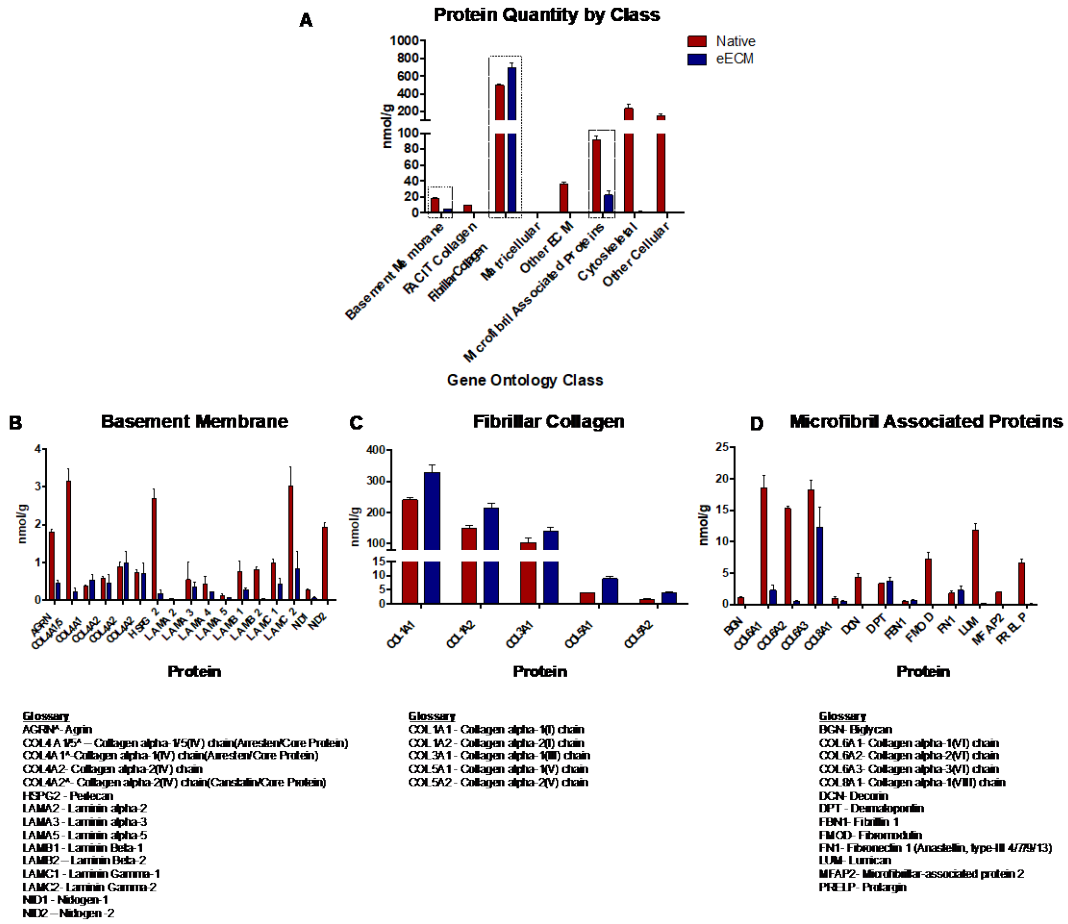

Figure 22. Proteomic signature of eECM

A. Absolute quantification of ECM proteins, binned by gene ontology class, for native esophageal mucosa tissue and eECM (n=3, error bars represent SEM). Top classes of proteins that showed retention of ECM proteins in eECM compared to native esophageal mucosa tissue included (B) basement membrane, (C) fibrillar collagens and (D) microfibril associated proteins (boxed). Proteins within the gene ontology classes are further shown (B-D).

8.5.5 Intestinal metaplasia of the esophagus occurs after 90 days post surgery

Overview of the animal model is presented in Figure 19. A modified version of the model developed by Henessy et al was used [253]. All animals underwent surgery to induce reflux by 1) creating a hiatal hernia, 2) performing a Heller myotomy to loosen the lower esophageal sphincter and 3) performing an endoscopic mucosal resection (2 cm x 3 cm circumferential) for new epithelium to grow in the presence of refluxing stomach acid.

Animals received pentagastrin at a dose of 100ug daily for at least 90 d after the procedure. Three out of 9 animals presented gastric symptoms such as anorexia or emetic episodes during this period. Pentagastrin administration was suspended temporarily for these 3 animals, and continued after the animals recovered. Two animals required reoperation due to hernia related complications i.e., a type IV diaphragmatic hernia. The animals with hernia complications underwent a second operation in which the stomach's greater curvature was fixed with prolene sutures to the left inner abdominal wall. One animal developed a bleeding gastric ulcer which was treated with sucralfate, ranitidine and temporary suspension of pentagastrin. All dogs recovered without further complications.

Esophageal acid reflux was established before surgery and 2 weeks post-surgery by 3 measurements: intraluminal esophageal pH readings, pH reflux events, and impedance reflux events. Readings were averaged over 1h. Intraluminal esophageal pH was 6.4 ± 0.414 at baseline and 6.2 ± 0.57 post-surgery. All animals had a drop in pH post-surgery compared to baseline, except for NMD-C and NMD-4 (Figure 23A). Reflux was measured with the pH probe for 1 hour and only 1 animal presented a reflux event pre-operatively (NMD-C), and 4 animals showed one event post-operatively (NMD-1, NMD-2, MD-C, MD-1) (Figure 23B). None of the animals showed any impedance events at baseline and 4 out of 8 animals had one impedance

event post-surgery (NMD-1, NMD-2, MD-1, MD-2) (Figure 23C). All animals showed at least 1 positive reflux readings 2 weeks post-surgery during the 1h period, except for NMD-C.

Animals underwent a second endoscopy to evaluate the gastroesophageal junction (GEJ) and lower esophagus macroscopically and to collect biopsies before the start of treatment. Endoscopy was performed at 90d, or longer (90-124d) to compensate if the animal had suspended pentagastrin due to complications post-surgery. Biopsies were taken from areas that showed the greatest severity of disease. The proximal border of the stomach (z-line) was first identified before biopsy collection to ensure no gastric tissue was collected with the forceps. A representative image from endoscopy at the distal esophagus (Figure 23D) and corresponding biopsies (H&E staining) shows metaplastic Barrett's esophagus from an area of macroscopic esophagitis (Figure 23E), dysplasia at the defect site (Figure 23F) and normal squamous epithelium from a macroscopic normal area (Figure 23G).

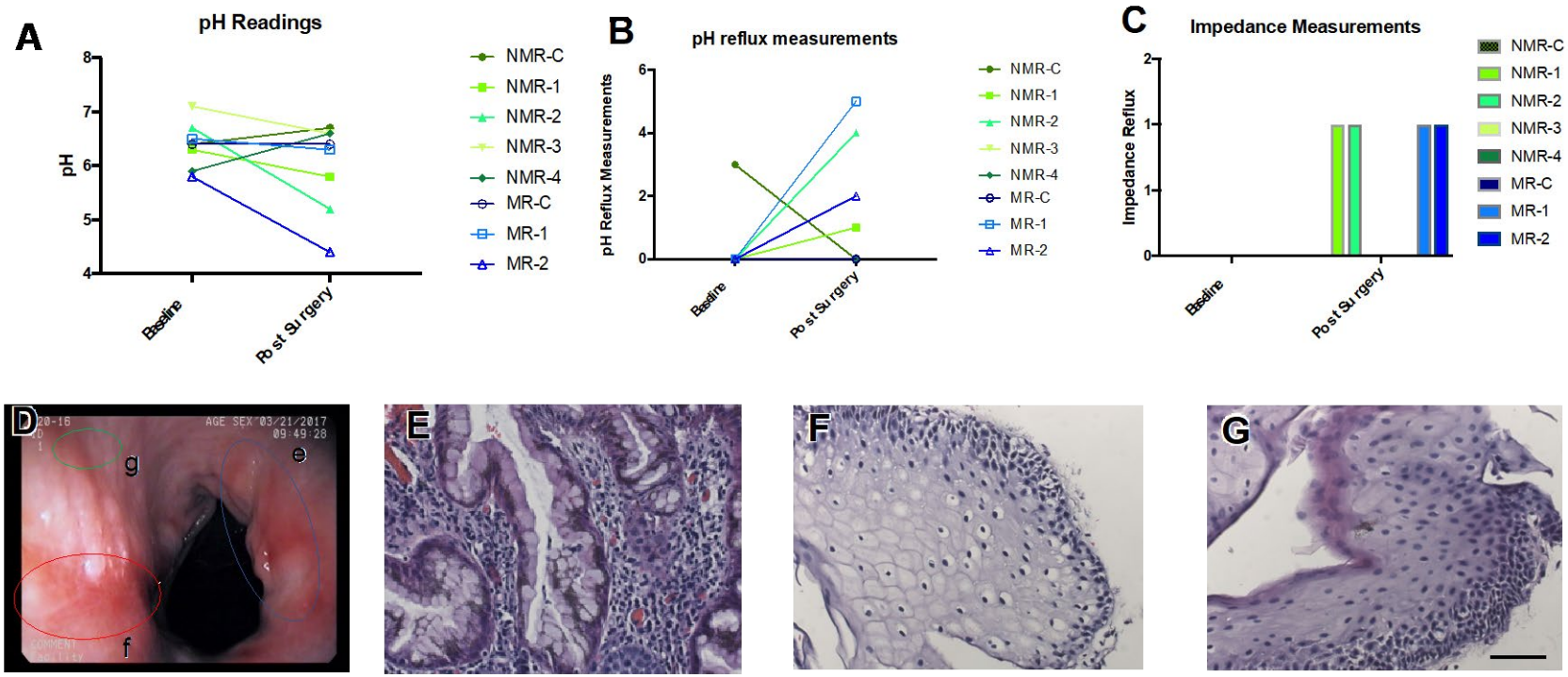

Figure 23. Induction of Reflux and columnar metaplasia.
A. Two-hour pH readings in the distal esophagus were obtained for all animals before ("Basline") and after reflux-inducing surgery. Average pH before the procedure was 6.4±0.41 at baseline and 6.2± 0.57 post-surgery. All animals except NMD-4 and NMD-C had a decrease in pH post-surgery when compared to baseline. **B.** Only one dog had reflux events at baseline during the 2-hour pH readings however, 4 dogs presented at least one reflux episode as measured by pH post-surgery. **C.** None of the animals had any reflux events, as measured by impedance events, during the 2-hour readings at baseline. Four dogs showed at least one reflux episode as measured by impedance events post-surgery. **D.** Representative image of distal esophageal mucosa at endoscopy before treatment with eECM. Biopsies were taken at area of (*e*) macroscopic esophagitis, (*f*) defect and (*g*) normal and stained with H&E. **E**. H&E stained biopsy harvested from an area of macroscopic esophagitis (e) showed Barrett's epithelium. **F.** H&E stained biopsy harvested at the defect site (f) showed dysplasia. **G**. Normal esophageal epithelium (g) stained with H&E showed normal epithelium. Scale bar = 50um

Macroscopic endoscopic evaluation showed that the animals had developed esophagitis to different degrees of severity before treatment (D0) (Figure 24). In the NMD group, one of the animals showed areas of scarring with columnar metaplasia upon macroscopic evaluation (NMD-4). NMD-1 and NMD-2 presented with non-confluent reddish areas with no apparent signs of ulceration, whereas NMD-C, NMD-3, NMD-4 showed areas of ulceration. For the MD group, MD-C had macroscopically the least severe esophagitis, with MD-1 and MD-2 both showing ulceration and erythema on opposite walls of the esophagus. MD-2 had the most severe disease of all animals with ulcers and erythema that compromised approximately 60% of the esophageal circumference. The initial mucosal resection had completely healed in all dogs with some scarring and non-inflammatory epithelium. Animals that were randomized to have a second mucosal defect created (MD group) had so at this point.

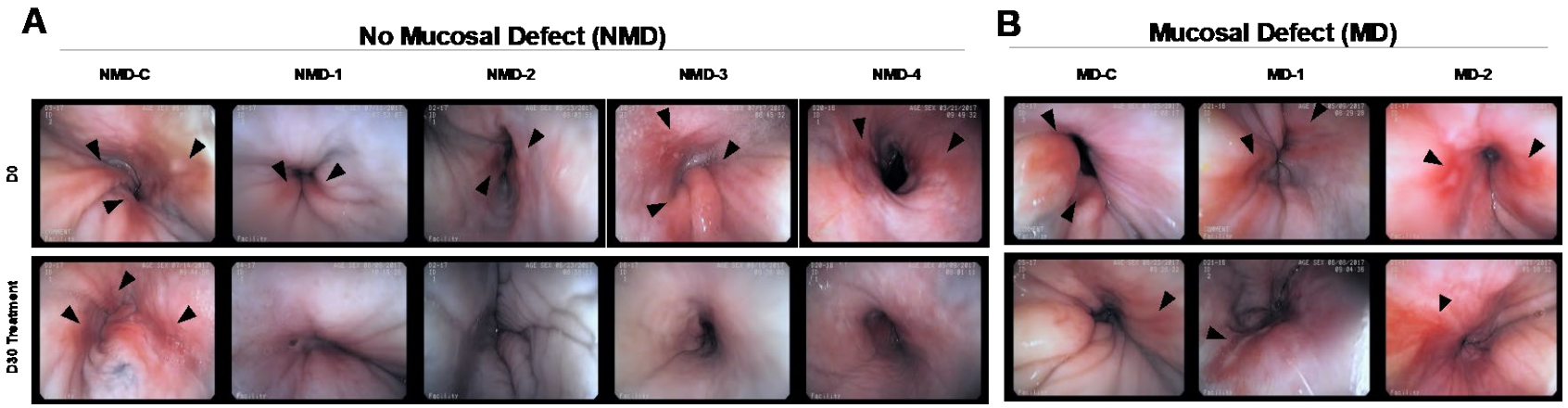

Figure 24. Esophageal mucosa before and after eECM treatment.
A. No mucosal defect. Top. After pentagastrin treatment all animals underwent an endoscopic procedure to evaluate the gastro-esophageal junction (GEJ) and the distal esophagus. Dogs had various degrees of esophagitis and ulceration (arrows). **Bottom.** Lower esophagus and GEJ after 30 days of eECM treatment. Improvement was seen in all animals except NMD-C that did not receive eECM. **B. Mucosal Defect group.** Animals received a second mucosal defect. **Top.** All animals had focal reddish areas and different degrees of esophageal inflammation. **Bottom.** After 30 days the focal reddish area and esophageal inflammation persisted in all animals (arrows) regardless of treatment.

Histologic analysis of biopsies at D0 showed the presence of columnar metaplastic cells in 7 of 8 dogs: all but MD-C. However, MD-C did show dysplastic cells (Figure 25B).

8.5.6 eECM hydrogel mitigates macroscopic esophageal inflammation of the epithelium in the distal esophagus compared to omeprazole alone control, and the effect is enhanced in the NMD group

Pentagastrin was suspended and omeprazole therapy (20 mg daily) was initiated in all animals. Animals either received eECM hydrogel (12 mg/mL, 25 mL, twice daily) administered orally at 15˚C plus omeprazole, or omeprazole alone control.

A final endoscopic examination and biopsy were conducted to evaluate the mucosa at the distal esophagus following 30 days of treatment. The 2 omeprazole controls (NMD-C, MD-C) did not show macroscopic resolution of esophagitis (redness or areas of erosion) after 30 days of treatment (Figure 24A, B). In contrast, all eECM treated dogs in the NMD group (NMD 1-4) showed almost complete resolution of macroscopic esophagitis after 30d of treatment compared to D0 (Figure 24A).

The eECM treatment dogs in the MD group did not show complete healing of macroscopic esophagitis after 30d treatment (MD 1-2) (Figure 24B). All MD animals had macroscopic reddish areas and erosion still present at the site of the second EMR. On the opposite side of the esophageal lumen to the second EMR, where the initial EMR had been performed at the time of the initial surgery, esophageal inflammation had receded resembling the NMD results.

8.5.7 eECM hydrogel mitigates metaplastic change in esophageal mucosa

Histologic evaluation (H&E staining) and immunolabeling for normal differentiated epithelium markers (suprabasal CK13+/basal CK14+) and Barrett's markers (Sox9+/Alcian blue+ goblet cells) were conducted on pre-treatment biopsies (d0) and post-treatment location-matched samples (d30) (Figure 25). A lower magnification of the same areas is shown in Supplementary Figure 52**.**

At d0, 7 of 8 dogs (NMD-C, NMD 1-4, and MD 1-2) showed intestinal metaplasia of the esophageal epithelium consistent with Barrett's disease. The metaplastic tissue was Sox9+, with minimal expression of CK13+/CK14+. MD-C had a Sox9- dysplastic epithelium at d0 (Figure 25A, B).

The majority of the esophageal mucosa in dog NMD-C was still metaplastic (Sox9+) with some small areas of normal epithelium (CK13+/CK14+) after 30d of treatment. In contrast, all 4 eECM treated dogs (NMD 1-4) showed histologic reversion of Barrett's esophagus toward a normal, differentiated squamous epithelium (CK13+/CK14+/Sox9-) in areas where columnar metaplasia (Sox9+) had previously been identified.

A different pattern was observed within the MD group. MD-C showed an area of metaplasia that was Sox9+, with adjacent areas of normal epithelium (CK13+/Ck14+) after 30d of eECM hydrogel treatment. MD-1 at 30d showed no evidence of metaplastic change (Sox9-/CK13+/CK14+), while MD-2 showed small areas of metaplasia and adjacent areas of normal, differentiated squamous epithelium (Figure 25B). A magnified view of the H&E staining for MD-2 shows an area of metaplastic epithelium with a transition to a normal, squamous epithelium (Supplementary Figure 53).

Alcian blue stains goblet cells and is commonly used as a secondary marker of Barrett's esophagus, corroborated the Sox9+ staining results at d0 and d30 for both the NMD and MD groups (Supplementary Figure 54**).**

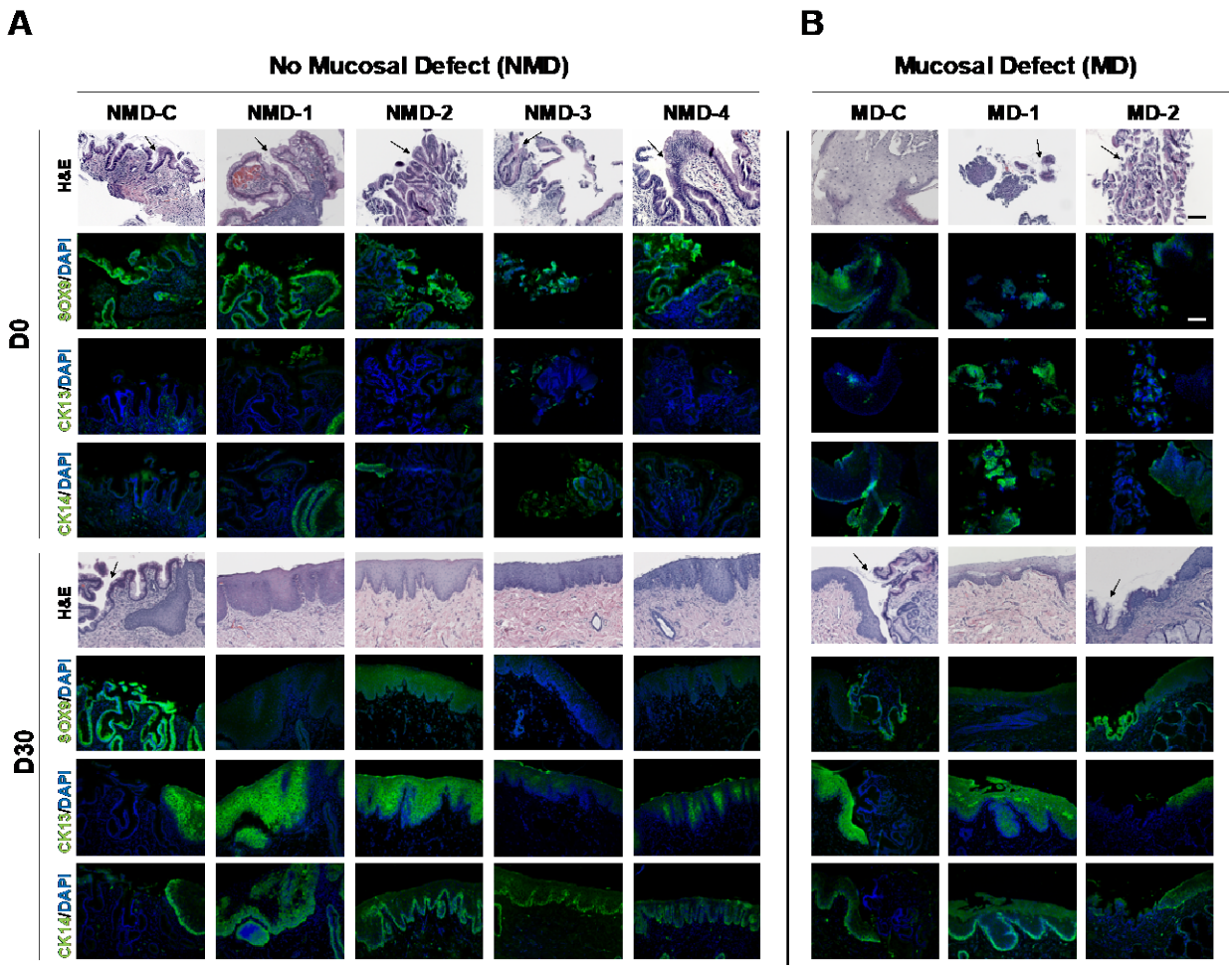

Figure 25. Effect of 30d eECM hydrogel on esophageal epithelial cell phenotype.
Animals were in one of two groups: no mucosal defect (NMD) (**A)** or mucosal defect (MD) (**B**). Biopsies (d0) were taken at the before treatment and following 30d of eECM treatment. Treatment was administered orally for 30d as eECM hydrogel (12 mg/mL 25 mL, BID) (NMD-1-4, MD-1-2) or control (Omeprazole 20 mg, QD) (NMD-C, MD-C). Samples were taken at necropsy in the same location as the biopsies, and stained with hematoxylin and eosin (H&E), Barrett's marker Sox9, or normal esophageal squamous epithelial markers CK13 and CK14. Arrows indicate goblet cells characteristic of intestinal metaplasia and Barrett's esophagus. Scale bar = 100 um.

8.5.8 eECM hydrogel downregulates TNFα+ expressing cells

Immunolabeling for TNFα was performed to characterize the pro-inflammatory cell infiltrate in the remodeled tissue. Three images per sample were quantified, with a representative picture shown (Figure 26).

There was a decrease in TNFα+ cells for NMD-1 (p=0.0055), NMD-2 (p=0.0004), and NMD-3 (p=0.0001) compared to the control NMD-C (Figure 26A) after 30d of treatment. There was no difference in the number of TNFα+ cells for MD-1 or MD-2 when compared to MD-C after 30d of treatment (Figure 26B).

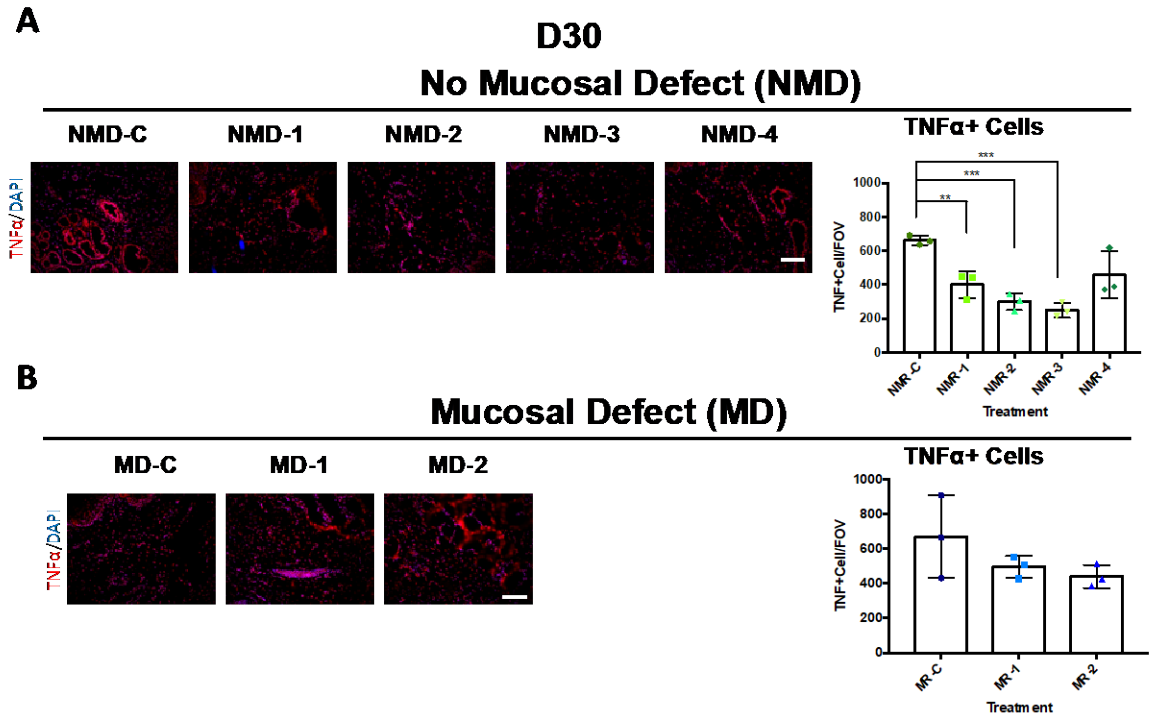

Figure 26. Effect of eECM hydrogel on TNFα+ pro-inflammatory cell infiltrate at D30. TNFα immunolabeling and DAPI counterstain was performed on the no mucosal defect (**NMD**) (**A**) or mucosal defect (**MD**) (**B**) animals after 30d of treatment. Three pictures per section per dog were imaged and quantified using Cell Profiler and compared to control. Representative images for each treatment are shown. Scale bar = 100 um. (** p≤0.01, *** p≤ 0.001). Values express mean ± SD.

8.5.9 Safety of eECM hydrogel oral administration for 30d: Does not induce gastrointestinal adverse effects and does not alter normal physiologic parameters

To evaluate safety of oral administration of the eECM hydrogel, animals were monitored for adverse gastroenterological events throughout administration of the therapy; weight was recorded and blood serum levels of electrolytes and proteins indicating organ status were measured before and after finalizing treatment.

No episodes of emesis or diarrhea occurred during the 30d treatment period. The animal's weight did not change throughout the course of the study (Figure 27A, B) and there were no abnormalities in electrolyte levels before or after treatment (Figure 27C).

Serum chemistries for liver function (ALB, ALP, ALT, TBIL), pancreatic function (AMY) and renal function (BUN/CRE) were conducted and showed no abnormalities before the initiation of the administration of eECM and at the conclusion of the study. No physiological parameters were outside the normal range in each of the in the evaluated body systems (Figure 27C).

A

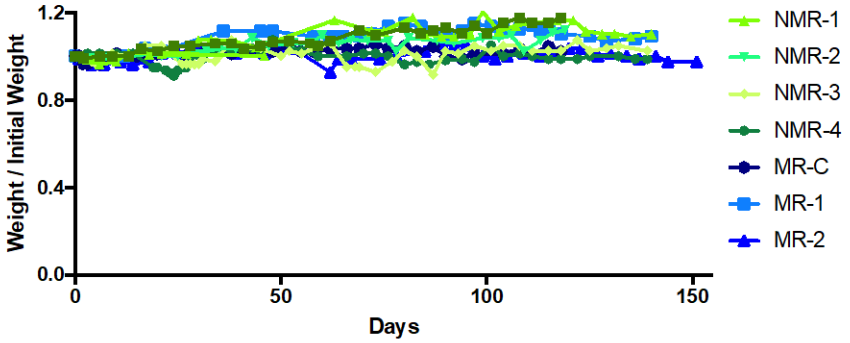

B

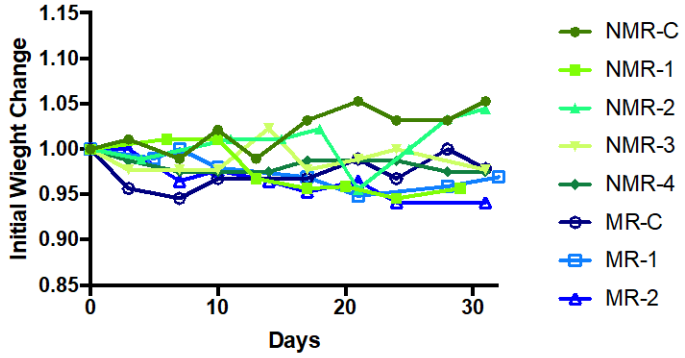

C

ANALYSIS	Before ECM Treatment (n=3)	After 30 days ECM Treatment (n=3)	Normal Range	Units
ALB (Albumin)	3.325	3.4	2.5 - 4.4	G/DL
ALP (Alkaline Phosphatase)	15	17.33	20 – 150	U/L
ALT (Alanine aminotransferase)	42.25	57.67	10 – 118	U/L
AMY (Amylase)	339	427	200 – 1200	U/L
TBIL (Total Bilirubin)	0.275	0.2	0.1 – 0.6	MG/DL
BUN (Blood urea nitrogen)	12.75	11.67	7 – 25	MG/DL
CA (Calcium)	10.15	10.2	8.6 – 11.8	MG/DL
PHOS (Phosphorus)	4.9	4.17	2.9 – 6.6	MG/DL
CRE (Creatinine)	0.75	0.87	0.3 – 1.4	MG/DL
GLU (Glucose)	92.75	112	60 – 110	MG/DL
NA^+ (Sodium)	153	137. 67	138 – 160	MMOL/L
K+ (Potassium)	4.35	4	3.7 – 5.8	MMOL/L
GLOB (globulin)	1.525	1.7	2.3 – 5.2	G/DL

Figure 27. Safety of 30 days of eECM administration.
A. Weight recording for all animals during the period of study. There was no overall weight change with a final weight of 106.23% ±6.60%. **B.** Animal weights during eECM administration. There was also no change with a 98.7%±3.75%. **C.** Average of veterinary blood scan did not show any physiological parameters out of range. Individual animals did not present any values out of range.

8.6 DISCUSSION

Results of the present study suggest that metaplastic changes induced in the esophageal mucosa as a result of chronic gastric reflux can be mitigated or reversed by exposure of the affected epithelial cells to a hydrogel composed of normal esophageal ECM components. These findings are consistent with a recently reported *in vitro* study in which neoplastic esophageal epithelial cells markedly downregulated the pathologic gene expression patterns following addition of normal esophageal matrix molecules to the culture medium (Chapter 7.0).

The concept of cell phenotype and morphogenetic patterning being directed or at least modulated by microenvironmental cues is not new [5, 238, 254]. Bissell et al. first described a model that postulates a relationship between the ECM and the cytoskeleton and nuclear matrix [5]. Kratochwil showed that normal breast epithelial cells cultured upon the ECM of salivary gland tissue assumed not only a salivary gland phenotype, but also the glandular patterning of salivary gland tissue [238].

Cell behavior, including proliferation, metabolic activity, and differentiation, is closely linked to the influence of microenvironmental cues [21]. The reciprocal flow of information between cells and the surrounding ECM directly impacts developing tissues and organs [4]. Factors present in cells' microenvironmental niche are continuously responding to and sending signals, which in turn modulates cell behavior and function during development [255]. The crosstalk between individual cells and their immediate surrounding microenvironment, which is largely represented by the ECM, is a key component of "dynamic reciprocity" [256]. That is, individual cells respond to the dynamic changes in their microenvironment by changing or

adapting their metabolic activity and consequent secretome [257]. The altered secretome in turn modifies the microenvironment (i.e., the ECM), which influences cell behavior.

The present study evaluated in a canine model, involved a surgical creation of a non-physiologic environment in the distal esophagus and the chronic, intermittent exposure to acidic gastric content. This condition mimics the clinical scenario of gastroesophageal reflux disease (GERD) and subsequent chronic inflammation that results in metaplastic transformation of the esophageal epithelium (i.e., Barret's esophagus) [11]. In our hands, the canine surgical model developed columnar metaplasia in 7 out of 8 animals after 3 months of daily pentagastrin injections, which correlated with previous findings, and further validated this experimental model [253, 258]. The large animal canine model was selected because of the comparable size to a human esophagus for endoscopic manipulation, and to evaluate cross-species effects from the porcine-derived ECM hydrogel.

The results of this preliminary study suggest that potentially harmful pathologic changes induced in the esophageal mucosa by chronic gastric reflux can be halted or reversed by exposure to normal esophageal ECM components. Thirty days of eECM hydrogel delivery reversed the macroscopic pro-inflammatory changes that had developed after inducing reflux for the non-mucosal defect (NMD) group. Furthermore, immunohistochemical analysis showed reversal of columnar metaplasia with decreased SOX9+/Alcian blue+ goblet cells, and an increase in CK13+/CK14+ differentiated esophageal epithelial cells. This reversal was accompanied by a reduction of overall TNFα+ pro-inflammatory cells in the remodeled tissue. No adverse gastrointestinal effects occurred after 30d of twice daily digestion, and blood serum protein levels representative of multiple body functions (liver, pancreas, kidney) remained within normal, physiologic ranges during the treatment period.

ECM bioscaffolds have been shown to promote esophageal reconstruction in pre-clinical [26-33] and human studies [30]. Heterologous and homologous eECM bioscaffolds have prevented stricture after full circumferential resection [29], augmented the gastroesophageal

anastomosis [28], reformed normal esophageal tissue layers after full-thickness defects [32, 43], and reformed near-normal mucosal epithelium after mucosal resection of esophageal adenocarcinoma (T1A) [30]. The mechanisms are not completely understood but the degradation of the ECM scaffolds [27, 29], promotion of re-epithelialization [27, 29] and downregulation of the pro-inflammatory response [29] have been proposed to be important. The present study shows that eECM in the hydrogel form can provide similar constructive effects as the previous bioscaffold studies, and can promote disease regression in a pathologic setting. The hydrogel form has the added advantages over the bioscaffold of being minimally invasive (liquid at room temperature and gels *in vivo*) and obviates the need for a stent to hold the bioscaffold in place [30].

What components in the eECM hydrogel may be regressing metaplastic cell phenotype via dynamic reciprocity? Targeted proteomics revealed the eECM composition includes structural proteins (e.g., collagen types I, III, and V), matrix-cell attachment proteins (e.g., fibronectin 1, dermatopontin, and fibrillin-1) and basement membrane proteins related to matrix-cell signaling (e.g., laminins, perlecan, nidogen, agrin, and collagen type IV). Laminin-311 is one protein that is plausibly retained in the eECM because of the retention of its heterotrimer subunits α3, β1, and γ1 (Error! Reference source not found.). Laminin-311 is not extensively studied, but was shown to be enriched in the basement membrane of lung tissue that is subjected to cyclic stretch, and promoted lung epithelial cell differentiation through β1 integrin [259], and the mechanotransduction of pro-survival MAPK signaling through its cable-like rope structure [260]. The esophagus is an organ that also undergoes cyclic stretch through peristalsis and could necessitate a similar mechanoresponsive basement membrane. Laminin-311 forms a complex with perlecan and nidogen-1 *[260]*, which were retained in eECM in the present study (Error! Reference source not found.), and it is thought that this complex mediates epithelial cell attachment and basement membrane assembly [261]. These complexes show the coordination

between components in the biochemically complex eECM which acts to influence cell behavior, and the advantage of isolating the template that Mother Nature has engineered. However, the constructive effects upon the inflammatory response and epithelial cell phenotype that occurred in response to the hydrogel cannot be attributed to any single component or combination of components. There is a differential expression of ECM components in the various segments of the GI tract and the functional and structural roles of these components during morphogenesis and homeostasis is only partially understood [262].

Which cell types may be influenced by the eECM hydrogel? Two main drivers of Barrett's pathogenesis are (1) transformation of the esophageal epithelial cells (differentiated epithelial cells and esophageal epithelial stem cells) [13, 17] and (2) chronic pro-inflammatory cells [11]. First, in a previous study eECM hydrogel robustly downregulated metaplastic (CP-A) and neoplastic (SK-GT-4, OE33) esophageal epithelial cell proliferation, downregulated signaling pathways associated with cell cycle, PI3K-Akt, and G1 to S phase transition, and interestingly increased the same signaling pathways in non-malignant epithelial cells (Chapter 7.0). The divergent effects on neoplastic and non-malignant cells would be advantageous for a pre-malignant therapy delivered to the esophagus. eECM hydrogel also promoted basally polarized, normally differentiated (CK13+/CK14+) stem cell organoids [33]. The eECM therapy could plausibly promote normal differentiation of stem or progenitor cells and normalize dysregulated stem cell signaling.

Second, the present study also robustly downregulated the TNFα+ pro-inflammatory cell infiltrate in 3 of the 4 NMD treatment dogs compared to control. TNFα is a potent pro-inflammatory cytokine that is upregulated with GERD-Barrett's-EAC progression [19]. Chronic levels of TNFα contribute to multiple mechanisms of Barrett's disease including upregulating matrix metalloproteinases (MMPs) to further remodel the matrix [19], inducing epithelial cells to proliferate and secrete reactive oxygen species (ROS) that can lead to DNA damage [20]; and

reducing E-cadherin levels/cell-cell adhesions [10] that can expose resident stem cells to bile salts and acid [11, 12, 19]. The present study results corroborated a previous study that delivered ECM hydrogel via enema in a rat model of ulcerative colitis, another chronic inflammatory-driven disease of the lower GI tract [140]. ECM hydrogel downregulated TNFα+ macrophages, which correlated with the restoration of a near normal epithelium, restoration of mucosal epithelial barrier function, and increased Ecadherin+ cell-cell adhesions [140]. In summary, eECM hydrogel most likely does not target one aspect of the Barrett's esophagus molecular pathogenesis, but rather acts through a "whole microenvironmental" approach, such as modulating epithelial cell phenotype and reducing the pro-inflammatory TNFα+ cell infiltrate.

Finally, from a more practical perspective, the success of a therapy delivered to the esophagus is highly dependent upon its ability to reach and remain at the desired location for its bioinductive effect. Rheologic and *ex vivo* testing demonstrated that the material properties of the ECM hydrogel such as gelation time, stiffness and mucoadhesion of the ECM hydrogel could be tailored by varying ECM concentration, temperature and tissue source. Based on our results, eECM at 12 mg/mL was selected as the preferred tissue source and ECM concentration. eECM at 12 mg/mL showed the highest mucoadhesion strength compared to heterologous sources, suggesting a tissue-specific effect. Increased mucoadhesion has been observed for "like" polymers, and it is plausible that the native esophageal mucosa and mucosa ECM hydrogel share similar biochemical and/or ultrastructural composition allowing for interdiffusion mucoadhesion at the interface [263]. Another important factor is the ability of the eECM hydrogel to be pushed through a catheter (e.g., shear-thinning viscosity), and showing a relatively fast gelation time (~5 min), which would be preferable because of esophageal peristalsis and swallowing. The results of the rheologic and *ex vivo* testing were confirmed *in vivo*, where the eECM hydrogel adhered up to 40 minutes after oral delivery in a healthy esophagus. It is suspected that the hydrogel would adhere equally, if not better, to the ulcerated

Barrett's tissue, as was shown previously wherein ECM hydrogel adhered equally to healthy or ulcerated colonic tissue [140].

The potential clinical implications of the present study are noteworthy. GERD, BE, and EAC are serious problems that have limited therapeutic options. Barrett's patients have persistent chronic inflammation, despite treatment for the gastric acid [11, 12]. An alternative therapy is needed. eECM hydrogel therapy could be incorporated into routine care of Barrett's patients, i.e., provided at the time of diagnosis endoscopically and at routine endoscopies, or prescribed to a patient to take home (oral administration). Further studies are required to investigate the efficacy of an eECM hydrogel as a treatment option for the esophageal pathology caused by gastric reflux.

The main limitations of this pilot study are the low animal number for the various treatment groups and the single time point (30d following initiation of treatment) of evaluation. There were also no dogs that received the eECM hydrogel alone during the post 90-day treatment period. However, neither of the two control dogs that received omeprazole alone showed any mitigation of the chronic inflammation. Further studies are required to investigate the efficacy of an ECM hydrogel as a treatment option for the esophageal pathology caused by gastric reflux, but the results of this pilot study are promising and importantly based upon accepted concepts of cell:matrix interactions.

8.7 CONCLUSION

The results show that non-malignant eECM retains a biochemically complex protein signature from the native mucosal tissue that includes basement membrane proteins, structural collagens, and microfibril associated proteins that can direct cell-matrix attachment. Consistent with our hypothesis, eECM hydrogel delivered orally for 30d in a canine model of Barrett's esophagus

can mitigate macroscopic esophagitis and mitigate the metaplastic epithelium from Sox9+/Alcian blue+ goblet cells toward normal, differentiated squamous epithelium (CK13+/CK14+). In contrast, the controls showed maintenance of Barrett's epithelium or progression from dysplasia to Barrett's. eECM treatment decreased the TNFα+ cell infiltrate in the remodeled tissue compared to control, suggesting that the non-malignant eECM hydrogel mitigated pro-inflammation and promoted constructive tissue remodeling, highlighting the interplay between non-malignant ECM, pro-inflammatory cells, and epithelial cells.

9.0 ECM AS A SUBMUCOSAL FLUID CUSHION AND TO PREVENT STRICTURE: A PILOT STUDY IN A DOG MODEL

9.1 HYPOTHESIS

Chapter 8.0 showed that eECM delivered orally for 30d in a canine model of Barrett's esophagus could mitigate metaplastic epithelium. The present study hypothesized that the eECM hydrogel mechanical and bioactive properties could be used for an alternative delivery method, i.e., delivering eECM hydrogel as a submucosal fluid cushion at the time of endoscopic resection of diseased esophageal epithelium. Previous studies have shown that the ECM scaffold in sheet form can mitigate stricture, and it was hypothesized that the eECM hydrogel would similarly mitigate stricture through its bioactive properties.

9.2 INTRODUCTION

Esophageal endoscopic submucosal dissection (ESD) [264] and endoscopic mucosal resection (EMR) [265] are two procedures that can be used to resect Barrett's esophagus with high grade dysplasia and neoplastic lesions. ESD cuts the submucosa with a specialized knife (e.g., Triangle Tip Knife), with the potential for deeper and more precise resection and requires ~60-120 minutes per procedure. EMR uses a snare or suction to resect the lesion, is less precise than ESD, but is significantly faster (~10 minutes per procedure). Gastroenterologists are

cautioned by their ability to aggressively resect pre-malignant and neoplastic lesions greater than 75% of the circumference because of the high risk for stricture [266].

During both EMR and ESD procedures, a fluid is injected into the submucosal space to elevate the mucosa while not damaging the underlying muscle layer. A stably formed submucosal fluid cushion (SFC) will provide better visualization of the margins for a complete resection, help to preserve the *en bloc* tissue for pathology, minimize the risk of perforation and bleeding during the procedure, and reduce the time per procedure i.e., endoscopic instruments need to be switched out for SFC injection versus resection [267-269]. Normal saline is typically used for SFC, but dissipates quickly into the mucosa. The only FDA approved medical device for SFC is Eleview®, an inert synthetic material that is designed for the physical lifting of the mucosa.

An ideal biomaterial would form a stably formed cushion in the submucosal space and mitigate stricture. Previously, multilayered UBM-ECM bioscaffolds mitigated stricture after placement on the autologous muscle tissue (at least 30% present) following full circumferential resection (5 cm) in the cervical esophagus [27, 29]. The UBM-ECM degraded as early as 13d, and was indistinguishable from the host tissue [27]. ECM degradation products can be simulated with pepsin digestion, and also form an ECM hydrogel. It is not known if the ECM hydrogel can similarly prevent stricture as the UBM-ECM bioscaffold. An ECM hydrogel that mitigates stricture would expand the clinical utility of the therapy for use in combination with standard esophageal treatments, including EMR and ESD.

The objectives of the present pilot study were to investigate the use of ECM hydrogel (12 mg/mL) to 1) mitigate stricture after full circumferential resection (5 cm) *in vivo* and 2) its characterize the SFC products *in vitro*. Outcome measures for the *in vivo* experiments included measuring the esophageal circumference after necropsy and assessment of epithelium reformation *in vivo*. Outcome measures for the *in vitro* study included evaluating mechanical

properties (viscoelasticity, mucoadhesion, and cushion formation *ex vivo*) and effects on macrophage phenotype, as a determinant of downstream tissue remodeling.

9.3 METHODS

9.3.1 Overview of animal study

A full circumferential mucosal resection of 5 cm of longitudinal width was performed in 3 dogs using a combination of EMR and ESD techniques as similarly described [29]. Evaluated treatments were twice daily administration of UBM-ECM hydrogel (n=2) and an untreated control (n=1). Endoscopy was performed 1 month after the procedure or if animals presented any clinical signs of stricture. A dilation was performed if possible and necessary according to the endoscopic findings on the animals. Animals were euthanized if they presented severe stricture or reached the 2 month timepoint after the balloon dilation. At the necropsy, animal tissue was measured to determine stricture and samples were harvested for histologic analysis. This animal model allowed measuring the following endpoints:

1. Endoscopic appearance of resection area
2. Esophageal measurements
3. Histologic assessment at final timepoint

9.3.2 Surgical procedure and postoperative care

All procedures complied with the University of Pittsburgh Institutional Animal Care and Use Program Policy for Large and Small Animal Surgery revision 12/14/2015. Each dog was induced with acepromazine (0.01 mg/kg, SC) and ketamine (5-11 mg/kg), and surgical plane anesthesia

maintained with 1-5% Isoflurane via endotracheal tube. After induction, the animal was moved to the surgery table and positioned inside the sterile surgical theater. Throughout the procedure and observation animals were infused with 2 ml/kg/h of lactated Ringer's solution. Temperature was controlled through warm water recirculating heating pads placed under the animal. Physiologic parameters such as heart rate, respiration rate, body temperature, and responsiveness were monitored during the procedure. Antibiotic prophylaxis with 25mg/kg of Cefazolin was administered before starting the procedure.

The animal was placed in supine decubitus with and a Pentax EG3430K endoscope was used to evaluate the esophagus. Distance from the mouth to the GE junction was measured. After identifying reference points in the esophagus, the mucosa and submucosa were separated with an injection of saline using a Olympus Injectorforce 4mm 23G needle. The full circumference of the mucosa (100%) for a length of 5 cm was removed using the ESD and Loop EMR technique. The ESD technique was done by injecting fluid or ECM into the mucosa/submucosa to separate the mucosa from the submucosa then using an endoscopic TT knife to cut the area. To perform EMR, a Cook Duette Kit with a ligation band was used. The mucosa was then excised with the use of a snare. The area of resection was demarked using Spot Endoscopic Marker.

For animals receiving UBM-ECM hydrogel treatment, after the mucosa was removed, and during the procedure, 50 mL of 12mg/mL of the UBM hydrogel were delivered and applied to the area of excision using a MILA EDC190 Endoscopic delivery catheter. The animals were maintained under anesthesia for 5 mins to allow gelation of the hydrogel. After the procedure animals were recovered and placed in observation.

Following the surgical procedure and cessation of inhalation anesthesia, animals were continually monitored for 24 hours. Body temperature was determined and recorded every 12 hours. The animals were kept warm and dry to prevent hypothermia and rotated once per half-hour until they maintained a sternal position.

Dogs were held in single housing with other animals in the room until animals were stable as determined by the Animal Research personnel, and then placed in normal living facilities. Buprenorphine (0.005-0.01 mg/kg intramuscular or intravenous, q12h), was administered following each surgical procedure for 5 days for pain and was continued if signs of pain were present and cephalexin (35 mg/kg q12) for 5 days.

After the procedure and until the end of the study, animals were monitored for signs of esophageal stenosis such as a decrease in food consumption, loss of body weight, and signs of distress, as determined by increases in breathing patterns, vocal expression, emetic episodes or difficulty swallowing food and/or decreased activity. If these signs were present, animals were evaluated with a contrast esophagogram and/or endoscopy.

9.3.3 Endoscopic monitoring and balloon dilation

One month after the initial surgical procedure animals underwent an endoscopy if any clinical signs of stricture were present. Additionally, all animals underwent an endoscopic procedure prior to euthanasia. Anesthesia was induced with acepromazine (0.1-0.5mg/kg) and maintained on isoflurane (1-5%) to perform the endoscopy.

If the animal was diagnosed with a mild or moderate stricture during the endoscopy, a balloon dilation was performed. To perform the dilation procedure an Olympus 20mm balloon dilator was used. Under endoscopic guidance, the balloon was inflated until moderate or significant amount of resistance could be identified with approximately 10 mL of 0.9% NaCl sterile and was kept inflated for 30-60 seconds. After dilation in UBM-ECM hydrogel treated animals, 50 mL of ECM was immediately applied to the injured area using a MILA EDC 190 catheter and left to gel for 5 minutes. After the procedure animals were not given access to food or water for at least an hour.

9.3.4 ECM delivery

ECM was delivered orally to the animals with the use of a 60 ml catheter tip syringe at 15°C. 50 mL were delivered twice daily from day 0 until completion of the study. Animals were not allowed to eat or drink for an hour after delivery of the hydrogel.

9.3.5 Necropsy

At the moment of necropsy, an endoscopy was performed as previously described. Euthanasia was performed by administering pentobarbital sodium IV (390 mg/kg) under anesthesia. After death was confirmed, the esophagus was harvested maintaining the same dimensions it had in the body. Measurements of the esophagus were taken 0.5 cm apart and recorded.

9.3.6 Rheology

The viscoelastic properties of Eleview® and eECM 12 mg/mL were determined with a temperature-controlled, 40 mm parallel plate rheometer (AR2000). The samples were kept at 4°C and loaded onto the rheometer with a parallel plate geometry pre-cooled to 10ºC. Mineral oil was used to seal the sample-plate interface and to minimize evaporation during the testing. A series of rheological tests were conducted for each sample in sequence. A steady state flow curve at 10°C was performed to determine the viscosity profile of the samples at a range of shear rates (0.1-1000 s^{-1}). Plate temperature was rapidly raised from 10°C to 37ºC, and an oscillatory time sweep was performed at 37ºC, by applying a small, 0.5% oscillatory strain at a frequency of 1 rad/s to measure the maximum storage modulus (G'), maximum loss modulus (G'') and gelation kinetics. Data was extracted and analyzed in Prism (Version 6, GraphPad) for statistical analysis (n=3).

9.3.7 Mucoadhesion to muscularis

A schematic of the experimental set-up to measure mucoadhesion of Eleview® and eECM hydrogel to porcine esophageal mucosa and muscularis is shown in Supplementary Figure 56. The test was performed as described in 8.4.3. Measurements were only accepted if the detachment occurred between the mucosa or muscularis and the hydrogel (n=3).

9.3.8 Ex-vivo submucosal fluid cushion performance

Porcine esophagus, colon and stomach were placed in a 37˚C incubator and their temperature was monitored with a thermometer until tissues reached 37˚C. After reaching the target temperature, a 23G needle was used to inject 2mL of either Eleview® or neutralized eECM at 12 mg/mL. eECM was kept on ice during the procedure. Tissues were evaluated and photographed alongside a metric witness at 15 minutes intervals for up to 75 minutes. Tissues were kept incubated at 37˚C throughout the procedure. After 75 minutes, the area injected with the test agents was dissected and evaluated. ImageJ was used to quantify the elevation of the mucosa after injection of the agent throughout the experiment.

9.3.9 Macrophage isolation and activation

Mouse bone marrow was harvested as previously described [131, 270]. Briefly, female 6 to 8 week old C57bl/6 mice (Jackson Laboratories, Bar Harbor, ME) were euthanized via CO_2 inhalation and cervical dislocation. Aseptically, the skin from the proximal hind limb to the foot was removed, the tarsus and stifle disarticulated, and the tibia isolated. The coxafemoral joint was disarticulated for isolation of the femur. After removal of excess tissue, bones were kept on ice and rinsed in a sterile dish containing macrophage complete medium consisting of DMEM

(Gibco, Grand Island, NY), 10% fetal bovine serum (FBS) (Invitrogen, Carlsbad, CA), 10% L929 supernatant[270], 50 uM beta-mercaptoethanol (Gibco), 100 U/ml penicillin, 100 ug/ml streptomycin, 10 mM non-essential amino acids (Gibco) and 10 mM HEPES buffer. The ends of the bones were transected and the marrow cavity was flushed with complete medium to collect bone marrow. Cells were washed, plated at 2 x 10^6 cells/ml, and allowed to differentiate into macrophages for 7 days at 37°C, 5% CO_2 with complete media changes every 48 hours as previously described [271]. After 7 days, resulting naïve macrophages were treated with basal media consisting of 10% FBS, 100 ug/ml streptomycin, 100 U/ml penicillin in DMEM and one of the following conditions as previously described: (1) 20 ng/ml IFNγ and 100 ng/ml of LPS to promote an M1-like phenotype, (2) 20 ng/ml IL-4 to promote an M2-like phenotype, (3) 250 ug/ml of pepsin control buffer, (4) 250 ug/ml of esophageal ECM, or (5) same volume of Eleview® for 24 hours at 37°C, 5% CO_2 [272].

9.3.10 Immunolabeling of macrophages

After 24 hours, macrophages were washed and fixed with 2% paraformaldehyde. Following PBS washes, cells were incubated in blocking solution consisting of 0.1% Triton-X 100, 0.1% Tween 20, 4% normal goat serum, and 2% bovine serum albumin (BSA) for 1 hour at room temperature to prevent non-specific antibody binding. The following primary antibodies were diluted in blocking solution: (1) monoclonal anti-F4/80 (Abcam, Cambridge, MA) at 1:100 dilution for a pan-macrophage marker, (2) polyclonal anti-iNOS (Abcam, Cambridge, MA) at 1:100 dilution for a M1-like marker, (3) polyclonal anti-Fizz1 (Peprotech, Rocky Hill, NJ) at 1:100 dilution for a M2-like marker, (4) polyclonal to liver Arginase (Abcam, Cambridge, MA) at 1:100 dilution for a M2-like marker [273-275]. Cells were incubated in primary antibodies for 16 h at 4°C. After PBS washes, cells were incubated in fluorophore-conjugated secondary antibodies (Alexa Fluor goat anti-rat 488 or goat anti-rabbit 488, Invitrogen) for 1 hour at room temperature.

After PBS washes, nuclei were counterstained with 4’6’diamidino-2-phenylindole (DAPI) prior to imaging three 200X fields using a live-cell microscope. Light exposure times were standardized to a negative isotype control and kept constant across images. Images were quantified utilizing CellProfiler Image Analysis software to obtain positive F4/80, iNOS, Fizz1, and Arginase1 percentages.

9.3.11 In-vivo use of ECM as submucosal fluid cushion for EMR

All procedures complied with the University of Pittsburgh Institutional Animal Care and Use Program Policy for Large and Small Animal Surgery revision 12/14/2015 with approved protocol number 17050670. Anesthesia was induced with acepromazine (0.01 mg/kg, SC) and ketamine (5-11 mg/kg), and surgical plane anesthesia maintained with 1-5% Isoflurane via endotracheal tube. Throughout the procedure and immediate post-operative period, animals were administered 2 ml/kg/h of lactated Ringer’s solution intravenously. Temperature was controlled through warm water recirculating heating pads placed under the animal. Physiologic parameters such as heart, respiration rate, body temperature, and responsiveness were monitored during the procedure. Antibiotic prophylaxis with 25mg/kg of cefazolin was administered before starting the procedure.

The animal was placed in supine position and a Pentax EG3430K endoscope was used to evaluate the esophagus. Distance from the mouth to the GE junction was measured. After identifying reference points in the esophagus the mucosa and submucosa at the site of excision were separated by with injection blue-dyed Urinary Bladder Matrix - hydrogel at 8mg/ml using a Olympus Injectorforce 4mm 23G needle. at 4˚C. This temperature was maintained at all times to prevent gelation and potential plugging of the needle. Approximately 2-5 ml of blue gel were injected per site. The full circumference of the mucosa (100%) for a length of 5 cm was removed

using band-ligation EMR technique. For EMR a Cook Duette Kit with a ligation band was used. The mucosa was then excised with the use of a snare.

9.3.12 Statistics

A 2-way ANOVA was used to compare the effect of the independent variables shear rate and sample on the dependent variable viscosity; and also to compare the effect of the independent variables sample and modulus type on the dependent variable modulus. A Sidak post-hoc multiple comparisons test was used and significance was determined using the 95% confidence interval and p-values were adjusted for multiple comparisons. A t-test was performed for the mucoadhesive strength comparing Eleview® and eECM 12 mg/mL.

9.4 RESULTS

Part I: Use of UBM-ECM hydrogel to mitigate stricture

9.4.1 Stricture study overview

Figure 28 shows the study design. The pilot study used 3 dogs, each of which received a full circumferential resection of 5 cm. Endoscopy was performed one month after the procedure or sooner if animals showed clinical signs of stricture. Based upon the endoscopy results a dilation could be performed if deemed necessary. Animals were sacrificed if they presented with intractable stricture or at the pre-determined endpoint 2 months after balloon dilation.

After resection, the control dog did not receive additional treatment, whereas the two UBM-ECM dogs received hydrogel treatment twice daily for 2 months post-balloon dilation.

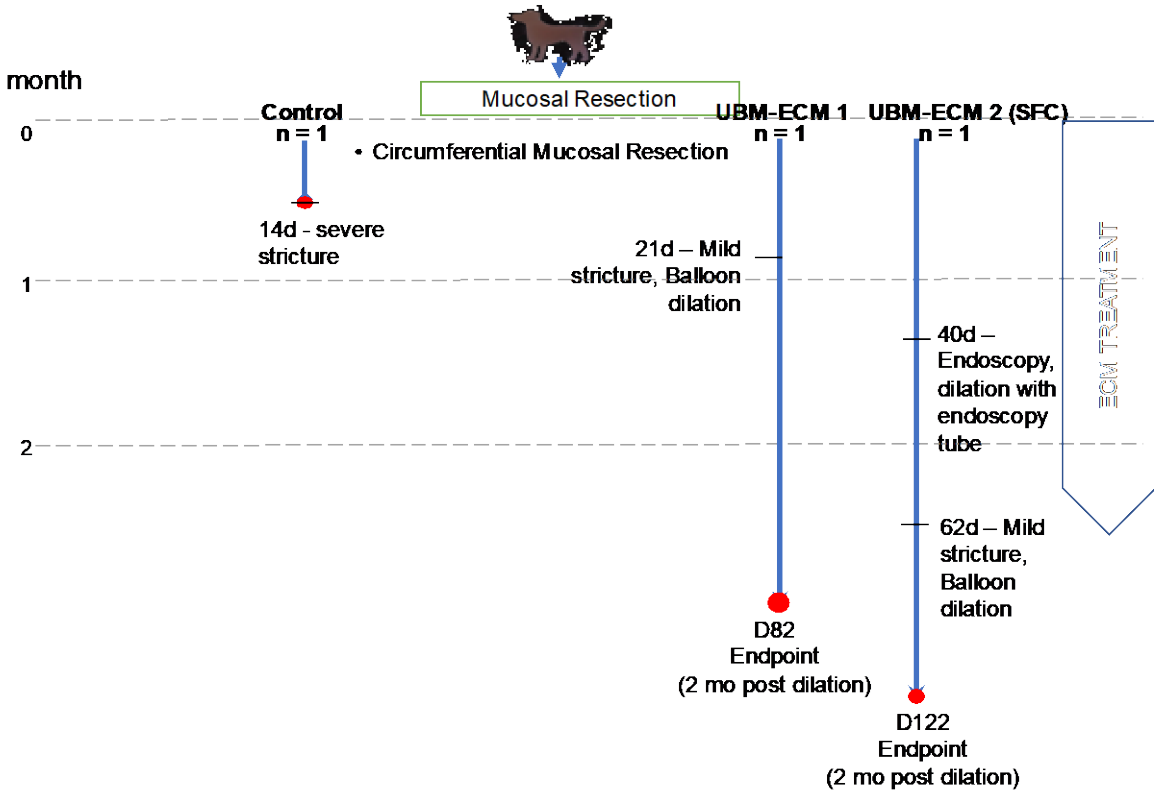

Figure 28 Study Overview: Use of UBM-ECM hydrogel to mitigate stricture in vivo. Control and UBM-ECM 1 had a 5cm circumferential resection created by a combination of EMR and ESD. UBM-ECM-2 used the UBM-ECM hydrogel as a submucosal fluid cushion and EMR was performed to resect the tissue. UBM-ECM treatment dogs received twice daily oral treatment (50 mL/treatment) for 2 months post-balloon dilation.

9.4.2 Efficacy of UBM-ECM hydrogel to mitigate stricture and promote re-epithelialization

Control (no treatment) had a full circumferential resection using a combination of EMR and ESD. The control dog developed a severe stricture after 14d and was euthanized (Figure 29A). UBM-ECM hydrogel treatment dog 1 had a full circumferential resection using a combination of EMR and ESD, was provided UBM-ECM hydrogel immediately after application (endoscopically), and then provided orally (12 mg/mL, 50 mL, twice daily) for the duration of the

study. The UBM-ECM dog 1 had a soft stricture at 21d that was easily dilated, and reached endpoint at 2 months post balloon dilation (Day 82) (Figure 29A). The UBM-ECM dog 1 was eating a normal diet at the time of sacrifice. Dog 2 used UBM-ECM hydrogel at the time of EMR resection (8 mg/mL), and was provided orally thereafter (12 mg/mL, 50 mL, twice daily). A soft stricture was apparent at 40d but was dilated by the endoscope. Twenty-two days later (d62) the esophagus showed a mild stricture and was balloon dilated. UBM-ECM dog 2 reached endpoint 2 months later, at 122 days, and was tolerating a normal diet (Figure 29A).

The esophagus circumference was measured after necropsy and the UBM-ECM treatment dog 1 and UBM-ECM treatment dog 2 had a smaller decrease in circumference compared to the control dog, suggesting that the UBM-ECM hydrogel mitigated stricture (Figure 29B).

The UBM-ECM treatment dogs 1 and 2 showed reformation of a stratified squamous epithelium in the middle of the defect compared to control, which showed erosion (Figure 29C).

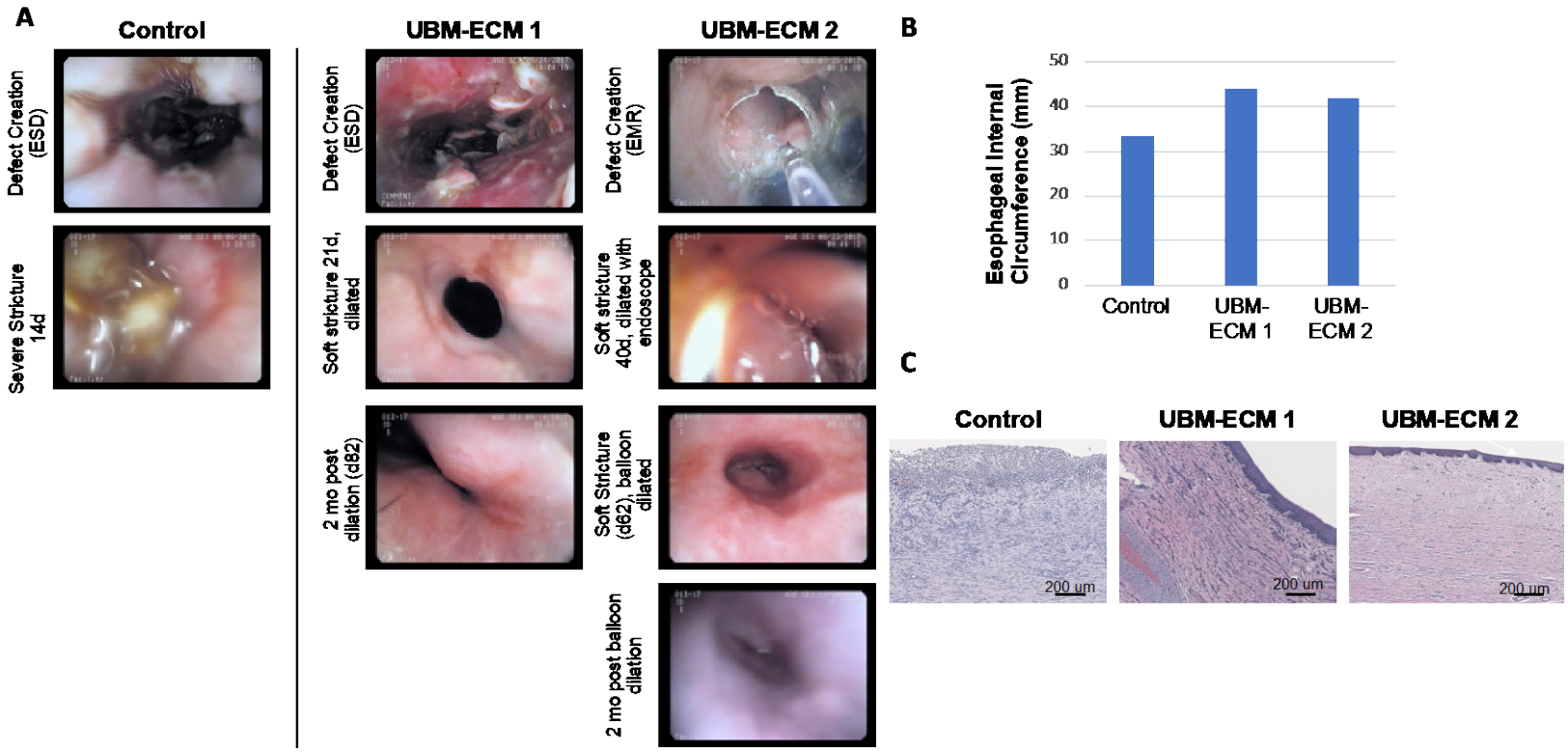

Figure 29. UBM-ECM hydrogel mitigated stricture and promoted re-epithelialization.
(A) Endoscopy pictures taken of Control (no treatment), UBM-ECM hydrogel treatment 1, and UBM-ECM hydrogel treatment 2 at the time of defect creation, when a soft or severe stricture developed, and before endpoint. (B). Circumference of the esophagus was measured after necropsy and shows UBM-ECM hydrogel treatment reduced the percentage decrease in circumference. (C). H&E staining of the center of the defect shows that the UBM-ECM 1 and 2 promoted reformation of a stratified squamous epithelium while control showed erosion. Scale bar= 200 um.

Phase II: **: Evaluation of ECM hydrogel as SFC**

9.4.3 *In vivo* use of UBM-ECM hydrogel as submucosal fluid cushion for EMR

UBM-ECM hydrogel was evaluated as a SFC in the UBM-ECM dog 2 as previously described. The UBM-ECM hydrogel was dyed blue and delivered through the long endoscopic needle without any resistance. Elevation of the mucosa was successfully achieved and maintained to facilitate the EMR procedure and the blue dye was visible indicating the places were the dissection had been created for removal (Figure 30A). Tissue was easily removed with the use of the snare. Upon macroscopic observation, the removed esophageal mucosal tissue included part of the gel (Figure 30B). The blue dye in the hydrogel appeared to diffuse across the circumference of the esophagus after removing the mucosa and a full-circumferential resection was achieved with the use of the hydrogel (Figure 30C). Further studies will be required to determine if the diffused blue material was hydrogel or the dye/water fraction that spread to the adjacent muscle.

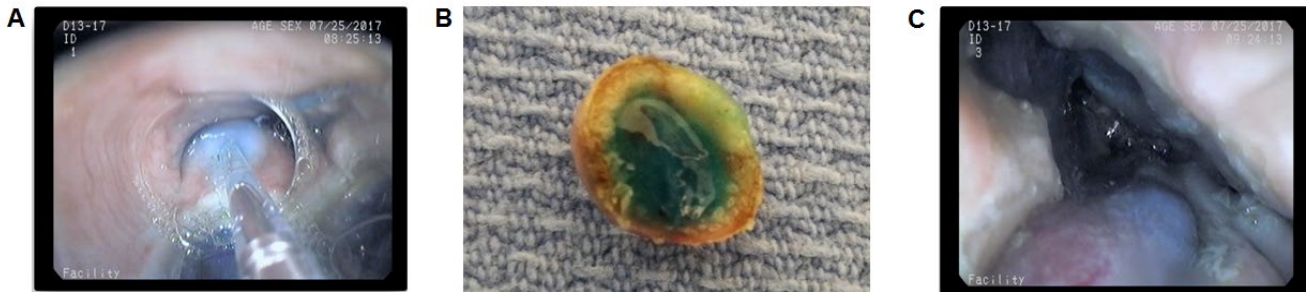

Figure 30. In-vivo use of UBM-ECM hydrogel as submucosal fluid cushion.
(A) Use of ECM hydrogel as a submucosal fluid cushion with visible areas where EMR has already been performed. (B) Esophageal tissue removed with SFC shows gel present on the removed piece. (C) Result of full circumferential EMR with full circumference of mucosa excised.

The *in vivo* results support the use of UBM-ECM as a SFC. The study will be appropriately powdered and repeated, and would use eECM hydrogel as the SFC. eECM hydrogel will be used because of more recent studies that show eECM can downregulate neoplastic esophageal cell phenotype (Chapter 7.0) and regress Barrett's epithelium in a canine model (Chapter 8.0). Hence, eECM was evaluated *in vitro* compared to Eleview® in the follow-up *in vitro* studies.

9.4.4 Viscoelastic properties of eECM and Eleview®

Eleview® was less viscous than eECM 12 mg/mL at 0.1 1/s shear rate ($p<0.0001$), and trended towards being less viscous at 1 1/s ($p=0.054$) (Figure 31A). Eleview® does not form a stably formed hydrogel because the loss modulus (G'') average (0.09 ± 0.04 Pa) is greater than the storage modulus (G') average (0.05 ± 0.01 Pa), while eECM 12 mg/mL has a storage modulus (G') (56.95 ± 66.72 Pa) that is ~ order of magnitude greater than the loss modulus (G") (7.62 ± 6.30 Pa) following the definition of a stably formed ECM hydrogel [62] (Figure 31B). The representative graphs of the time sweep of Eleview® further demonstrate that Eleview® does not form a hydrogel (Figure 31C), while the eECM 12 mg/mL storage modulus increases sigmoidally and plateaus over time (Figure 31D). Therefore, the gelation time to 50% gelation could be calculated for eECM 12 mg/mL (4.5 ± 3.5 min), but not for Eleview® (Figure 31E).

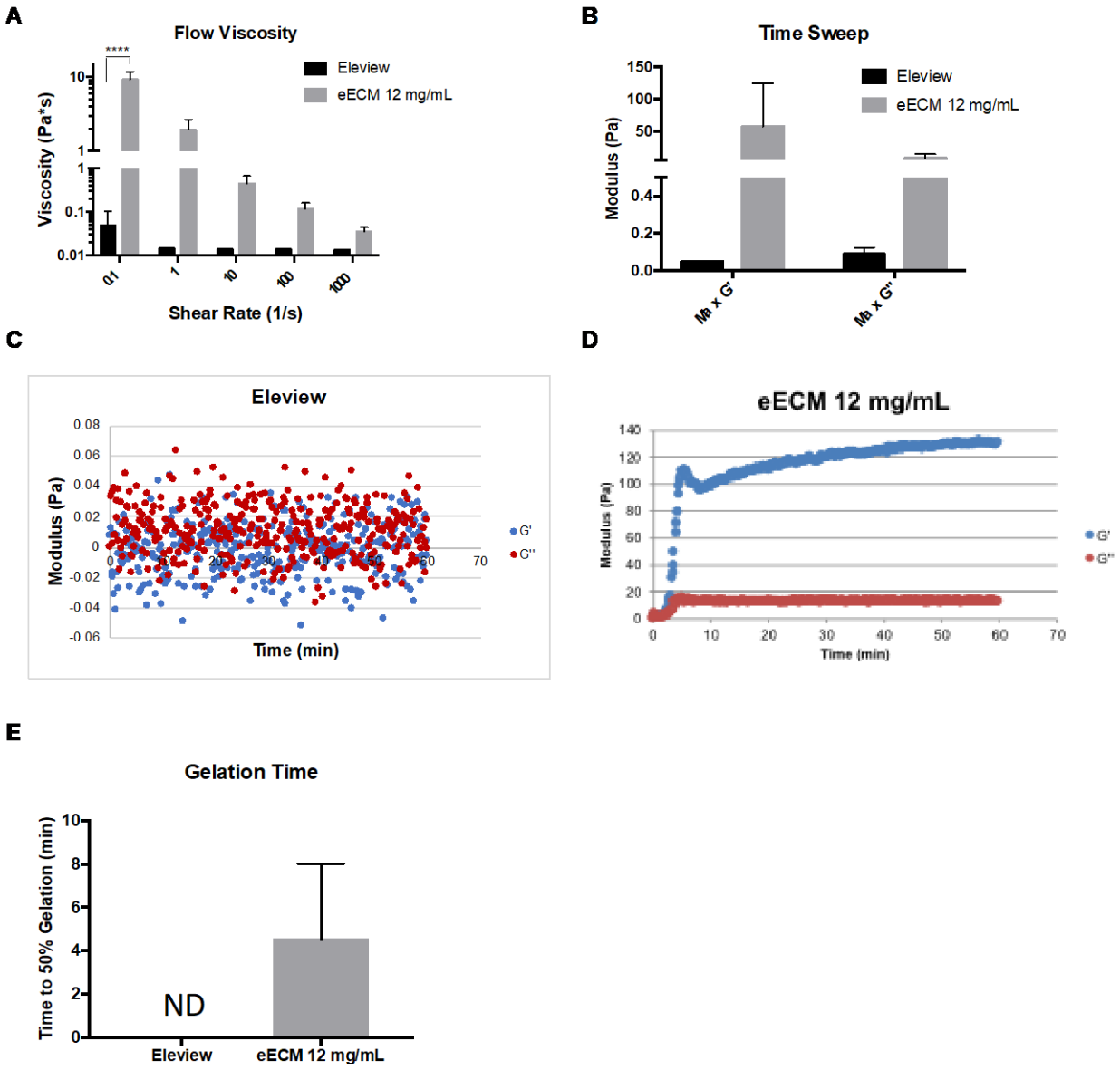

Figure 31. Viscoelastic properties.
(A) The viscosity profile of Eleview® and eECM 12 mg/mL was tested with increasing shear rate 0.1 – 1000 1/s) at 10°C. (B) Temperature was rapidly raised to 37°C to induce gelation and to measure the maximum storage and loss modulus. Representative graphs of the time sweep are shown for (C) Eleview® and (D) eECM hydrogel at 12 mg/mL. (E) Time to 50% gelation was measured for Eleview® and eECM at 12 mg/mL, but because Eleview® did not gel (G''>G' during the time sweep test), a gelation time is not shown (ND- Not determined). Values are expressed as mean ± SD.

9.4.5 Mucoadhesive force to the muscularis

Eleview® (0.16±0.05 N) and eECM (0.21±0.08 N) did not show significantly different mucoadhesion to the muscularis (Figure 32A). eECM had a higher mucoadhesive strength to the mucosa (0.37±0.02 N) than Eleview® (0.15±0.06 N) (p=0.0053) (Figure 32B).

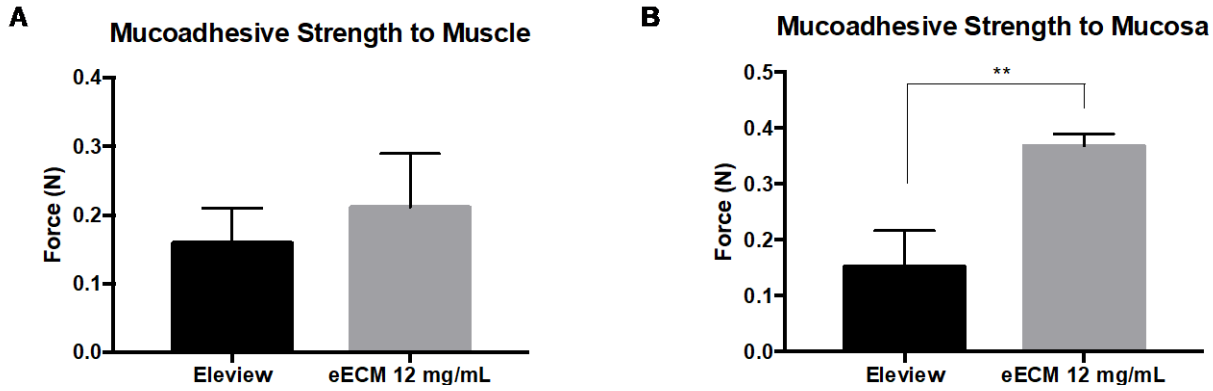

Figure 32. Mucoadhesive strength.
The mucoadhesive strength of Eleview® and eECM 12 mg/mL to (A) porcine muscularis or (B) mucosa. Values are expressed as mean ± SD.

9.4.6 Macrophage activation

Macrophages exposed to eECM showed activation of FIZZ1, an anti-inflammatory marker with minimal iNOS expression (a pro-inflammatory marker). iNOS expression was comparable between Eleview®, eECM and pepsin control (Figure 33). Eleview® did not show an effect on macrophage activation.

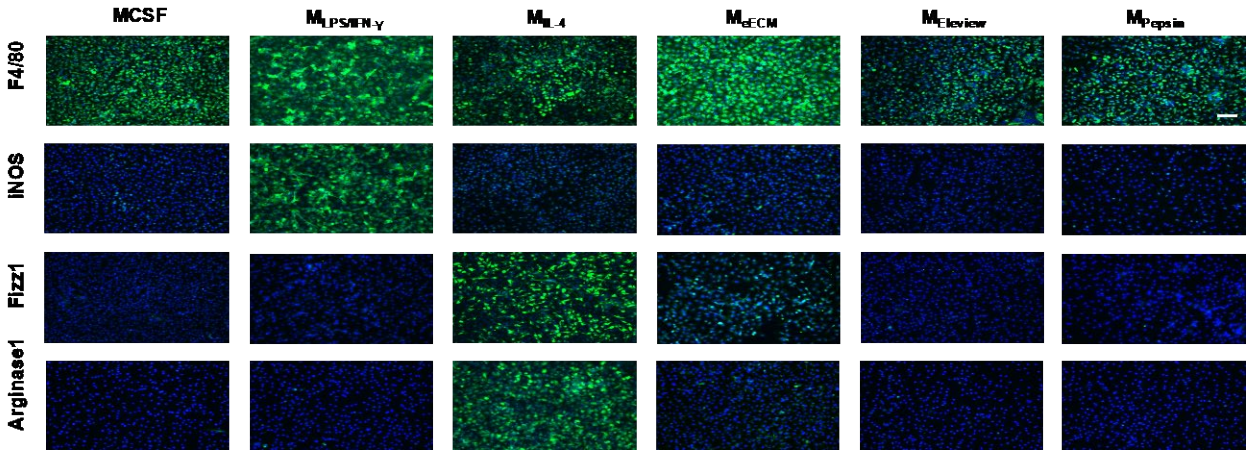

Figure 33. Macrophage activation.
Macrophage expression of anti-inflammatory (Fizz1, Arginase) and pro-inflammatory markers (iNOS) after exposure to eECM and Eleview®. F3/80 is a pan macrophage marker. Scale bar = 100 um.

9.4.7 Ex-vivo submucosal fluid cushion performance

Eleview® and eECM successfully created a fluid cushion with injection of 2mL of test agent. The two test agents were easily injectable with a 23G needle. Eleview® appeared to diffuse since the moment of injection. Measurements (Figure 34) and macroscopic appearance of the elevation confirmed this observation (Appendix F) for all three tissues tested.

eECM maintained a higher height compared to Eleview® for the duration of the test in the esophagus (Figure 34A) and colon (Figure 34B). The stomach, however had similar heights for both test agents (Figure 34C).

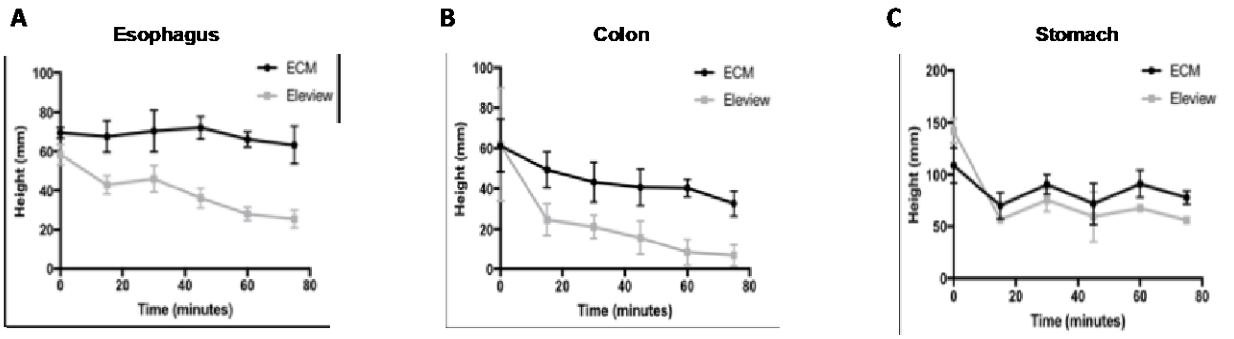

Figure 34. Ex vivo submucosal fluid cushion heights over time.
Heights were measured after injection of 2 mL of eECM or Eleview® over time in the (A) esophagus, (B) colon, and (C) stomach. Values are expressed as mean ± SD.

Dissection of test agent after 75 minutes showed differences between Eleview® and eECM in all tissues (Appendix F). Areas injected with Eleview® showed a viscous liquid with no clear adhesion to the mucosa or underlying muscle layer. Areas previously injected with eECM showed a clear and defined mass of gel that remained adhered to the mucosa and underlying muscle. The results support previous findings that demonstrated Eleview® was not able to form a gel (Figure 31C).

9.5 DISCUSSION

The results of the pilot study show that UBM-ECM hydrogel can mitigate stricture. UBM-ECM hydrogel delayed the onset of stricture, and the strictures that formed were soft and easily dilated using balloon dilation. In contrast, the stricture with the control dog was severe, not letting water or food pass, and the dog had to be euthanized. The two UBM-ECM treatment dogs were taken out to 2 months post dilation, and although the esophagi appeared slightly narrowed, were able to drink and eat a normal diet. The circumference measurements at

necropsy corroborated the macroscopic observations where the UBM-ECM hydrogel treatment reduced the decrease in circumference compared to control, i.e., mitigated stricture.

The results of the pilot study corroborated previous studies that used multilayered UBM-ECM bioscaffolds sheets placed after circumferential resection [27, 29] of the same size (5 cm). It was not obvious that the UBM-ECM hydrogel would recapitulate the effects of the UBM-ECM bioscaffold sheet. The multilayered UBM-ECM bioscaffolds were placed with a sidedness (i.e., abluminal side toward the muscle, and the luminal side toward the esophageal lumen) [27, 29]. It was suggested that the sidedness may have promoted esophageal epithelial cell migration across the basement membrane side of the UBM-ECM bioscaffolds, which is still plausible. However, somewhat surprising, even when the UBM-ECM was digested, and lost the sidedness and architecture of the scaffold, a similar result was still seen with mitigation of stricture and promotion of a near normal looking epithelium. This may suggest that the biochemical cues of the UBM-ECM degradation products are dominant over the physical structure of the bioscaffold.

What could be the mechanism for the mitigation of stricture? The pathogenesis of stricture is not well understood, however early epithelialization and minimization of the pro-inflammatory cell infiltrate are thought to be critical to prevent stricture [29]. In the present pilot study, the control dog showed erosion while the UBM-ECM hydrogel treatment dogs showed a near normal, stratified squamous epithelium at the center of the defect. Solubilized UBM-ECM has repeatedly been shown to promote an M2-like macrophage activation [131, 169], which could modulate from a pro-inflammatory (“M1-like”) to immunomodulatory (“M2-like”) microenvironment.

The study results also identified an alternative method to deliver the ECM hydrogel at the time of resection, by injecting into the submucosa. This delivery technique would provide an early, therapeutic dose to influence downstream esophageal tissue remodeling. ECM hydrogel would also obviate the need for stents, which is how the UBM-ECM bioscaffold was held in

place, and which requires another procedure to remove the stent and has a risk of stent migration.

The *in vivo* stricture study will need to be repeated, and eECM hydrogel will be used because of more recent results that indicate eECM can downregulate neoplastic phenotype (Chapter 7.0 and regress Barrett's epithelium (Chapter 8.0 eECM was compared to the current standard Eleview® as a submucosal fluid cushion *in vitro* for this reason. Eleview® and eECM are different biomaterials. Eleview® did not form a stably formed hydrogel at 37°C, but rather remained liquid over an hour at 37°C. Eleview® is a reverse phase poloxamer: a temperature-dependent liquid-to-gel material [267], however, it did not form a hydrogel *in vitro* during the rheology testing or during the *ex vivo* cushion testing in the present study.

In contrast, eECM formed a hydrogel that is stably formed at 37°C. This stably formed hydrogel could explain why the eECM hydrogel showed greater submucosal fluid cushion height than Eleview® for 75 minutes *ex vivo*; which would be sufficient for EMR procedures and some ESD procedures (60-120 minutes). In contrast, Eleview® only maintained an SFC for 10 minutes *in vivo* [267], requiring multiple injections during the ESD procedure.

An ideal SFC biomaterial would also adhere to both the underlying muscle and overlying mucosa. There was no difference in mucoadhesive strength to the muscle, but eECM 12 mg/mL showed greater mucoadhesion than Eleview® to the mucosa. eECM 12 mg/mL activated "M2-like" Fizz1 expression, a marker commonly associated with an immunomodulatory "M2-like" macrophage phenotype. Eleview® did not show "M2-like" activation, as was expected for its synthetic formulation.

Limitations of the present pilot study include the low n number, and the use of different time points *in vivo* for endoscopy and sacrifice. UBM-ECM hydrogel was evaluated in the *in vivo* study and eECM hydrogel was evaluated in the *in vitro* study. However, the results are encouraging and warrant a more robustly powered *in vivo* study.

A biomaterial that prevents stricture in the esophagus is of great clinical need, as any therapeutic intervention (endoscopic mucosal resection, radiofrequency ablation, photodynamic therapy) in the esophagus has a risk for stricture, and can make the treatment worse than the disease. The stricture risk is magnified to 70-80% with large lesions (75% circumferential) [29], and even resections of less than 50% circumference have been associated with a 25% stricture risk [276]. ECM hydrogel could allow surgeons to resect pre-malignant lesions that would otherwise not be indicated because of the risk for stricture. eECM hydrogel could also be investigated with other treatments to resect pre-malignant and neoplastic lesions, including radiofrequency ablation (RFA), which has a 6% risk of stricture. The *ex vivo* SFC results also suggest that ECM hydrogel could be used as a SFC product in other parts of the body for resections of the mucosa.

9.6 CONCLUSION

The results show that eECM hydrogel material properties can be tailored for endoscopic submucosal fluid cushion delivery, further expanding the clinical utility of the therapy. eECM hydrogel would have several advantages to the current clinical standard Eleview because it formed a stable hydrogel with a longer-lasting cushion *ex vivo*, and activated macrophages toward anti-inflammatory Fizz1+ expression *in vitro*. Most importantly, ECM hydrogel mitigated stricture in 2 dogs compared to the no treatment control, suggesting that ECM hydrogel can have a beneficial, bioinductive effect on stricture mechanisms of action.

9.7 ACKNOWLEDGEMENTS

This study is in progress and acknowledges the contributions of the following people: Dr. Juan Diego Naranjo, Dr. Alejandro Nieponice, Dr. Bas Weusten, Dr. Kevin McGrath, Dr. Patrick Chan, Eric Sobieski, Dr. Lina Quijano, Dr. Catalina Pineda, Madeline Cramer, Anant Bajwa, Tucker Pavelek, and Dr. Stephen F. Badylak.

The help of Pitt LARF staff and attending veterinarians, Lori Walton for histology, and Dr. Bryan Brown's laboratory for granting access to the rheometer are appreciated.

10.0 ECM HYDROGEL AS AN ORAL THERAPEUTIC FOR HIGH GRADE DYSPLASIA AND CANCER IN A RAT MODEL: PRELIMINARY RESULTS

10.1 INTRODUCTION

Esophageal mucosa extracellular matrix (eECM) hydrogel downregulated neoplastic esophageal cell phenotype and signaling pathways (PI3K-Akt, cell cycle, DNA replication) *in vitro* (Chapter 7.0). Additionally, eECM hydrogel regressed Barrett's epithelium toward a near normal, stratified squamous epithelium without mucosal resection in a canine model (Chapter 8.0). The present study evaluated the potential of eECM hydrogel to mitigate or regress more advanced esophageal disease, including esophageal high grade dysplasia (HGD) and neoplasia, in a rodent model without mucosal resection.

The Levrat model is a validated surgical model of EAC [157], wherein the distal esophagus is anastomosed to the jejunum of the small intestine. Constant duodenal and gastric reflux bathes the lower esophagus, and over time recapitulates the metaplastic and dysplastic changes to the mucosa as seen in humans. Barrett's esophagus generally appears after 17 weeks, high grade dysplasia after 24 weeks, and EAC after 31 weeks in this model. eECM (12 mg/mL), UBM (12 mg/mL), and pepsin control (1.2 mg/mL) (n=8) were administered orally by oral gavage for 21d, twice daily. Interim results are presented for macroscopic mucosal healing by endoscopy and histologic changes to the differentiation state of the mucosa by H&E staining. A 3d timepoint for eECM, UBM, and pepsin (n=3) was performed for an early evaluation of macrophage phenotype (CD206+/TNFα+).

10.2 MATERIALS AND METHODS

10.2.1 Experimental design

Experimental design is shown in Figure 35. UBM-ECM and eECM (12 mg/mL) were evaluated compared to pepsin control (1.2 mg/mL) (n=8). Disease developed for 24 weeks and treatment was provided for 3 weeks. A pre-treatment endoscopy and biopsy was performed at week 23 (1 week before treatment) and before necropsy. Treatment was administered twice daily by oral gavage.

10.2.2 Levrat model

The IACUC was approved by the Institutional Animal Care and Use Committee (IACUC) of the Allegheny Health Network Research Institute. All animals received humane care according to the standards set in "The Guide for the Care and Use of Animals." Sprague-Dawley rats (6-8 week old, 250 ± 30 g) underwent the modified Levrat's surgical procedure as previously described [277, 278]. Briefly, animals were placed on modified diets and withheld from food and water before surgery. The Levrat's surgical procedure creates an end-to-side esophagojejunal anastomosis, wherein constant duodenal and gastric reflux enters the esophagus. Animals were closely monitored during the post-operative period, given Lactate Ringer' solution (25 mL/kg), and Enrofloxin (5 mg/kg) and Ketoprofen (3 mg/kg) for infection and pain, respectively, for 3d, and transitioned over a 10d period from a liquid to full-solid diet to allow the healing of the fragile anastomosis if ingested. Animals were housed on raised wire cage inserts to prevent access to the bedding, which can rip the anastomosis. Animals were weighed weekly for the duration of the study. Animals were provided with modified diets and weighed more frequently if weight loss was >30%, and sacrificed if animals experienced >45% weight loss or fit alternate euthanasia

criteria. Despite the animals being closely monitored, treated for pain, and conservatively sacrificed based on the euthanasia criteria, the accepted mortality of the model is still 55%. This is a severe, category E reflux animal model that creates uncontrolled, continuous reflux.

10.2.3 Endoscopic analysis

Animals received endoscopy before treatment at week 23, and after 3 weeks of treatment, prior to sacrifice at week 27. Animals were anesthetized with isoflurane and intubated before the procedure as previously described [279]. A small animal, rigid endoscope and forceps (Storz Endoskope) were used, and videos were recorded during the procedure. Biopsies were taken from the highest level of disease (as visualized macroscopically) that was also accessible, from each animal before treatment and either formalin fixed for histology or flash frozen for RNA and protein analysis. Animals were provided modified diets, withheld from food and water on the day of endoscopy, and transitioned to solid diets over 3d after endoscopy. Animals were treated with Ringer's lactate solution (25 mL/kg) d0, Ketoprofen (3 mg/kg) 1d and Baytril (5 mg/kg) 5d for pain and infection post-endoscopy.

Endoscopy videos were blinded and stills were taken at the highest level of disease before treatment and at the matched location in the esophagus post-treatment.

10.2.4 ECM hydrogel and pepsin control preparation

UBM-ECM and eECM were prepared as previously described [42, 62], by using tissue-specific protocols to meet criteria for decellularization. ECM hydrogels were prepared into a hydrogel as previously described [62]. UBM-ECM and eECM (15 mg/mL) were digested with pepsin (1 mg/mL) in 0.01 M HCl with a constant stir for 48 hours, and stored at -20°C. Pepsin control (1 mg/mL) was similarly prepared without addition of ECM. ECM was thawed overnight at 4°C

before use, and neutralized to physiologic pH and salt with 1/10 pre-gel volume of 0.1 M NaOH and 1/9 pre-gel volume of 10x PBS, and diluted to the final ECM concentration (12 mg/mL). Pepsin was prepared the same way for a final concentration of 1.2 mg/mL.

10.2.5 Oral gavage treatment

Neutralized eECM, UBM, and pepsin were kept on ice. The samples were mixed and administered by oral gavage (Instech, 18G x 50mm) to the rat esophagus, 2x per day for 21d. Rats were also injected with Enrofloxin (5 mg/kg) at the same time as the oral gavage treatment to prevent respiratory infection. Water and food were withheld for 1 h after oral gavage treatment to allow the treatment to adhere to the mucosa.

10.2.6 Necropsy

Animals were sacrificed either after 3d or 3 weeks of treatment, by carbon dioxide inhalation and diaphragm puncture to confirm death. The esophagus, including the esophagojejunostomy, was dissected and the distal blue sutures marking the anastomosis were preserved. The explanted esophagus was opened longitudinally, rinsed in 1x phosphate buffer solution (PBS), and macroscopic pictures were taken. Half of the longitudinal esophagus was pinned to cork and formalin fixed, and the other half was flash frozen in OCT (Tissue-Tek). Samples of the small intestine and large intestine were formalin fixed to assess the treatment effect, if any, on the lower parts of the gastrointestinal tract. Similarly, a lobe of the liver, section of the lung, and the lymph nodes were formalin fixed for histology as primary sites of esophageal adenocarcinoma metastases.

Samples for histology were paraffin embedded, cut in 5 um sections, and stained with hematoxylin and eosin (H&E) for evaluation of the tissue disease state.

10.2.7 Macrophage triple stain

Blank sections (5 um) were stained with a macrophage triple stain protocol, as previously described [140]. Briefly, samples were deparaffinized, and antigen retrieval was performed using citrate buffer. Samples were stained for pan macrophage marker CD68 (mouse anti-rat, ED1 clone, Serotec, MCA341R, 1:150), "M1" pro-inflammatory marker TNFα (rabbit anti-human, Abcam 6671, 1:100), "M2" anti-inflammatory marker CD206 (goat anti mouse, R&D AF2535, 1:100), and DAPI. The secondary antibodies used were Alexa 594 (donkey anti-mouse, Invitrogen A21203, 1:200), Alexa 488 (donkey anti-goat, Invitrogen A1105, 1:200), PerCP-Cy6.6 (Donkey anti-rabbit, Santa Cruz sc-45106, 1:200).

Primary antibodies were confirmed to cross-react with rat epitopes. Primary deletes were performed to confirm absence of nonspecific binding. Antibodies were diluted in blocking buffer (2% normal horse serum, 1% bovine serum albumin, 0.1% Triton X-100, 0.1% tween 20 in 1xPBS). Slides were imaged on a multispectral fluorescence microscope (Nikon E600 with Cri Nuance Fx Multispectral Imaging system).

The immunolabeled esophagus was split into 6 sections, proximal to distal. Representative images of each section were taken at 20x magnification, channels were unmixed, and quantified using a custom CellProfiler pipeline to quantify DAPI+/CD68+/TNFα + and DAPI+/CD68+/CD206+ cells. Thresholds were set for positive staining above background, and the fluorescent images were quantified using an ImageJ macro.

10.2.8 H&E scoring

The complete H&E stained esophagus was imaged for each animal. Each esophagus was divided into 6 segments, proximally to distally. Reviewers were blinded to treatment groups and scored the percentage of the disease state of the esophagus (normal, hyperplasia, Barrett's,

EAC) and submucosal inflammation score (0 normal, 1 mild, 2 severe). Scoring criteria and a representative esophageal segment are shown in Appendix G.

10.3 INTERIM RESULTS

10.3.1 Experimental overview

An experimental overview is provided in Figure 35. Levrat surgery was performed and the disease developed for 24 weeks before treatment. Pre-treatment endoscopy was performed at 23 weeks to separate the animals into groups and to collect a pre-treatment biopsy. Treatment was for 21d, twice daily with eECM 12 mg/mL, UBM 12 mg/mL, or pepsin 1.2 mg/mL (n=8). A final endoscopy was performed and the animals were sacrificed at week 27.

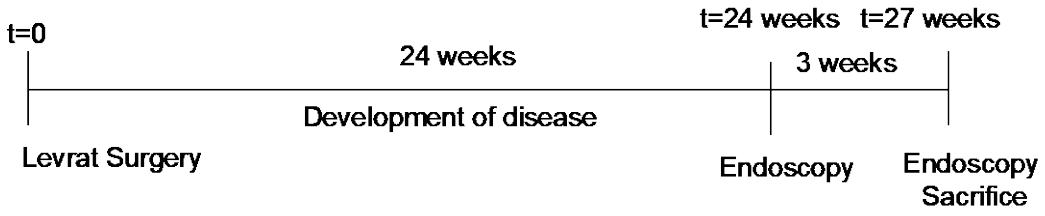

Figure 35. Levrat experimental overview.

10.3.2 UBM and eECM can modulate early macrophage phenotype in the most distal segment of the esophagus

A 3d time point was performed to assess the early macrophage phenotype in response to eECM, UBM, and pepsin treatment. The esophagus was divided into 6 segments from proximal to distal. CD206 is an anti-inflammatory (“M2”) marker and TNFα is a pro-inflammatory (“M1”) marker.

There was a spatial macrophage response along the length of the esophagus from proximal to distal. The most distal segment, which is also the most diseased region, showed an increase in the CD206+CD68+/TNFα+CD68+ ratio with UBM and eECM treatment compared to pepsin control (Figure 36A), which is corroborated by representative images taken from the most distal segment (Figure 36B). Appendix G shows that the increase in the M2/M1 ratio with UBM and eECM treatment is largely due to a decrease in TNFα+CD68+ cell numbers in the most distal segment.

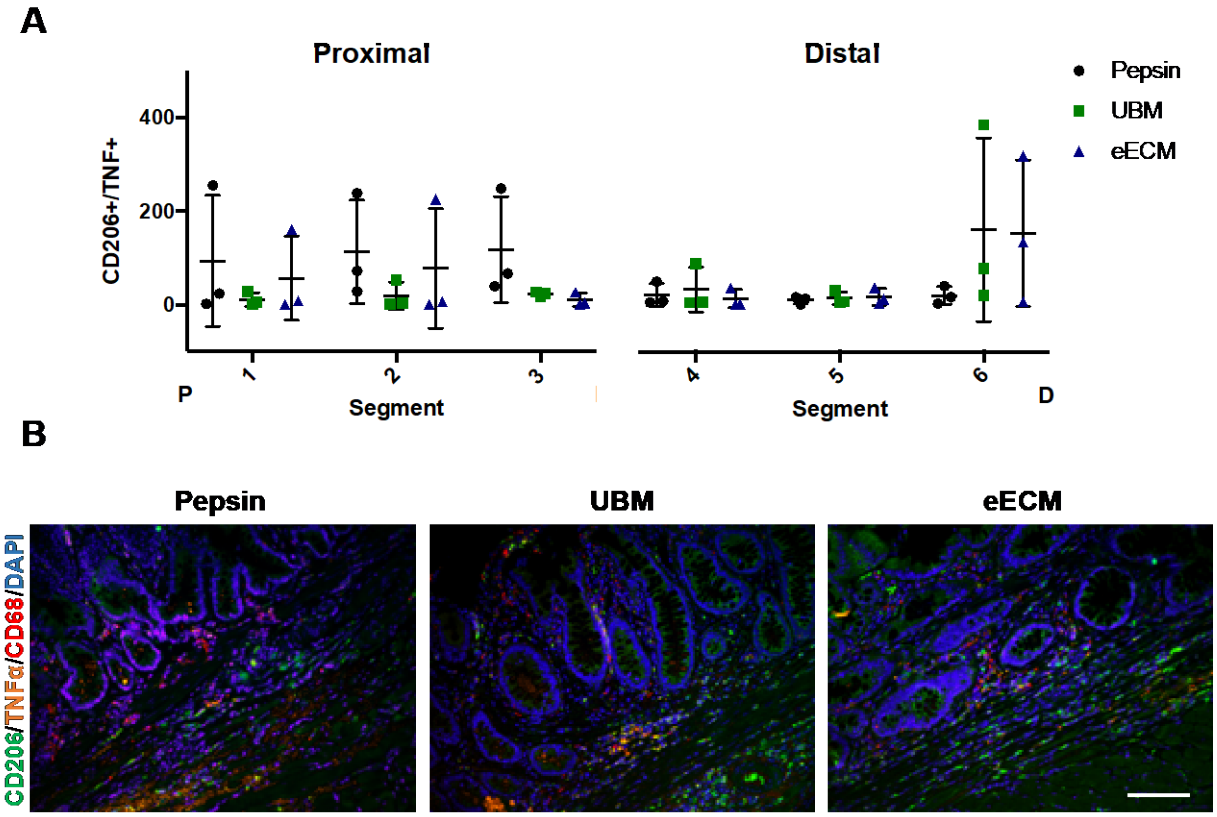

Figure 36. Macrophage activation (CD206+CD68+/TNF+CD68+) after 3d treatment.
The esophagus was immunolabeled for pro-inflammatory TNFα, anti-inflammatory CD206, and pan macrophage CD68. The esophagus was divided into 6 segments proximal (P) to distal (D), with a picture taken in each segment. The (CD206+/TNFα+) ("M2"/"M1") ratio of CD68+ macrophages was quantified for the 6 segments. At the most distal diseased region, there was a change in the M2/M1 ratio with UBM and eECM treatment compared to pepsin control (A). Representative pictures at the distal, most diseased region show a shift away from pro-inflammatory TNFα+/CD68+ cells with UBM and eECM treatment. CD206=green. TNFα=orange. CD68= red. DAPI=blue. Scale bar = 100 um. Values expressed as mean ± SD.

10.3.3 eECM can show macroscopic improvements in disease state by endoscopy

Endoscopy was performed 1 week prior to treatment, and after 21d of treatment (Figure 37). Each animal was identified by the highest stage of disease, although multiple disease types could be seen along the length of the esophagus. In general, most animals in the pepsin group

seemed to progress from their starting disease state toward a more advanced disease state (e.g., esophagitis to BE, BE to potential tumors), UBM seemed to regress slightly (e.g., Barrett's towards esophagitis), and eECM showed the most striking regression, from macroscopic Barrett's esophagus/dysplasia toward a more normal looking epithelium, and Barrett's toward normal.

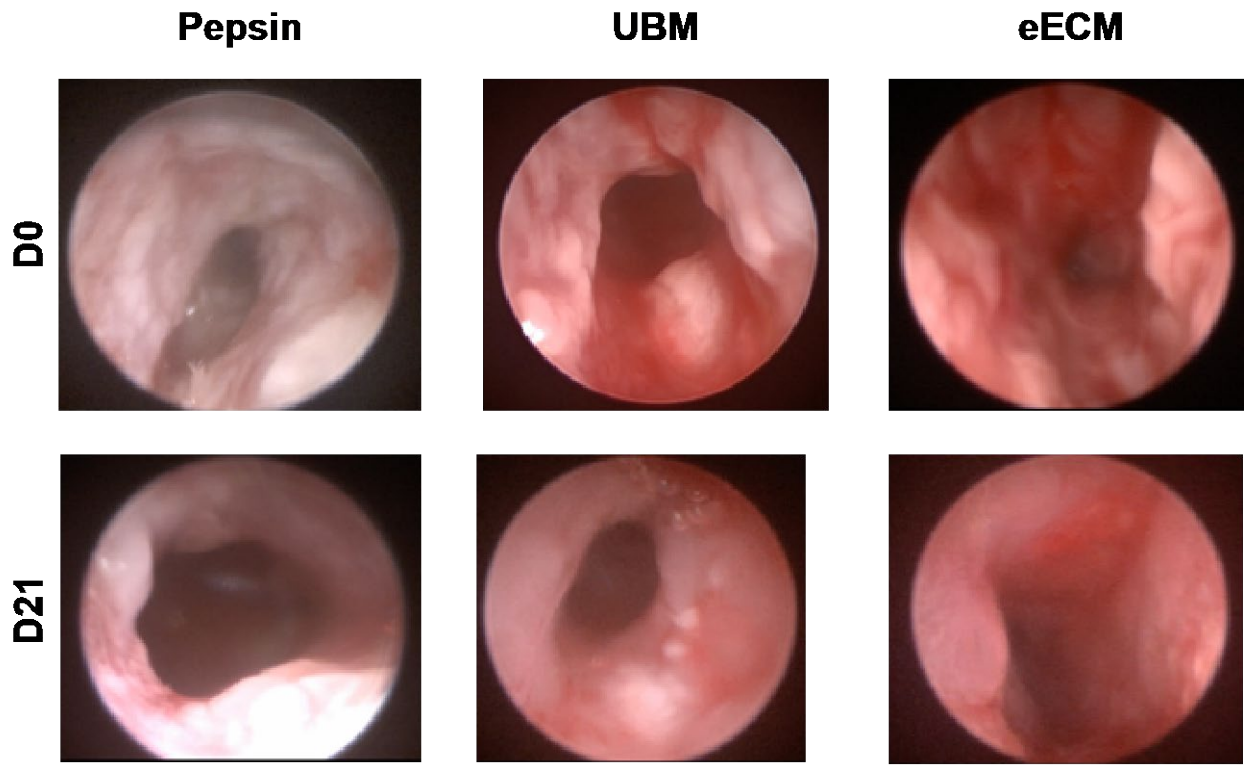

Figure 37. eECM appears to regress esophageal epithelial disease macroscopically. Endoscopies were performed before treatment started at week 24 (d0) and after 21d of treatment. Evaluated treatments were pepsin, UBM, and eECM (12 mg/mL). Representative pictures are shown. Pepsin shows an esophagus with esophagitis and Barrett's at d0 that progresses toward a small tumor protruding into the lumen at d21. UBM regresses slightly from esophagitis and Barrett's (d0) toward focal patches of esophagitis at d21. eECM regresses from esophagitis and Barrett's (d0) toward a more normal looking epithelium.

10.3.4 H&E scoring

Scoring of the esophagi for the proportion of disease states (normal, hyperplastic, Barrett's, EAC, erosion) and submucosal inflammation for each animal were performed. Scoring criteria and a representative esophagus is shown in the Appendix G. The initial scoring shows a trend toward regression of Barrett's and EAC disease state with eECM and UBM treatment compared to pepsin control in the most distal esophagus (Appendix G**)**, however, these are still interim results that need to be confirmed because of inter-observer variability.

10.4 DISCUSSION

The Levrat surgical model is an *in vivo* animal model of a highly aggressive EAC. The gastroesophageal reflux is created through an esophagojejunostomy, resulting in continuous esophageal insult and injury and animals were treated while the disease can still progress.

In this model, UBM and eECM showed a modulation of macrophage activation state in the most distal region of the esophagus, away from pro-inflammatory TNFα+CD68+ state, with an increase in the overall CD206+CD68+/TNFα+CD68+ ratio. TNFα is progressively activated in macrophages after exposure to metaplastic and neoplastic ECM (Chapter 5.0) and TNFα is progressively increased in the progression from GERD to EAC [19]. Therefore, a decrease in TNFα+ macrophages could be favorable for treatment of a chronic inflammatory-driven disease. However, caution needs to be exercised because some of the animals had progressed to small tumors in the distal region of the esophagus at the start of treatment, and there are reports of tumor-associated macrophages (TAM) expressing CD206 [280].

A more thorough analysis should be performed with multiple pro-inflammatory ("M1") and anti-inflammatory ("M2") macrophage markers, at 3d and 21d, to understand the balance

between macrophage activation that promotes constructive tissue remodeling versus the macrophage activation that promotes potential progression of cancer. However, the interim endoscopy results were promising, and showed relatively significant progression in pepsin control animals, a slight regression in the UBM-ECM treated animals, and mostly regression in the eECM treated animals.

The complete study (21d) will evaluate the histologic scoring of the esophagi disease state, expression of genes related to PI3K-Akt signaling, safety of 21d ECM treatment by blood serum chemistry, and macrophage phenotype at 21d to further understand the role of using an M2-promoting biomaterial in a setting of chronic inflammation and early cancer.

10.5 ACKNOWLEDGEMENTS

This study, including the supplementary material in the appendix, is in progress and acknowledges the contributions of the following people: Dr. Lina Quijano, David Nascari, Dr. Xue Li, Ashten Omstead, Paul Joseph, Mark Biedka, Dr. Juan Diego Naranjo, Joseph Bartolacci, Dr. Blair Jobe, Dr. Ali Zaidi, and Dr. Stephen F. Badylak.

The Allegheny Health Network Research Institute and the dedicated supervisors and staff of the Pre-clinical health team are also acknowledged for their assistance: Dr. Krista Gibbs, Amie Barrett, Amy Cupps, Marlena K., Rachel K., Heather E, Britta, Helen Scala, and Tara Fraser.

11.0 SUMMARY OF MILESTONES AND FUTURE DIRECTIONS

The central hypothesis of the present dissertation is that extracellular matrix (ECM) isolated from non-malignant, metaplastic, and neoplastic esophageal tissue has distinct effects upon esophageal epithelial cell phenotype and macrophage activation. Delivering non-malignant ECM hydrogel to a diseased esophagus will halt or revert disease progression *in vivo* via macrophage-mediated repolarization and restoration of dysregulated matrix-cell signaling.

Milestone 1: The effect of non-malignant, metaplastic, and neoplastic ECM upon macrophage activation *in vitro* was determined.

Summary Milestone 1: Esophageal adenocarcinoma (EAC) is a chronic inflammatory driven cancer. Macrophages are plastic innate immune cells that are responsive to microenvironmental signals in chronic inflammation, cancer, and tissue remodeling. ECM directs cell phenotype by dynamic reciprocity, however, the effect of non-malignant, metaplastic, and neoplastic esophageal ECM on macrophage phenotype remains unknown. An increased understanding of progressively diseased esophageal ECM could inform treatment of EAC, and provide a rationale for the therapeutic use of non-malignant ECM in EAC patients.

Neoplastic ECM had increased amounts of ECM proteins functionally related to inflammatory response and tumorigenesis including, but not limited to, COL8A1, lumican, and elastin. ECM samples also contained matrix-bound nanovesicles (MBV), a recently described,

bioactive component of the matrix. Metaplastic and neoplastic MBV had distinct miRNA profiles functionally related to epithelial-mesenchymal transition; gastrointestinal cancer, and inflammatory activation. The present dissertation determined metaplastic and neoplastic ECM progressively activated pro-inflammatory TNFα at the gene and protein level, and increased, via paracrine effects, migration of a normal esophageal epithelial cell, i.e., a tumorigenic behavior. The results suggest metaplastic ECM (found in Barrett's esophagus) contains similar signals to neoplastic ECM, despite Barrett's being considered a clinically benign condition.

Future Directions Milestone 1: Future experiments should further determine the molecular mechanisms regulating activation of macrophages by the metaplastic and neoplastic ECM. The macrophage cell surface receptors activated in response to metaplastic and neoplastic ECM could be clinically relevant targets to guide EAC immunotherapy strategies. Comparing the effect of ECM isolated from Barrett's esophagus "progressors" versus "non-progressors" upon macrophage phenotype could identify potential signaling pathways, and accurate markers, that further distinguish these two patient populations.

The contribution of specific components in the metaplastic and neoplastic ECM should be investigated. The functional relevance of metaplastic and neoplastic MBV on important cell types in the neoplastic niche (fibroblasts, epithelial cells, and macrophages) should be determined. miRNA inhibition experiments could be performed to determine the specific miRNA within the metaplastic and neoplastic MBV that regulate tumorigenic cell functions. The non-malignant, metaplastic, and neoplastic ECM could be fractionated and exposed to macrophages to identify specific ECM proteins or cryptic peptides that recapitulate the effects of the parent ECM. COL8A1, lumican, and elastin could be investigated as biomarkers in EAC patient biopsies, similarly to ECM proteins being used as biomarkers for breast cancer [281].

Milestone 2: The effect of non-malignant ECM hydrogel from two distinct tissue sources upon normal, metaplastic, and neoplastic esophageal cell phenotype and neoplastic signaling pathways was characterized.

Summary Milestone 2: ECM can have a dramatic effect to direct cell differentiation during development [238, 239], and correction of dysregulated cell surface receptors can revert cancer cells toward a more polarized, non-malignant phenotype [21]. ECM degradation products showed potential to mitigate EAC neoplastic cell phenotype as indicated by the success of 14 human patients treated with ECM bioscaffolds after cancer resection, however the molecular mechanisms remain unknown. Furthermore, the preference for homologous versus heterologous ECM after neoplastic esophageal mucosal resection is not known.

Heterologous ECM (urinary bladder matrix, UBM) showed a decrease in neoplastic cell metabolism and increased Barrett's metaplastic cell apoptosis. Homologous ECM (eECM) strikingly downregulated neoplastic cell proliferation and neoplastic signaling pathways e.g., PI3K-Akt, cell cycle, DNA replication, and showed minimal or opposite effects upon normal cells. The results suggest eECM may show a more pronounced therapeutic effect compared to UBM. Preliminary experiments suggest that UBM and eECM may also have distinct effects on neoplastic esophageal cell surface receptors, downregulating EGFR and CD164, respectively.

Future Directions Milestone 2: Future studies will determine non-malignant and neoplastic cell surface receptors activated in response to UBM and eECM and further validate the downstream signaling pathways (e.g., PI3K-Akt, cell cycle) from the cell surface receptor to the nucleus. eECM could be fractionated and provided to neoplastic and non-malignant cells to determine components that recapitulate the effects of the parent ECM. Future work should use primary non-malignant and neoplastic cells and culture the cells in 3D hydrogels to validate the findings.

The present dissertation focused on the effect of epithelial cells, but likely non-malignant ECM degradation products have a direct or indirect effect on other cell types in the tumor niche (e.g., tumor-associated fibroblasts, endothelial cells, tumor-associated macrophages).

Milestone 3: The effect of non-malignant ECM hydrogel upon macrophage activation and epithelial cell phenotype in a canine model of Barrett's esophagus and rat model of EAC was evaluated. Practical aspects of clinical translation (e.g., tissue source, ECM concentration, delivery method) were also determined.

Summary Milestone 3: ECM degradation products did not promote cancer recurrence in 14 patients. ECM degradation products were simulated *in vitro* using pepsin digestion, resulting in an ECM hydrogel form that was clinically translatable.

The present dissertation identified esophageal mucosa ECM (eECM) hydrogel at 12 mg/mL as the preferred formulation because of its viscoelastic properties (e.g., shear thinning, stably formed gel, fast (~5 min) gelation time), and the greatest mucoadhesion to the mucosa *in vitro* compared to heterologous UBM and dermal ECM. Targeted proteomics revealed that eECM retains structural collagen types I, III, and V, matrix-cell attachment proteins (e.g., fibronectin 1, dermatopontin, and fibrillin-1) and basement membrane proteins related to matrix-cell signaling (e.g., laminins, perlecan, nidogen, agrin, and collagen type IV). Esophageal mucosa ECM hydrogel was evaluated in a pre-clinical, large animal model of Barrett's esophagus that corroborated the *in vitro* results shown in Milestone 1 and 2. Specifically, 30 days of twice daily eECM hydrogel treatment (oral administration) showed a direct effect on the differentiation status of the epithelial cells, regressing Sox9+/Alcian blue+ goblet cells before treatment toward normal, stratified squamous CK13+/CK14+ epithelial cells after treatment; and concomitant reduction in TNF+ pro-inflammatory cell infiltrate. Omeprazole control did not promote the same

tissue-healing properties. ECM hydrogel is also safe, as evaluated by blood serum chemistry and animal weights. Injecting the eECM into the submucosa to facilitate mucosal resection is an alternative delivery method that was identified in a canine pilot study, and showed biological and mechanical advantages compared to Eleview®, the clinical standard submucosal fluid cushion product. Preliminary results in a small animal model with higher stage of disease (high grade dysplasia and EAC) show that the CD206+/TNF+ ratio is increased in the most distal, diseased region, and appears to regress macroscopic disease by endoscopy compared to pepsin control.

The present dissertation results corroborate the pre-clinical studies over the past decade [26-33] that have proven efficacy of ECM bioscaffolds in esophageal reconstruction, provides a rationale to use the minimally invasive, hydrogel form that could also treat the pre-malignant disease, and provides a molecular rationale for the use of the tissue-specific ECM (eECM).

Future Directions Milestone 3: The small n value is the primary limitation of the pre-clinical, large animal study. Nevertheless, the results of this study upon Barrett's epithelial cell phenotype, pro-inflammatory TNFα+ infiltrate, and the regression of more advanced esophageal stages (e.g., high grade dysplasia, tumor) in the rat model, are encouraging. Dosing regimens and the optimal therapeutic window to treat esophageal disease will need to be determined in pre-clinical studies, and a clinical trial will need to be performed.

The role of PI3K-Akt signaling and recruited esophageal stem cells in the reformation of the normal epithelium with eECM hydrogel treatment should be further investigated. Signaling pathways to mitigate stricture with eECM treatment should also be explored. Another important future application is the use of eECM hydrogel in combination with radiofrequency ablation (RFA), which is rapidly becoming the most widely used method of treating pre-neoplastic lesions.

APPENDIX A

OVERVIEW OF TISSUE DECELLULARIZATION AND SOLUBLIZATION PROTOCOLS

Table 8. Overview of tissue decellularization and solubilization protocols.
Decellularization reagents and solubilization protocol used to produce ECM hydrogels for each source tissue and species. The fundamental solubilization protocols are referred to as Voytik-Harbin, Freytes and Uriel as defined below. Any modifications to the base protocol are indicated within the table.

Source Tissue	Decellularization Reagents	Solubilization Protocol	Ref.
Adipose			
Human *(Lipoaspirate)*	• 1% SDS, or 2.5 mM sodium deoxycholate • 2.5 mM sodium deoxycholate with 500 U lipase and 500 U colipase	• Freytes • 3200 IU pepsin • 0.1 M HCl	108]
	• 0.5% SDS • Isopropanol • 0.1% peracetic acid/4% ethanol	• Voytik-Harbin • 10 mg pepsin • RT, 48 hr	114]
Rat *(Subcutaneous)*	• 2 mL dispase/ g tissue □	• Uriel	84, 85, 88]
Porcine	• 10 mM Tris and 5 mM EDTA • 99% isopropanol • HBSS with 10000 U DNase, 12.5 mg RNase, 1000 U lipase	• Freytes • 37ºC, 24 hr	282]

Table 8 (continued)

Source Tissue	Decellularization Reagents	Solubilization Protocol	Ref.
Bone			
Bovine *(Cancellous Tibia)*	• 0.5 M HCl • 1:1 Chloroform:methanol • 0.05% trypsin/0.02% EDTA • 1% w/v pen/strep in PBS	• Freytes • 96 hr	113, 127, 283]
Cartilage			
Porcine *(Articular)*	• 10 mM Tris-HCl at pH 8 • 0.25% trypsin • 1.5 M NaCl in 50 mM Tris-HCl at pH 7.6 • 50 U/mL DNase and 1 U/mL RNase in 10 mM Tris-HCl • 1% Triton X-100 • 10 mM Tris-HCl • 0.1% peracetic acid/4% ethanol	• Voytik-Harbin • 10 mg pepsin • RT, 48 hr	114]
Porcine *(Meniscus)*	• 1% SDS • 0.1% EDTA	• Freytes • 1.5 mg/mL pepsin	111]
Central Nervous System			
Porcine *(Adult Brain, Spinal Cord)*	• 0.02% trypsin/0.05% EDTA • 3% Triton X-100 • 1 M sucrose • 4% deoxycholate • 0.1% peracetic acid/4% ethanol	• Freytes	95, 124, 132, 284]
Porcine *(Fetal Brain)*	• 0.05% trypsin-EDTA with 0.2% DNase I • 3% Triton X-100 with 0.2% DNase I • 1 M sucrose • 1% sodium deoxycholate • 0.2% peracetic acid in 4% ethanol	• Freytes • 24 hr	285]
Colon			
Porcine *(Submucosa)*	• 2:1 Chloroform:methanol • Graded ethanol (100%, 90%, 70%) • 0.02% trypsin/0.05% EDTA • 4% sodium deoxycholate • 0.1% peracetic acid/4% ethanol	• Freytes • 0.1 M HCl	112]

Table 8 (continued)

Source Tissue	Decellularization Reagents	Solubilization Protocol	Ref.
Cornea			
Porcine	• 10 U/ml DNAse and 10 U/mL RNAse in 10 nM $MgCL_2$	• Freytes • 0.1 M HCl • 72 hr	110]
Esophagus			
Porcine *(Mucosa/submucosa)*	• 1% trypsin/0.05% EDTA • 1 M sucrose • 3% Triton X-100 • 10% deoxycholate • 0.1% peracetic acid/4% ethanol	• Freytes	33]
Heart			
Porcine, Rat *(Ventricular Myocardium)*	• 1% SDS • 1% Triton X-100	• Freytes • 0.1 M HCl	99, 117, 119, 121-123, 286]
Porcine *(Ventricular Myocardium)*	• 1% SDS and 0.5% pen/strep	• Freytes • 0.1 M HCl	83, 101, 115, 287-290]
	• 1% SDS • 1% Triton X-100 • 0.1% peracetic acid/4% ethanol	• Voytik-Harbin • 10 mg pepsin • RT, 48 hr	114, 291]
	• 0.02% trypsin-EDTA • 3% Tween-20 • 102 mM sodium deoxycholate • 0.1% peracetic acid • 1% pen/strep	• Freytes	292]
	• 1% SDS • 0.1% Triton X-100	• Freytes • 0.1 M HCl • 12 hr	293]

Table 8 (continued)

Source Tissue	Decellularization Reagents	Solubilization Protocol	Ref.
	Perfusion • 0.02% trypsin/0.05% EDTA • 3% Triton X-100/0.05% EDTA • 4% deoxycholic acid • 0.1% peracetic acid • 2:1 chloroform:methanol • 100-70% ethanol	• Freytes • 2 mg/mL pepsin	294]
Human *(Ventricular Myocardium)*	• 1% SDS and 0.5% pen/strep • Isopropyl alcohol • 40 U/mL DNase and 1 U/mL RNase in 40 mM HCl, 6 mM $MgCl_2$, 1 mM $CaCl_2$, and 10 mM NaCl • 1% SDS/0.5% pen/strep • 0.001% Triton X-100	• Freytes	101]
	• 10 mM Tris and 0.1% EDTA • 0.5% SDS • 100 U/mL pen/strep and nystatin in DPBS • Fetal bovine serum • 100 U/mL pen/strep and nystatin in DPBS	• Freytes • pH 1 • 37°C • Salts were not neutralized	295]
	• 10 mM Tris and 0.1% EDTA • 0.5% SDS • 100 U/mL pen/strep and nystatin in DPBS • Fetal bovine serum • 100 U/mL pen/strep and nystatin in DPBS	• Freytes • pH 2	295]
Goat *(Ventricle)*	• 0.1% peroxyacetic acid/4% ethanol • 1% SDS • 1% Triton X-100	• Freytes • 60-72 hr	296]
Porcine, Human *(Pericardium)*	• 1% SDS	• Freytes • 0.1 M HCl	96, 116, 120, 135, 297]

Table 8 (continued)

Source Tissue	Decellularization Reagents	Solubilization Protocol	Ref.
Kidney			
Human *(Cortex)*	• 1% SDS	• Freytes	[102]
Liver			
Rat	*Perfusion* • 1% Triton X-100 and 0.1% ammonium hydroxide	• Freytes • 10% (w/w) pepsin • 0.1 M HCl	98]
Rat, Porcine, Canine, Human	• 0.02% trypsin and 0.05% EGTA • 3% Triton X-100 • 0.1% peracetic acid	• Freytes • 24-72 hr (until no particulate)	97]
Porcine	• 0.02% trypsin and 0.05% EDTA • 3% Triton X-100 • 4% sodium deoxycholic acid • 0.1% peracetic acid	• Freytes • 72 hr	128, 129]
	• 0.1% SDS	• Freytes • 3 mg/mL pepsin • 0.1 M HCl • 72 hr	93]
Lung			
Porcine	*Perfusion* • 1x pen/strep • 0.1% Triton X-100 • 2% sodium deoxycholate • DNase solution • NaCl	• Freytes	90]
Pancreas			
Porcine	• 1.1% NaCl • 0.7% NaCl • 0.05% trypsin/0.02% EDTA, pH 8.2 • 1% Triton X-100/1% ammonium hydroxide • 70% ethanol	• Freytes • 5 mg/mL pepsin • 0.1 M HCl	103]
Skeletal Muscle			
Porcine *(Intercostal, Hindleg)*	• 1% SDS	• Freytes • 0.1 M HCl	99, 118]

Table 8 (continued)

Source Tissue	Decellularization Reagents	Solubilization Protocol	Ref.
Porcine *(Psoas)*	• 1% SDS • 1% SDS and 0.5% pen/strep • Isopropyl alcohol	• Freytes • 0.1 M HCl	288]
	• 1% SDS and 0.5% pen/strep • Isopropyl alcohol • 0.001% Triton X-100	• Freytes • 0.1 M HCl	104]
Porcine	• 0.2% trypsin/0.1% EDTA • 0.5% Triton X-100 • 1% Triton X-100/ 0.2% sodium deoxycholate • Isopropanol • $5x10^7$ U/l DNase-I and $1x10^6$ U/l RNase	• Freytes	105]
Skin			
Rat *(Dermis)*	• 2 mL dispase/ g tissue □	• Uriel	84-87, 106]
Porcine *(Dermis)*	• 0.25% trypsin • 70% ethanol • 3% H_2O_2 • 1% Triton X-100 in 0.26% EDTA/0.69% Tris • 0.1% peracetic acid/4% ethanol	• Freytes • 72 hr	65, 298-300]
Small Intestine			
Porcine *(Submucosa/muscularis mucosa/stratum compactum/lamina propria)*	*Mechanical delamination of other tissue layers only*	• Voytik-Harbin • Additional step: centrifuged, dialyzed against 0.01 M acetic acid	58, 75]
Porcine (*Submucosa/muscularis mucosa/stratum compactum)*	• 0.1% peracetic acid/4% ethanol	• Freytes • 72 hr	33, 68, 97, 131]
	• 0.1% peracetic acid/4% ethanol	• Freytes • 0.5 mg/mL pepsin	94]

Table 8 (continued)

Source Tissue	Decellularization Reagents	Solubilization Protocol	Ref.
	• 0.1% peracetic acid/4% ethanol	• Freytes • 24 hr	92]
Tendon			
Human *(Flexor digitorum profudus, flexor digitorum superficialis, flexor pollicic longus)*	• 0.1% EDTA • 0.1% SDS in 0.1% EDTA	• Freytes • 0.02 M HCl • 24 hr	100, 125]
Tooth			
Human *(Dentin)*	• 10% HCl • 0.5% pen/strep • 0.5M HCl • 0.05% trypsin/0.025% EDTA	• Freytes • 84 hr	137]
Umbilical Cord			
Human	• 1% SDS and 0.5% pen/step • 0.001% Triton X-100 • 40 U/mL DNase and 1 U/mL RNase in 10 mM NaCl, 1 mM $CaCl_2$ 6 mM $MgCl_2$, and 40 mM HCl • 1% SDS and 0.5% pen/strep • 0.001% Triton X-100	• Freytes • 0.1 M HCl	104]
Urinary Bladder			
Porcine *(Basement membrane/lamina propria)*	• 0.1% peracetic acid/4% ethanol	• Freytes	33, 62-66, 95, 97, 124, 132, 134, 284, 300]

Key
Freytes:

- 1 mg/mL pepsin in 0.01 M HCl
- Stir plate, RT, 48 hr
- Neutralized to pH 7.4 and physiological salt with NaOH and 10x PBS

Uriel:

- High salt buffer solution (0.05 M Tris pH 7.4, 3.4 M sodium chloride, 4 mM of ethylenediaminete- traacetic acid, and 2 mM of N-ethylmaleimide) containing protease inhibitors (0.001mg/mL pepstatin, 0.01mg/mL aprotonin, 0.001mg/mL leupeptin, 2mM sodium orthova- nadate, and 1mM phenylmethylsulfonyl fluoride)
- Homogenized with mortar and pestle
- 2 M urea buffer

Voytik-Harbin:

- 2 mg pepsin per 100 mg ECM in 0.5 M acetic acid
- 4°C, 72 hr
- Neutralized to pH 7.4 and physiological salt with NaOH and 10x PBS

⌘ Was not lyophilized/powdered prior to solubilization
RT – room temperature

APPENDIX B

THE EFFECT OF NORMAL, METAPLASTIC, AND NEOPLASTIC ESOPHAGEAL EXTRACELLULAR MATRIX UPON MACROPHAGE ACTIVATION

B.1 SUPPLEMENTARY FIGURES

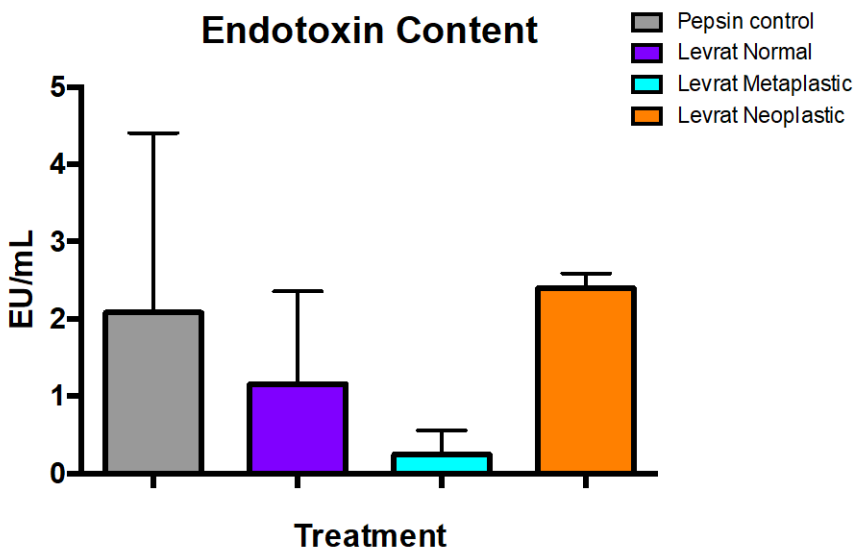

Figure 38. Endotoxin concentration
Endotoxin is a ubiquitous environmental contaminant and activates macrophages toward an "M1" phenotype. Endotoxin was measured to confirm that the distinctive M1 signaling pathway activation by the normal, metaplastic, and neoplastic ECM was not due to a difference in endotoxin concentration. Endotoxin concentration was measured by the limulus amoebocyte assay and was not significantly different between samples.

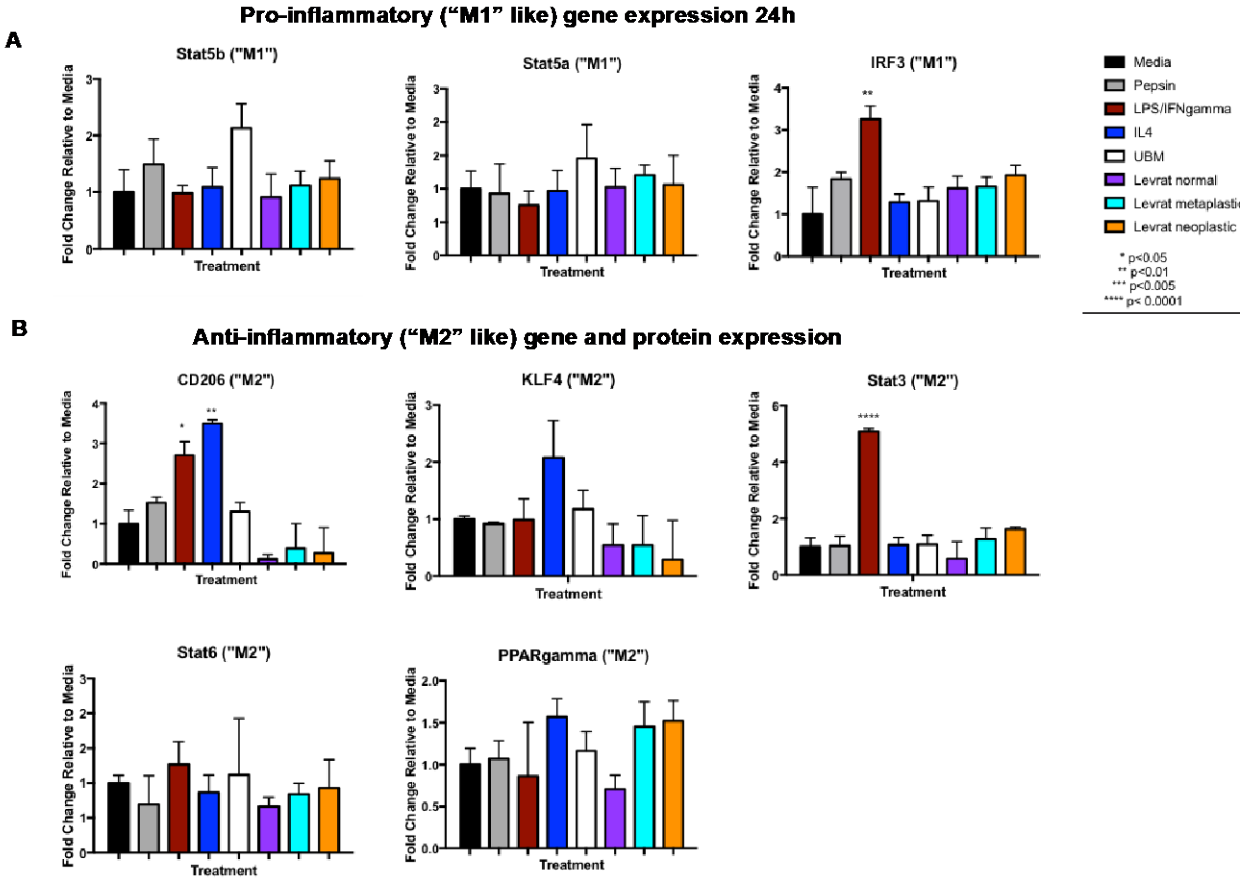

Figure 39. Pro-inflammatory and anti-inflammatory THP-1 gene expression in response to normal, metaplastic, and neoplastic ECM

(A) Pro-inflammatory ("M1-like") and (B) anti-inflammatory ("M2-like") genes that were tested but not found to be activated in THP-1 cells by the normal, metaplastic, and neoplastic ECM after 24h.

APPENDIX C

C.1 INTRODUCTION

The long-term objective is to isolate MBV from human normal and neoplastic esophageal ECM. The MBV isolation protocol was first optimized for porcine esophageal ECM because human esophageal ECM is limited.

The MBV isolation protocol was optimized to determine a preferred digestion time (3h, 18h), the minimum amount of ECM needed to provide a quantifiable amount of MBV (10-100 mg tested), and the quantification method to standardize the MBV preparations (internal RNA cargo or external MBV protein). UBM was used as a positive control as a tissue source with a relatively high yield of MBV.

C.2 MATERIALS AND METHODS

C.2.1 MBV Isolation

Liberase enzyme (TM) (Roche) was used. The choice of enzyme used for MBV isolation is critical to balance yield with specificity. For example, collagenase and Proteinase K as used previously [6] have high yield, but Proteinase K can clip surface antigens and collagenase is non-specific. Liberase has higher purity and specificity than collagenase and is therefore being

investigated as a gentler method to extract MBV from ECM. Liberase (0.1 mg/mL) was suspended in buffer (0.05 M Tris, 0.2 M NaCl, and 0.005 M CaCl2 in water). UBM and eECM were weighed and added to the Liberase buffer at a concentration of 10 mg/mL. Samples were inverted and placed in a rotating mixer (max speed 18) for either 1) 3h at 37°C or 2) overnight at room temperature for 18h.

After the digestion, samples were centrifuged: 500 g for 10 minutes, 2,500 g for 20 min, and 10,000 g for 30 minutes (last step 3 times). Between each centrifugation step, samples were decanted. Samples were sterile filtered with a 0.2 um filter into ultra-clear centrifugation tubes. The samples were ultracentrifuged at 100,000 g for 2h, the supernatant was aspirated and discarded, and the MBV pellet was re-suspended in 1x PBS and stored at -80°C.

C.2.2 MBV quantification

Internal MBV RNA was quantified as a potential standard. MBV were first treated with DNAse (RQ1 Promega) and RNAse (RNase A Ambion) at 37°C for 30 minutes. The MBV samples were then lysed and RNA was isolated using the EconoSpin columns and Exiqon solutions (miRCURY RNA isolation kit- cell and plant) following the Exiqon protocol. External MBV protein was quantified using the NanoDrop (A280).

C.2.3 Cell Culture

Het-1A cells were cultured as described in Chapter 5.5.3.2, and THP-1 cells were cultured as described in Chapter 5.4.3. Primary esophageal fibroblasts were isolated from mouse esophagus as described in [301].

MBV were added to the cell culture media at the specified concentration by internal RNA standardization and treated for 24h before isolating RNA for gene expression or performing the MTT assay.

C.2.4 Gene Expression

RNA and qPCR were performed as described in Chapter 5.4.3.1. Primers were validated by annealing temperature and specificity as described in Chapter 7.5.8.2. Primers used are shown in Table 9.

Table 9. Primers for qPCR

Gene	Forward	Reverse
COL8A1 (mouse)	TGCCCCGGTAAAGTATGTGC	GCATCGGTAGAGGCATTTCCA
Elastin (mouse)	TTGCTGATCCTCTTGCTCAAC	GCCCCTGGATAATAGACTCCAC
Lumican (mouse)	TAAGCTTAAGAGTATACCAACAGTTAATG	GCGCAGATGCTTGATCTTG
CK14 (Human)	GAAGTGAAGATCCGTGACTGGT	GTGGCTGTGAGAATCTTGTTCC
Vimentin (human)	AGTCCACTGAGTACCGGAGAC	CATTTCACGCATCTGGCGTTC
Sox9 (human)	AGCGAACGCACATCAAGAC	CTGTAGGCGATCTGTTGGGG
Muc5AC (human)	CAGCACAACCCCTGTTTCAAA	GCGCACAGAGGATGACAGT

C.2.5 MTT Viability Assay.

MTT assay was performed using the Vybrant quick protocol option according to Chapter 7.5.6.

C.3 RESULTS

MBV were isolated from 10, 20, and 30 mg of porcine eECM (Figure 40B,D) and UBM (Figure 40A,C) and quantified for RNA (Figure 40A,B) and protein (Figure 40C,D). The eECM MBV internal RNA concentrations were nearly the same as PBS background control (Figure 40B). The RNA and external protein measurements give similar trends. Internal RNA standardization was chosen as a subsequent metric because the eventual application is the miRNA cargo mediated effect on cells.

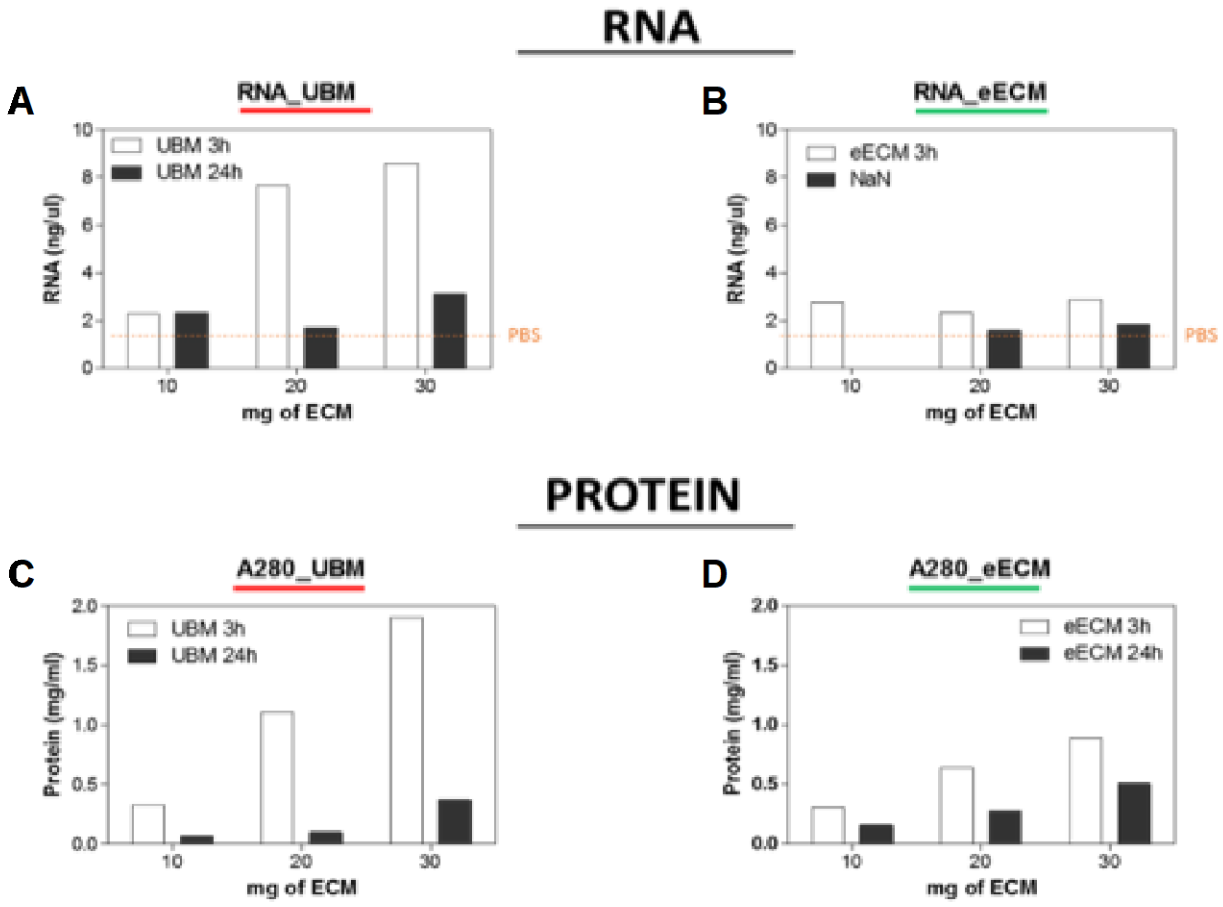

Figure 40. MBV yield from 10, 20, and 30 mg of ECM

The experiment was repeated with 50, 75, and 100 mg of eECM (Figure 41B) and UBM (Figure 41D). eECM at 50, 75, and 100 mg was able to provide an internal RNA reading above background, and 3h digestion yielded a higher RNA concentration than 18h digestion (Figure 41B). 50 mg was identified as the minimum amount of ECM required, and internal RNA cargo was selected as the quantification method. As seen previously, UBM had a higher yield than eECM for both the 3h (Figure 41A) and 18h (Figure 41C) digestion .

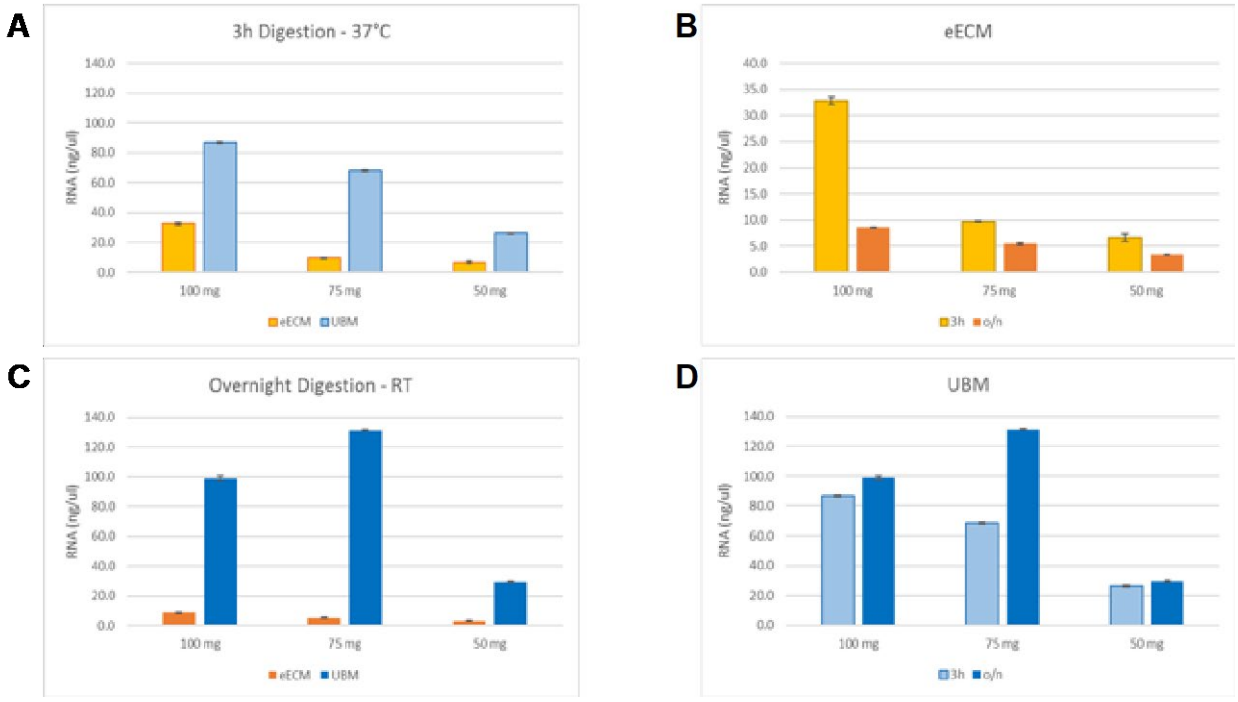

Figure 41. Isolating MBV from 50, 75 and 100 mg of eECM and UBM.

The bioactivity of porcine eECM MBV was tested on THP-1 macrophages, Het-1A epithelial cells, and primary fibroblasts. The concentration of MBV used in the bioactivity experiments was based upon the MBV internal RNA concentration. Bioactivity was assessed by activation of THP-1 macrophages, Het-1A gene expression, and primary fibroblast gene expression. MTT was also used as a measure of cell viability.

THP-1 cells were treated with 20-500 ng/mL porcine eECM MBV and 500 ng/mL UBM MBV as a positive control (Figure 42A), and RNA was isolated for “M1” pro-inflammatory genes IRF5, TNF, Stat2, iNOS, and “anti-inflammatory” gene IL1RN. These genes were selected as the genes that changed with the metaplastic and neoplastic esophageal ECM (Chapter 5.5.3). Twenty-five ng/mL was selected as the preferred MBV concentration, having an effect upon THP-1 gene expression compared to media, and having the highest viability by MTT assay (Figure 42B). A slight dose response with increasing MBV concentration and decreasing viability was seen with porcine eECM MBV on THP-1 cells.

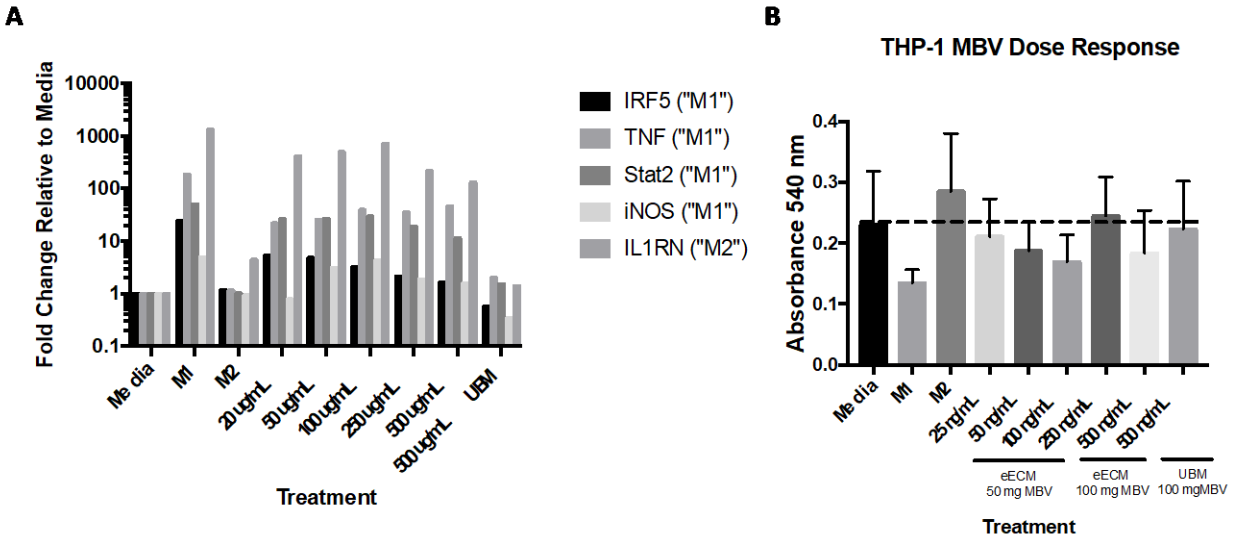

Figure 42. Effect of porcine eECM MBV on THP-1 cells.
(A). Effect upon THP-1 gene expression. (B) Effect upon THP-1 cell viability (MTT assay).

Primary esophageal fibroblasts were isolated from mouse, and showed characteristic fibroblast morphology by brightfield microscopy and stained positively for Vimentin (Figure 45A). Gene expression was performed for COL8A1, elastin, and lumican (Figure 45B). These genes were selected because these proteins were upregulated in the neoplastic esophageal ECM compared to normal esophageal ECM (Chapter 5.5.2.3). MBV treatment at 50 and 100 ng/mL

interestingly decreased elastin compared to media control. No significant effect on fibroblast viability was seen with increasing eECM MBV concentration (Figure 45C). 50 ng/mL was selected as a starting concentration for the human normal and neoplastic ECM MBV future experiments.

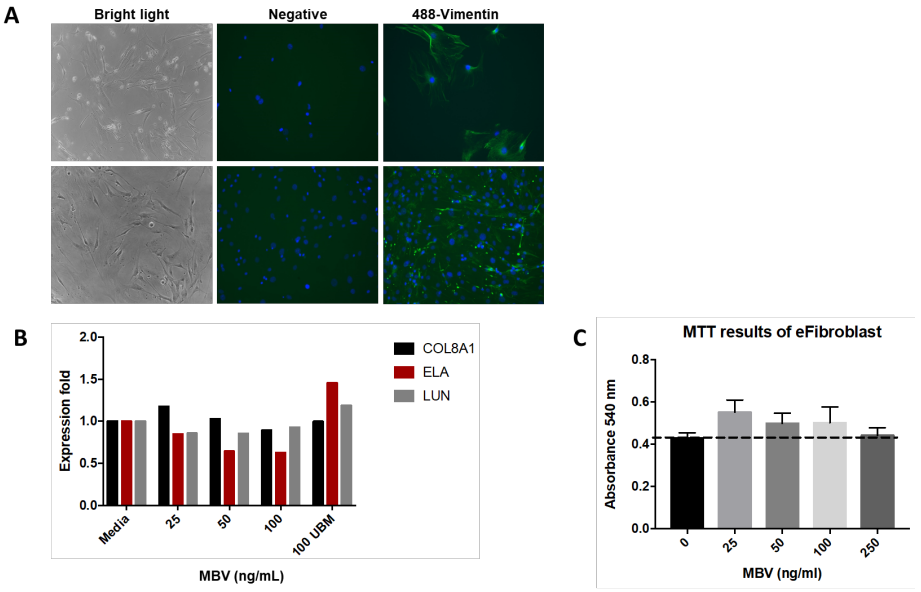

Figure 43. Effect of porcine eECM MBV on primary fibroblasts.
(A) Primary fibroblast phenotype by bright field and Vimentin staining (488 positive). (B) Effect upon primary fibroblast gene expression (C) Effect upon Fibroblast viability.

Het-1A epithelial cells were evaluated for gene expression related to disease state: normal (CK14), Barrett's (Sox9), and Muc5AC (EAC), and epithelial-mesenchymal transition (Vimentin). Surprisingly, the porcine eECM MBV showed a striking increase of genes related to Sox9 and Muc5Ac with 50 and 100 ng/mL MBV treatment (Figure 44A). A concentration dependent decrease in Het-1A viability was seen with increasing MBV concentration (Figure 44B). MBV at 50 ng/mL balanced viability and gene expression for Het-1A cells, and will be used as a starting concentration for future human normal and neoplastic MBV experiments.

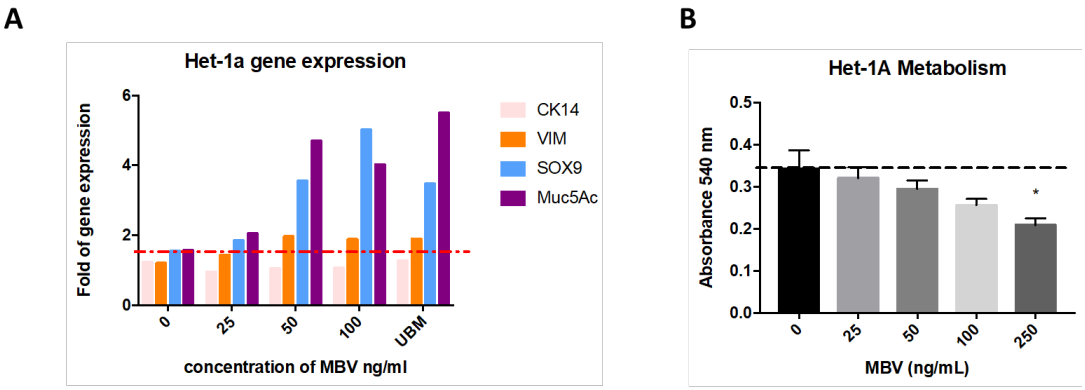

Figure 44. Effect of porcine eECM MBV on Het-1A epithelial cells.
(A) Effect upon Het-1A gene expression. (B) Effect upon Het-1A viability.

C.4 SUMMARY AND FUTURE DIRECTIONS

The results of the optimization experiments show that 50 mg of porcine ECM can be digested to isolate a quantifiable amount of MBV, as determined by internal RNA cargo. Digestion time of 3h was selected because it showed a higher yield of MBV compared to overnight digestion. The optimization experiments with porcine eECM MBV identified 25 ng/mL as an ideal starting concentration for THP-1 cells and 50 ng/mL for primary fibroblasts and Het-1A epithelial cells, based upon gene expression and viability, which will be repeated with the human normal and neoplastic ECM MBV.

APPENDIX D

ECM DOWNREGULATED NEOPLASTIC ESOPHAGEAL CELL PHENOTYPE: SUPPLEMENTARY MATERIALS

D.1 SUPPLEMENTARY METHODS

D.1.1 SDS-PAGE and Silver Stain

The neutralized pepsin, pepsin-digested UBM-ECM, and eECM samples were centrifuged at 10,000 g to collect the soluble components and 50 ug were combined with Laemmli buffer, heated at 95°C for 5 minutes, and loaded onto a 4-20% mini-PROTEAN gel (Bio-Rad). Gel electrophoresis was performed at 120V for 1 hour. The gel was fixed overnight at 4°C and the Pierce Silver Stain Kit (Thermo Fisher) was used according to manufacturer's instructions.

D.1.2 Cell Morphology

Immunolabeling was performed on the fixed OE33 cancer cell bridges for actin and tubulin to determine the bridge biochemical content. Cells were cultured and fixed in 6-well plates for actin staining, or grown on cover slips and fixed for tubulin staining. Fixation was performed using 4% paraformaldehyde (PFA) and washed 2x 5 min in 1x PBS for all stains. For actin staining, cells

were permeabilized with 0.1% Triton X-100 in PBS for 5 minutes, washed 2x5min with 1x PBS, and stained with Alexa Fluor 547 phalloidin (2 units/mL, Molecular Probes, Thermo Fisher #A22283) for 20 min at room temperature. Cells were rinsed 2 more times with 1x PBS. For tubulin staining, cells were blocked with 2% BSA/4% horse serum/0.1% Triton X-100/0.1% Tween-20 in PBS for 1 hour at room temperature, and stained with mouse monoclonal tubulin primary antibody (12G10 anti-alpha-tubulin, Developmental Hybridoma Bank, 0.1 mL concentrate, 1:50) overnight at 4°C. Cells were washed 3x5 min with 1x PBS, and incubated with Alexa Fluor 594 donkey anti-mouse secondary antibody (1:200, Invitrogen #A21203) for 1 h at room temperature. Cells were washed 3x5 min with 1x PBS, and DAPI was added for 5 min at room temperature. The cells were washed 3x5 min with 1x PBS. Images were taken with a fluorescence microscope at 20x magnification. A plasma DIC overlay was used to visualize the structure of the cell bridge at 40x magnification for tubulin staining.

D.1.3 Apoptosis

Live, non-permeabilized cells were washed, trypsinized and 200,000 – 1 million live cells/treatment were prepared for staining with the Annexin V Apoptosis Detection Kit (eBioscience) and with PI viability dye according to manufacturer's instructions. Cellular debris were gated out, and the mean side scatter intensity was measured within 4 hours at excitation 552 nm and 640 nm for PI and Annexin V-APC, respectively, using the BD FACSAria II (n=3).

D.1.4 Gene Expression: Whole Transcriptome Analysis

Human Clariom S Pico array (Thermo Fisher Scientific) was performed with 5 ng total RNA and the IVT Pico reagent kit (Thermo Fisher) according to manufacturer instructions. Amplified

cDNA was fragmented, end-labeled with biotin and hybridized to the Human Clariom S array. Following overnight (16h) hybridization at 45°C with rotational mixing at 60 RPM, arrays were processed on a GeneChip® 450 Fluidics Station using manufacturer specified protocols and scanned using the GeneArray® 3000 scanner. First level data analysis was then performed using Affymetrix Expression Console and an RNA normalization algorithm. Data was presented as the Tukey bi-weight average signal.

D.1.5 qPCR – Primer Validation

Primer annealing temperature was optimized using gradient PCR (MasterCycler gradient, Eppendorf) and melting curve analysis (QuantStudio 6 Flex, Applied Biosystems by Life Technologies). Primer specificity was evaluated using PCR gel electrophoresis and SYBR Green Master Mix for 40 PCR cycles, to confirm the presence of a single PCR product, separated on a 3% agarose gel at 70V for 1 hour.

D.1.6 Western Immunoblotting

Het-1A and OE33 cells were washed in cold PBS and then collected with lysis buffer (20 uM Tris, 137 uM NaCl, 1% Triton, 0.1% SDS, 10% glycerol, 20 uM Na3VO4, and protease/phosphatase inhibitor (Pierce Protease/phosphatase inhibitor Mini Tablets, EDTA-free Thermo Scientific)). The lysates were centrifuged at 13,000 g for 5 minutes and protein concentration was determined by the Pierce Bicinchoninic acid (BCA) assay (Thermo Fisher). Fifteen ug of Het-1A extracts and 100 ug of OE33 lysates were separated by SDS-PAGE in 4-20% Mini-PROTEAN precast protein gels (Bio-Rad), and transferred to EMD Millipore Immobilon-P polyvinylidene difluoride (PVDF) transfer membrane (Fisher Scientific) for 4 hours using wet transfer. The membranes were incubated with primary antibodies against rabbit pAKT

(Ser473) (1:1,000, Cell Signaling #9271), rabbit polyclonal AKT 1/2/3 (H-136) (1:1,000, Santa Cruz Biotechnology #SC-8302), or mouse monoclonal ACTB (8H10D10) (1:1,000, Cell Signaling #3700) overnight at 4°C. The membranes were washed and incubated with secondary antibodies for 1 h at room temperature: polyclonal goat anti-mouse immunoglobulins/HRP (Dako, #P0447) diluted 1:10,000 for ACTB; polyclonal goat anti-rabbit immunoglobulins/HRP (Dako, #P0448) diluted 1:1,000 for pAKT or diluted 1:10,000 for AKT. pAKT primary and secondary antibodies were diluted in Pierce Protein Free Blocking Buffer (Thermo Fisher Scientific), and AKT and ACTB primary and secondary antibodies were diluted in 5% milk in Tris-buffered saline with 1x Tween-20 (1x TBST). The membranes were washed and imaged with Clarity Western ECL substrate (Bio-Rad) and imaged with the ChemiDoc Touch Imaging System (Bio-Rad). Independent blots were run for each antibody for the two cell lines. The blots within each cell line were loaded with the same protein concentration, and equal protein loading was confirmed by ACTB immunoblot.

D.2 SUPPLEMENTARY TABLES

Table 10: Functionality of candidate genes grouped by signaling pathway analysis
Differentially expressed genes (>2 or <-2 fold change, p< 0.05) from the whole transcriptome analysis of Het-1A and OE33 cells treated with UBM-ECM or eECM (n=3) are grouped by top signaling pathway. Top signaling pathways include focal adhesion-PI3K-Akt-mTOR, Wnt, senescence and autophagy, cell cycle, and DNA replication. Table shows the gene ID, gene description, fold change with UBM-ECM or eECM treatment in Het-1A cells or OE33 cells compared to pepsin treatment, and biologic function. Up arrow is upregulated, down arrow is downregulated, and the parenthesis show the fold change of the treatment compared to pepsin control. Genes were excluded from the table if ECM treatment changed the normal and neoplastic cell in the same direction (both upregulation, both downregulation) for the same ECM treatment, unless the relative fold change between the normal and neoplastic cell for the same ECM treatment was >2 or <-2.

Focal Adhesion-PI3K-Akt-mTOR							
Gene ID	**Description**	**Het-1A**		**OE33**		**Function**	**Ref.**
		UBM	**eECM**	**UBM**	**eECM**		
Focal Adhesion							
FN1	Fibronectin 1				↑(2.3)	Downregulated in breast cancer metastasis	[302]
LAMB3	Laminin subunit beta 3				↑(3.4)	Basement membrane protein	[303]
ITGA3	Integrin subunit alpha 3				↑(2.4)	Overexpression results in increased head/neck cancer cell migration	[304]
ITGAE	Integrin subunit alpha E				↓(2.1)	Overexpression associated with treatment-resistant ovarian cancer	[305]
Growth Factors and RTK							
VEGFA	Vascular endothelial growth factor A		↑(16.5)		↑(3.2)	Growth factor associated with endothelial cell migration and proliferation. Activated by PI3K/Akt in tumor cells	[306]

Table 10 (continued)

ANGPT2	Angiopoietin 2				↑(2.16)	Upstream growth factor of PI3K/Akt pathway	[307]
EPHA2	EPH receptor A2				↑(2.4)	Part of the receptor tyrosine kinases upstream of the PI3K complex	[303]
GRB10	Growth factor receptor bound protein 10		↑(9.2)		↑(4.1)	Adaptor protein connecting cell surface receptor kinases to downstream signaling pathways; reduces AKT1 phosphorylation with high insulin exposure. Negative regulator of Wnt pathway	[303]
PI3K-Akt-mTOR							
PIK3IP1	Phosphoinositide-3-Kinase Interacting Protein 1				↑(2.2)	Negative regulator of PI3K activity	[303]
HRAS	HRas proto-oncogene GTPase				↓(2.2)	Positive regulator of PI3K activity	[308]
PIK3R3	Phosphoinositide-3-kinase Regulatory subunit 3			↓(2.3)		Positive regulator of PI3K: phosphorylates PIP_2 to PIP_3 which activates AKT	[309]
GSK3B	Glycogen synthase kinase 3 Beta		↓(2.3)		↑(2.5)	Negative regulator of PI3K activity: downstream molecule of AKT that can phosphorylate cyclin D1 and lower the levels necessary to drive G1/S transition	[310]

Table 10 (continued)

SLC2A3	Solute carrier family 2 member 3			↓(6.4)	↓(3.6)	Facilitates uptake of glucose needed to support proliferation and metabolic activity	[303]
PFKFB3	6-phosphofructo-2-kinase-/fructose-2,6-biphosphatase 3				↓(4.2)	Positive regulator of glycolysis	[303]
PPP2CB	Protein phosphatase 2 catalytic subunit B				↑(2.2)	Catalytic subunit of PP2A, a serine/threonine phosphatase that can dephosphorylate AKT	[311]
PPP2R5C	Protein phosphatase regulatory subunit B' gamma				↑(2.0)	Regulatory subunit of PP2A, a serine/threonine phosphatase that can dephosphorylate AKT	[311]
PPP2R3A	Protein phosphatase 2 regulatory subunit B'' alpha			↓(3.1)		Regulatory subunit of PP2A, a serine/threonine phosphatase that can dephosphorylate AKT	[311]
PPP2R2D	Regulatory subunit B delta			↓(3.3)		Regulatory subunit of PP2A, a serine/threonine phosphatase that can dephosphorylate AKT	[311]
FOXO3	Forkhead Box 3				↑(2.7)	Transcription factor downstream of the activated AKT complex that induces apoptosis in the absence of survival signals	[312]
mTOR							
DDIT4	DNA Damage inducible transcript 4 protein			↓(2.5)	↑(5.0)	Negative regulator of mTORC1	[313]

Table 10 (continued)

ULK1	Unc-51 like autophagy activating kinase 1				↑(4.1)	Downstream target of mTORC1 and also negative regulator of mTORC1	[314]
PRKAG2	5'-AMP-activated protein kinase subunit gamma-2 i				↑(3.7)	Genetic variant is highly associated with colorectal cancers	[315]
TSC2	Tuberous sclerosis complex 2				↑(2.5)	Negative regulator of mTORC1	[316]
RRAGC	Ras Related GTP-Binding C				↑(2.3)	Mutation upregulates the mTORC1 pathway	[317]
RICTOR	RPTOR independent complex of MTOR complex 2		↑(2.1)	↓(2)	↑(2.1)	Positively regulates AKT activation with mTORC1	[318]
PRKAB2	Protein Kinase AMP-Activated Non-Catalytic Subunit Beta 2		↑(2.7)	↓(3.4)		Upregulation results in increased expression of several oncogenes	[319]

Wnt Signaling							
Gene ID	**Description**	**Het-1A**		**OE33**		**Function**	**Ref.**
		UBM	**eECM**	**UBM**	**eECM**		
GSK3B	Glycogen synthase kinase 3 Beta		↓(2.3)		↑(2.5)	Negative regulator of Wnt signaling: Part of the destruction complex that phosphorylates CTNNB and marks it for destruction	310]
PPP2R3A	Protein phosphatase 2 regulatory subunit B'' alpha			↓(3.1)		Regulatory subunit of PP2A, a component of the destruction complex that binds Axin and APC and dephosphorylates GSK3B	320]

Table 10 (continued)

PPP2CB	Protein phosphatase catalytic subunit B				↑(2.2)	Catalytic subunit of PP2A, a component of the destruction complex that binds Axin and APC and dephosphorylates GSK3B	320]
PPP2R5C	Protein phosphatase regulatory subunit B' gamma				↑(2.0)	Regulatory subunit of PP2A, a component of the destruction complex that binds Axin and APC and dephosphorylates GSK3B	320]
PPARD	Peroxisome proliferator activated receptor delta			↓(2.7)		Target gene of Wnt	321]
RACGAP1	Rac GTPase Activating Protein 1		↓(3.1)		↓(8.1)	Modulating protein of the Wnt pathway, regulating cytokinesis; upregulated in gastrointestinal cancers	322]
APC	Adenomatous polyposis coli			↓(2.5)		Part of the Wnt destruction complex; Negative regulator of Wnt signaling	321]
PLAU	Plasminogen activator urokinase				↑(6.9)	Degrades extracellular matrix	323]

Senescence and Autophagy							
Gene ID	**Description**	**Het-1A**		**OE33**		**Function**	**Ref.**
		UBM	**eECM**	**UBM**	**eECM**		
FN1	Fibronectin 1				↑(2.3)	Positively correlated with autophagy related genes	[324]

Table 10 (continued)

GSK3B	Glycogen synthase kinase 3 Beta		↓(2.3)		↑(2.5)	Positive regulator of autophagy activated upon growth factor deprivation. Inversely regulated by PI3K-Akt-mTOR pathway	[325]
ULK1	Unc-51 like autophagy activating kinase 1				↑(4.1)	Positive regulator of autophagy	[314]
E2F1	E2F transcription factor 1				↓(3.1)	Promotes neoplastic cell proliferation, positive regulator of autophagy	[326]
PCNA	Proliferating cell nuclear antigen				↓(3.1)	High expression associated with neoplasia, promotes cell proliferation. Negatively related to autophagy	[327]
PLAU	Plasminogen activator urokinase				↑(6.9)	Degrades extracellular matrix	[328]
BMP2	Bone morphogenetic protein 2				↑(2.6)	Prevents metastasis into bone	[329]
MAP1LC3B	Microtubule associated protein 1 light chain 3 beta				↑(2.6)	Induces autophagy through autophagosome biogenesis	[330]
GABARAPL2	GABA type A receptor associated protein like 2				↑(2.5)	Associates with autophagic vesicles	[331]
SRC	SRC proto-oncogene non-receptor tyrosine kinase				↑(2)	Activates mTOR, repressor of autophagy	[332]
HRAS	HRas proto-oncogene GTPase				↓(2.2)	Regulates cellular response to extracellular signals, including growth factors, can positively regulate autophagy	[333]
CDK2	Cyclin dependent kinase 2				↓(3.2)	Activates mTOR, autophagy repressor	[334]

Table 10 (continued)

Cell Cycle							
Gene ID	**Description**	**Het-1A**		**OE33**		**Function**	**Ref.**
		UBM	**eECM**	**UBM**	**eECM**		
APC	Adenomatous polyposis coli			↓(2.5)		Tumor suppressor gene, loss associated with hyperplastic epithelium	[335]
PRKDC	Protein kinase DNA-activated catalytic polypeptide				↓(2.2)	Central regulator of the DNA damage response; repairs double stranded DNA break repair	[336]
YWHAH	Tyrosine 3-monooxygenase/tryptophan 5-monooxygenase activation protein				↓(2.3)	Binds phosphoserine-containing proteins to regulate the cell cycle; oncoprotein for cancer genesis	[337]
PLK1	Polo like kinase 1		↓(6.7)		↓(2.4)	Regulates the mitotic spindle during chromosome segregation; decrease in expression leads to cell proliferation and induces apoptosis	[338]
ORC5	Origin Recognition Complex Subunit 5				↓(2.6)	Essential to start DNA replication; binds to replication origins throughout the cell cycle; platform for assembly of other DNA replication initiation factors	[339]

Table 10 (continued)

CDC6	Cell division cycle 6		↑(2.6)		↓(2.7)	Helicase loading protein that localizes in the nucleus during G1, and part of the prereplicative complex at each origin; when phosphorylated, the pre-replicative complex dissembles and, CDC6 translocates to the cytoplasm at the start of S phase.	[335, 339]
BUB18	Bub1 mitotic checkpoint serine/threonine kinase B				↓(2.9)	Checkpoint protein that prevents cell division if sister chromatids are unattached to a spindle microtubule	[339]
MCM8	Minichromosome maintenance 8 homologous recombination repair factor				↓(3.1)	Binds chromatin after initiation of DNA synthesis; depletion of protein slows down DNA synthesis	[340]
CDK2	Cyclin dependent kinase 2				↓(3.2)	Regulates cell cycle control G_1→S phase, Activity increased in tumors	[341, 342]
MCM10	Minichromosome maintenance 10 replication initiation factor				↓(3.9)	Component of the pre-replication complex that assembles in G1; involved in formation of replication fork during S phase	[339]

Table 10 (continued)

ORC6	Origin recognition complex subunit 6				↓(4.0)	Essential to start DNA replication; ORC6 mediates the stability of prereplicative complexes in G1 stage; phosphorylated and inactivated to complete DNA replication	[339]
MCM4	Minichromosome Maintenance Complex Component 4				↓(4.0)	Component of the pre-replication complex that assembles in G1; has DNA helicase activity, involved in formation of replication fork during S phase	[335, 339]
MCM3	Minichromosome maintenance complex component 3				↓(4.2)	Component of the pre-replication complex that assembles in G1; has DNA helicase activity, involved in formation of replication fork during S phase	[339]
MCM7	Minichromosome maintenance complex component 7				↓(4.6)	Component of the pre-replication complex that assembles in G1; has DNA helicase activity, involved in formation of replication fork during S phase	[339]
PCNA	Proliferating cell nuclear antigen				↓(4.8)	Aids and controls DNA replication by forming a ring around DNA; cofactor for DNA polymerase	[343]

Table 10 (continued)

CCNE2	Cyclin E2				↓(4.9)	Regulator of CDK2; helps in cell cycle G1→ S transition; Shown to increase proliferation, migration, and invasion in lung cancer cells (increased expression in tumor cells)	[339, 344]
RBL1	RB transcriptional corepressor like 1				↓(5.0)	Tumor suppressor protein that regulates entry into cell division; phosphorylated in S to M phase and dephosphorylated in G1 phase	[303, 339]
CDC45	Cell division cycle 45				↓(5.2)	Recruits DNA polymerase α into pre-replication complexes essential for DNA replication and cell cycle progression	[345]
CDC20	Cell Division Cycle 20		↓(2.7)		↓(5.4)	Regulatory protein necessary for nuclear movement before anaphase and chromosome separation	[339]
CCNA2	Cyclin A2		↓(2.2)		↓(5.5)	Regulates cell cycle at G1 to S and G2 to M transitions; overexpressed in many cancer types	[346]
CDK1	Cyclin dependent kinase 1				↓(5.6)	Key regulator of G1/S and G2/M transition	[335]

Table 10 (continued)

ORC1	Origin recognition complex subunit 1				↓(5.8)	Essential to start DNA replication; binds to replication origins throughout the cell cycle; platform for assembly of other DNA replication initiation factors.	[339]
MCM6	Minichromosome maintenance complex component 6				↓(6.1)	Component of the pre-replication complex that assembles in G1; has DNA helicase activity, involved in formation of replication fork during S phase	[339]
MCM5	Minichromosome maintenance complex component 5				↓(6.3)	Component of the pre-replication complex that assembles in G1; has DNA helicase activity, involved in formation of replication fork during S phase	[339]
MCM2	Minichromosome maintenance complex component 2				↓(6.6)	Component of the pre-replication complex that assembles in G1; has DNA helicase activity, involved in formation of replication fork during S phase	

Table 10 (continued)

DNA replication							
Gene ID	**Description**	**Het-1A**		**OE33**		**Function**	**Ref.**
		UBM	**eECM**	**UBM**	**eECM**		
RPA3	Replication protein A3				↓(2.0)	Binds single stranded DNA during DNA replication	[347]
RPA2	Replication protein A2				↓(2.2)	Binds single stranded DNA during DNA replication	[347]
POLD2	DNA polymerase delta 2				↓(2.4)	Component of the DNA polymerase delta complex	[303]
CDC6	Cell division cycle 6		↑(2.6)		↓(2.7)	Part of the pre-replication complex that attaches to origins of replication to start DNA replication	[339]
RFC5	Replication factor c subunit 5				↓(2.9)	Required to load the DNA clamp (PCNA) during DNA replication	[348]
POLD3	DNA polymerase delta 3				↓(3.1)	Regulates double stranded DNA break repair; depletion prevents replication fork progression	[349]
PRIM1	Primase (dna) subunit 1				↓(3.2)	Subunit of a primase that synthesizes Okazaki fragments and initiates DNA replication	[303]

Table 10 (continued)

CDK2	Cyclin dependent kinase 2				↓(3.2)	Peak activation during G1-S and S phase to phosphorylate components of the pre-replication complex and prevent replication from occurring more than once per cycle; Activity increased in tumors	[342, 350]
MCM10	Minichromosome maintenance 10 replication initiation factor				↓(3.9)	Component of the pre-replication complex; involved in formation of replication fork during DNA replication	[339]
MCM4	Minichromosome Maintenance Complex Component 4x				↓(4.1)	Component of the pre-replication complex; has DNA helicase activity, involved in formation of replication fork during DNA replication	[339, 351]
MCM3	Minichromosome maintenance complex component 3				↓(4.2)	Component of the pre-replication complex; has DNA helicase activity, involved in formation of replication fork during DNA replication	[351]
MCM7	Minichromosome maintenance complex component 3				↓(2.9)	Component of the pre-replication complex; has DNA helicase activity, involved in formation of replication fork during DNA replication	[351]

Table 10 (continued)

PCNA	Proliferating cell nuclear antigen				↓(4.8)	Facilitates and controls DNA replication by forming a ring around the DNA; cofactor for DNA polymerase	[343]
RFC4	Replication Factor C Subunit 4				↓(5.8)	Required to load the DNA clamp (PCNA) during DNA replication; Involved in DNA damage checkpoint pathways	[348, 352]
MCM6	Minichromosome maintenance complex component 6				↓(6.1)	Component of the pre-replication complex; has DNA helicase activity, involved in formation of replication fork during DNA replication	[339, 351]
MCM5	Minichromosome maintenance complex component 5				↓(6.3)	MCM2-7 proteins make up pre-replicative complex formed at replication origin; ability to induce DNA replication	[351]
MCM2	Minichromosome maintenance complex component 2				↓(6.6)	Component of the pre-replication complex; has DNA helicase activity, involved in formation of replication fork during DNA replication	[351]
GMNN	Geminin				↓(6.6)	DNA replication inhibitor	[350]
RFC2	Replication factor subunit 2				↓(7.5)	Required to load the DNA clamp (PCNA) during DNA replication	[348]

Abbreviations:
UBM – Urinary bladder matrix
eECM – Esophageal mucosa ECM

Table 11. Primers list.

Human candidate genes selected for validation by qPCR with the forward and reverse primer sequences. Primers were designed using qPrimer Depot (NCI NIH) or referenced from the literature.

Gene	Forward Primer (5'-3')	Reverse Primer (5'-3')	Ref
PIK3R3	TTAGGTGGCTTTGGTGGAAG	AGACTGGAGGGAGGTGATGA	PrimerDepot
SLC2A3	GATGGGCTCTTGAACACCTG	GACAGCCCATCATCATTTCC	PrimerDepot
RICTOR	GGAAGCCTGTTGATGGTGAT	GGCAGCCTGTTTTATGGTGT	[353]
PP2A	AGTTGGCCAAATGTGTCTCC	GAGTTGCGGTACAAGGAAGG	[354]
PIK3IP1	TGGCATCATCTTGGGCTACTC	GGGTTGGTGAAGGCAGACAA	[355]
HRAS	CCAGCTTATATTCCGTCATCG	CAGTCGCGCCTGTGAAC	PrimerDepot
GSK3B	CCACTGTTGTCACCTTGCTG	GAGTGATCATGTCAGGGCG	PrimerDepot
TSC2	CCAGCATCTCATACACACGC	CTTGGAGGATGTGAAGACAGC	PrimerDepot
DDIT4	GGACGCACTTGTCTTAGCAGTTCTC	CCAGGGCGTTGCTGATGAA	[356]
PFKFB3	CCGCGTACCATCTACCTGTG	CAGAGCACTGGCAAACTTCTTG	[357]
FOXO3A	CCCAACCAGCTCCTTTAACA	GAGTCCGAAGTGAGCAGGTC	[358]
ULK1	CGTTGCAGTACTCCATAACCAG	GGGGAAGGAAATCAAAATCC	PrimerDepot
PPARD	GCGCAGCTGCAAGATTCAGAAGAA	AACGGATAGCGTTGTGTGACATGC	PrimerDepot
RACGAP1	TCCTCTGCCACTTTTTACGG	TCTGTTTGAGCAGCTTGTGC	PrimerDepot
E2F1	AGCTGGACCACCTGATGAAT	GTCCTGACACGTCACGTAGG	[359]
PCNA	AAGAGAGTGGAGTGGCTTTTG	TGTCGATAAAGAGGAGGAAGC	PrimerDepot
MAP1LC3B	AAACGGGCTGTGTGAGAAAAC	TGAGGACTTTGGGTGTGGTTC	[360]
CDK2	AGAAAATCCGCCTGGACACT	GAGAGCAGAGGCATCCATGA	PrimerDepot
GABARAPL2	GTGTTCTCTCCGCTGTAGGC	TGTGGATAAGACAGTCCCACA	PrimerDepot
MCM4	TTGAAGCCATTGATGTGGAA	GGCACTCATCCCCGTAGTAA	[361]
MCM6	TCTACTATGCGCCTGGCAAT	TTGTCAGCTCCCATCATGTC	PrimerDepot

Table 11 (continued)

MCM7	GGTCAGTTCTCCACTCACGG	CATACATTGATCGACTGGCG	PrimerDepot
CDK1	TGAAACTGCTCGCACTTG	ATGGTAGATCCCGGCTTATT	[362]
CDC6	GGGAATCAGAGGCTCAGAAG	CACTGGATGTTTGCAGGAGA	PrimerDepot
CCNE2	GTTCTTCTACCTCAGTATTCTC	AGCAGCAGTCAGTATTCT	[363]
RPA2	ACAGTGTTTTCACTGCTGGTG	CAGAGAAGGCTCCAACCAAC	PrimerDepot
PRIM1	TTTCACATAAGGTGCTAGACTGG	GAATTGGATGCCATTTCCAC	PrimerDepot
CDKN2B	CCCAACTCCACCAGATAGCA	GGGATTTCCGCATCCTAGCA	[364]
CDC45	TGGACTGCACACGGATCT	AACCTGGCTGCGGTATAG	[365]
ACTB	AGAGCTACGAGCTGCCTGAC	AGCACTGTGTTGGCGTACAG	[366]

D.3 SUPPLEMENTARY FIGURES

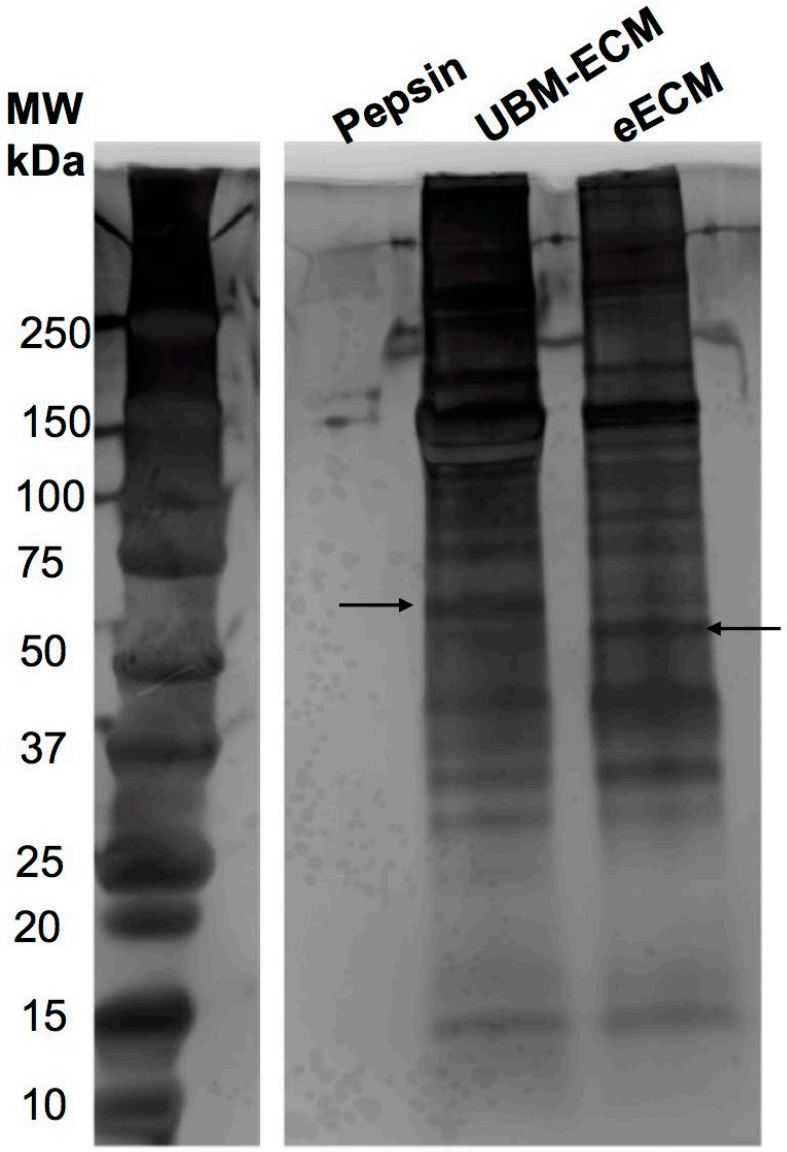

Figure 45. The soluble proteins of pepsin, UBM-ECM, and eECM were separated by gel chromatography and stained with silver stain.

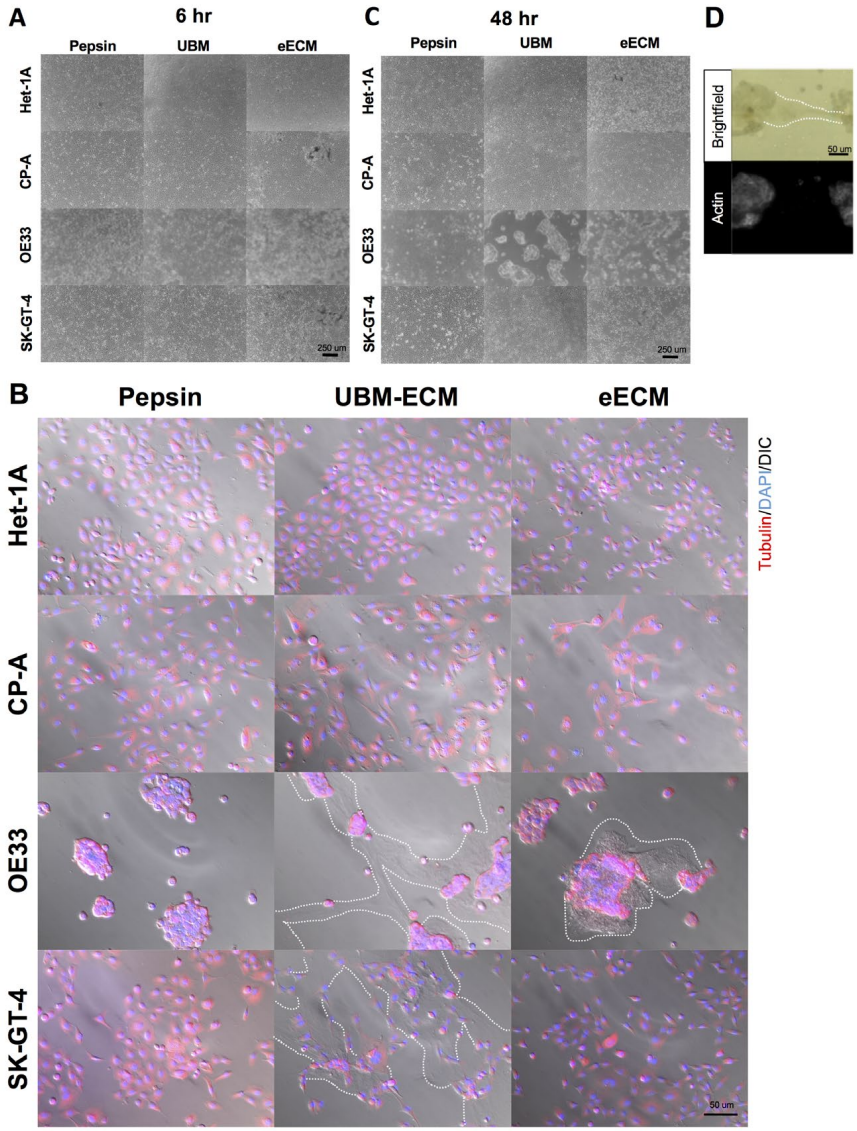

Figure 46. Cell morphology

Het-1A, CP-A, OE33, and SK-GT-4 cells were cultured with media supplemented with pepsin (25 ug/mL), UBM-ECM (250 ug/mL), or eECM (250 ug/mL). (**A)** No drastic change in cell morphology was shown with UBM-ECM or eECM treatment compared to pepsin control after 6h. Scale bar= 250 um. (**B)** Complete differential interference contrast (DIC) microscopy panel, showing the presence of cell bridges at 24h in OE33 cells treated with UBM-ECM and eECM, but not in Het-1A or CP-A cells, compared to pepsin control. Fixed cells were stained with tubulin and DAPI, and cell bridges are outlined in white dotted lines. Scale bar = 50 um (**C)** Cells treated with UBM-ECM and eECM treatment for 48h showed a similar phenotype to 24h with a reduced confluency for OE33 cells compared to pepsin control, with little change in the Het-1A or CP-A cells. SK-GT-4 cells also showed a slightly reduced confluency with UBM-ECM and eECM treatment compared to pepsin at 48h. Scale bar = 250 um. (**D**) Fixed OE33 cells treated with UBM-ECM (250 ug/mL) after 24h were stained with phalloidin actin. The cell bridge seen in the brightfield image did not stain positively for actin. Scale bar = 50 um.

Figure 47. Top differentially expressed pathways for Het-1A and OE33 cells treated with UBM-ECM normalized to pepsin, or eECM normalized to pepsin.
Green bars refer to downregulated genes, red bars refer to upregulated genes, and yellow bars refers to the Gene Count within that pathway. Top candidate pathways selected for further analysis are marked (*).

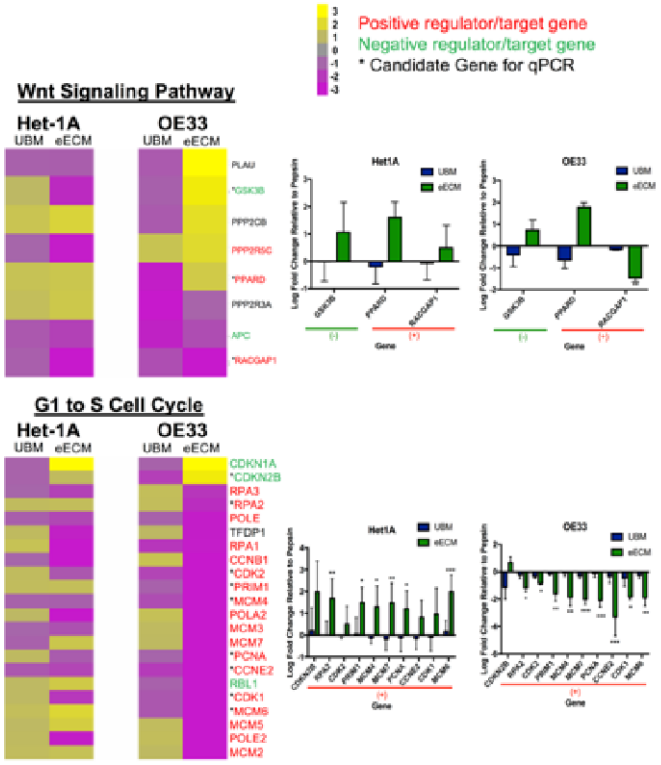

Figure 48. Signaling pathway analysis shown for Wnt signaling and G1 to S Cell Cycle. Differentially expressed genes (>2 or <-2 fold change, p< 0.05) for Het-1A and OE33 cells treated with UBM-ECM (250 ug/mL) or eECM (250 ug/mL) for 24h, and normalized to pepsin control treatment (25 ug/mL). Purple bars represent downregulated genes, and yellow bars represent upregulated genes compared to pepsin control. Genes are labeled as positive regulators (red) or negative regulators (green) and candidate genes that were further validated by qPCR are marked (*).

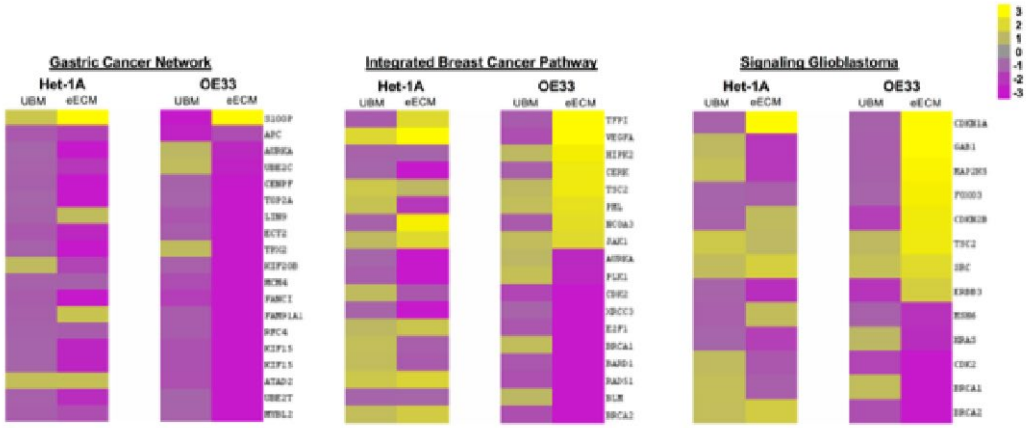

Figure 49. Signaling pathway networks for other cancer types were also shown to be downregulated in OE33 cells with ECM treatment including gastric cancer network, integrated breast cancer pathway, and signaling glioblastoma, but not further validated by qPCR.

Purple bars represent downregulated genes, and yellow bars represent upregulated genes compared to pepsin control.

APPENDIX E

ESOPHAGEAL EXTRACELLULAR MATRIX HYDROGEL MITIGATES METAPLASTIC CHANGE IN A DOG MODEL: SUPPLEMENTARY MATERIAL

E.1 SUPPLEMENTARY FIGURES

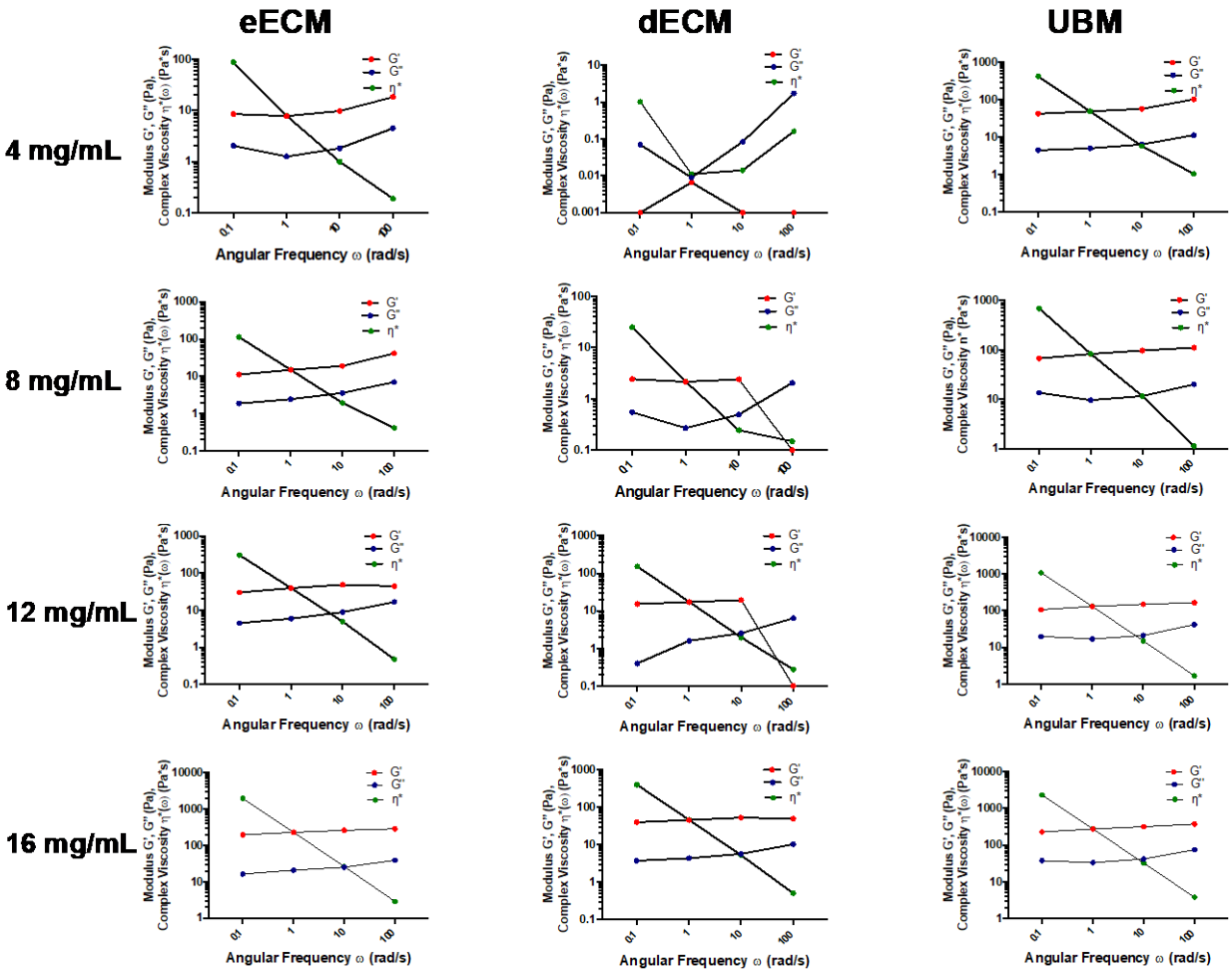

Figure 50. ECM hydrogel stability.
ECM hydrogels of the 3 sources (eECM, dECM, UBM) and the 4 ECM concentrations (4, 8, 12, 16 mg/mL) were tested for gel stability by applying a small 0.5% oscillatory strain and measuring the storage modulus G', loss modulus G'', and complex viscosity $\eta^*(\omega)$ plotted over angular frequencies (ω) (0.1-100 rad/s) on a log-log scale at 37°C. Representative graphs are shown (n=3).

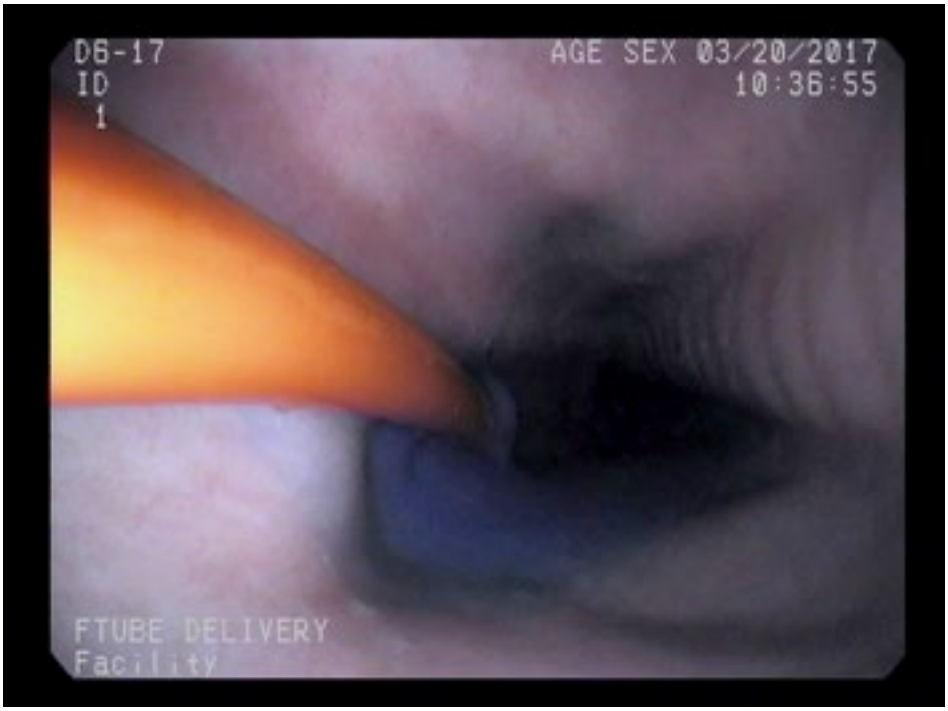

Figure 51. Blue-dyed eECM hydrogel is identifiable by endoscopy after feeding tube delivery at 15°C.

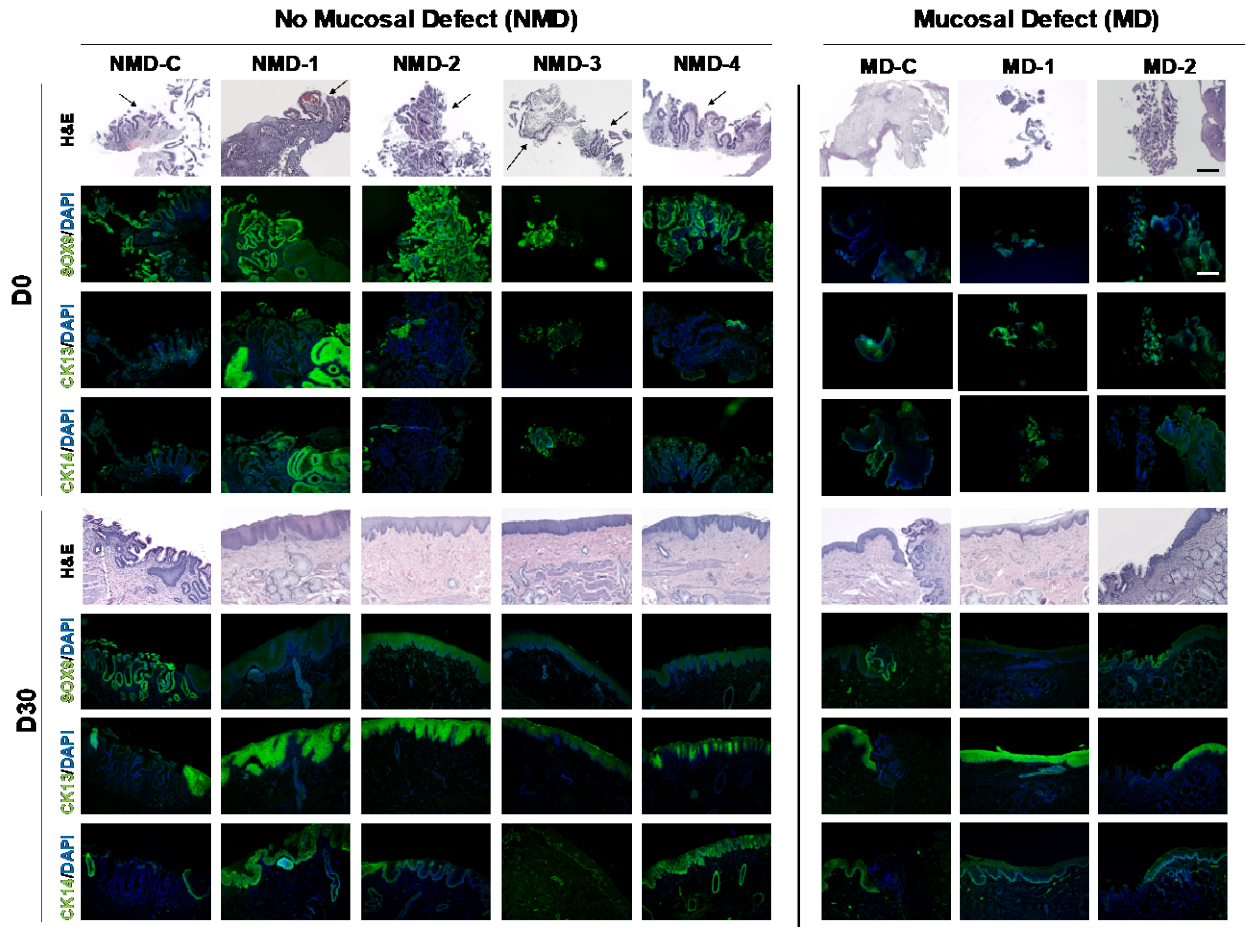

Figure 52. Effect of 30d eECM hydrogel on esophageal epithelial cell phenotype.
Animals were in one of two groups: no mucosal defect (NMD) (**A)** or mucosal defect (MD) (**B**). Biopsies (d0) were taken at the highest level of esophageal disease before treatment. Treatment was delivered orally for 30d as eECM hydrogel (12 mg/mL, 25 mL, BID) (NMD-1-4, MD-1-2) or control (Omeprazole, 20 mg, QD) (NMD-C, MD-C). Samples were taken at necropsy in the same location as the biopsies, and stained with hematoxylin and eosin (H&E), Barrett's marker Sox9, or normal squamous epithelial markers CK13 and CK14. Arrows indicate goblet cells characteristic of intestinal metaplasia and Barrett's esophagus. Scale bar = 250 um.

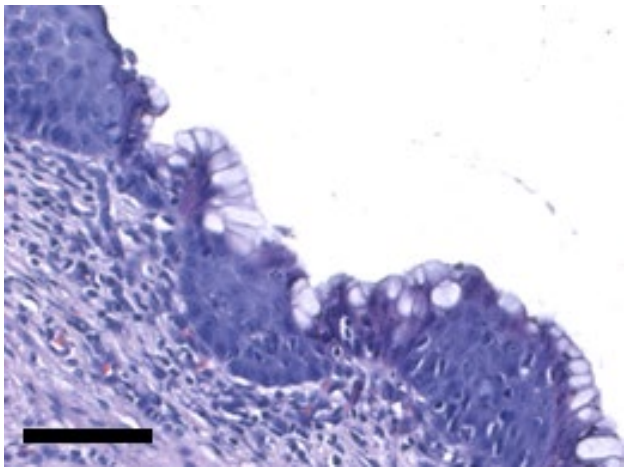

Figure 53. H&E staining for MD-2 appears to show the metaplastic epithelium in the process of transitioning to a normal, squamous epithelium because columnar and squamous cells are intermixed.

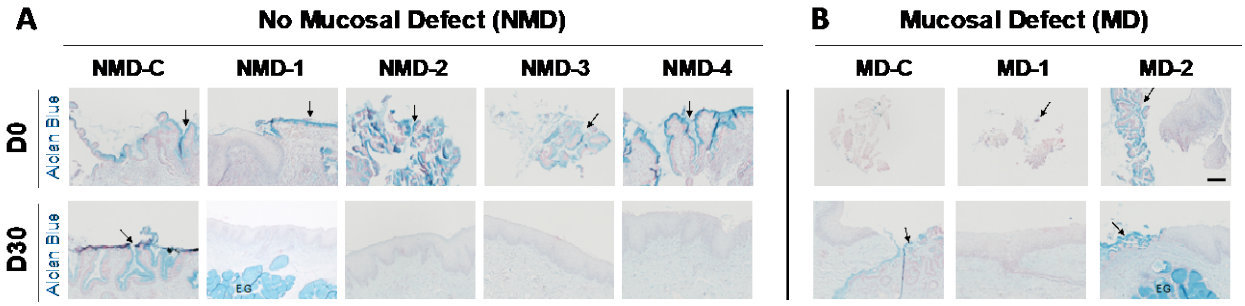

Figure 54. Alcian blue staining.
Animals were in one of two groups: no mucosal defect (NMD) (**A)** or mucosal defect (MD) (**B**). Biopsies (d0) were taken at the highest level of esophageal disease before treatment. Treatment was delivered orally for 30d as eECM hydrogel (12 mg/mL, 25 mL, BID) (NMD-1-4, MD-1-2) or control (Omeprazole, 20 mg, QD) (NMD-C, MD-C). Samples were taken at necropsy in the same location as the biopsies, and stained with Alcian blue. Alcian blue labels the intracytoplasmic acidic mucin of goblet cells**.** Arrows indicate goblet cells characteristic of intestinal metaplasia and Barrett's esophagus. Non-metaplastic, mucin containing esophageal glands (EG) can also stain positively for alcian blue and are not a marker of Barrett's esophagus. Scale bar = 100 um.

Table 12. Quantitative proteomics of porcine esophageal tissue and ECM.
Protein abundance of proteins in the native tissue and eECM (n=3), and separated by function (e.g., Basement membrane, fibrillar collagen, Structural, Cytoskeletal).

Protein Abundance (nmol/g*)												
Protein	GENE	Uniprot	Functional	Matrisome	Esophagus						Trend	Tech CV (%)
					Native			ECM				
					eN1	eN2	eN3	eE1	eE2	eE3		
Agrin(iso 2,3,4,5,&6)	AGRN^	O00468	Basement Membrane	Glycoprotein	1.71	1.73	1.96	0.34	0.57	0.45		31%
Collagen alpha-1/5(IV) chain(Arresten/Core Protein)	COL4A1/5^	160613	Basement Membrane	Collagen	2.62	3.13	3.73	0.36	0.27	0.07		6%
Collagen alpha-1(IV) chain(Arresten/Core Protein)	COL4A1^	160613	Basement Membrane	Collagen	0.37	0.42	0.32	0.80	0.36	0.45		8%
Collagen alpha-2(IV) chain	COL4A2	P08122	Basement Membrane	Collagen	0.52	0.63	0.61	0.91	0.20	0.22		10%
Collagen alpha-2(IV) chain(Canstatin/Core Protein)	COL4A2^	161386	Basement Membrane	Collagen	0.73	1.11	0.80	1.59	0.70	0.64		4%
Perlecan	HSPG2	375271	Basement Membrane	Proteoglycan	3.23	2.43	2.41	0.36	0.08	0.07		9%
Laminin alpha-2	LAMA2	P24043	Basement Membrane	Glycoprotein	0.04	0.04	0.04					17%
Laminin alpha-3	LAMA3	Q61789	Basement Membrane	Glycoprotein	0.07	1.01		0.30	0.57	0.16		13%
Laminin alpha-4	LAMA4	201819	Basement Membrane	Glycoprotein	0.18	0.23	0.85			0.23		6%
Laminin alpha-5	LAMA5	O15230	Basement Membrane	Glycoprotein	0.07	0.23	0.08	0.07				19%
Laminin Beta-1	LAMB1	197090	Basement Membrane	Glycoprotein	0.50	1.31	0.47	0.22	0.35	0.27		13%
Laminin Beta-2	LAMB2	196474	Basement Membrane	Glycoprotein	0.79	0.93	0.70	0.03	0.03			13%
Laminin Gamma-1	LAMC1	177387	Basement Membrane	Glycoprotein	0.84	1.17	0.97	0.73	0.28	0.24		8%
Laminin Gamma-2	LAMC2	Q13753	Basement Membrane	Glycoprotein	2.01	3.48	3.58		1.30	0.37		11%
Nidogen-1	NID1	137039	Basement Membrane	Glycoprotein	0.26	0.31	0.24	0.08	0.03			16%
Nidogen-2	NID2	Q14112	Basement Membrane	ECM Glycoproteins	1.88	2.19	1.73					8%
Collagen alpha-1(XII) chain	COL12A1	340214	FACIT Collagen	Collagen	0.59	0.51	0.61	0.30	0.66	0.52		15%
Collagen alpha-1(XIV) chain	COL14A1	191772	FACIT Collagen	Collagen	7.71	8.96	8.70					12%
Collagen alpha-1(I) chain	COL1A1	137953	Fibrillar Collagen	Collagen	237.83	232.07	252.01	292.35	327.58	368.50		4%
Collagen alpha-1(I) chain(Gal Glu-K)	COL1A1^	137953	Fibrillar Collagen	Collagen	0.20	0.18	0.12					11%
Collagen alpha-2(I) chain	COL1A2	129564	Fibrillar Collagen	Collagen	152.85	132.47	160.71	188.21	220.13	237.05		4%
Collagen alpha-2(I) chain(C-term Propeptide)	COL1A2^	129564	Fibrillar Collagen	Collagen	2.11	1.76	1.63					24%
Collagen alpha-1(III) chain	COL3A1	138936	Fibrillar Collagen	Collagen	127.05	113.94	72.61	115.35	142.76	158.29		8%
Collagen alpha-1(V) chain	COL5A1	183987	Fibrillar Collagen	Collagen	3.94	4.06	3.84	8.81	7.50	10.45		2%
Collagen alpha-2(V) chain	COL5A2	145018	Fibrillar Collagen	Collagen	1.86	1.70	1.54	3.98	3.97	4.42		7%
Fibulin 5	FBLN5	50160	Matricellular	Glycoprotein	0.48	0.28	0.29					25%
Periostin	POSTN	93155	Matricellular	Glycoprotein	1.03	0.90	0.29	0.99	0.90	0.48		16%
Secreted protein, acidic, cysteine-rich (osteonectin)	SPARC	34296	Matricellular	Glycoprotein	0.05	0.08	0.08					9%
Thrombospondin 2	THBS2	P35442	Matricellular	Glycoprotein			0.04					12%
Tenascin-X	TNXB	126729	Matricellular	Glycoprotein	0.12	0.15	0.09					13%
Annexin A2	ANXA2	38678	Other ECM	ECM-affiliated	6.24	6.06	6.58	0.40	0.29	0.16		17%
Asporin	ASPN	42573	Other ECM	Proteoglycan	1.20	1.24	1.03					16%
Galectin-1	LGALS1	14857	Other ECM	ECM-affiliated	9.54	16.52	7.98					10%
Galectin-3	LGALS3	27202	Other ECM	ECM-affiliated	6.76	7.07	7.15					29%
Mimecan/Osteoglycin	OGN	34069	Other ECM	Proteoglycan	9.00	10.96	9.86					8%
Biglycan	BGN	41706	Structural ECM	Proteoglycan	0.92	1.44	0.91					20%
Collagen alpha-1(XVIII) chain	COL18A1	182881	Structural ECM	Collagen	0.05	0.06	0.04					6%
Collagen alpha-1(VI) chain	COL6A1	108806	Structural ECM	Collagen	15.81	22.33	17.56	3.90	1.50	1.46		9%
Collagen alpha-2(VI) chain	COL6A2	108579	Structural ECM	Collagen	14.57	15.98	15.30	0.83	0.35	0.16		7%
Collagen alpha-3(VI) chain	COL6A3	288133	Structural ECM	Collagen	16.49	21.23	17.03	18.48	10.28	8.16		3%
Collagen alpha-1(VIII) chain	COL8A1	P27658	Structural ECM	Collagens	0.94	1.36	0.53	0.63	0.57	0.37		15%
Decorin	DCN	39805	Structural ECM	Proteoglycan	5.57	3.97	3.45					5%
Dermatopontin	DPT	24203	Structural ECM	Glycoprotein	3.50	3.21	3.30	4.62	3.03	3.65		10%
Emilin 1	EMILIN1	106667	Structural ECM	Glycoprotein	0.05	0.07	0.03					7%
Fibrillin 1	FBN1	311952	Structural ECM	Glycoprotein	0.63	0.48	0.50	0.67	0.58	0.87		6%
Fibromodulin	FMOD	Q06828	Structural ECM	Proteoglycans	9.30	6.95	5.41					12%
Fibronectin 1(Anastellin, type III 4//9/13)	FN1	P02751	Structural ECM	Glycoprotein	1.38	2.65	1.39	3.65	1.91	1.27		9%
Latent transforming growth factor beta binding protein 1	LTBP1	Q14766	Structural ECM	Glycoprotein	0.14	0.03	0.05	0.04		0.14		9%
Lumican	LUM	38279	Structural ECM	Proteoglycan	9.83	12.86	12.74	0.03		0.16		7%
Microfibrillar-associated protein 2	MFAP2	20578	Structural ECM	Glycoprotein	2.05	1.89	1.96					14%
Prolargin	PRELP	43179	Structural ECM	Proteoglycan	7.62	5.74	6.70	0.10	0.04	0.06		5%
Versican	VCAN	300008	Structural ECM	Proteoglycans	0.37	0.52	0.30					13%
Target of Nesh-SH3	ABI3BP	Q7Z7G0	Secreted	ECM Glycoproteins	1.06	1.17	0.78					29%
Transforming growth factor-beta-induced protein ig-h3	TGFBI	74597	Secreted	Glycoprotein	0.53	0.86	0.13	0.28		0.05		12%
Actin (All isoforms)	ACT	42051	Cytoskeletal	Cellular	146.62	253.09	147.65	0.32	0.10	0.11		4%
Actin, cytoplasmic 1/2	ACTB	41737	Cytoskeletal	Cellular	32.82	60.80	33.55	1.14	0.53	0.21		12%
Myosin(Myosin-3,4,6,7)	MYH^	P12882	Cytoskeletal	Cellular	6.54	1.43	1.10					10%
Spectrin alpha chain, non-erythrocytic 1	SPTA2	284637	Cytoskeletal	Cellular	1.22	1.46	1.27	0.42	0.50	0.33		6%
Tubulin beta-4 B chain(4b & 5 chain)	TUBB^	49586	Cytoskeletal	Cellular	1.97	2.80	2.09	0.14	0.08	0.04		2%
Vimentin	VIM	53733	Cytoskeletal	Cellular	3.51	3.68	3.35	0.04	0.08	0.07		6%
Glyceraldehyde-3-phosphate dehydrogenase	GAPDH	35828	Other Cellular	Cellular	67.15	72.07	43.30					6%
Histone H1 (H1.1,H1.2,H1.3,H1.4)	H1^	20863	Other Cellular	Cellular	49.67	58.69	31.24					7%
Histone 2A(H2A-A-K)	H2A^	14077	Other Cellular	Cellular	15.39	15.42	9.97					7%
Lamin-A/C	LMNA		Other Cellular	Cellular	50.40	12.28	16.02	0.54		0.05		16%
^indicates peptide that was used to identify protein may be homologus to multiple protein isoforms, cryptic peptides, or susceptiple to PTM and is explain in paranthesis next to the protein name												

APPENDIX F

ECM HYDROGEL AS A SUBMUCOSAL FLUID CUSHION AND TO PREVENT STRICTURE

F.1 SUPPLEMENTARY MATERIALS

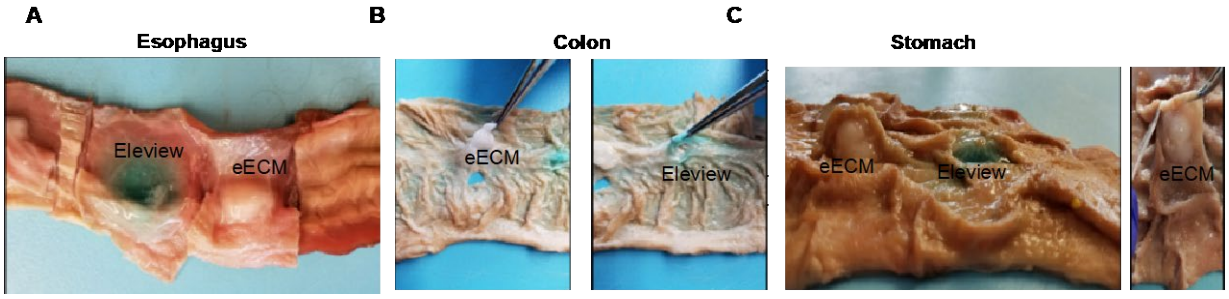

Figure 55. Macroscopic appearance of submucosal fluid cushion (SFC) *ex vivo*.
SFC was performed with two test agents: Eleview® (dyed blue) and esophageal mucosa ECM hydrogel (eECM, 12 mg/mL), for porcine esophagus (A), colon (B), and stomach (C). Pictures were taken after 75 minutes.

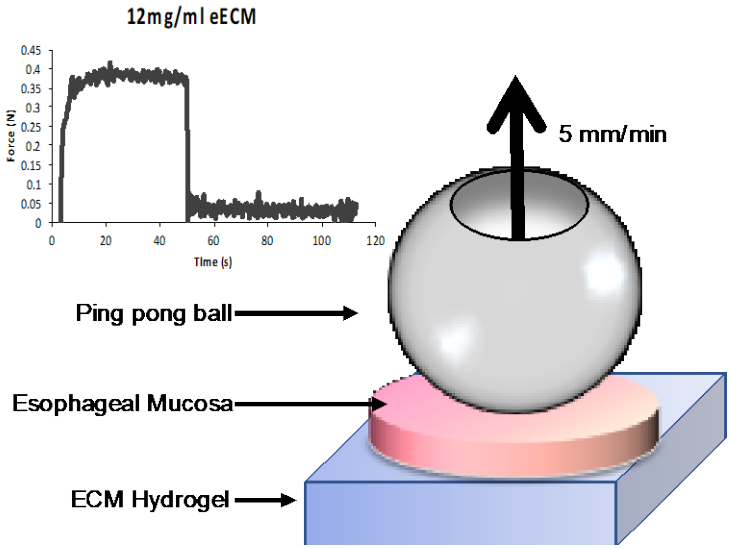

Figure 56. Schematic illustrating the experimental set-up to measure ECM hydrogel mucoadhesion to porcine mucosa and muscle tissue.
Schematic shows the new test that was developed to measure the strength of the bond between the ECM hydrogel and porcine mucosa. The test was based upon indentation tests for measuring hydrogel adhesion [367]. The ECM hydrogel is at the bottom of the test construct. The porcine esophageal tissue (mucosa or muscle) is glued to a half-sphere and allowed to adhere for 1h at 37°C. The half-sphere is raised at a speed of 5 mm/min. A representative graph of a mechanical Instron test is shown. The peak force is calculated.

APPENDIX G

ECM AS AN ORAL THERAPEUTIC FOR HIGH GRADE DYSPLASIA AND CANCER IN A RAT MODEL: SUPPLEMENTARY MATERIAL

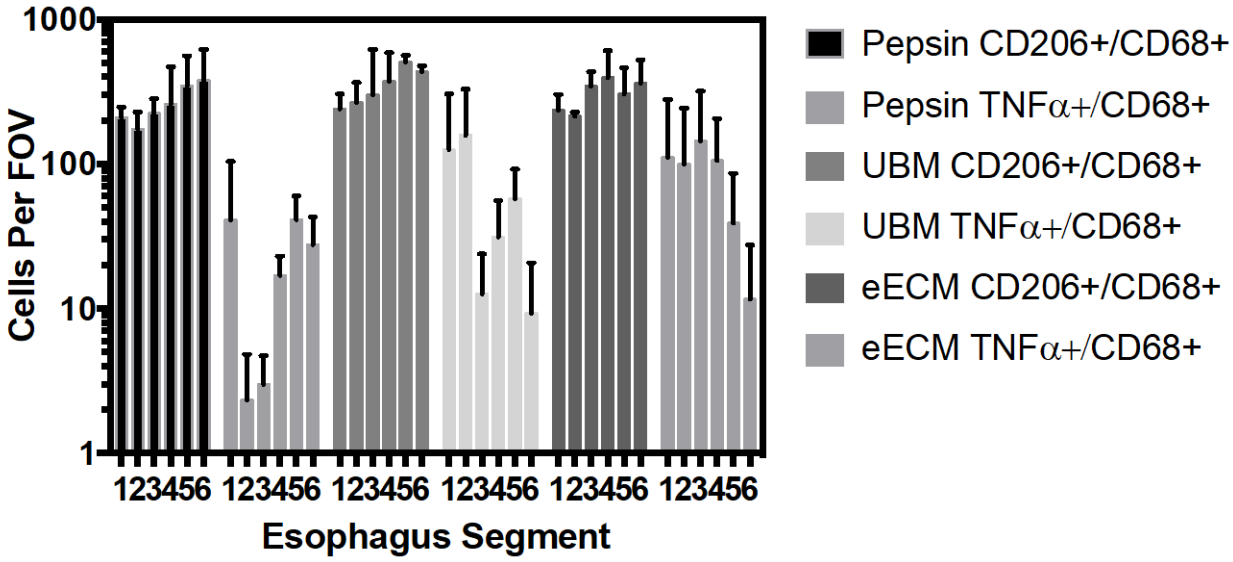

Figure 57. 3d Macrophage phenotype.
CD206+/CD68+ cells per field of view for each of the segments (1-6) listed proximally to distally (oral to gastric).

A

Feature	Disease State
Disease State	Normal Hyperplasia Esophagitis Barrett's EAC Erosion *Mark each disease state as a percentage from 0-100 for the coverage of the esophagus segment
Inflammation Score	0 – no inflammation 1- mild inflammation in the submucosa 2- severe inflammation in the submucosa

B

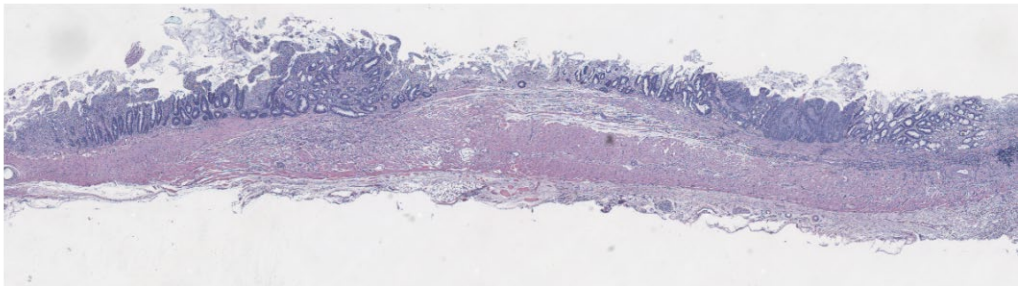

Figure 58. Scoring of disease state and inflammation after 21d of treatment.
(A) Scoring criteria used. Esophagi are divided into 6 segments. Reviewers are blinded and asked to score the percentage of disease length/segment for the different disease states and to score the inflammation. (B) Representative esophageal segment (1 of 6) being graded per animal.

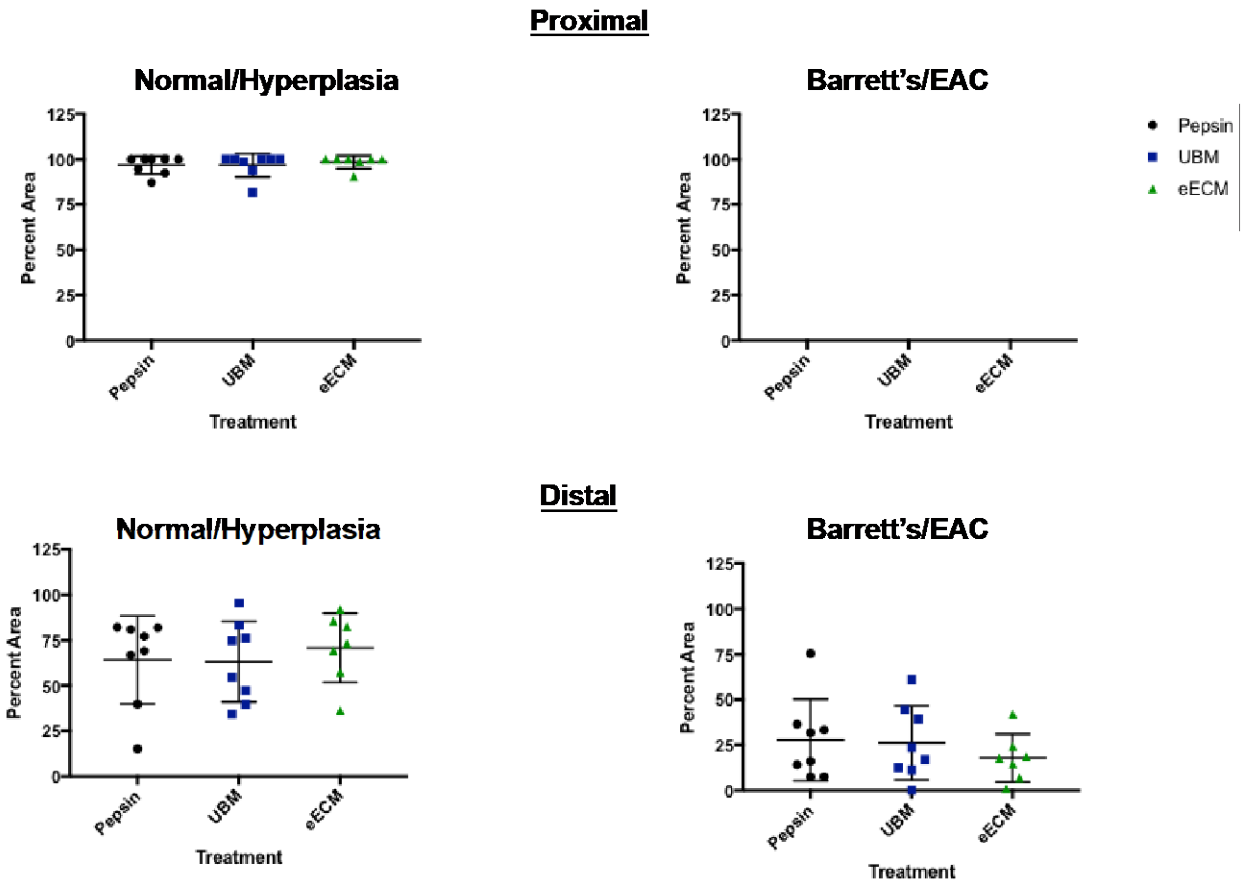

Figure 59 Scoring of the proximal (segments 1-3) and distal (segments 4-6) for normal/hyperplastic percentage and Barrett's/EAC percentage with each treatment.
The scores suggest a trend toward a decrease in the percentage of Barrett's/EAC disease state in the distal esophagus with ECM treatment, however, the scores showed some inter-observer variability and need to be confirmed.

APPENDIX H

ABBREVIATIONS

BE	Barrett's esophagus
EAC	esophageal adenocarcinoma
ECM	extracellular matrix
eECM	esophageal mucosa ECM
EMR	endoscopic mucosal resection
EMT	epithelial-mesenchymal transition
ESD	endoscopic submucosal dissection
GERD	gastroesophageal reflux disease
HGD	high grade dysplasia
MBV	matrix-bound nanovesicle
PPIs	proton pump inhibitors
SFC	submucosal fluid cushion
UBM	urinary bladder matrix

BIBLIOGRAPHY

1. Pohl, H. and H.G. Welch, *The role of overdiagnosis and reclassification in the marked increase of esophageal adenocarcinoma incidence.* J Natl Cancer Inst, 2005. **97**(2): p. 142-6.

2. Pennathur, A., et al., *Oesophageal carcinoma.* Lancet, 2013. **381**(9864): p. 400-12.

3. Londono, R., et al., *Esophagus and regenerative medicine.* World J Gastroenterol, 2012. **18**(47): p. 6894-9.

4. Nelson, C.M. and M.J. Bissell, *Of extracellular matrix, scaffolds, and signaling: tissue architecture regulates development, homeostasis, and cancer.* Annu Rev Cell Dev Biol, 2006. **22**: p. 287-309.

5. Bissell, M.J., H.G. Hall, and G. Parry, *How does the extracellular matrix direct gene expression?* J Theor Biol, 1982. **99**(1): p. 31-68.

6. Huleihel, L., et al., *Matrix-bound nanovesicles within ECM bioscaffolds.* Sci Adv, 2016. **2**(6): p. e1600502.

7. Mantovani, A., et al., *Macrophage polarization: tumor-associated macrophages as a paradigm for polarized M2 mononuclear phagocytes.* Trends Immunol, 2002. **23**(11): p. 549-55.

8. Kalluri, R. and R.A. Weinberg, *The basics of epithelial-mesenchymal transition.* J Clin Invest, 2009. **119**(6): p. 1420-8.

9. Solinas, G., et al., *Tumor-associated macrophages (TAM) as major players of the cancer-related inflammation.* J Leukoc Biol, 2009. **86**(5): p. 1065-73.

10. Mantovani, A., et al., *Cancer-related inflammation.* Nature, 2008. **454**(7203): p. 436-44.

11. Jankowski, J.A., et al., *Barrett's metaplasia.* Lancet, 2000. **356**(9247): p. 2079-85.

12. Rieder, F., et al., *Inflammatory mediators in gastroesophageal reflux disease: impact on esophageal motility, fibrosis, and carcinogenesis.* Am J Physiol Gastrointest Liver Physiol, 2010. **298**(5): p. G571-81.

13. Spechler, S.J., et al., *History, molecular mechanisms, and endoscopic treatment of Barrett's esophagus.* Gastroenterology, 2010. **138**(3): p. 854-69.

14. Wang, D.H., et al., *Aberrant epithelial-mesenchymal Hedgehog signaling characterizes Barrett's metaplasia.* Gastroenterology, 2010. **138**(5): p. 1810-22.

15. Song, S., et al., *COX-2 induction by unconjugated bile acids involves reactive oxygen species-mediated signalling pathways in Barrett's oesophagus and oesophageal adenocarcinoma.* Gut, 2007. **56**(11): p. 1512-21.

16. Gaman, A., Kuo B., *Esophageal Embryology and Congenital Disorders*, in *Esophageal Cancer: Principles and Practice*, B.T. Jobe, C.R., Hunter, J.G., Editor. 2009, DemosMedical: New York, NY. p. 3-10.

17. Jankowski, J.A., et al., *Molecular evolution of the metaplasia-dysplasia-adenocarcinoma sequence in the esophagus.* Am J Pathol, 1999. **154**(4): p. 965-73.

18. Morales, C.P., R.F. Souza, and S.J. Spechler, *Hallmarks of cancer progression in Barrett's oesophagus.* Lancet, 2002. **360**(9345): p. 1587-9.

19. Tselepis, C., et al., *Tumour necrosis factor-alpha in Barrett's oesophagus: a potential novel mechanism of action.* Oncogene, 2002. **21**(39): p. 6071-81.

20. Balkwill, F. and A. Mantovani, *Inflammation and cancer: back to Virchow?* Lancet, 2001. **357**(9255): p. 539-45.

21. Weaver, V.M., et al., *Reversion of the malignant phenotype of human breast cells in three-dimensional culture and in vivo by integrin blocking antibodies.* J Cell Biol, 1997. **137**(1): p. 231-45.

22. Weaver, V.M., et al., *beta4 integrin-dependent formation of polarized three-dimensional architecture confers resistance to apoptosis in normal and malignant mammary epithelium.* Cancer Cell, 2002. **2**(3): p. 205-16.

23. Liu, H., et al., *Polarity and proliferation are controlled by distinct signaling pathways downstream of PI3-kinase in breast epithelial tumor cells.* J Cell Biol, 2004. **164**(4): p. 603-12.

24. Hiles, M. and J. Hodde, *Tissue engineering a clinically useful extracellular matrix biomaterial.* Int Urogynecol J Pelvic Floor Dysfunct, 2006. **17 Suppl 1**: p. S39-43.

25. Keane, T.J., Saldin, L.T., Badylak S.F., *Decellularization of mammalian tissues: Preparing extracellular matrix bioscaffolds*, in *Characterisation and Design of Tissue Scaffolds*, P. Tomlins, Editor. 2016, Woodhead Publishing. p. 75-103.

26. Badylak, S., et al., *Resorbable bioscaffold for esophageal repair in a dog model.* J Pediatr Surg, 2000. **35**(7): p. 1097-103.

27. Badylak, S.F., et al., *Esophageal reconstruction with ECM and muscle tissue in a dog model.* J Surg Res, 2005. **128**(1): p. 87-97.

28. Nieponice, A., T.W. Gilbert, and S.F. Badylak, *Reinforcement of esophageal anastomoses with an extracellular matrix scaffold in a canine model.* Ann Thorac Surg, 2006. **82**(6): p. 2050-8.

29. Nieponice, A., et al., *An extracellular matrix scaffold for esophageal stricture prevention after circumferential EMR.* Gastrointest Endosc, 2009. **69**(2): p. 289-96.

30. Badylak, S.F., et al., *Esophageal preservation in five male patients after endoscopic inner-layer circumferential resection in the setting of superficial cancer: a regenerative medicine approach with a biologic scaffold.* Tissue Eng Part A, 2011. **17**(11-12): p. 1643-50.

31. Nieponice, A., et al., *Bone marrow-derived cells participate in the long-term remodeling in a mouse model of esophageal reconstruction.* J Surg Res, 2013. **182**(1): p. e1-7.

32. Nieponice, A., et al., *Patch esophagoplasty: esophageal reconstruction using biologic scaffolds.* Ann Thorac Surg, 2014. **97**(1): p. 283-8.

33. Keane, T.J., et al., *Tissue-Specific Effects of Esophageal Extracellular Matrix.* Tissue Eng Part A, 2015. **21**(17-18): p. 2293-300.

34. Hodde, J.P., et al., *Small intestinal submucosa does not promote PAIII tumor growth in Lobund-Wistar rats.* J Surg Res, 2004. **120**(2): p. 189-94.

35. Phillips, J., K.O. Riley, and B.A. Woodworth, *Porcine small intestine submucosal grafts for post-tumor resection orbital reconstruction.* Laryngoscope, 2014. **124**(6): p. E219-23.

36. Hurst, R.E., et al., *Matrix-dependent plasticity of the malignant phenotype of bladder cancer cells.* Anticancer research, 2003. **23**(4): p. 3119-28.

37. Hurst, R.E., et al., *Proteome-level display by 2-dimensional chromatography of extracellular matrix-dependent modulation of the phenotype of bladder cancer cells.* Proteome Sci, 2006. **4**: p. 13.

38. Dozmorov, M.G., et al., *Analysis of the interaction of extracellular matrix and phenotype of bladder cancer cells.* BMC Cancer, 2006. **6**: p. 12.

39. Hurst, R.E., et al., *Suppression and activation of the malignant phenotype by extracellular matrix in xenograft models of bladder cancer: a model for tumor cell "dormancy".* PLoS One, 2013. **8**(5): p. e64181.

40. Suckow, M.A., et al., *Use of an extracellular matrix material as a vaccine carrier and adjuvant.* Anticancer Res, 2008. **28**(5A): p. 2529-34.

41. Badylak, S.F., et al., *Resorbable bioscaffold for esophageal repair in a dog model.* J Pediatr Surg, 2000. **35**(7): p. 1097-103.

42. Keane, T.J., et al., *Preparation and characterization of a biologic scaffold from esophageal mucosa.* Biomaterials, 2013. **34**(28): p. 6729-37.

43. Dua, K.S., et al., *In-vivo oesophageal regeneration in a human being by use of a non-biological scaffold and extracellular matrix.* Lancet, 2016. **388**(10039): p. 55-61.

44. Drury, J.L. and D.J. Mooney, *Hydrogels for tissue engineering: scaffold design variables and applications.* Biomaterials, 2003. **24**(24): p. 4337-51.

45. Choi, J.S., et al., *In vitro cartilage tissue engineering using adipose-derived extracellular matrix scaffolds seeded with adipose-derived stem cells.* Tissue Engineering Part A, 2012. **18**(1-2): p. 80-92.

46. Mercuri, J.J., S.S. Gill, and D.T. Simionescu, *Novel tissue-derived biomimetic scaffold for regenerating the human nucleus pulposus.* J Biomed Mater Res A, 2011. **96**(2): p. 422-35.

47. Mercuri, J.J., et al., *Regenerative potential of decellularized porcine nucleus pulposus hydrogel scaffolds: stem cell differentiation, matrix remodeling, and biocompatibility studies.* Tissue Eng Part A, 2013. **19**(7-8): p. 952-66.

48. Beck, E.C., et al., *Chondroinduction from Naturally Derived Cartilage Matrix: A Comparison Between Devitalized and Decellularized Cartilage Encapsulated in Hydrogel Pastes.* Tissue Eng Part A, 2016. **22**(7-8): p. 665-79.

49. Beck, E.C., et al., *Chondroinductive Hydrogel Pastes Composed of Naturally Derived Devitalized Cartilage.* Ann Biomed Eng, 2016. **44**(6): p. 1863-80.

50. Hynes, R.O., *The evolution of metazoan extracellular matrix.* J Cell Biol, 2012. **196**(6): p. 671-9.

51. Tibbitt, M.W. and K.S. Anseth, *Hydrogels as extracellular matrix mimics for 3D cell culture.* Biotechnol Bioeng, 2009. **103**(4): p. 655-63.

52. Elliott, R.A., Jr. and J.G. Hoehn, *Use of commercial porcine skin for wound dressings.* Plast Reconstr Surg, 1973. **52**(4): p. 401-5.

53. Badylak, S.F., et al., *Small intestinal submucosa as a large diameter vascular graft in the dog.* J Surg Res, 1989. **47**(1): p. 74-80.

54. Lantz, G.C., et al., *Small intestinal submucosa as a small-diameter arterial graft in the dog.* J Invest Surg, 1990. **3**(3): p. 217-27.

55. Lantz, G.C., et al., *Small intestinal submucosa as a superior vena cava graft in the dog.* J Surg Res, 1992. **53**(2): p. 175-81.

56. Sandusky, G.E., Jr., et al., *Histologic findings after in vivo placement of small intestine submucosal vascular grafts and saphenous vein grafts in the carotid artery in dogs.* Am J Pathol, 1992. **140**(2): p. 317-24.

57. Lantz, G.C., et al., *Small intestinal submucosa as a vascular graft: a review.* J Invest Surg, 1993. **6**(3): p. 297-310.

58. Voytik-Harbin, S.L., A.O. Brightman, *Small intestinal submucosa: A tissue derived extracellular matrix that promotes tissue-specific growth and differentiation of cells in vitro.* Tissue Eng, 1998. **4**: p. 157-174.

59. Badylak, S.F., D.O. Freytes, and T.W. Gilbert, *Extracellular matrix as a biological scaffold material: Structure and function.* Acta Biomater, 2009. **5**(1): p. 1-13.

60. Zantop, T., et al., *Extracellular matrix scaffolds are repopulated by bone marrow-derived cells in a mouse model of Achilles tendon reconstruction.* J Orthop Res, 2006. **24**(6): p. 1299-309.

61. Gilbert, T.W., et al., *Production and characterization of ECM powder: implications for tissue engineering applications.* Biomaterials, 2005. **26**(12): p. 1431-5.

62. Freytes, D.O., et al., *Preparation and rheological characterization of a gel form of the porcine urinary bladder matrix.* Biomaterials, 2008. **29**(11): p. 1630-7.

63. Ghuman, H., et al., *ECM hydrogel for the treatment of stroke: Characterization of the host cell infiltrate.* Biomaterials, 2016. **91**: p. 166-81.

64. Massensini, A.R., et al., *Concentration-dependent rheological properties of ECM hydrogel for intracerebral delivery to a stroke cavity.* Acta Biomater, 2015. **27**: p. 116-30.

65. Wolf, M.T., et al., *A hydrogel derived from decellularized dermal extracellular matrix.* Biomaterials, 2012. **33**(29): p. 7028-7038.

66. Zhang, L., et al., *Effect of an inductive hydrogel composed of urinary bladder matrix upon functional recovery following traumatic brain injury.* Tissue Eng Part A, 2013. **19**(17-18): p. 1909-18.

67. Bible, E., et al., *Non-invasive imaging of transplanted human neural stem cells and ECM scaffold remodeling in the stroke-damaged rat brain by (19)F- and diffusion-MRI.* Biomaterials, 2012. **33**(10): p. 2858-71.

68. Fisher, M.B., et al., *Potential of healing a transected anterior cruciate ligament with genetically modified extracellular matrix bioscaffolds in a goat model.* Knee Surg Sports Traumatol Arthrosc, 2012. **20**(7): p. 1357-65.

69. Badylak, S.E., *The extracellular matrix as a scaffold for tissue reconstruction.* Seminars in Cell & Developmental Biology, 2002. **13**(5): p. 377-383.

70. Londono, R. and S.F. Badylak, *Biologic scaffolds for regenerative medicine: mechanisms of in vivo remodeling.* Ann Biomed Eng, 2015. **43**(3): p. 577-92.

71. Sarikaya, A., et al., *Antimicrobial activity associated with extracellular matrices.* Tissue Eng, 2002. **8**(1): p. 63-71.

72. Brennan, E.P., et al., *Antibacterial activity within degradation products of biological scaffolds composed of extracellular matrix.* Tissue Eng, 2006. **12**(10): p. 2949-55.

73. Agrawal, V., et al., *Recruitment of progenitor cells by an extracellular matrix cryptic peptide in a mouse model of digit amputation.* Tissue Eng Part A, 2011. **17**(19-20): p. 2435-43.

74. Reing, J.E., et al., *Degradation products of extracellular matrix affect cell migration and proliferation.* Tissue Eng Part A, 2009. **15**(3): p. 605-14.

75. Brightman, A.O., et al., *Time-lapse confocal reflection microscopy of collagen fibrillogenesis and extracellular matrix assembly in vitro.* Biopolymers, 2000. **54**(3): p. 222-34.

76. Crapo, P.M., T.W. Gilbert, and S.F. Badylak, *An overview of tissue and whole organ decellularization processes.* Biomaterials, 2011. **32**(12): p. 3233-43.

77. Keane, T.J., et al., *Consequences of ineffective decellularization of biologic scaffolds on the host response.* Biomaterials, 2012. **33**(6): p. 1771-81.

78. Drake, M.P., et al., *Action of proteolytic enzymes on tropocollagen and insoluble collagen.* Biochemistry, 1966. **5**(1): p. 301-12.

79. Miller, E.J., *Structural studies on cartilage collagen employing limited cleavage and solubilization with pepsin.* Biochemistry, 1972. **11**(26): p. 4903-9.

80. Hulmes, D.J.S., *Collagen Diversity, Synthesis, and Assembly*. Collagen: Structure and Mechanics, ed. P. Fratzl. 2008: Springer.

81. Agrawal, V., et al., *An isolated cryptic Peptide influences osteogenesis and bone remodeling in an adult Mammalian model of digit amputation.* Tissue Eng Part A, 2011. **17**(23-24): p. 3033-44.

82. Parkinson, J., K.E. Kadler, and A. Brass, *Simple physical model of collagen fibrillogenesis based on diffusion limited aggregation.* J Mol Biol, 1995. **247**(4): p. 823-31.

83. Johnson, T.D., S.Y. Lin, and K.L. Christman, *Tailoring material properties of a nanofibrous extracellular matrix derived hydrogel.* Nanotechnology, 2011. **22**(49): p. 494015.

84. Uriel, S., et al., *The role of adipose protein derived hydrogels in adipogenesis.* Biomaterials, 2008. **29**(27): p. 3712-9.

85. Uriel, S., et al., *Extraction and Assembly of Tissue-Derived Gels for Cell Culture and Tissue Engineering.* Tissue Eng Part C, 2009. **15**(309-321).

86. Cheng, M.-H., et al., *Dermis-derived hydrogels support adipogenesis in vivo.* Journal of Biomedical Materials Research Part A, 2010. **92A**(3): p. 852-858.

87. Pilipchuk, S.P., et al., *Influence of crosslinking on the stiffness and degradation of dermis-derived hydrogels.* Journal of Biomedical Materials Research Part A, 2013. **101**(10): p. 2883-2895.

88. Poon, C.J., et al., *Preparation of an adipogenic hydrogel from subcutaneous adipose tissue.* Acta Biomaterialia, 2013. **9**(3): p. 5609-5620.

89. Kadler, K.E., A. Hill, and E.G. Canty-Laird, *Collagen fibrillogenesis: fibronectin, integrins, and minor collagens as organizers and nucleators.* Curr Opin Cell Biol, 2008. **20**(5): p. 495-501.

90. Pouliot, R.A., et al., *Development and characterization of a naturally derived lung extracellular matrix hydrogel.* J Biomed Mater Res A, 2016. **104**(8): p. 1922-35.

91. Kim, E.J., et al., *Injectable and Thermosensitive Soluble Extracellular Matrix and Methylcellulose Hydrogels for Stem Cell Delivery in Skin Wounds.* Biomacromolecules, 2016. **17**(1): p. 4-11.

92. Keane, T.J., et al., *Restoring Mucosal Barrier Function and Modifying Macrophage Phenotype with an Extracellular Matrix Hydrogel: Potential Therapy for Ulcerative Colitis.* Journal of Chron's and Colitis, 2016.

93. Park, K.M., et al., *Decellularized Liver Extracellular Matrix as Promising Tools for Transplantable Bioengineered Liver Promotes Hepatic Lineage Commitments of Induced Pluripotent Stem Cells.* Tissue Eng Part A, 2016. **22**(5-6): p. 449-60.

94. Liang, R., et al., *Positive effects of an extracellular matrix hydrogel on rat anterior cruciate ligament fibroblast proliferation and collagen mRNA expression.* Journal of Orthopaedic Translation, 2015. **3**(3): p. 114-122.

95. Medberry, C.J., et al., *Hydrogels derived from central nervous system extracellular matrix.* Biomaterials, 2013. **34**(4): p. 1033-40.

96. Seif-Naraghi, S., et al., *Design and Characterization of an Injectable Pericardial Matrix Gel: A Potentially Autologous Scaffold for Cardiac Tissue Engineering.* Tissue Eng Part A, 2010. **16**(6): p. 2017-2027.

97. Loneker, A.E., et al., *Solubilized liver extracellular matrix maintains primary rat hepatocyte phenotype in-vitro.* J Biomed Mater Res A, 2016. **104**(4): p. 957-65.

98. Lee, J.S., et al., *Liver extracellular matrix providing dual functions of two-dimensional substrate coating and three-dimensional injectable hydrogel platform for liver tissue engineering.* Biomacromolecules, 2014. **15**(1): p. 206-18.

99. DeQuach, J.A., et al., *Simple and high yielding method for preparing tissue specific extracellular matrix coatings for cell culture.* PLoS One, 2010. **5**(9): p. e13039.

100. Farnebo, S., et al., *Design and characterization of an injectable tendon hydrogel: a novel scaffold for guided tissue regeneration in the musculoskeletal system.* Tissue Eng Part A, 2014. **20**(9-10): p. 1550-61.

101. Johnson, T.D., et al., *Human versus porcine tissue sourcing for an injectable myocardial matrix hydrogel.* Biomater Sci, 2014. **2014**: p. 60283D.

102. Nagao, R.J., et al., *Decellularized Human Kidney Cortex Hydrogels Enhance Kidney Microvascular Endothelial Cell Maturation and Quiescence.* Tissue Eng Part A, 2016.

103. Chaimov, D., et al., *Innovative encapsulation platform based on pancreatic extracellular matrix achieve substantial insulin delivery.* J Control Release, 2016.

104. Ungerleider, J.L., et al., *Extracellular Matrix Hydrogel Promotes Tissue Remodeling, Arteriogenesis, and Perfusion in a Rat Hindlimb Ischemia Model.* JACC Basic Transl Sci, 2016. **1**(1-2): p. 32-44.

105. Fu, Y., et al., *Decellularization of porcine skeletal muscle extracellular matrix for the formulation of a matrix hydrogel: a preliminary study.* J Cell Mol Med, 2016. **20**(4): p. 740-9.

106. Engel, H., et al., *Investigation of Dermis-derived hydrogels for wound healing applications.* Biomed J, 2015. **38**(1): p. 58-64.

107. D'Amore, A., et al., *Characterization of the complete fiber network topology of planar fibrous tissues and scaffolds.* Biomaterials, 2010. **31**(20): p. 5345-54.

108. Young, D.A., et al., *Injectable hydrogel scaffold from decellularized human lipoaspirate.* Acta Biomater, 2011. **7**(3): p. 1040-9.

109. Engler, A., H. Sweeney, and D. Discher, *Matrix Elasticity Directs Stem Cell Lineage Specification.* Cell, 2006. **126**: p. 677-689.

110. Ahearne, M. and A.P. Lynch, *Early Observation of Extracellular Matrix-Derived Hydrogels for Corneal Stroma Regeneration.* Tissue Eng Part C Methods, 2015. **21**(10): p. 1059-69.

111. Wu, J., et al., *An injectable extracellular matrix derived hydrogel for meniscus repair and regeneration.* Acta Biomater, 2015. **16**: p. 49-59.

112. Keane, T.J., et al., *Preparation and characterization of a biologic scaffold and hydrogel derived from colonic mucosa.* J Biomed Mater Res B Appl Biomater, 2015.

113. Sawkins, M.J., et al., *Hydrogels derived from demineralized and decellularized bone extracellular matrix.* Acta Biomater, 2013. **9**(8): p. 7865-73.

114. Pati, F., et al., *Printing three-dimensional tissue analogues with decellularized extracellular matrix bioink.* Nat Commun, 2014. **5**: p. 3935.

115. Wassenaar, J.W., et al., *Modulating in vivo degradation rate of injectable extracellular matrix hydrogels.* J. Mater. Chem. B, 2016. **4**(16): p. 2794-2802.

116. Seif-Naraghi, S.B., et al., *Injectable extracellular matrix derived hydrogel provides a platform for enhanced retention and delivery of a heparin-binding growth factor.* Acta Biomater, 2012. **8**(10): p. 3695-703.

117. Singelyn, J.M. and K.L. Christman, *Modulation of material properties of a decellularized myocardial matrix scaffold.* Macromol Biosci, 2011. **11**(6): p. 731-8.

118. Dequach, J., et al., *Injectable skeletal muscle matrix hydrogel promotes neovascularization and muscle cell infiltration in a hindlimb ischemia model.* Eur Cell Mater., 2013. **23**: p. 400-412.

119. Singelyn, J.M., et al., *Naturally derived myocardial matrix as an injectable scaffold for cardiac tissue engineering.* Biomaterials, 2009. **30**(29): p. 5409-16.

120. Seif-Naraghi, S.B., et al., *Patient-to-patient variability in autologous pericardial matrix scaffolds for cardiac repair.* J Cardiovasc Transl Res, 2011. **4**(5): p. 545-56.

121. Seif-Naraghi, S.B., et al., *Safety and efficacy of an injectable extracellular matrix hydrogel for treating myocardial infarction.* Sci Transl Med, 2013. **5**(173): p. 173ra25.

122. Singelyn, J.M., et al., *Catheter-deliverable hydrogel derived from decellularized ventricular extracellular matrix increases endogenous cardiomyocytes and preserves cardiac function post-myocardial infarction.* J Am Coll Cardiol, 2012. **59**(8): p. 751-63.

123. Wassenaar, J.W., et al., *Evidence for Mechanisms Underlying the Functional Benefits of a Myocardial Matrix Hydrogel for Post-MI Treatment.* J Am Coll Cardiol, 2016. **67**(9): p. 1074-86.

124. Tukmachev, D., et al., *Injectable Extracellular Matrix Hydrogels as Scaffolds for Spinal Cord Injury Repair.* Tissue Eng Part A, 2016. **22**(3-4): p. 306-17.

125. Kim, M.Y., et al., *Augmentation of tendon healing with an injectable tendon hydrogel in a rat Achilles tendon model.* Plast Reconstr Surg, 2014. **133**(5): p. 645e-653e.

126. Ravi, S., et al., *Effect of bone marrow-derived extracellular matrix on cardiac function after ischemic injury.* Biomaterials, 2012. **33**(31): p. 7736-45.

127. Paduano, F., et al., *Odontogenic Differentiation of Human Dental Pulp Stem Cells on Hydrogel Scaffolds Derived from Decellularized Bone Extracellular Matrix and Collagen Type I.* PLoS One, 2016. **11**(2): p. e0148225.

128. Sellaro, T.L., et al., *Maintenance of hepatic sinusoidal endothelial cell phenotype in vitro using organ-specific extracellular matrix scaffolds.* Tissue Eng, 2007. **13**(9): p. 2301-10.

129. Sellaro, T.L., et al., *Maintenance of human hepatocyte function in vitro by liver-derived extracellular matrix gels.* Tissue Eng Part A, 2010. **16**(3): p. 1075-82.

130. Badylak, S.F. and T.W. Gilbert, *Immune response to biologic scaffold materials.* Semin Immunol, 2008. **20**(2): p. 109-16.

131. Sicari, B.M., et al., *The promotion of a constructive macrophage phenotype by solubilized extracellular matrix.* Biomaterials, 2014. **35**(30): p. 8605-12.

132. Meng, F.W., et al., *Solubilized extracellular matrix from brain and urinary bladder elicits distinct functional and phenotypic responses in macrophages.* Biomaterials, 2015. **46**: p. 131-40.

133. Ventrix, I. *A Study of VentriGel in Early and Late Post-myocardial Infarction Patients*. Available from: NLM Identifier: NCT02305602.

134. Wang, R.M. and K.L. Christman, *Decellularized myocardial matrix hydrogels: In basic research and preclinical studies.* Adv Drug Deliv Rev, 2016. **96**: p. 77-82.

135. Sonnenberg, S.B., et al., *Delivery of an engineered HGF fragment in an extracellular matrix-derived hydrogel prevents negative LV remodeling post-myocardial infarction.* Biomaterials, 2015. **45**: p. 56-63.

136. Smith, E.L., et al., *Evaluation of skeletal tissue repair, part 2: enhancement of skeletal tissue repair through dual-growth-factor-releasing hydrogels within an ex vivo chick femur defect model.* Acta Biomater, 2014. **10**(10): p. 4197-205.

137. Viswanath, A., et al., *Extracellular Matrix-Derived Hydrogels for Dental Stem Cell Delivery.* J Biomed Mater Res A, 2016.

138. Huleihel, L., et al., *Matrix-Bound Nanovesicles Recapitulate Extracellular Matrix Effects on Macrophage Phenotype.* Tissue Eng Part A, 2017. **23**(21-22): p. 1283-1294.

139. Saldin, L.T., et al., *Extracellular matrix hydrogels from decellularized tissues: Structure and function.* Acta Biomater, 2017. **49**: p. 1-15.

140. Keane, T.J., et al., *Restoring Mucosal Barrier Function and Modifying Macrophage Phenotype with an Extracellular Matrix Hydrogel: Potential Therapy for Ulcerative Colitis.* J Crohns Colitis, 2017. **11**(3): p. 360-368.

141. Mosser, D.M. and J.P. Edwards, *Exploring the full spectrum of macrophage activation.* Nat Rev Immunol, 2008. **8**(12): p. 958-69.

142. Gordon, S. and P.R. Taylor, *Monocyte and macrophage heterogeneity.* Nat Rev Immunol, 2005. **5**(12): p. 953-64.

143. Badylak, S.F., et al., *Macrophage phenotype as a determinant of biologic scaffold remodeling.* Tissue Eng Part A, 2008. **14**(11): p. 1835-42.

144. Pollard, J.W., *Trophic macrophages in development and disease.* Nat Rev Immunol, 2009. **9**(4): p. 259-70.

145. Godwin, J.W., A.R. Pinto, and N.A. Rosenthal, *Macrophages are required for adult salamander limb regeneration.* Proc Natl Acad Sci U S A, 2013. **110**(23): p. 9415-20.

146. Yun, M.H., H. Davaapil, and J.P. Brockes, *Recurrent turnover of senescent cells during regeneration of a complex structure.* Elife, 2015. **4**.

147. Wynn, T.A. and K.M. Vannella, *Macrophages in Tissue Repair, Regeneration, and Fibrosis.* Immunity, 2016. **44**(3): p. 450-462.

148. Mantovani, A., *Cancer: Inflaming metastasis.* Nature, 2009. **457**(7225): p. 36-7.

149. Hay, E.D., ed. *Cell Biology of Extracellular Matrix*. Second ed. 2013, Springer Science & Business Media. 468.

150. Frantz, C., K.M. Stewart, and V.M. Weaver, *The extracellular matrix at a glance.* J Cell Sci, 2010. **123**(Pt 24): p. 4195-200.

151. Bonnans, C., J. Chou, and Z. Werb, *Remodelling the extracellular matrix in development and disease.* Nat Rev Mol Cell Biol, 2014. **15**(12): p. 786-801.

152. Cox, T.R. and J.T. Erler, *Remodeling and homeostasis of the extracellular matrix: implications for fibrotic diseases and cancer.* Dis Model Mech, 2011. **4**(2): p. 165-78.

153. Lu, P., V.M. Weaver, and Z. Werb, *The extracellular matrix: a dynamic niche in cancer progression.* J Cell Biol, 2012. **196**(4): p. 395-406.

154. Lu, H., et al., *A breast cancer stem cell niche supported by juxtacrine signalling from monocytes and macrophages.* Nat Cell Biol, 2014. **16**(11): p. 1105-17.

155. Klug, F., et al., *Low-dose irradiation programs macrophage differentiation to an iNOS(+)/M1 phenotype that orchestrates effective T cell immunotherapy.* Cancer Cell, 2013. **24**(5): p. 589-602.

156. Allavena, P. and A. Mantovani, *Immunology in the clinic review series; focus on cancer: tumour-associated macrophages: undisputed stars of the inflammatory tumour microenvironment.* Clin Exp Immunol, 2012. **167**(2): p. 195-205.

157. Macke, R.A., et al., *Barrett's esophagus and animal models.* Ann N Y Acad Sci, 2011. **1232**: p. 392-400.

158. Sutherland, R.S., et al., *Regeneration of bladder urothelium, smooth muscle, blood vessels and nerves into an acellular tissue matrix.* J Urol, 1996. **156**(2 Pt 2): p. 571-7.

159. Calle, E.A., et al., *Targeted proteomics effectively quantifies differences between native lung and detergent-decellularized lung extracellular matrices.* Acta Biomater, 2016. **46**: p. 91-100.

160. Pratt, J.M., et al., *Multiplexed absolute quantification for proteomics using concatenated signature peptides encoded by QconCAT genes.* Nat Protoc, 2006. **1**(2): p. 1029-43.

161. Goddard, E.T., et al., *Quantitative extracellular matrix proteomics to study mammary and liver tissue microenvironments.* Int J Biochem Cell Biol, 2016. **81**(Pt A): p. 223-232.

162. Hill, R.C., et al., *Quantification of extracellular matrix proteins from a rat lung scaffold to provide a molecular readout for tissue engineering.* Mol Cell Proteomics, 2015. **14**(4): p. 961-73.

163. Slivka, P.F., et al., *Fractionation of an ECM hydrogel into structural and soluble components reveals distinctive roles in regulating macrophage behavior.* Biomaterials Science, 2014. **2**(10): p. 1521.

164. Huleihel, L., et al., *Macrophage phenotype in response to ECM bioscaffolds.* Semin Immunol, 2017. **29**: p. 2-13.

165. Allavena, P., et al., *The inflammatory micro-environment in tumor progression: the role of tumor-associated macrophages.* Crit Rev Oncol Hematol, 2008. **66**(1): p. 1-9.

166. Mantovani, A., A. Sica, and M. Locati, *Macrophage polarization comes of age.* Immunity, 2005. **23**(4): p. 344-6.

167. Mantovani, A., et al., *The chemokine system in diverse forms of macrophage activation and polarization.* Trends Immunol, 2004. **25**(12): p. 677-86.

168. Kusmartsev, S. and D.I. Gabrilovich, *STAT1 signaling regulates tumor-associated macrophage-mediated T cell deletion.* J Immunol, 2005. **174**(8): p. 4880-91.

169. Dziki, J.L., et al., *Solubilized extracellular matrix bioscaffolds derived from diverse source tissues differentially influence macrophage phenotype.* J Biomed Mater Res A, 2017. **105**(1): p. 138-147.

170. Provenzano, P.P., et al., *Collagen density promotes mammary tumor initiation and progression.* BMC Med, 2008. **6**: p. 11.

171. Ma, Z.H., et al., *Effect of enhanced expression of COL8A1 on lymphatic metastasis of hepatocellular carcinoma in mice.* Exp Ther Med, 2012. **4**(4): p. 621-626.

172. Vecchi, M., et al., *Gene expression analysis of early and advanced gastric cancers.* Oncogene, 2007. **26**(29): p. 4284-94.

173. Giussani, M., et al., *Tumor-extracellular matrix interactions: Identification of tools associated with breast cancer progression.* Semin Cancer Biol, 2015. **35**: p. 3-10.

174. Seya, T., et al., *Lumican expression in advanced colorectal cancer with nodal metastasis correlates with poor prognosis.* Oncol Rep, 2006. **16**(6): p. 1225-30.

175. Venturi, M., Bonavina, L., Colombo, L., Mussini, E., Bauer, D., and Peracchia, A., *Collagen and elastin distribution in the human esophagus*, in *Recent Advances in Diseases of the Esophagus*, R.R. A. Peracchia, L. Bonavina, U. Fumagalli, S. Bona, and B. Chella, Editor. 1996: Bologna. p. 865–870.

176. Houghton, A.M., et al., *Elastin fragments drive disease progression in a murine model of emphysema.* J Clin Invest, 2006. **116**(3): p. 753-9.

177. Adair-Kirk, T.L. and R.M. Senior, *Fragments of extracellular matrix as mediators of inflammation.* Int J Biochem Cell Biol, 2008. **40**(6-7): p. 1101-10.

178. Salmela, M.T., et al., *Upregulation and differential expression of matrilysin (MMP-7) and metalloelastase (MMP-12) and their inhibitors TIMP-1 and TIMP-3 in Barrett's oesophageal adenocarcinoma.* Br J Cancer, 2001. **85**(3): p. 383-92.

179. Bernard, M.P., et al., *Nucleotide sequences of complementary deoxyribonucleic acids for the pro alpha 1 chain of human type I procollagen. Statistical evaluation of structures that are conserved during evolution.* Biochemistry, 1983. **22**(22): p. 5213-23.

180. Bernard, M.P., et al., *Structure of a cDNA for the pro alpha 2 chain of human type I procollagen. Comparison with chick cDNA for pro alpha 2(I) identifies structurally conserved features of the protein and the gene.* Biochemistry, 1983. **22**(5): p. 1139-45.

181. Constantinou, C.D. and S.A. Jimenez, *Structure of cDNAs encoding the triple-helical domain of murine alpha 2 (VI) collagen chain and comparison to human and chick*

homologues. Use of polymerase chain reaction and partially degenerate oligonucleotide for generation of novel cDNA clones. Matrix, 1991. **11**(1): p. 1-9.

182. Exposito, J.Y., et al., *Sea urchin collagen evolutionarily homologous to vertebrate pro-alpha 2(I) collagen.* J Biol Chem, 1992. **267**(22): p. 15559-62.

183. Nelson, C.M. and M.J. Bissell, *Modeling dynamic reciprocity: Engineering three-dimensional culture models of breast architecture, function, and neoplastic transformation.* Seminars in Cancer Biology, 2005. **15**(5): p. 342-352.

184. Villasante, A. and G. Vunjak-Novakovic, *Tissue-engineered models of human tumors for cancer research.* Expert Opin Drug Discov, 2015. **10**(3): p. 257-68.

185. Yanez-Mo, M., et al., *Biological properties of extracellular vesicles and their physiological functions.* J Extracell Vesicles, 2015. **4**: p. 27066.

186. Weissleder, R., et al., *Cell-specific targeting of nanoparticles by multivalent attachment of small molecules.* Nat Biotechnol, 2005. **23**(11): p. 1418-23.

187. Insua-Rodriguez, J. and T. Oskarsson, *The extracellular matrix in breast cancer.* Adv Drug Deliv Rev, 2016. **97**: p. 41-55.

188. Bissell, M.J., et al., *The organizing principle: microenvironmental influences in the normal and malignant breast.* Differentiation, 2002. **70**(9-10): p. 537-46.

189. Dauth, S., et al., *Extracellular matrix protein expression is brain region dependent.* J Comp Neurol, 2016. **524**(7): p. 1309-36.

190. Loessner, D., et al., *Bioengineered 3D platform to explore cell-ECM interactions and drug resistance of epithelial ovarian cancer cells.* Biomaterials, 2010. **31**(32): p. 8494-506.

191. Sherman-Baust, C.A., et al., *Remodeling of the extracellular matrix through overexpression of collagen VI contributes to cisplatin resistance in ovarian cancer cells.* Cancer Cell, 2003. **3**(4): p. 377-86.

192. Nadiarnykh, O., et al., *Alterations of the extracellular matrix in ovarian cancer studied by Second Harmonic Generation imaging microscopy.* BMC Cancer, 2010. **10**: p. 94.

193. Fleszar, A.J., et al., *The extracellular matrix of ovarian cortical inclusion cysts modulates invasion of fallopian tube epithelial cells.* 2018. **2**(3): p. 031902.

194. Luo, M.L., et al., *An ADAM12 and FAK positive feedback loop amplifies the interaction signal of tumor cells with extracellular matrix to promote esophageal cancer metastasis.* Cancer Lett, 2018. **422**: p. 118-128.

195. Groblewska, M., et al., *The role of matrix metalloproteinases (MMPs) and their inhibitors (TIMPs) in the development of esophageal cancer.* Folia Histochem Cytobiol, 2012. **50**(1): p. 12-9.

196. Bobryshev, Y.V., M.C. Killingsworth, and R.V. Lord, *Structural alterations of the mucosa stroma in the Barrett's esophagus metaplasia-dysplasia-adenocarcinoma sequence.* J Gastroenterol Hepatol, 2012. **27**(9): p. 1498-504.

197. Lin, S. and R.I. Gregory, *MicroRNA biogenesis pathways in cancer.* Nat Rev Cancer, 2015. **15**(6): p. 321-33.

198. Banerjee, S., et al., *MicroRNA let-7c regulates macrophage polarization.* J Immunol, 2013. **190**(12): p. 6542-9.

199. Banerjee, S., et al., *miR-125a-5p regulates differential activation of macrophages and inflammation.* J Biol Chem, 2013. **288**(49): p. 35428-36.

200. Brown, B.N. and S.F. Badylak, *Extracellular matrix as an inductive scaffold for functional tissue reconstruction.* Transl Res, 2014. **163**(4): p. 268-85.

201. Parenteau-Bareil R., G., R. and Berthod F., *Collagen-Based Biomaterials for Tissue Engineering Applications.* Materials, 2010. **3**(3): p. 1863-1887.

202. Chattopadhyay, S. and R.T. Raines, *Review collagen-based biomaterials for wound healing.* Biopolymers, 2014. **101**(8): p. 821-33.

203. Kogan, G., et al., *Hyaluronic acid: a natural biopolymer with a broad range of biomedical and industrial applications.* Biotechnol Lett, 2007. **29**(1): p. 17-25.

204. Spechler, S.J., *Barrett's esophagus and esophageal adenocarcinoma: pathogenesis, diagnosis, and therapy.* Med Clin North Am, 2002. **86**(6): p. 1423-45, vii.

205. Prasad, G.A., et al., *Endoscopic and surgical treatment of mucosal (T1a) esophageal adenocarcinoma in Barrett's esophagus.* Gastroenterology, 2009. **137**(3): p. 815-23.

206. Nieponice, A., et al., *Bone marrow-derived cells participate in the long-term remodeling in a mouse model of esophageal reconstruction.* J Surg Res, 2012.

207. Hussey, G.S., Dziki, J. L., and Badylak, S.F., *Extracellular matrix-based materials for regenerative medicine.* Nature Reviews Materials, 2018.

208. Gerdes, H.H., A. Rustom, and X. Wang, *Tunneling nanotubes, an emerging intercellular communication route in development.* Mech Dev, 2013. **130**(6-8): p. 381-7.

209. Lou, E., et al., *Tunneling Nanotubes: A new paradigm for studying intercellular communication and therapeutics in cancer.* Commun Integr Biol, 2012. **5**(4): p. 399-403.

210. Rustom, A., et al., *Nanotubular highways for intercellular organelle transport.* Science, 2004. **303**(5660): p. 1007-10.

211. Wang, Y., et al., *Tunneling-nanotube development in astrocytes depends on p53 activation.* Cell Death Differ, 2011. **18**(4): p. 732-42.

212. Vivanco, I. and C.L. Sawyers, *The phosphatidylinositol 3-Kinase AKT pathway in human cancer.* Nat Rev Cancer, 2002. **2**(7): p. 489-501.

213. Sagatys, E., et al., *Activation of the serine/threonine protein kinase Akt during the progression of Barrett neoplasia.* Hum Pathol, 2007. **38**(10): p. 1526-31.

214. Nicholson, K.M. and N.G. Anderson, *The protein kinase B/Akt signalling pathway in human malignancy.* Cell Signal, 2002. **14**(5): p. 381-95.

215. Roesly, H.B., et al., *The decreased expression of Beclin-1 correlates with progression to esophageal adenocarcinoma: the role of deoxycholic acid.* Am J Physiol Gastrointest Liver Physiol, 2012. **302**(8): p. G864-72.

216. Barkan, D., et al., *Inhibition of metastatic outgrowth from single dormant tumor cells by targeting the cytoskeleton.* Cancer Res, 2008. **68**(15): p. 6241-50.

217. Roth, J.M., et al., *Recombinant alpha2(IV)NC1 domain inhibits tumor cell-extracellular matrix interactions, induces cellular senescence, and inhibits tumor growth in vivo.* Am J Pathol, 2005. **166**(3): p. 901-11.

218. Chen, J., et al., *The key regulatory roles of the PI3K/Akt signaling pathway in the functionalities of mesenchymal stem cells and applications in tissue regeneration.* Tissue Eng Part B Rev, 2013. **19**(6): p. 516-28.

219. Pickup, M.W., J.K. Mouw, and V.M. Weaver, *The extracellular matrix modulates the hallmarks of cancer.* EMBO Rep, 2014. **15**(12): p. 1243-53.

220. Barkan, D., J.E. Green, and A.F. Chambers, *Extracellular matrix: a gatekeeper in the transition from dormancy to metastatic growth.* Eur J Cancer, 2010. **46**(7): p. 1181-8.

221. Spencer, V.A., R. Xu, and M.J. Bissell, *Gene expression in the third dimension: the ECM-nucleus connection.* J Mammary Gland Biol Neoplasia, 2010. **15**(1): p. 65-71.

222. Dameron, K.M., et al., *The p53 tumor suppressor gene inhibits angiogenesis by stimulating the production of thrombospondin.* Cold Spring Harb Symp Quant Biol, 1994. **59**: p. 483-9.

223. Iotsova, V. and D. Stehelin, *Down-regulation of fibronectin gene expression by the p53 tumor suppressor protein.* Cell Growth Differ, 1996. **7**(5): p. 629-34.

224. Lukashev, M.E. and Z. Werb, *ECM signalling: orchestrating cell behaviour and misbehaviour.* Trends Cell Biol, 1998. **8**(11): p. 437-41.

225. Dulak, A.M., et al., *Exome and whole-genome sequencing of esophageal adenocarcinoma identifies recurrent driver events and mutational complexity.* Nat Genet, 2013. **45**(5): p. 478-86.

226. Saldin, L.T., et al., *Extracellular Matrix Hydrogels from Decellularized Tissues: Structure and Function.* Acta Biomater, 2016.

227. Wilkinson, N.W., et al., *Epidermal growth factor receptor expression correlates with histologic grade in resected esophageal adenocarcinoma.* J Gastrointest Surg, 2004. **8**(4): p. 448-53.

228. Ferry, D.R., et al., *A phase II study of gefitinib monotherapy in advanced esophageal adenocarcinoma: evidence of gene expression, cellular, and clinical response.* Clin Cancer Res, 2007. **13**(19): p. 5869-75.

229. Huang, A.F., et al., *CD164 regulates the tumorigenesis of ovarian surface epithelial cells through the SDF-1alpha/CXCR4 axis.* Mol Cancer, 2013. **12**(1): p. 115.

230. Prasad, G.A., et al., *Long-term survival following endoscopic and surgical treatment of high-grade dysplasia in Barrett's esophagus.* Gastroenterology, 2007. **132**(4): p. 1226-1233.

231. Spechler, S.J. and R.F. Souza, *Barrett's esophagus.* N Engl J Med, 2014. **371**(9): p. 836-45.

232. Coleman, H.G., Bhat S.K., and Murray L.J., *Epidemiology and prevalance of Barrett's esophagus*, in *Esophageal cancer and Barrett's esophagus*, S.R. Sharma P., and Ilson D., Editor. 2015, John Wiley & Sons.

233. Wang, K.K., R.E. Sampliner, and G. Practice Parameters Committee of the American College of, *Updated guidelines 2008 for the diagnosis, surveillance and therapy of Barrett's esophagus.* Am J Gastroenterol, 2008. **103**(3): p. 788-97.

234. Hvid-Jensen, F., et al., *Incidence of adenocarcinoma among patients with Barrett's esophagus.* N Engl J Med, 2011. **365**(15): p. 1375-83.

235. Sikkema, M., et al., *Risk of esophageal adenocarcinoma and mortality in patients with Barrett's esophagus: a systematic review and meta-analysis.* Clin Gastroenterol Hepatol, 2010. **8**(3): p. 235-44; quiz e32.

236. Corley, D.A., et al., *Protective association of aspirin/NSAIDs and esophageal cancer: a systematic review and meta-analysis.* Gastroenterology, 2003. **124**(1): p. 47-56.

237. Abnet, C.C., et al., *Non-steroidal anti-inflammatory drugs and risk of gastric and oesophageal adenocarcinomas: results from a cohort study and a meta-analysis.* Br J Cancer, 2009. **100**(3): p. 551-7.

238. Kratochwil, K., *Organ specificity in mesenchymal induction demonstrated in the embryonic development of the mammary gland of the mouse.* Dev Biol, 1969. **20**(1): p. 46-71.

239. Bissell, M.J., A. Rizki, and I.S. Mian, *Tissue architecture: the ultimate regulator of breast epithelial function.* Curr Opin Cell Biol, 2003. **15**(6): p. 753-62.

240. Allman, A.J., et al., *Xenogeneic extracellular matrix grafts elicit a TH2-restricted immune response.* Transplantation, 2001. **71**(11): p. 1631-40.

241. Sadtler, K., et al., *Developing a pro-regenerative biomaterial scaffold microenvironment requires T helper 2 cells.* Science, 2016. **352**(6283): p. 366-70.

242. Beattie, A.J., et al., *Chemoattraction of progenitor cells by remodeling extracellular matrix scaffolds.* Tissue Eng Part A, 2009. **15**(5): p. 1119-25.

243. Dziki, J.B.S.Y., M.; Sicari, B.; Ambrosio, F.; Stearns, K.; Turner, N.; and A.B. Wyse, M.L.; Brown, E.H.P.; Rubin, J.P., *An acellular biologic scaffold treatment for volumetric muscle loss: results of a 13-patient cohort study.* NPJ Regenerative Medicine, 2016.

244. Brennan, E.P., et al., *Chemoattractant activity of degradation products of fetal and adult skin extracellular matrix for keratinocyte progenitor cells.* J Tissue Eng Regen Med, 2008. **2**(8): p. 491-8.

245. Agrawal, V., et al., *Epimorphic regeneration approach to tissue replacement in adult mammals.* Proc Natl Acad Sci U S A, 2010. **107**(8): p. 3351-5.

246. F2900-11, A., *Standard Guide for Characterization of Hydrogels used in Regenerative Medicine*, A. International, Editor. 2011: West Conshohocken, PA.

247. Mako, A., et al., *Formulation of thermoresponsive and bioadhesive gel for treatment of oesophageal pain and inflammation.* Eur J Pharm Biopharm, 2009. **72**(1): p. 260-5.

248. Wisniewski, J.R., et al., *Universal sample preparation method for proteome analysis.* Nat Methods, 2009. **6**(5): p. 359-62.

249. Goddard, E.T., et al., *The Rodent Liver Undergoes Weaning-Induced Involution and Supports Breast Cancer Metastasis.* Cancer Discov, 2017. **7**(2): p. 177-187.

250. MacLean, B., et al., *Skyline: an open source document editor for creating and analyzing targeted proteomics experiments.* Bioinformatics, 2010. **26**(7): p. 966-8.

251. *Bancroft's Theory and Practice of Histological Techniques E-Book*, C.L. KS Suvarna, JD Bancroft Editor. 2018, Elsevier Health Sciences.

252. Johnson, D.R., et al., *CDX2 protein expression compared to alcian blue staining in the evaluation of esophageal intestinal metaplasia.* World J Gastroenterol, 2015. **21**(9): p. 2770-6.

253. Gillen, P., et al., *Experimental columnar metaplasia in the canine oesophagus.* Br J Surg, 1988. **75**(2): p. 113-5.

254. Schmeichel, K.L., V.M. Weaver, and M.J. Bissell, *Structural cues from the tissue microenvironment are essential determinants of the human mammary epithelial cell phenotype.* J Mammary Gland Biol Neoplasia, 1998. **3**(2): p. 201-13.

255. Roskelley, C.D., A. Srebrow, and M.J. Bissell, *A hierarchy of ECM-mediated signalling regulates tissue-specific gene expression.* Curr Opin Cell Biol, 1995. **7**(5): p. 736-47.

256. Bissell, M.J. and J. Aggeler, *Dynamic reciprocity: how do extracellular matrix and hormones direct gene expression?* Prog Clin Biol Res, 1987. **249**: p. 251-62.

257. Roskelley, C.D. and M.J. Bissell, *Dynamic reciprocity revisited: a continuous, bidirectional flow of information between cells and the extracellular matrix regulates mammary epithelial cell function.* Biochem Cell Biol, 1995. **73**(7-8): p. 391-7.

258. Li, H., et al., *Mechanisms of columnar metaplasia and squamous regeneration in experimental Barrett's esophagus.* Surgery, 1994. **115**(2): p. 176-81.

259. DeBiase, P.J., et al., *Laminin-311 (Laminin-6) fiber assembly by type I-like alveolar cells.* J Histochem Cytochem, 2006. **54**(6): p. 665-72.

260. Jones, J.C., et al., *Laminin-6 assembles into multimolecular fibrillar complexes with perlecan and participates in mechanical-signal transduction via a dystroglycan-dependent, integrin-independent mechanism.* J Cell Sci, 2005. **118**(Pt 12): p. 2557-66.

261. Hirosaki, T., et al., *Laminin-6 is activated by proteolytic processing and regulates cellular adhesion and migration differently from laminin-5.* J Biol Chem, 2002. **277**(51): p. 49287-95.

262. Hussey, G.S., T.J. Keane, and S.F. Badylak, *The extracellular matrix of the gastrointestinal tract: a regenerative medicine platform.* Nat Rev Gastroenterol Hepatol, 2017. **14**(9): p. 540-552.

263. Peppas, N.A.a.S., J.J., *Hydrogels as mucoadhesive and bioadhesive materials: A review.* Biomaterials, 1996. **17**(16): p. 1553-1561.

264. Committee, A.T., et al., *Endoscopic submucosal dissection.* Gastrointest Endosc, 2015. **81**(6): p. 1311-25.

265. Committee, A.T., et al., *Endoscopic mucosal resection.* Gastrointest Endosc, 2015. **82**(2): p. 215-26.

266. Katada, C., et al., *Esophageal stenosis after endoscopic mucosal resection of superficial esophageal lesions.* Gastrointest Endosc, 2003. **57**(2): p. 165-9.

267. Girotra, M., G. Triadafilopoulos, and S. Friedland, *Utility and performance characteristics of a novel submucosal injection agent (Eleview(TM)) for endoscopic mucosal resection and endoscopic submucosal dissection.* Transl Gastroenterol Hepatol, 2018. **3**: p. 32.

268. Repici, A., et al., *Standard needle versus needleless injection modality: animal study on different fluids for submucosal elevation.* Gastrointest Endosc, 2017. **86**(3): p. 553-558.

269. Mehta, N., et al., *Optimal injection solution for endoscopic submucosal dissection: A randomized controlled trial of Western solutions in a porcine model.* Dig Endosc, 2018. **30**(3): p. 347-353.

270. Englen, M.D., et al., *Granulocyte/macrophage colony-stimulating factor is expressed and secreted in cultures of murine L929 cells.* J Immunol Methods, 1995. **184**(2): p. 281-3.

271. Zhang, X., R. Goncalves, and D.M. Mosser, *The isolation and characterization of murine macrophages.* Curr Protoc Immunol, 2008. **Chapter 14**: p. Unit 14 1.

272. Shearer, J.D., et al., *Differential regulation of macrophage arginine metabolism: a proposed role in wound healing.* Am J Physiol, 1997. **272**(2 Pt 1): p. E181-90.

273. Ho, V.W. and L.M. Sly, *Derivation and characterization of murine alternatively activated (M2) macrophages.* Methods Mol Biol, 2009. **531**: p. 173-85.

274. Nelson, S.M., X. Lei, and K.S. Prabhu, *Selenium levels affect the IL-4-induced expression of alternative activation markers in murine macrophages.* J Nutr, 2011. **141**(9): p. 1754-61.

275. Veremeyko, T., et al., *IL-4/IL-13-dependent and independent expression of miR-124 and its contribution to M2 phenotype of monocytic cells in normal conditions and during allergic inflammation.* PLoS One, 2013. **8**(12): p. e81774.

276. Lewis, J.J., et al., *Factors associated with esophageal stricture formation after endoscopic mucosal resection for neoplastic Barrett's esophagus.* Gastrointest Endosc, 2011. **74**(4): p. 753-60.

277. Gibson, M.K., et al., *Prevention of Barrett esophagus and esophageal adenocarcinoma by smoothened inhibitor in a rat model of gastroesophageal reflux disease.* Ann Surg, 2013. **258**(1): p. 82-8.

278. Zaidi, A.H., et al., *Associations of microbiota and toll-like receptor signaling pathway in esophageal adenocarcinoma.* BMC Cancer, 2016. **16**: p. 52.

279. Kosovec, J.E., et al., *Establishing magnetic resonance imaging as an accurate and reliable tool to diagnose and monitor esophageal cancer in a rat model.* PLoS One, 2014. **9**(4): p. e93694.

280. Liu, C.Y., et al., *M2-polarized tumor-associated macrophages promoted epithelial-mesenchymal transition in pancreatic cancer cells, partially through TLR4/IL-10 signaling pathway.* Lab Invest, 2013. **93**(7): p. 844-54.

281. Bergamaschi, A., et al., *Extracellular matrix signature identifies breast cancer subgroups with different clinical outcome.* J Pathol, 2008. **214**(3): p. 357-67.

282. Lin, C.Y., et al., *An injectable extracellular matrix for the reconstruction of epidural fat and the prevention of epidural fibrosis.* Biomed Mater, 2016. **11**(3): p. 035010.

283. Gothard, D., et al., *In Vivo Assessment of Bone Regeneration in Alginate/Bone ECM Hydrogels with Incorporated Skeletal Stem Cells and Single Growth Factors.* PLoS One, 2015. **10**(12): p. e0145080.

284. Crapo, P.M., et al., *Effects of biologic scaffolds on human stem cells and implications for CNS tissue engineering.* Tissue Eng Part A, 2014. **20**(1-2): p. 313-23.

285. Sood, D., et al., *Fetal Brain Extracellular Matrix Boosts Neuronal Network Formation in 3D Bioengineered Model of Cortical Brain Tissue.* ACS Biomaterials Science & Engineering, 2016. **2**(1): p. 131-140.

286. Stoppel, W.L., et al., *Anisotropic silk biomaterials containing cardiac extracellular matrix for cardiac tissue engineering.* Biomed Mater, 2015. **10**(3): p. 034105.

287. Johnson, T.D., R.L. Braden, and K.L. Christman, *Injectable ECM scaffolds for cardiac repair.* Methods Mol Biol, 2014. **1181**: p. 109-20.

288. Ungerleider, J.L., et al., *Fabrication and characterization of injectable hydrogels derived from decellularized skeletal and cardiac muscle.* Methods, 2015. **84**: p. 53-9.

289. Gaetani, R., et al., *Cardiac derived extracellular matrix enhances cardiogenic properties of human cardiac progenitor cells.* Cell Transplant, 2015.

290. Grover, G.N., N. Rao, and K.L. Christman, *Myocardial matrix-polyethylene glycol hybrid hydrogels for tissue engineering.* Nanotechnology, 2014. **25**(1): p. 014011.

291. Jang, J., et al., *Tailoring mechanical properties of decellularized extracellular matrix bioink by vitamin B2-induced photo-crosslinking.* Acta Biomater, 2016. **33**: p. 88-95.

292. Freytes, D.O., et al., *Natural cardiac extracellular matrix hydrogels for cultivation of human stem cell-derived cardiomyocytes.* Methods Mol Biol, 2014. **1181**: p. 69-81.

293. Stoppel, W.L., et al., *Elastic, silk-cardiac extracellular matrix hydrogels exhibit time-dependent stiffening that modulates cardiac fibroblast response.* J Biomed Mater Res A, 2016.

294. D'Amore, A., et al., *Bi-layered polyurethane - Extracellular matrix cardiac patch improves ischemic ventricular wall remodeling in a rat model.* Biomaterials, 2016. **107**: p. 1-14.

295. Kappler, B., et al., *The cytoprotective capacity of processed human cardiac extracellular matrix.* J Mater Sci Mater Med, 2016. **27**(7): p. 120.

296. Fujita, K., et al., *Characterizing and modulating the mechanical properties of hydrogels from ventricular extracellular matrix.* IEEE, 2015: p. 1-5.

297. Seif-Naraghi, S., et al., *Fabrication of biologically derived injectable materials for myocardial tissue engineering.* J Vis Exp, 2010(46).

298. Faulk, D.M., et al., *ECM hydrogel coating mitigates the chronic inflammatory response to polypropylene mesh.* Biomaterials, 2014. **35**(30): p. 8585-95.

299. Wolf, M.T., et al., *Polypropylene surgical mesh coated with extracellular matrix mitigates the host foreign body response.* J Biomed Mater Res A, 2014. **102**(1): p. 234-46.

300. Wolf, M.T., et al., *Macrophage polarization in response to ECM coated polypropylene mesh.* Biomaterials, 2014. **35**(25): p. 6838-49.

301. Kalabis, J., et al., *Isolation and characterization of mouse and human esophageal epithelial cells in 3D organotypic culture.* Nat Protoc, 2012. **7**(2): p. 235-46.

302. Vecchi, M., et al., *Breast cancer metastases are molecularly distinct from their primary tumors.* Oncogene, 2008. **27**(15): p. 2148-58.

303. Crown Human Genome Center, W.I.o.S.i.I. 1996-2017.

304. Kurozumi, A., et al., *Tumor-suppressive microRNA-223 inhibits cancer cell migration and invasion by targeting ITGA3/ITGB1 signaling in prostate cancer.* Cancer Sci, 2016. **107**(1): p. 84-94.

305. Helleman, J., et al., *Molecular profiling of platinum resistant ovarian cancer.* Int J Cancer, 2006. **118**(8): p. 1963-71.

306. Karar, J. and A. Maity, *PI3K/AKT/mTOR Pathway in Angiogenesis.* Front Mol Neurosci, 2011. **4**: p. 51.

307. Semenza, G.L., *Hypoxia-inducible factors: mediators of cancer progression and targets for cancer therapy.* Trends Pharmacol Sci, 2012. **33**(4): p. 207-14.

308. Thevathasan, J.V., et al., *The small GTPase HRas shapes local PI3K signals through positive feedback and regulates persistent membrane extension in migrating fibroblasts.* Mol Biol Cell, 2013. **24**(14): p. 2228-37.

309. Wang, G., et al., *PIK3R3 induces epithelial-to-mesenchymal transition and promotes metastasis in colorectal cancer.* Mol Cancer Ther, 2014. **13**(7): p. 1837-47.

310. Luo, J., B.D. Manning, and L.C. Cantley, *Targeting the PI3K-Akt pathway in human cancer: rationale and promise.* Cancer Cell, 2003. **4**(4): p. 257-62.

311. Peifer, M. and P. Polakis, *Wnt signaling in oncogenesis and embryogenesis--a look outside the nucleus.* Science, 2000. **287**(5458): p. 1606-9.

312. Fu, Z. and D.J. Tindall, *FOXOs, cancer and regulation of apoptosis.* Oncogene, 2008. **27**(16): p. 2312-9.

313. Knowles, L.M., et al., *Inhibition of fatty-acid synthase induces caspase-8-mediated tumor cell apoptosis by up-regulating DDIT4.* J Biol Chem, 2008. **283**(46): p. 31378-84.

314. Egan, D.F., et al., *Phosphorylation of ULK1 (hATG1) by AMP-activated protein kinase connects energy sensing to mitophagy.* Science, 2011. **331**(6016): p. 456-61.

315. Slattery, M.L., et al., *Genetic variation in a metabolic signaling pathway and colon and rectal cancer risk: mTOR, PTEN, STK11, RPKAA1, PRKAG2, TSC1, TSC2, PI3K and Akt1.* Carcinogenesis, 2010. **31**(9): p. 1604-11.

316. Ma, L., et al., *Phosphorylation and functional inactivation of TSC2 by Erk implications for tuberous sclerosis and cancer pathogenesis.* Cell, 2005. **121**(2): p. 179-93.

317. Okosun, J., et al., *Recurrent mTORC1-activating RRAGC mutations in follicular lymphoma.* Nat Genet, 2016. **48**(2): p. 183-8.

318. Sarbassov, D.D., et al., *Phosphorylation and regulation of Akt/PKB by the rictor-mTOR complex.* Science, 2005. **307**(5712): p. 1098-101.

319. Monteverde, T., et al., *Evidence of cancer-promoting roles for AMPK and related kinases.* FEBS J, 2015. **282**(24): p. 4658-71.

320. Nam, J.S., et al., *Src family kinase inhibitor PP2 restores the E-cadherin/catenin cell adhesion system in human cancer cells and reduces cancer metastasis.* Clin Cancer Res, 2002. **8**(7): p. 2430-6.

321. Barker, N. and H. Clevers, *Mining the Wnt pathway for cancer therapeutics.* Nat Rev Drug Discov, 2006. **5**(12): p. 997-1014.

322. Wang, S.M., L.L. Ooi, and K.M. Hui, *Upregulation of Rac GTPase-activating protein 1 is significantly associated with the early recurrence of human hepatocellular carcinoma.* Clin Cancer Res, 2011. **17**(18): p. 6040-51.

323. Lu, P., et al., *Extracellular matrix degradation and remodeling in development and disease.* Cold Spring Harb Perspect Biol, 2011. **3**(12).

324. Cann, G.M., et al., *Developmental expression of LC3alpha and beta: absence of fibronectin or autophagy phenotype in LC3beta knockout mice.* Dev Dyn, 2008. **237**(1): p. 187-95.

325. Lin, S.Y., et al., *GSK3-TIP60-ULK1 signaling pathway links growth factor deprivation to autophagy.* Science, 2012. **336**(6080): p. 477-81.

326. Polager, S., M. Ofir, and D. Ginsberg, *E2F1 regulates autophagy and the transcription of autophagy genes.* Oncogene, 2008. **27**(35): p. 4860-4.

327. Qiu, D.M., et al., *The expression of beclin-1, an autophagic gene, in hepatocellular carcinoma associated with clinical pathological and prognostic significance.* BMC Cancer, 2014. **14**: p. 327.

328. Baker, M.S., et al., *Inhibition of cancer cell urokinase plasminogen activator by its specific inhibitor PAI-2 and subsequent effects on extracellular matrix degradation.* Cancer Res, 1990. **50**(15): p. 4676-84.

329. Arnold, S.F., E. Tims, and B.E. McGrath, *Identification of bone morphogenetic proteins and their receptors in human breast cancer cell lines: importance of BMP2.* Cytokine, 1999. **11**(12): p. 1031-7.

330. Hanna, R.A., et al., *Microtubule-associated protein 1 light chain 3 (LC3) interacts with Bnip3 protein to selectively remove endoplasmic reticulum and mitochondria via autophagy.* J Biol Chem, 2012. **287**(23): p. 19094-104.

331. Boyer-Guittaut, M., et al., *The role of GABARAPL1/GEC1 in autophagic flux and mitochondrial quality control in MDA-MB-436 breast cancer cells.* Autophagy, 2014. **10**(6): p. 986-1003.

332. Pal, R., et al., *Src-dependent impairment of autophagy by oxidative stress in a mouse model of Duchenne muscular dystrophy.* Nat Commun, 2014. **5**: p. 4425.

333. Lock, R., et al., *Autophagy-dependent production of secreted factors facilitates oncogenic RAS-driven invasion.* Cancer Discov, 2014. **4**(4): p. 466-79.

334. Su, M., et al., *MicroRNA-221 inhibits autophagy and promotes heart failure by modulating the p27/CDK2/mTOR axis.* Cell Death Differ, 2015. **22**(6): p. 986-99.

335. Bruce Alberts, A.J., Julian Lewis, Martin Raff, Keith Roberts, Peter Walter, *Molecular Biology of the Cell*. 2007, New York: Garland Science.

336. Yu, Y., et al., *Elevated breast cancer risk in irradiated BALB/c mice associates with unique functional polymorphism of the Prkdc (DNA-dependent protein kinase catalytic subunit) gene.* Cancer Res, 2001. **61**(5): p. 1820-4.

337. Namkoong, H., et al., *The bone morphogenetic protein antagonist gremlin 1 is overexpressed in human cancers and interacts with YWHAH protein.* BMC Cancer, 2006. **6**: p. 74.

338. Spankuch-Schmitt, B., et al., *Effect of RNA silencing of polo-like kinase-1 (PLK1) on apoptosis and spindle formation in human cancer cells.* J Natl Cancer Inst, 2002. **94**(24): p. 1863-77.

339. (US), N.L.o.M., *Genetics Home Reference [Internet]*. 2013: Bethesda, MD.

340. Danis, E., et al., *Specification of a DNA replication origin by a transcription complex.* Nat Cell Biol, 2004. **6**(8): p. 721-30.

341. Deshpande, A., P. Sicinski, and P.W. Hinds, *Cyclins and cdks in development and cancer: a perspective.* Oncogene, 2005. **24**(17): p. 2909-15.

342. Tetsu, O. and F. McCormick, *Proliferation of cancer cells despite CDK2 inhibition.* Cancer Cell, 2003. **3**(3): p. 233-45.

343. Stoimenov, I. and T. Helleday, *PCNA on the crossroad of cancer.* Biochem Soc Trans, 2009. **37**(Pt 3): p. 605-13.

344. Chen, D., et al., *MicroRNA-30d-5p inhibits tumour cell proliferation and motility by directly targeting CCNE2 in non-small cell lung cancer.* Cancer Lett, 2015. **362**(2): p. 208-17.

345. Kastan, M.B. and J. Bartek, *Cell-cycle checkpoints and cancer.* Nature, 2004. **432**(7015): p. 316-23.

346. Gao, T., et al., *CCNA2 is a prognostic biomarker for ER+ breast cancer and tamoxifen resistance.* PLoS One, 2014. **9**(3): p. e91771.

347. Salas, T.R., et al., *Evidence for direct contact between the RPA3 subunit of the human replication protein A and single-stranded DNA.* Nucleic Acids Res, 2009. **37**(1): p. 38-46.

348. Schar, P., *Spontaneous DNA damage, genome instability, and cancer--when DNA replication escapes control.* Cell, 2001. **104**(3): p. 329-32.

349. Hirota, K., et al., *The POLD3 subunit of DNA polymerase delta can promote translesion synthesis independently of DNA polymerase zeta.* Nucleic Acids Res, 2015. **43**(3): p. 1671-83.

350. Woo, R.A. and R.Y. Poon, *Cyclin-dependent kinases and S phase control in mammalian cells.* Cell Cycle, 2003. **2**(4): p. 316-24.

351. Ishimi, Y., et al., *Enhanced expression of Mcm proteins in cancer cells derived from uterine cervix.* Eur J Biochem, 2003. **270**(6): p. 1089-101.

352. Lowndes, N.F. and J.R. Murguia, *Sensing and responding to DNA damage.* Curr Opin Genet Dev, 2000. **10**(1): p. 17-25.

353. Rogers-Broadway, K.R., et al., *Differential effects of rapalogues, dual kinase inhibitors on human ovarian carcinoma cells in vitro.* Int J Oncol, 2016. **49**(1): p. 133-43.

354. Dong, L., et al., *Involvement of SET in the Wnt signaling pathway and the development of human colorectal cancer.* Oncol Lett, 2014. **7**(4): p. 1203-1208.

355. Li, S., et al., *EphA6 promotes angiogenesis and prostate cancer metastasis and is associated with human prostate cancer progression.* Oncotarget, 2015. **6**(26): p. 22587-97.

356. Costa, J.L., et al., *Anti-proliferative action of vitamin D in MCF7 is still active after siRNA-VDR knock-down.* BMC Genomics, 2009. **10**: p. 499.

357. Domenech, E., et al., *AMPK and PFKFB3 mediate glycolysis and survival in response to mitophagy during mitotic arrest.* Nat Cell Biol, 2015. **17**(10): p. 1304-16.

358. Levanon, K., et al., *FOXO3a loss is a frequent early event in high-grade pelvic serous carcinogenesis.* Oncogene, 2014. **33**(35): p. 4424-32.

359. Haller, F., et al., *Prognostic role of E2F1 and members of the CDKN2A network in gastrointestinal stromal tumors.* Clin Cancer Res, 2005. **11**(18): p. 6589-97.

360. Galluzzi, L., et al., *Induction of endoplasmic reticulum stress response by the indole-3-carbinol cyclic tetrameric derivative CTet in human breast cancer cell lines.* PLoS One, 2012. **7**(8): p. e43249.

361. Li, T., et al., *miR-31 promotes proliferation of colon cancer cells by targeting E2F2.* Biotechnol Lett, 2015. **37**(3): p. 523-32.

362. Wang, Y.X., et al., *Silibinin inhibits proliferation, induces apoptosis and causes cell cycle arrest in human gastric cancer MGC803 cells via STAT3 pathway inhibition.* Asian Pac J Cancer Prev, 2014. **15**(16): p. 6791-8.

363. Zhang, Z., et al., *METTL13 is downregulated in bladder carcinoma and suppresses cell proliferation, migration and invasion.* Sci Rep, 2016. **6**: p. 19261.

364. Bork, S., et al., *DNA methylation pattern changes upon long-term culture and aging of human mesenchymal stromal cells.* Aging Cell, 2010. **9**(1): p. 54-63.

365. Li, J.N., et al., *mRNA expression of the DNA replication-initiation proteins in epithelial dysplasia and squamous cell carcinoma of the tongue.* BMC Cancer, 2008. **8**: p. 395.

366. Doster, A., et al., *Phosphorothioate-modified CpG oligodeoxynucleotides mimic autoantigens and reveal a potential role for Toll-like receptor 9 in receptor revision.* Immunology, 2013. **139**(2): p. 166-78.

367. Pliszczak, D., et al., *Mucoadhesion evaluation of polysaccharide gels for vaginal application by using rheological and indentation measurements.* Colloids Surf B Biointerfaces, 2012. **92**: p. 168-74.